

In vivo visualization
of intestinal stem cell
and crypt dynamics

Lotte Bruens

COLOFON

The work described in this thesis was performed at the Hubrecht Institute for Developmental Biology and Stem Cell Research (Royal Netherlands Academy of Arts and Sciences, KNAW), University Medical Center Utrecht and the Netherlands Cancer Institute within the framework of the research school Cancer, Stem Cells & Developmental Biology (CS&D), which is part of the Utrecht Graduate School of Life Sciences (Utrecht University).

Printed by: Ridderprint | www.ridderprint.nl

Layout by: Lotte Bruens

Cover design by: Lotte Bruens

Cover: Intestinal villi stained against E-cadherin for cell-cell contacts (magenta), phalloidin for F-actin (grey) and Dapi for nuclei (cyan).

Title pages: 3D rendering in Imaris of intestinal stem cells (marked by Lgr5) at the bottom of crypts.

ISBN: 978-94-6375-856-7

Copyright © 2020 by Lotte Bruens. All rights reserved. No part of this book may be reproduced, stored in a retrieval system or transmitted in any form or by any means, without prior permission of the author.

***IN VIVO* VISUALIZATION OF INTESTINAL STEM CELL AND CRYPT DYNAMICS**

IN VIVO VISUALISATIE VAN STAMCEL- EN CRYPTDYNAMIEK IN DE DARM
(met een samenvatting in het Nederlands)

Proefschrift

ter verkrijging van de graad van doctor aan de Universiteit Utrecht op gezag van de rector magnificus, prof.dr. H.R.B.M. Kummeling, ingevolge het besluit van het college voor promoties in het openbaar te verdedigen op donderdag 19 november 2020 des middags te 16.15 uur

door

Lotte Bruens

geboren op 11 januari 1990
te Neuss, Duitsland

PROMOTOR:

Prof. dr. J.E. van Rheenen

COPROMOTOR:

Dr. H.J.G. Snippert

TABLE OF CONTENTS

<i>Thesis scope and outline</i>		7
<i>Chapter 1</i>	Capturing Stem Cell Behavior Using Intravital and Live Cell Microscopy	9
<i>Chapter 2</i>	Cellular Dynamics that Minimize the Accumulation of Mutations in the Intestinal Epithelium	31
<i>Chapter 3</i>	Retrograde Movement Determines the Number of Cells with Stem Cell Potential in Small and Large Intestinal Crypts	45
<i>Chapter 4</i>	Wnt Ligands Influence Tumor Initiation by Controlling the Number of Intestinal Stem Cells	79
<i>Chapter 5</i>	Calorie Restriction Decreases Retention of Intestinal Mutations by Increasing the Number of Wild-type Stem Cell Competitors	107
<i>Chapter 6</i>	<i>In Vivo</i> Imaging Reveals Existence of Crypt Fission and Fusion in Adult Mouse Intestine	123
<i>Chapter 7</i>	Summarizing discussion	135
<i>Addendum</i>	Nederlandse samenvatting Curriculum vitae List of publications Acknowledgements	149

THESIS SCOPE AND OUTLINE

To cope with the hazardous environment in the lumen, the intestinal epithelium is renewed every 3-5 days. This rapid tissue turnover is fueled by stem and progenitor cells at the bottom of crypts – small invaginations into the intestinal wall – that proliferate approximately once a day. The proliferation pushes postmitotic cells upward towards the lumen where they get shed. In this thesis, we use intravital microscopy to visualize this highly dynamic intestinal epithelium in real time. We aim to understand the dynamics that underlie stem cell competition at the base of small and large intestinal crypts and how stem cell and crypt dynamics in the healthy epithelium can affect mutation accumulation and ultimately tumor initiation.

In **Chapter 1** we highlight how over the recent years live cell and intravital microscopy have contributed to the understanding of stem cell dynamics and plasticity during development, homeostasis, regeneration and tumor formation.

In **Chapter 2** we give our perspective on how intestinal stem cell and crypt dynamics minimize the retention of mutations in the intestinal epithelium by ensuring that most mutated cells get lost.

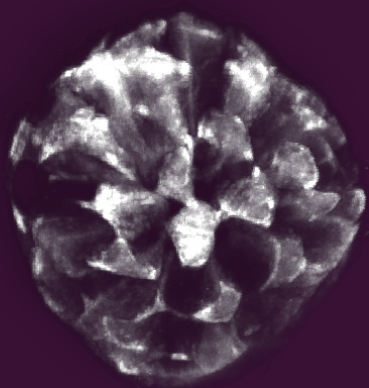
In **Chapter 3** we describe the differences in stem cell dynamics in small and large intestinal crypts. We find that the amount of retrograde movement of the cells within the crypt determines which cells can act as long-term stem cells, as this allows gaining a favorable position in the niche center. While in the small intestine we do observe retrograde movement resulting in functional stemness of cells further away from the crypt base, this retrograde movement is (near) absent in the large intestine. Therefore, only cells at the center of the crypt can function as long-term stem cells in the large intestine, while cells further away from the crypt base are destined to be lost.

In **Chapter 4** we investigate how Wnt ligands influence tumor initiation by controlling the number of intestinal stem cells. We show that when Wnt secretion is reduced using a Porcupine inhibitor, stem cells located further away from the crypt base are lost, resulting in a smaller pool of competing stem cells. When APC is deleted in this scenario, APC mutated stem cells can take over the crypt more rapidly, leading to accelerated tumorigenesis.

In **Chapter 5** we study the effects of enlarging the stem cell pool by a calorie restricted diet. We demonstrate that a larger stem cell pool induced by this diet results in a lower retention of mutated cells, since there are more wild-type stem cell competitors that can outcompete mutated cells.

In **Chapter 6** we uncover the previously unobserved phenomenon of crypt fusion. We show that in addition to crypt duplication through crypt fission, two crypts can fuse together to form one daughter crypt. We propose that crypt fission and crypt fusion can function as counterbalancing processes.

In **Chapter 7** I summarize the results described in this thesis, discuss the findings in the light of the current literature, and propose future research directions.



Chapter I

Capturing Stem Cell Behavior Using Intravital and Live Cell Microscopy

Fumagalli A, Bruens L*, Scheele C and van Rheenen J*

Adapted from Cold Spring Harbor Perspectives in Biology pii: a035949 (2019)

* Equal contribution

ABSTRACT

Stem cells maintain tissue homeostasis by driving cellular turnover and regeneration upon damage. They reside within specialized niches that provide the signals required for stem cell maintenance. Stem cells have been identified in many tissues and cancer types, but their behavior within the niche and their reaction to microenvironmental signals were inferred from limited static observations. Recent advances in live imaging techniques, such as live cell imaging and intravital microscopy, have allowed the visualization of stem cell behavior and dynamics over time in their (near) native environment. Through these recent technological advances, it is now evident that stem cells are much more dynamic than previously anticipated, resulting in a model in which stemness is a state that can be gained or lost over time. In this review, we will highlight how live imaging and intravital microscopy have unraveled previously unanticipated stem cell dynamics and plasticity during development, homeostasis, regeneration, and tumor formation.

INTRODUCTION

Decades ago, clonogenic assays suggested that adult tissues are composed of heterogeneous cells that are hierarchically organized. Long-lived and self-renewing adult stem cells (SCs) are at the top of the hierarchy, whereas short-lived progenitors and differentiated cells with limited clonogenic capacity are at the bottom. Over the years, various techniques confirmed the existence of SC populations that maintain the dynamic equilibrium of tissue homeostasis in adult organs. In this review, we will highlight recent advances in the SC field, focusing on the new insights provided by live cell imaging and intravital microscopy (IVM). First, we will briefly describe the history of techniques used to study SCs and the advantages that live cell imaging brings to the field. Next, we will highlight how live imaging has revealed previously unanticipated dynamics and plasticity of SCs during development, homeostasis, and regeneration. Last, we will touch on the role of SCs in tumor initiation and progression.

REVEALING THE PRESENCE OF SCs – A PLETHORA OF TECHNIQUES

For a long time, clonogenic assays were used as the gold standard to identify adult SC populations *in vitro*^{1,2}. Similarly, transplantation studies enabled the first identification of adult SCs *in vivo*^{3,4}. These methods proved the capacity of specific subpopulations of cells, that is the SCs, to give rise to progeny (form cell colonies *in vitro*) or repopulate organs (*in vivo*). Although powerful, these methods were based on repopulation of ablated or damaged niches, or introduction of cells in ectopic environments. These non-physiologic contexts might affect and alter the behavior of the transplanted cells, triggering regeneration-like responses, rather than recapitulating homeostatic cell turnover.

The advent of lineage tracing contributed to resolve tissue hierarchy in an unperturbed tissue or tumor. Lineage tracing is the identification of all the progeny of a single cell by a heritable mark such as (multi) color fluorescent reporters, Brainbow⁵, or Confetti^{6,7}. When crossed with a line expressing an inducible Cre-recombinase under a promoter of choice (e.g., tissue or cell-type-specific promoters), expression of the reporter construct can be precisely induced through the activation of the Cre-recombinase by Tamoxifen injection. In contrast to transplantation-based or *in vitro* approaches, static lineage tracing provides quantitative information on the number, localization, and differentiation status of the progeny of a mother cell in its intact and native *in vivo* environment at a specific chosen time. Nevertheless, most lineage-tracing approaches rely on static images that fail to describe the full dynamics of a complex tissue.

The implementation of fluorescent probes together with high-resolution microscopy technologies (such as confocal, multiphoton, and light-sheet microscopy) opened a whole world of opportunities to study real time (stem) cell dynamics in living organisms (**Figure 1a**). Live cell imaging and IVM are unique compared with any other technique because they allow tracking of the same cells over time, thereby collecting coupled spatial and temporal information. For this reason, these techniques have made a strong contribution to the SC field, revealing SC dynamics in development, homeostasis, as well as in regeneration and cancer. Over the years, live cell imaging has been widely applied to *in vitro* 2D culture systems to study SC maintenance and differentiation. However, cell lines cultured in 2D fail to recapitulate the complexity of cell–cell interactions within living tissues. During the last decade, *in vitro* 3D cultured organoids allowed for the application of live cell imaging in more organotypic settings⁸. Organoids represent miniature reconstructions of epithelial tissues that can be propagated indefinitely *in*

in vitro, whereby the epithelial hierarchy of the tissue of origin is maintained (i.e., adult SCs generate all the tissue-specific differentiated cells)⁹. Although very useful to study cell–cell interactions over time, these 3D *in vitro* studies are largely lacking the context and natural niches in which the SCs reside.

The development of IVM marks a huge step forward in the need to visualize cells in their native environment. Most IVM studies make use of microscopes equipped with a multiphoton laser that generates long wavelengths (i.e., within the infrared spectrum) and ultra-short, high-energy laser pulses, which confine excitation (by simultaneous absorption of two photons) to the focal plane, creating optical sectioning while minimizing light scattering and allowing high-imaging quality up to 1 mm imaging depth^{10,11}. In addition, the usage of low energy wavelengths and excitation only at the focal plane reduces photobleaching and phototoxicity. Although the imaging quality of multiphoton excitation is not hampered as much as single-photon excitation at great imaging depth, the anatomical location of many different organs is too deep in the animal to obtain high-resolution images. To image these organs, tissues of interest can be surgically exposed; however, this does not allow imaging over multiple days (**Figure 1b**). To overcome this, different optical imaging windows have been developed; small devices equipped with a cover glass that can be surgically implanted onto the organ of interest to reach deeper tissues and to image for longer times. This approach allows visual access to the mammary gland, intestine, liver, pancreas, kidney, spleen, lungs, and brain, enabling visualization of the dynamic behavior of individual cells in their natural environment (**Figure 1c**;¹²⁻¹⁷).

FILMING ORGAN DEVELOPMENT AND THE ORIGIN OF SCs

Tissue-specific SCs and their niches are formed during organogenesis in the developing embryo. Starting from the multipotent blastula, cells proliferate and migrate while undergoing a sequence of developmental decisions that force them in more and more differentiated lineages. This ultimately results in the formation of adult SCs that sustain the tissue for the lifetime of the organism. Although static analysis can reveal different (stem) cell populations at different embryonic stages, live imaging enables linking these populations over time. An early example of this is the imaging of hematopoietic stem cell (HSC) generation from the aortic hemogenic endothelial cells. Although it had been postulated before, live imaging in zebrafish embryos showed that HSCs emerge from the aortic floor into the subaortic space through a process called endothelial hematopoietic transition. This live imaging allowed for direct visualization of the emergence of HSCs in the embryo that had not been possible through static analyses^{18,19}. The recently developed adaptive light-sheet technology now enables to even follow every single cell, and its fate in a developing postimplantation mouse embryo in real time²⁰. These emerging techniques have the power to reveal the role of SC dynamics and plasticity during organogenesis and adult SC formation.

An excellent example showing that cell dynamics play a crucial role in the formation of SC niches can be found in the fetal intestine, which consists of a continuous sheet of nonproliferative Lgr5⁻ villi and proliferative Lgr5⁺ intervillus regions. Adult crypts harboring the intestinal Lgr5⁺ SCs arise from these intervillus regions²¹. However, how these crypts form and multiply while the developing intestine elongates remained unknown. Only recently, live imaging of intestinal explants from E16.5 mouse embryos showed that fetal villi undergo gross remodeling and fission thereby increasing intestinal length (**Figure 2a**)²². These fission events bring the nonproliferative villus cells into the proliferative intervillus region where they are exposed to SCs-inducing factors and become a new intestinal SC pool. As a

result of this cellular plasticity, villus and intervillus cells have similar capacity to contribute to the growth of the intestinal epithelium during development, as shown by lineage-tracing experiments²². Thus, live imaging showed that adult intestinal SCs arise from equipotent precursors that get into the right niche through villus fission²².

Because adult SCs are dedicated to sustain tissue renewal for the entire lifetime of an organism, quality control mechanisms take place in the developing embryo to select and optimize tissue and organ development, including cell competition. This protective mechanism of cell competition, in which more fit “winner” cells actively sense and eliminate less fit “loser” cells was originally discovered in *Drosophila* (for review, see²³). Live embryo imaging, in combination with lineage tracing and single-cell transcriptomics, revealed two distinct modes of cell competition during skin development in mice (**Figure 2b**)²⁴. In the early single-layered epithelium, loser cells are actively killed and subsequently engulfed by neighboring winner progenitors. Later, when the tissue begins to stratify, loser cells are expelled from the proliferative basal layer from which later the epidermal SCs will arise through differentiation. Loser cells more often divide perpendicular to the basal layer than their winner counterparts, a mechanism that also has been shown to play a role in SC competition in the aging skin²⁵. Together, these mechanisms serve as quality control for the barrier function of the skin²⁴. Future live imaging studies will have to show how cell competition plays a role in the development of other mammalian organs.

Another developmental process during which cell dynamics is key, is branching morphogenesis. Branching morphogenesis leads to epithelial expansion generating extensively branched but compact organs, like the kidney, pancreas, lungs, and glands, including the salivary, mammary, and prostate glands (for review, see²⁶). An organ where branching morphogenesis can be followed by IVM is the

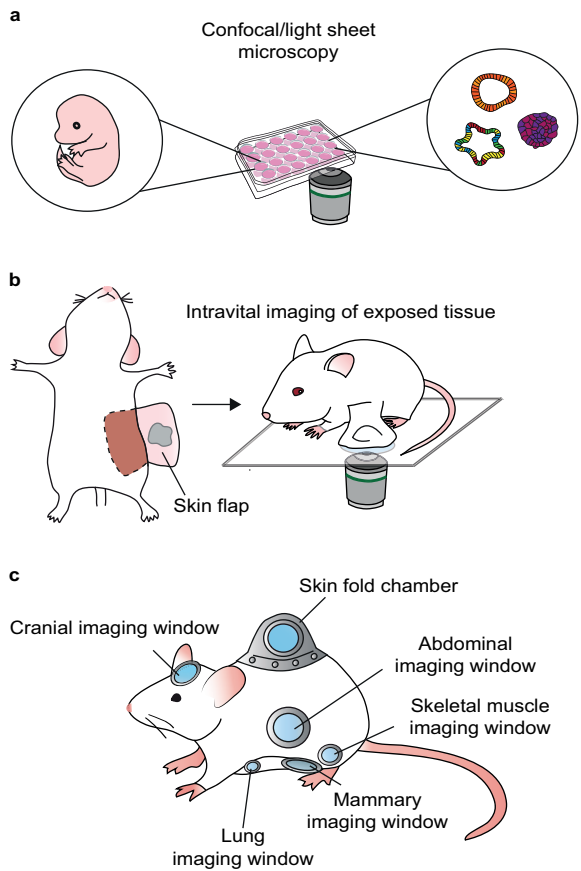


Figure 1. Overview of techniques for live cell imaging and intravital microscopy. *a.* Confocal and light-sheet technologies to visualize stem cell dynamics in 3D organoids and embryo explants enabling high-throughput and high-resolution time-lapse imaging. *b,c.* Intravital microscopy combined with multiphoton excitation allows in vivo stem cell imaging at great imaging depth at high resolution over time, either by surgically exposing the tissue for multiple hours (*b*) or by implantation of optical imaging windows for multiple days to weeks (*c*).

mammary gland as it occurs after birth. During embryonic development, a rudimentary tree is formed by multipotent progenitors that give rise to both basal and luminal cells^{27,28}. After birth, multipotent progenitors are rapidly replaced by lineage-restricted progenitors but these cells are quiescent until puberty. During puberty, the lineage-restricted developmental progenitors that drive branching morphogenesis are localized in the terminal end buds^{29,30}. IVM revealed that cells in the terminal end buds are the driving forces of ductal extension, whereas cells appeared to be static along the ducts (**Figure 2c**)²⁹. Cells in the terminal end buds were shown to continuously proliferate and intermix, resulting in an equipotent pool of developmental progenitors in the terminal end buds equally contributing to ductal growth. Because of the proliferation in the end bud, cells at the edge are left behind to elongate the duct while the end bud

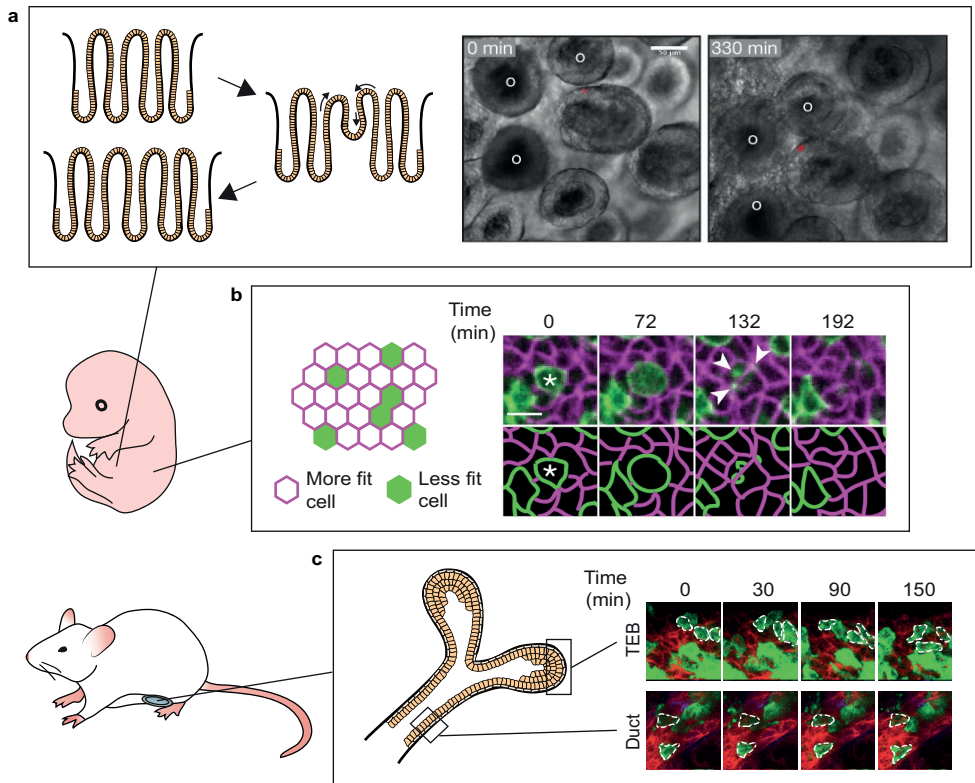


Figure 2. Intravital microscopy of organ development and the origin of stem cells. **a.** Live imaging of intestinal explants (E16.5) shows the dynamics of crypt formation through extensive remodeling and fission events. Fission event is indicated with the red star, white circles indicate villi. Scale bar, 50 μm. (Photos in panel A are reprinted from Guiu et al. 2019, with permission, from Springer Nature © 2019.) **b.** Live embryo imaging reveals that embryonic skin development is regulated by a process of cell competition. During early skin development, less fit cells (depicted in green) are actively eliminated and engulfed by neighboring more fit cells (depicted in magenta). Scale bar, 10 μm. (Photos in panel b are reprinted from Ellis et al. 2019, with permission, from Springer Nature © 2019.) **c.** Intravital microscopy of the developing mammary gland uncovers the terminal end bud (TEB) cells as the driving forces of ductal extension and bifurcation, in contrast to the ductal cells that stay static and nonproliferative. (Photos in panel c are reprinted from Scheele et al. 2017, with permission from the authors.)

is pushed further²⁹. From these dynamic insights, together with static analysis of the branching networks in the mammary gland, kidney, and human prostate, a simple parameter-free model for branching morphogenesis could be deduced. Branched organs self-organize into a network of ducts following three rules: (1) equipotent ductal tips proliferate and stochastically branch, (2) they randomly explore their environment, and (3) they become proliferatively inactive when they come into close proximity with neighboring ducts³¹.

IMAGING SC PLASTICITY DURING TISSUE HOMEOSTASIS

Over the past few years, lineage tracing and clonal analysis have enabled quantitative modeling of SC behavior in adult organs, resulting in precise models of SC behavior of the different SC compartments. However, these analyses relied on static views of very dynamic processes, urging for techniques that allow for dynamic measures of SC fate³². In this section, we will highlight how *in vivo* imaging exemplified the role of SC plasticity in space and time under homeostatic conditions.

In the skin, lineage-tracing studies have led to a detailed model of tissue turnover, with distinct unipotent SC populations driving the homeostatic turnover in their specific compartment³³⁻³⁹. However, this dogma of static SC compartments has been challenged by several studies. IVM of individual SCs over multiple generations revealed that each hair follicle SC has an equal potential to differentiate or divide⁴⁰. More recently, it was shown in mouse ear and paw skin that SC fate decisions (division or differentiation) are a direct consequence of neighboring cell behavior⁴¹. Differentiation of an SC and the subsequent transit into the upward layers of the skin, thereby leaving the niche partially vacant, is the trigger for neighboring SCs to divide symmetrically⁴¹. These two *in vivo* imaging studies clearly show that SC fate (symmetric or asymmetric division) is not a hard-wired intrinsic feature, but a flexible trait defined by the environment of an SC. Similarly, in the mouse hair follicle, *in vivo* imaging revealed that hair follicle SC fate is dictated by its location in the hair follicle niche⁴². During the hair growth cycle (anagen), *in vivo* imaging with high spatial and temporal resolution uncovered what dynamic cellular processes take place, including long-range migration and major reorganization of epithelial SC progeny, that could not have been observed in static analyses⁴³. By tracking the same SC and their progeny over multiple days, it was shown that hair follicle SC location changes during the hair follicle growth cycle⁴⁴. As each hair follicle SC moves along its niche, it produces distinct differentiated cell types based on its location, indicating that hair follicle SCs have a flexible fate and differentiation potential determined by the direct environment (**Figure 3a**)⁴⁴. Upon hair follicle regression, the same SCs can act as phagocytes to clear the dying neighboring cells and this mechanism was shown to be essential to maintain tissue homeostasis and prevent overgrowth after hair follicle regression⁴⁵. In conclusion, these studies show a previously unanticipated plasticity of SC commitment in the homeostatic hair follicle and interfollicular epidermis of the skin, enabling them to respond to changing conditions in the tissue.

Such plasticity of cellular identity has also been observed in the testis during spermatogenesis. Sperm SCs mainly undergo incomplete divisions generating syncytia of undifferentiated spermatogonia. Classically, spermatogonia are subclassified into differentiated and undifferentiated subpopulations, based on relative expression levels of GFR α 1 (SC marker) and receptor tyrosine kinase KIT (differentiation marker). Based on fixed samples, it was thought that SC activity was limited to the undifferentiated spermatogonia (mainly expressing GFR α 1), whereas more differentiated spermatogonia (mainly expressing Kit) irreversibly lost SC potential⁴⁶. However, *in vivo* time-lapse imaging unraveled that these

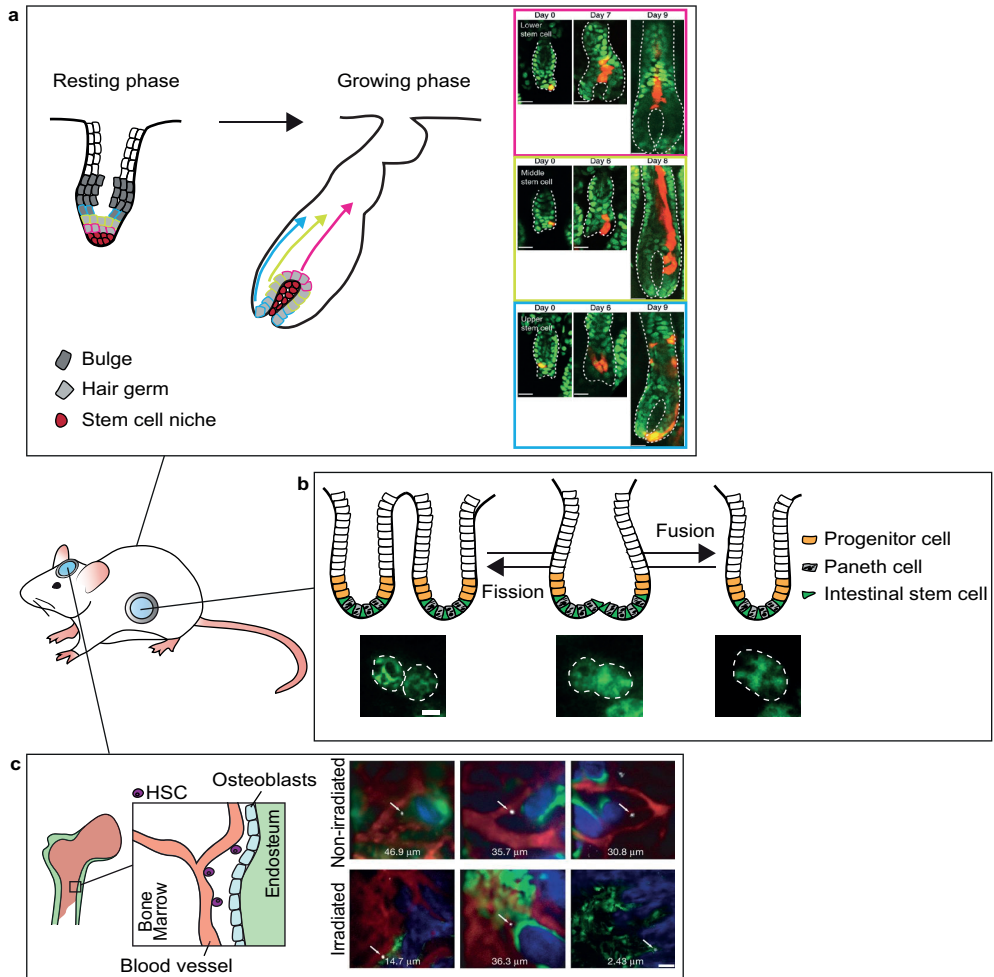


Figure 3. In vivo imaging of stem cell plasticity during tissue homeostasis. a. Intravital microscopy of the hair follicle stem cells reveals a previously unanticipated plasticity of the stem cells dictated by their positioning in the stem cell niche. Clones of progeny arising from a single stem cell are depicted in red. Scale bar, 20 μm. (Photos in panel **a** are reprinted from Xin et al. 2018, with permission, from Nature Publishing Group © 2018.) **b.** Intravital microscopy of whole crypt dynamics reveals the presence of crypt fusion, as a counteracting mechanism for crypt fission. Scale bar, 20 μm. (Photos in panel **b** are reprinted from Bruens et al. 2017 courtesy of the Creative Commons CC BY-NC-ND 4.0 License.) **c.** Intravital microscopy of the hematopoietic stem cells and its niche is dynamically regulated depending on the environmental cues (upper panel: normal conditions, lower panel: irradiation). Bone collagen is depicted in blue (second harmonics generation), osteoblasts in green, and vascularization in red. Scale bar, 50 μm. (Photos in panel **c** are reprinted from Lo Celso et al. 2009, with permission from the authors.)

syncytia are not irreversibly committed, and can undergo fragmentation and subsequently cells can regain stemness (measured by reexpression of the GFR α 1 SC marker)⁴⁷. Although cellular plasticity is rare in homeostatic spermatogenesis, it increases when the tissue is damaged upon administration of busulfan, a drug toxic to spermatogonia including SCs, leading to regeneration^{47,48}. In conclusion, these *in vivo* imaging studies point toward a revised model of sperm SC dynamics, in which stemness is more flexible than previously anticipated.

In the intestine, an epithelial system with high-cellular turnover driven by SCs at the bottom of the crypt, live imaging has also greatly contributed to our understanding of the SC niche dynamics and plasticity. In contrast to the skin, only a single SC compartment is fueling tissue renewal. Lineage-tracing studies have been crucial to determine the SC identity and dynamics in the intestine. After the identification of the specific SC marker Lgr5 in the intestine, lineage-tracing studies revealed that these Lgr5+ cells at the base of the intestinal crypts generate all the differentiated cell types of the intestine along the crypt villus axis⁴⁹. Further modeling of the clonal dynamics showed that the intestinal SCs in each crypt are equipotent, and by undergoing symmetric cell divisions they neutrally compete for niche space^{6,50}. Through this neutral competition, SC clones can be lost over time eventually leading to monoclonal crypts. Although the static lineage-tracing measurements revealed the long-term potential of the intestinal SCs, the short-term crypt dynamics were not resolved. To this end, multiday IVM was used to investigate the dynamic competition between different SCs within their niche. Strikingly, *in vivo* imaging revealed that positioning in the niche space is an important determinant of SCs to win the competition, and that this potential is reversible. Monitoring fluorescently labeled SCs (expressing the recombined Confetti construct) in the same crypts over multiple days revealed that “central” Lgr5+ SCs (i.e., residing at bottom of the crypt base) are likely to stay within the niche and give rise to progeny that will colonize the entire crypt and villus. In contrast, Lgr5+ SCs residing in the upper part of the crypt base (called “border cells”) are more susceptible to be displaced into the above transient-amplifying compartment⁵¹. Moreover, IVM showed that SCs can change position within the niche over time, so that cells at a favorable position in the niche center can lose their potential when entering the border of the crypt, and vice versa⁵¹. In addition, manipulation of the SC niche by, for example, reducing Wnt secretion (e.g., with administration of the porcupine inhibitor LGK974) down-regulates the expression of Lgr5 in the crypt base. Thereby, the number of SCs decreases leading to less competitors resulting in faster competition⁵².

Live cell imaging of intestinal organoids was used to further elucidate cell dynamics and fate decisions in the intestine. Time-lapse phase contrast imaging combined with fluorescent lineage tracing confirmed that small intestinal organoids contain crypt-like buds harboring functional Lgr5+ SCs resembling the *in vivo* intestine⁸. Lgr5+ SCs give rise to a wide range of specialized cell types that intermix into one intestinal epithelial lining, thus creating a mosaic pattern of cell types. Time-lapse imaging of organoids revealed that postmitotic positioning predicts long-term placement along the crypt axis and subsequent differentiation potential of the daughter cells⁵³. This positioning occurs during cytokinesis on the apical surface of the epithelium (toward the lumen) in an actin-dependent manner⁵⁴. During this process, neighboring cells can intrude within the cytokinetic furrow as a consequence of the elongated cell shape. Thus, neighboring cells can position themselves in between the daughter cells. Interference with cell shape abrogated cell intermixing, indicating that cell shape differences and apicobasal positioning are essential determinants of correct spatial organization of the intestinal epithelium⁵⁴.

Another crucial factor determining tissue patterning is symmetry breaking, the process in which a pool of identical cells change their differentiation potential with respect to neighboring cells creating asymmetric tissue structures, such as the intestinal SC niche and crypt–villus axis. Large-scale quantitative light-sheet imaging of intestinal organoid development, combined with single-cell genomics, identified heterogeneity in YAP1 expression between identical cells as the driver of symmetry breaking in intestinal spheres⁵⁵. Cell-to-cell variability in YAP1 activation promotes lateral inhibition through Notch and DLL1, which in turn leads to the emergence of the first Paneth cell and subsequent organoid asymmetry and crypt-like bud formation⁵⁵. Together, these intravital and live imaging studies start to reveal the intricate and dynamic interplay between SCs and its niche, and show that previously unnoticed features such as cell shape, cell-to-cell variability, and relative cell position are crucial determinants of SC potential.

Cell dynamics in the intestine are further complicated by dynamics involving whole crypts. In the epithelium, crypts can be found in a bifurcating shape, which has been interpreted as crypts undergoing a fission event, during which one crypt splits into two. However, a recent IVM study revealed the presence of a counteracting mechanism called crypt fusion during which two independent crypts fuse into one (**Figure 3b**)⁵⁶. Although producing opposite outcomes, crypt fission and fusion appear as morphologically identical in static images, highlighting the importance of *in vivo* imaging in studying dynamic processes. High-resolution live imaging in intestinal organoids was used to follow the cellular dynamics of crypt fission. This imaging showed that upon the initiation of fission, the more rigid Paneth cells form two clusters at either side of the crypt flanking a more flexible Lgr5+ SC cluster. Subsequently, an invagination is formed at this Lgr5+ site, which splits the crypt into two in a zipper-like fashion⁵⁷. Together, these observations point toward a model in which the distribution and proportion of stiff cells determines the likelihood of *in vivo* tissue deformation events such as crypt fission⁵⁸. In conclusion, these studies emphasize the dynamic nature of SC potential and fate, and illustrate the power of live cell and IVM approaches to unravel new mechanisms of tissue organization and SC dynamics, otherwise indistinguishable when inspecting fixed tissue sections.

FOLLOWING SCs DURING REGENERATIVE PROCESSES

In many tissues, regenerative potential relies on the presence of SCs that respond to cues from the damaged niche by producing new cells repairing the damage. This response is highly dynamic as it relies on cell–cell interactions, microenvironmental changes, cell migration, and proliferation. Therefore, tissue regeneration is another example in which live cell imaging approaches can add important insights that cannot be captured using static models.

The bone marrow harboring the HSCs represents a highly dynamic SC niche that rapidly responds to various stress-inducing signals. Although the location of the HSC niche had been previously identified by immunohistochemistry, it still remained unknown how this niche was established. Live imaging experiments of the mouse calvarium revealed that HSCs injected in nonirradiated mice reside close to the vasculature but further away from the endosteum (**Figure 3c**)⁵⁹. However, when the HSCs were injected in an irradiated setting or in a niche with impaired endogenous HSCs (carrying a c-Kit mutation) they localized more closely to endosteum. This position within the niche correlated with the differentiation state; long-term and proliferative HSCs localized closest to the endosteum and osteoblasts, whereas more mature subsets resided progressively further away⁵⁹. Upon stress, however (such as acute infection), quiescent HSCs become motile and interact with wider osteoblastic regions, indicating that

the location and behavior of the HSCs dynamically respond to the environmental cues⁶⁰.

In the skeletal muscle, the SCs - called satellite cells - are reactivated upon damage and proliferate and differentiate to replace damaged muscle fibers. Although this is a relatively simple repair mechanism, only recently the dynamics of the response within the SC niche and the necessary cues have been studied by IVM. Under homeostasis, the satellite cells were found to be nondividing and immobile. However, upon injury remnants of the extracellular matrix of damaged fibers, called ghost fibers, guide satellite cells to proliferate and migrate along them. This results in the spreading of progenitors, which then form nascent myofibers replacing the damaged fibers. These findings show that the regeneration

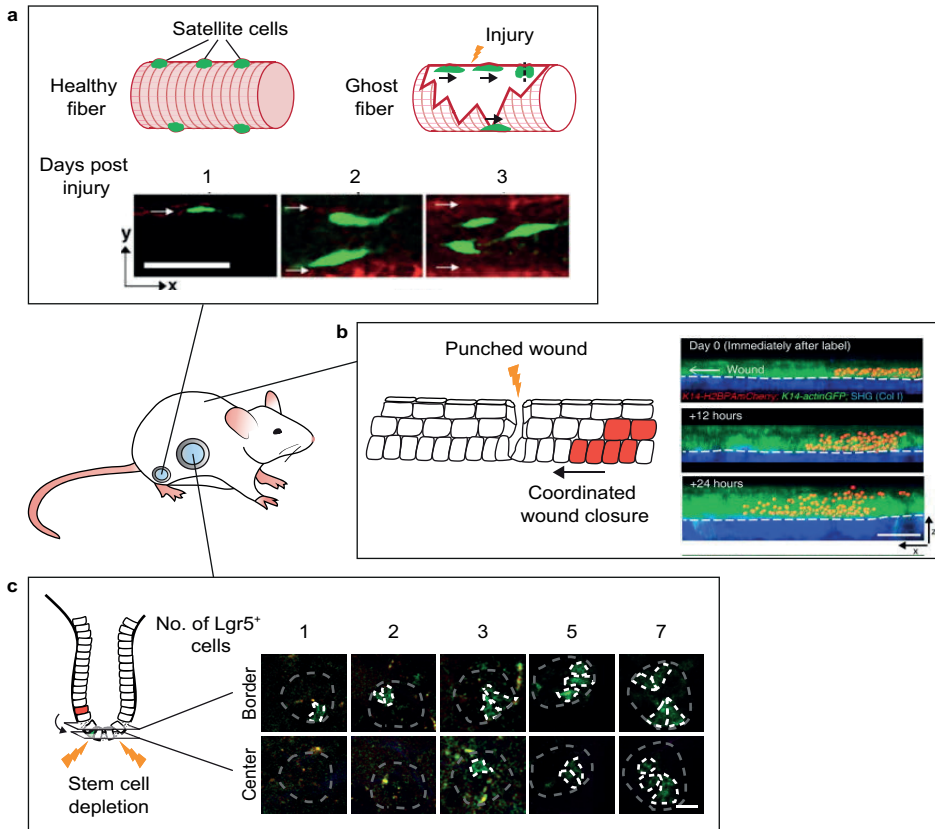


Figure 4. Following stem cells during regenerative processes by intravital microscopy. **a**. Intravital microscopy reveals the dynamics of satellite cell-mediated repair of injured muscle fibers. Remnants of damaged fibers form ghost fibers, which are used by satellite cells as guides for proliferation and migration. Scale bar, 50 μ m. (Photos in panel **a** are reprinted from Webster et al. 2016, with permission, from Elsevier © 2016.) **b**. Imaging of the cell dynamics during wound healing in the skin reveals the migratory and proliferative dynamics of the cells repairing the wound (migratory and proliferative cells are shown in red). Scale bar, 50 μ m. (Photos in panel **b** are reprinted from Park et al. 2017, with permission, from Springer Nature © 2017.) **c**. Multiday intravital microscopy shows the highly plastic nature of the intestinal cells. After ablation of all the stem cells, transit-amplifying cells fall back into the stem cell niche, adopt a stem cell fate, and repopulate the stem cell zone. Repopulating transit-amplifying cells are depicted in green. Scale bar, 20 μ m. (Photos in panel **c** are adapted from Ritsma et al. 2014, with permission from the authors.)

response in the skeletal muscle is not solely an SC intrinsic reaction but that the wound itself, in this case the ghost fibers, orchestrate the repair (**Figure 4a**)⁶¹.

In contrast to skeletal muscle, the skin is easily accessible for IVM. Laser ablation of SCs during the hair growth cycle (anagen) combined with multiday IVM showed that the position of a hair follicle SC is predictive for its differentiation potential into an uncommitted, committed, or differentiated cell type⁴². When hair follicle SCs are ablated, more differentiated epithelial cells can repopulate the SC compartment and sustain hair growth⁴². In addition, *in vivo* timelapse imaging has been used to study the cellular dynamics during the repair of a punch wound. During wound repair, directed division, differentiation, and migration are balanced to effectively repair the wound while maintaining tissue homeostasis⁶². Static analysis has shown that two zones appear after wounding: a migratory front that surrounds the wound edge surrounded by a ring of rapidly proliferation cells⁶³⁻⁶⁵. However, IVM revealed that these zones spatially overlap, with some cells performing both behaviors simultaneously (**Figure 4b**)⁶². These zones do not only serve as a source for new cells for wound closure, they also restrict the area of unwounded epithelium that is used for re-epithelialization⁶². Together, this shows how homeostatic mechanisms can be repurposed and integrated with wound-specific behaviors to restore homeostasis after damage.

As in many other tissues, stemness in the intestine has been shown to be highly plastic. When Lgr5+ SCs are ablated, cells from higher up in the crypt can fall back into the SC niche where they dedifferentiate and reexpress the SC marker Lgr5⁶⁶. Multiday IVM revealed that on ablation of all SCs, repopulation is a sporadic event. Individual cells transfer from the transit-amplifying zone into the SC niche border where they clonally expand and refill the SC niche (**Figure 4c**)⁵¹. When only one Lgr5+ SC is ablated, preexisting SCs rearrange to restore the alternation in pattern between Paneth and SCs within 2 hours and without cell division. Simultaneously, the damaged cell is forced out of the crypt by peristalsis-like motion of the crypt lumen⁶⁷. Thus, the intestinal crypt is highly dynamic and plastic, and the location within it defines stemness.

IMAGING OF SCs DURING TUMOR INITIATION AND PROGRESSION

Mechanisms used to maintain tissue homeostasis and regeneration, such as cell competition and cellular plasticity, are hijacked by cancer cells in the attempt to survive and infiltrate healthy tissues⁶⁸⁻⁷⁰. IVM experiments have unraveled differences and similarities between healthy tissues and cancers, and provided unexpected findings to increase understanding of cancer initiation, tumor maintenance, and spreading, and possibly contribute to fine tune treatment strategies.

Tumor Initiation

The human body has developed robust mechanisms to resist tumor growth and most of the time healthy tissues succeed in outcompeting mutant cells and reestablishing homeostasis. Both in intestine and in skin, it has been shown that tissue architecture and cellular turnover present protective mechanisms to oncogene-induced abnormalities. In the hair follicle, normal tissue dynamics lead to upward movement of the healthy hair follicle progenitor cells, resulting in relocation and subsequent differentiation of the mutant progenitor cells⁴⁴. Similarly, clonal analysis and *in vivo* imaging of cell fate choices in epidermal SCs harboring oncogenic Pik3ca mutations showed that oncogene-induced differentiation restricts clonal expansion of mutant cells, and eventually leads to the loss of oncogenic

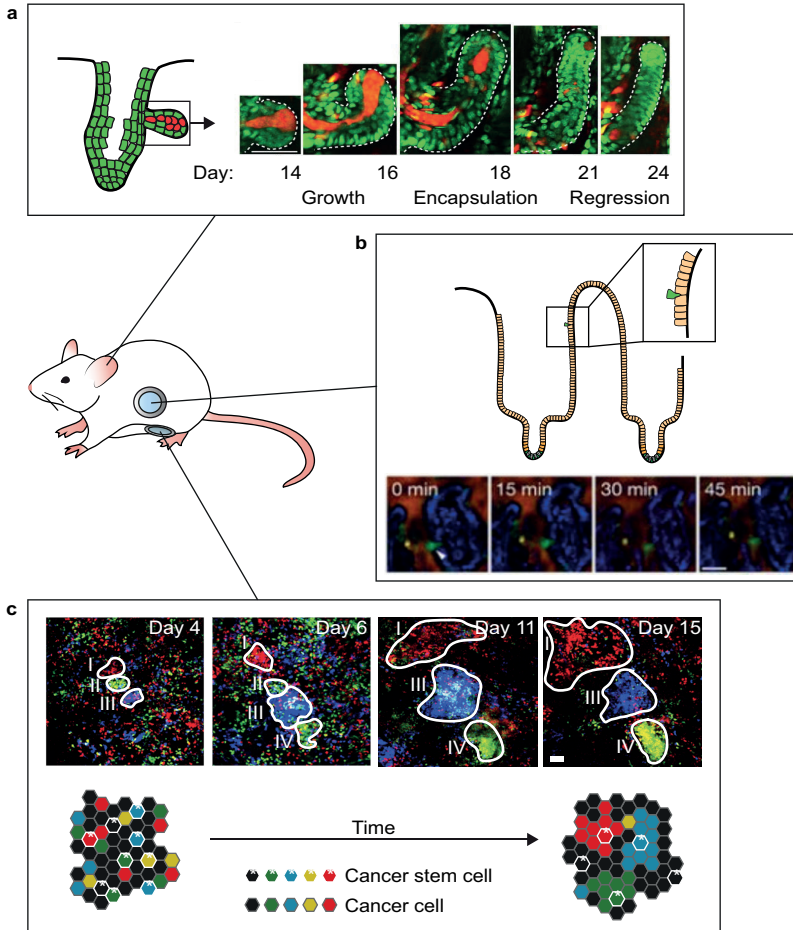


Figure 5. Imaging of stem cells during tumor initiation and progression. **a.** Repeated intravital imaging of a hair follicle harboring an oncogenic β -catenin mutation shows ectopic hair follicle outgrowth. Counteracting mechanisms result in encapsulation of the mutant cells, thereby actively eliminating them from the tissue. Mutant cells are depicted in red, wild-type cells are depicted in green. (Photos in panel **a** are reprinted from Brown et al. 2017, with permission, from Springer Nature © 2017.) **b.** Time-lapse intravital microscopy in the intestine shows that transformed cells (RasV12 mutant cells depicted in green) are actively expelled from the healthy intestinal epithelium. (Photos in panel **b** are reprinted from Kon et al. 2017, with permission, from Springer Nature © 2017.) **c.** Multiday intravital microscopy of labeled tumor cells in a growing mammary carcinoma shows different growth patterns. Only a small population of the tumor cells (cancer stem cells) drives the outgrowth of clones. Analysis of the clonal growth patterns reveals that cancer stem cell properties are plastic, and can be lost and gained over time. Scale bars, 50 μ m. (Photos in panel **c** are reprinted from Zomer et al. 2013, with permission from John Wiley & Sons © 2013.)

epithelial cells⁷¹. In addition, the skin has been shown to exploit regeneration processes that actively exclude potentially harmful cancer cells. Cre-induced activation of oncogenic β -catenin in the hair follicle SCs of a genetic mouse model produces benign deformations (i.e., new axes of hair growth), which expand in a way reminiscent of early-stage embryonic hair follicle formation. IVM showed that wild-type

(WT) cells are recruited to these new hair follicle branches and that Wnt signaling is activated in WT cells on the expression of Wnt ligands by neighboring mutant β -catenin cells, influencing the behavior of the WT⁷². Nevertheless, healthy tissue is able to counteract this ectopic growth by encapsulating the mutant cells (β -catenin or Hras) and actively eliminate them from the tissue (**Figure 5a**)⁷³. Together, these *in vivo* studies present a strong case for tissue autonomous mechanisms, such as tissue architecture and cell dynamics, that actively protect against the fixation of oncogenic mutations.

The removal of aberrant cells from the epithelium has also been shown to occur in the intestine. As in the skin, differentiated cells are thought to be incapable of inducing tumor formation because normal tissue dynamics push them upward to the tip of the villus where they undergo apoptosis giving them no time to form aberrant clones⁷⁴. In addition, neutral competition in the intestinal SC niche may be a protective mechanism against the acquisition of mutations, and subsequent tumor initiation⁷⁵. Several studies have investigated the effect of specific mutations on the SC competition in the niche^{76,77}. Indeed, introduction of sporadic mutations, such as Apc loss, Kras activation, or p53 mutations in the SC compartment, leads to a bias in the competition between WT and mutant SCs. As a result, the mutant clones have a slightly increased chance to expand and colonize a crypt^{76,77}. Nevertheless, because the number of WT SCs exceeds the number of mutant SCs, many mutated SCs are still replaced by the progeny of WT SCs, confirming the hypothesis that intestinal tissue architecture protects against mutation accumulation. This notion was further confirmed by a recent IVM study using a porcupine inhibitor to reduce the Wnt secretion, resulting in a reduction of the number of Lgr5+ SCs. Lineage tracing in an Apc-deficient background showed that the fixation speed of Apc-deficient SCs was increased, leading to accelerated adenoma formation⁵². Together these studies show that clonal drift and SC competition are protective against mutation fixation in the SC compartment.

In addition to SC competition in the crypt, it has been shown that cell competition – discussed in the section “Filming Organ Development and the Origin of SCs” – plays a role in eliminating transformed cells from the villus epithelium. Time-lapse IVM in the intestine showed that normal epithelial cells can recognize RasV12 transformed cells resulting in active elimination of the transformed cells (**Figure 5b**)⁷⁸. Upon contact with neighboring normal cells, the actin-binding protein epithelial protein lost in neoplasm (EPLIN) accumulates in transformed cells during a process called EDAC (epithelial defense against cancer^{78,79}). EDAC induces Warburg-effect-like metabolic changes in the transformed cells via up-regulation of pyruvate dehydrogenase kinase 4 (PDK4), leading to enhanced aerobic glycolysis and down-regulation of mitochondrial function. This PDK-mediated mitochondrial dysfunction results in apical extrusion of RasV12-transformed cells from the intestinal epithelium⁷⁸.

Even though many transformed cells are eliminated and do not have the chance to initiate tumorigenesis, some transformed cells escape these control mechanisms and give rise to cancer. When cancer progresses, the healthy tissue inevitably succumbs and loses cell–cell competition within the niche. IVM of leukemic cell colonization in the bone marrow revealed that unlike healthy HSCs, these cells are highly motile, migrate irrespective of any bone marrow subcompartment, and do not remain cohesive after cell division⁸⁰. Infiltrating leukemic cells force remodeling of the bone marrow and actively induce loss of osteoblastic SCs^{80,81}. Thus, due to the lack of a supporting niche, the fitness of resident healthy HSCs may be dramatically reduced, possibly leading to a progressive loss of normal hematopoiesis⁸¹. Together, these studies highlight the importance of the interaction between the SCs and their niche during cancer initiation and progression.

Tumor Maintenance by Cancer Stem Cells

Although SCs are believed to be the tumor-initiating cells in most tissues, it still remains unclear whether SCs are driving tumor progression and metastasis. At premalignant stages, lineage tracing studies have shown that tissue hierarchy is largely maintained; cells with stem-like properties drive clonal expansion leading to multiclonal tumors, supporting the cancer SC (CSC) hypothesis^{82,83}. According to the CSC theory, the majority of tumor cells within a tumor mass have limited proliferative potential and die after a few rounds of cell divisions, although a small proportion of tumor cells, the CSCs, can self-renew and sustain tumor (and metastasis) growth⁸⁴. In line with this hypothesis, a recent lineage-tracing study in human primary colon cancer xenografts showed evidence for a small subpopulation of CSCs, driving long-term tumor growth and progression⁸⁵. These CSC clones were predominantly found at the tumor edge in close proximity to osteopontin-producing cancer-associated fibroblasts⁸⁵. CSC behavior, however, changed over time depending on the location of the CSC within the tumor, indicating that functional CSC properties can be defined by microenvironmental factors⁸⁵.

What remains unclear from these static lineage-tracing studies is whether CSCs show a similar degree of plasticity compared with their healthy SC counterparts and how CSC plasticity contributes to tumor growth, progression, and resistance. To understand the role of plasticity in tumor maintenance, several live imaging studies have been conducted to follow CSC dynamics in their intact environment. For example, multicolor *in vivo* Confetti tracing of unperturbed mammary tumors (MMTV-PyMT tumor model) revealed that most cancer cells provide lineages that disappear over time and that only a minor population of cancer cells (i.e., CSCs) is able to generate large, long-lived single-colored Confetti clones during both adenoma and carcinoma stages (**Figure 5c**)⁸⁶. In addition, analysis of the clonal dynamics over time showed that cancer cells can form clones with delayed onset of growth or clones that suddenly undergo regression. This indicated that stem-like characteristics are highly dynamic and can be either acquired (upon plasticity) or lost (with differentiation) over time⁸⁶. Another study, in which human colorectal cancer organoids were followed by multiday confocal imaging, showed that non-CSCs (identified by the lack of expression of the fluorescent ASCL2-specific SC reporter STAR) were able to form organoids, and underwent cellular plasticity, gaining SC identity (visualized by reexpression of the STAR reporter) to further fuel organoid growth⁸⁷.

CSC plasticity not only plays a role in tumor growth, but also in the metastatic cascade. It has been extensively reported that cells that undergo epithelial-to-mesenchymal transition (EMT) may gain self-renewal potential (i.e., stemness), which enables them to efficiently fuel metastatic growth at distant sites⁸⁸. This view was recently challenged by static lineage-tracing experiments showing that metastases are not seeded by cells that have expressed specific mesenchymal markers (e.g., Fsp1)^{89,90}. However, it remains unknown whether all mesenchymal cells express the classical mesenchymal markers (such as N-cadherin, vimentin, fibronectin, and Fsp1), especially in light of recent findings revealing the existence of multiple EMT stages in skin and in mammary tumors, ranging from epithelial to completely mesenchymal states⁹¹. Cells can be in different hybrid EMT states leading to differences in cellular plasticity, invasiveness, and metastatic potential⁹¹. IVM of EMT and mesenchymal-to-epithelial-transition (MET) in mammary tumors using a fluorescent E-cadherin expression reporter showed that only a small population of cells undergoes EMT in an unperturbed system⁹². This small population of mesenchymal cells is motile and able to disseminate to a distant site, both in early- and late-stage tumors^{92,93}. However, at the distant site, mesenchymal cells switch back to an epithelial state already after a few cell divisions, rendering potential differences in self-renewal capacity between seeding epithelial and mesenchymal cells irrelevant⁹².

CSC identity and plasticity are also important in the context of treatment efficiency and treatment resistance. A recent study in basal cell carcinoma showed that these tumor cells can escape targeted therapy (smoothened inhibitor Vismodegib) by adopting a different cellular identity⁹⁴. Normally, basal cell carcinoma cells have an identity that closely resembles hair follicle bulge cells. However, on treatment with Vismodegib, a subset of basal cell carcinoma cells initiates a transcriptional program that resembles that of interfollicular and isthmus SCs⁹⁴. This involves transcriptional changes leading to a rapid Wnt activation, which renders these cells insensitive to the Smoothened inhibitor⁹⁴. Thus, cell identity switches may be a common way for tumor cells to escape drug-induced cell death.

To systematically understand cell identity switches as an escape mechanism in different tumor types and identify new potential drug combinations, more high-throughput methods are required. Now, with proper culture conditions, organoids can be efficiently generated from patient biopsies. The recent establishment of human tumor organoid libraries represents a breakthrough in cancer biology and expands the possibilities to look at tumor genetic heterogeneity⁹⁵⁻⁹⁷. Moreover, these patient-derived biobanks offer large platforms to test the response to old and new (combinations of) drugs. For example, a panel of human colorectal cancer organoids in combination with confocal live cell imaging was used to link appearance of chromosomal instability to specific colorectal cancer mutations, by looking at segregation errors over time in human colorectal cancer organoids carrying increasing mutational load^{98,99}. Similar approaches were used to monitor drug responses on a panel of KRAS-mutant versus KRAS-WT patient-derived colorectal cancer organoids and revealed that KRAS-mutant organoids are significantly less sensitive to EGFR inhibitors¹⁰⁰. Together with the development of new high-throughput screening platforms and microscopy, organoids systems will provide a powerful tool to understand cancer progression and mechanisms of cellular drug resistance¹⁰¹. Moreover, human tumor-derived organoids can be engineered with fluorescent markers, and subsequently be transplanted orthotopically into animals, providing a unique opportunity to track human CSC dynamics at a cellular resolution by IVM. The relevance of this unique combination of tools was recently shown by a study using engineered human colorectal cancer organoids to elucidate the contribution of defined mutations to metastasis formation¹⁰². The authors found that metastatic ability is directly caused by mutations that allow growth independent of certain niche signals, thereby identifying the cellular mechanisms of key drivers of progression in colorectal cancer¹⁰².

CONCLUDING REMARKS

The combination of *in vitro* live cell imaging, lineage tracing, and IVM has been essential to define the SC dynamics of healthy and tumorigenic tissues in the murine setting. Overall (*in vivo*), live cell imaging studies challenge the concept of fixed SCs populations with a determined and hardwired self-renewal capacity. It now appears that instead of a static one-way route, cellular hierarchy is much more plastic than previously thought, and stemness is a state that can be gained or lost, especially during regeneration responses and tumor growth.

Because most IVM data is based on imaging in animal models, the next challenge will be to understand whether these dynamics reflect the human situation. *In vitro*, the advent of organoid technology has allowed mapping cell dynamics of primary human cells in a 3D cellular organization, closely resembling the tissue of origin. However, these cultures are mostly limited to the epithelial component, and do not allow to study the interactions between cells and their microenvironment. Recent

efforts have succeeded in integrating some components of the microenvironment such as mesenchymal stroma¹⁰³⁻¹⁰⁶ and immune cells^{107,108} together with patient-derived organoids. To go one step further, orthotopic transplantation of human (tumor) organoids can be combined with *in vivo* live cell imaging techniques. For instance, healthy human colon organoids – derived from either iPS cells or adult tissues – can engraft and reconstruct the human colon epithelium in a mouse, allowing to study human tissue dynamics in an orthotopic environment using IVM^{106,109}. In addition, orthotopic transplantation of human tumor-derived organoids will open new avenues to study the dynamic processes occurring during tumor progression including the metastatic cascade. In conclusion, the combination of state-of-the-art live imaging techniques will have the unique potential to ultimately resolve the intricate dynamics of SCs and their niches.

ACKNOWLEDGEMENTS

We regret that owing to space limitations we could only describe a selection of papers and therefore have not been able to reference all literature relevant to the topic. The authors would like to thank members of the laboratory of JvR, for helpful discussions and their critical reading of the manuscript. JvR is supported by CancerGenomics.nl, a European Research Council Grant CANCER-RECURRENCE 648804, the Doctor Josef Steiner Foundation and the European Union's Horizon 2020 research and innovation program under the Marie Skłodowska-Curie grant agreement No 642866.

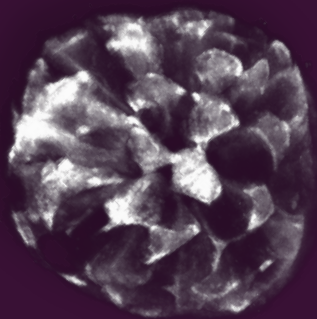
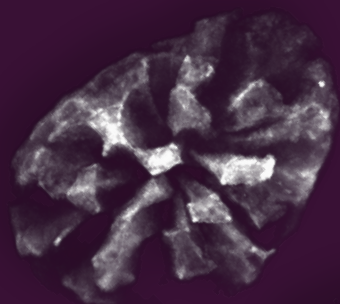
REFERENCES

1. Withers, H. R. & Elkind, M. M. Microcolony survival assay for cells of mouse intestinal mucosa exposed to radiation. *Int J Radiat Biol Relat Stud Phys Chem Med* **17**, 261-267 (1970).
2. Barrandon, Y. & Green, H. Three clonal types of keratinocyte with different capacities for multiplication. *Proc Natl Acad Sci U S A* **84**, 2302-2306 (1987).
3. Deome, K. B., Faulkin, L. J., Jr., Bern, H. A. & Blair, P. B. Development of mammary tumors from hyperplastic alveolar nodules transplanted into gland-free mammary fat pads of female C3H mice. *Cancer Res* **19**, 515-520 (1959).
4. Spangrude, G. J., Heimfeld, S. & Weissman, I. L. Purification and characterization of mouse hematopoietic stem cells. *Science* **241**, 58-62 (1988).
5. Livet, J. [The brain in color: transgenic "Brainbow" mice for visualizing neuronal circuits]. *Med Sci (Paris)* **23**, 1173-1176 (2007).
6. Snippert, H. J. *et al.* Intestinal crypt homeostasis results from neutral competition between symmetrically dividing Lgr5 stem cells. *Cell* **143**, 134-144 (2010).
7. Kretzschmar, K. & Watt, F. M. Lineage tracing. *Cell* **148**, 33-45 (2012).
8. Sato, T. *et al.* Single Lgr5 stem cells build crypt-villus structures in vitro without a mesenchymal niche. *Nature* **459**, 262-265 (2009).
9. Kretzschmar, K. & Clevers, H. Organoids: Modeling Development and the Stem Cell Niche in a Dish. *Dev Cell* **38**, 590-600 (2016).
10. Helmchen, F. & Denk, W. Deep tissue two-photon microscopy. *Nat Methods* **2**, 932-940 (2005).
11. Dunn, K. W. & Young, P. A. Principles of multiphoton microscopy. *Nephron Exp Nephrol* **103**, e33-40 (2006).
12. Huang, Q. *et al.* Noninvasive visualization of tumors in rodent dorsal skin window chambers. *Nat Biotechnol* **17**, 1033-1035 (1999).
13. Trachtenberg, J. T. *et al.* Long-term in vivo imaging of experience-dependent synaptic plasticity in adult cortex. *Nature* **420**, 788-794 (2002).
14. Kedrin, D. *et al.* Intravital imaging of metastatic behavior through a mammary imaging window. *Nat Methods* **5**, 1019-1021 (2008).
15. Ritsma, L. *et al.* Surgical implantation of an abdominal imaging window for intravital microscopy. *Nat Protoc* **8**, 583-594 (2013).
16. Alieva, M., Ritsma, L., Giedt, R. J., Weissleder, R. & van Rheenen, J. Imaging windows for long-term intravital imaging: General overview and technical insights. *Intravital* **3**, e29917 (2014).
17. Entenberg, D. *et al.* A permanent window for the murine lung enables high-resolution imaging of cancer metastasis. *Nat Methods* **15**, 73-80 (2018).
18. Boisset, J. C. & Robin, C. Imaging the founder of adult hematopoiesis in the mouse embryo aorta. *Cell Cycle* **9**, 2489-2490 (2010).
19. Kissa, K. & Herbomel, P. Blood stem cells emerge from aortic endothelium by a novel type of cell transition. *Nature* **464**, 112-115 (2010).
20. McDole, K. *et al.* In Toto Imaging and Reconstruction of Post-Implantation Mouse Development at the Single-Cell Level. *Cell* **175**, 859-876 e833 (2018).
21. Noah, T. K., Donahue, B. & Shroyer, N. F. Intestinal development and differentiation. *Exp Cell Res* **317**, 2702-2710 (2011).
22. Guiu, J. *et al.* Tracing the origin of adult intestinal stem cells. *Nature* **570**, 107-111 (2019).
23. Amoyel, M. & Bach, E. A. Cell competition: how to eliminate your neighbours. *Development* **141**, 988-1000 (2014).
24. Ellis, S. J. *et al.* Distinct modes of cell competition shape mammalian tissue morphogenesis. *Nature* **569**, 497-502 (2019).
25. Liu, N. *et al.* Stem cell competition orchestrates skin homeostasis and ageing. *Nature* **568**, 344-350 (2019).
26. Varner, V. D. & Nelson, C. M. Cellular and physical mechanisms of branching morphogenesis. *Development* **141**, 2750-2759 (2014).
27. Lilja, A. M. *et al.* Clonal analysis of Notch1-expressing cells reveals the existence of unipotent stem cells that retain long-term plasticity in the embryonic mammary gland. *Nat Cell Biol* **20**, 677-687 (2018).
28. Wuidart, A. *et al.* Early lineage segregation of multipotent embryonic mammary gland progenitors. *Nat Cell Biol* **20** (2018).
29. Scheele, C. L. *et al.* Identity and dynamics of mammary stem cells during branching morphogenesis. *Nature* **542**, 313-317 (2017).
30. Davis, F. M. *et al.* Single-cell lineage tracing in the mammary gland reveals stochastic clonal dispersion of stem/progenitor cell progeny. *Nat Commun* **7**, 13053 (2016).
31. Hannezo, E. *et al.* A Unifying Theory of Branching Morphogenesis. *Cell* **171**, 242-255 e227 (2017).
32. Krieger, T. & Simons, B. D. Dynamic stem cell heterogeneity. *Development* **142**, 1396-1406 (2015).
33. Jaks, V. *et al.* Lgr5 marks cycling, yet long-lived, hair follicle stem cells. *Nat Genet* **40**, 1291-1299 (2008).

34. Page, M. E., Lombard, P., Ng, F., Gottgens, B. & Jensen, K. B. The epidermis comprises autonomous compartments maintained by distinct stem cell populations. *Cell Stem Cell* **13**, 471-482 (2013).
35. Jensen, K. B. *et al.* Lrig1 expression defines a distinct multipotent stem cell population in mammalian epidermis. *Cell Stem Cell* **4**, 427-439 (2009).
36. Mascré, G. *et al.* Distinct contribution of stem and progenitor cells to epidermal maintenance. *Nature* **489**, 257-262 (2012).
37. Fullgrabe, A. *et al.* Dynamics of Lgr6(+) Progenitor Cells in the Hair Follicle, Sebaceous Gland, and Interfollicular Epidermis. *Stem Cell Reports* **5**, 843-855 (2015).
38. Snippert, H. J. *et al.* Lgr6 marks stem cells in the hair follicle that generate all cell lineages of the skin. *Science* **327**, 1385-1389 (2010).
39. Lim, X. *et al.* Interfollicular epidermal stem cells self-renew via autocrine Wnt signaling. *Science* **342**, 1226-1230 (2013).
40. Rompolas, P. *et al.* Spatiotemporal coordination of stem cell commitment during epidermal homeostasis. *Science* **352**, 1471-1474 (2016).
41. Mesa, K. R. *et al.* Homeostatic Epidermal Stem Cell Self-Renewal Is Driven by Local Differentiation. *Cell Stem Cell* **23**, 677-686 e674 (2018).
42. Rompolas, P., Mesa, K. R. & Greco, V. Spatial organization within a niche as a determinant of stem-cell fate. *Nature* **502**, 513-518 (2013).
43. Rompolas, P. *et al.* Live imaging of stem cell and progeny behaviour in physiological hair-follicle regeneration. *Nature* **487**, 496-499, doi:10.1038/nature11218 [pii] (2012).
44. Xin, T., Gonzalez, D., Rompolas, P. & Greco, V. Flexible fate determination ensures robust differentiation in the hair follicle. *Nat Cell Biol* **20**, 1361-1369 (2018).
45. Mesa, K. R. *et al.* Niche-induced cell death and epithelial phagocytosis regulate hair follicle stem cell pool. *Nature* **522**, 94-97 (2015).
46. Shinohara, T., Orwig, K. E., Avarbock, M. R. & Brinster, R. L. Spermatogonial stem cell enrichment by multiparameter selection of mouse testis cells. *Proc Natl Acad Sci U S A* **97**, 8346-8351 (2000).
47. Hara, K. *et al.* Mouse spermatogenic stem cells continually interconvert between equipotent singly isolated and syncytial states. *Cell Stem Cell* **14**, 658-672 (2014).
48. Nakagawa, T., Sharma, M., Nabeshima, Y., Braun, R. E. & Yoshida, S. Functional hierarchy and reversibility within the murine spermatogenic stem cell compartment. *Science* **328**, 62-67 (2010).
49. Barker, N. *et al.* Identification of stem cells in small intestine and colon by marker gene Lgr5. *Nature* **449**, 1003-1007 (2007).
50. Lopez-Garcia, C., Klein, A. M., Simons, B. D. & Winton, D. J. Intestinal stem cell replacement follows a pattern of neutral drift. *Science* **330**, 822-825 (2010).
51. Ritsma, L. *et al.* Intestinal crypt homeostasis revealed at single-stem-cell level by in vivo live imaging. *Nature* **507**, 362-365 (2014).
52. Huels, D. J. *et al.* Wnt ligands influence tumour initiation by controlling the number of intestinal stem cells. *Nat Commun* **9**, 1132 (2018).
53. Carroll, T. D. *et al.* Interkinetic nuclear migration and basal tethering facilitates post-mitotic daughter separation in intestinal organoids. *J Cell Sci* **130**, 3862-3877 (2017).
54. McKinley, K. L. *et al.* Cellular aspect ratio and cell division mechanics underlie the patterning of cell progeny in diverse mammalian epithelia. *Elife* **7** (2018).
55. Serra, D. *et al.* Self-organization and symmetry breaking in intestinal organoid development. *Nature* **569**, 66-72 (2019).
56. Bruens, L., Ellenbroek, S. I. J., van Rheeën, J. & Snippert, H. J. In Vivo Imaging Reveals Existence of Crypt Fission and Fusion in Adult Mouse Intestine. *Gastroenterology* **153**, 674-677 e673 (2017).
57. Langlands, A. J. *et al.* Paneth Cell-Rich Regions Separated by a Cluster of Lgr5+ Cells Initiate Crypt Fission in the Intestinal Stem Cell Niche. *PLoS Biol* **14**, e1002491 (2016).
58. Almet, A. A., Hughes, B. D., Landman, K. A., Nathke, I. S. & Osborne, J. M. A Multicellular Model of Intestinal Crypt Buckling and Fission. *Bull Math Biol* **80**, 335-359 (2018).
59. Lo Celso, C. *et al.* Live-animal tracking of individual haematopoietic stem/progenitor cells in their niche. *Nature* **457**, 92-96 (2009).
60. Rashidi, N. M. *et al.* In vivo time-lapse imaging shows diverse niche engagement by quiescent and naturally activated hematopoietic stem cells. *Blood* **124**, 79-83 (2014).
61. Webster, M. T., Manor, U., Lippincott-Schwartz, J. & Fan, C. M. Intravital Imaging Reveals Ghost Fibers as Architectural Units Guiding Myogenic Progenitors during Regeneration. *Cell Stem Cell* **18**, 243-252 (2016).
62. Park, S. *et al.* Tissue-scale coordination of cellular behaviour promotes epidermal wound repair in live mice. *Nat Cell Biol* **19**, 155-163 (2017).
63. Zhao, M., Song, B., Pu, J., Forrester, J. V. & McCaig, C. D. Direct visualization of a stratified epithelium reveals that wounds heal by unified sliding of cell sheets. *FASEB J* **17**, 397-406 (2003).
64. Usui, M. L. *et al.* Morphological evidence for the role of suprabasal keratinocytes in wound reepithelialization.

- Wound Repair Regen* **13**, 468-479 (2005).
65. Safferling, K. *et al.* Wound healing revised: a novel reepithelialization mechanism revealed by in vitro and in silico models. *J Cell Biol* **203**, 691-709 (2013).
 66. Bankaitis, E. D., Ha, A., Kuo, C. J. & Magness, S. T. Reserve Stem Cells in Intestinal Homeostasis and Injury. *Gastroenterology* **155**, 1348-1361 (2018).
 67. Choi, J. *et al.* Intestinal crypts recover rapidly from focal damage with coordinated motion of stem cells that is impaired by aging. *Sci Rep* **8**, 10989 (2018).
 68. Condeelis, J., Singer, R. H. & Segall, J. E. The great escape: when cancer cells hijack the genes for chemotaxis and motility. *Annu Rev Cell Dev Biol* **21**, 695-718 (2005).
 69. Ellenbroek, S. I. & van Rheenen, J. Imaging hallmarks of cancer in living mice. *Nat Rev Cancer* **14**, 406-418, (2014).
 70. Suijkerbuijk, S. J. E. & van Rheenen, J. From good to bad: Intravital imaging of the hijack of physiological processes by cancer cells. *Dev Biol* **428**, 328-337 (2017).
 71. Ying, Z., Sandoval, M. & Beronja, S. Oncogenic activation of PI3K induces progenitor cell differentiation to suppress epidermal growth. *Nat Cell Biol* **20**, 1256-1266 (2018).
 72. Deschene, E. R. *et al.* beta-Catenin activation regulates tissue growth non-cell autonomously in the hair stem cell niche. *Science* **343**, 1353-1356 (2014).
 73. Brown, S. *et al.* Correction of aberrant growth preserves tissue homeostasis. *Nature* **548**, 334-337 (2017).
 74. Barker, N. *et al.* Crypt stem cells as the cells-of-origin of intestinal cancer. *Nature* **457**, 608-611 (2009).
 75. van Rheenen, J. & Bruens, L. Cellular protection mechanisms that minimise accumulation of mutations in intestinal tissue. *Swiss Med Wkly* **147**, w14539 (2017).
 76. Snippert, H. J., Schepers, A. G., van Es, J. H., Simons, B. D. & Clevers, H. Biased competition between Lgr5 intestinal stem cells driven by oncogenic mutation induces clonal expansion. *EMBO Rep* **15**, 62-69 (2014).
 77. Vermeulen, L. *et al.* Defining stem cell dynamics in models of intestinal tumor initiation. *Science* **342**, 995-998 (2013).
 78. Kon, S. *et al.* Cell competition with normal epithelial cells promotes apical extrusion of transformed cells through metabolic changes. *Nat Cell Biol* **19**, 530-541 (2017).
 79. Ohoka, A. *et al.* EPLIN is a crucial regulator for extrusion of RasV12-transformed cells. *J Cell Sci* **128**, 781-789 (2015).
 80. Hawkins, E. D. *et al.* T-cell acute leukaemia exhibits dynamic interactions with bone marrow microenvironments. *Nature* **538**, 518-522 (2016).
 81. Duarte, D. *et al.* Inhibition of Endosteal Vascular Niche Remodeling Rescues Hematopoietic Stem Cell Loss in AML. *Cell Stem Cell* **22**, 64-77 e66 (2018).
 82. Schepers, A. G. *et al.* Lineage tracing reveals Lgr5+ stem cell activity in mouse intestinal adenomas. *Science* **337**, 730-735 (2012).
 83. Driessens, G., Beck, B., Caauwe, A., Simons, B. D. & Blanpain, C. Defining the mode of tumour growth by clonal analysis. *Nature* **488**, 527-530 (2012).
 84. Battle, E. & Clevers, H. Cancer stem cells revisited. *Nat Med* **23**, 1124-1134 (2017).
 85. Lenos, K. J. *et al.* Stem cell functionality is microenvironmentally defined during tumour expansion and therapy response in colon cancer. *Nat Cell Biol* **20**, 1193-1202 (2018).
 86. Zomer, A. *et al.* Intravital imaging of cancer stem cell plasticity in mammary tumors. *Stem Cells* **31**, 602-606 (2013).
 87. Oost, K. C. *et al.* Specific Labeling of Stem Cell Activity in Human Colorectal Organoids Using an ASCL2-Responsive Minigene. *Cell Rep* **22**, 1600-1614 (2018).
 88. Kalluri, R. & Weinberg, R. A. The basics of epithelial-mesenchymal transition. *J Clin Invest* **119**, 1420-1428 (2009).
 89. Zheng, X. *et al.* Epithelial-to-mesenchymal transition is dispensable for metastasis but induces chemoresistance in pancreatic cancer. *Nature* **527**, 525-530 (2015).
 90. Fischer, K. R. *et al.* Epithelial-to-mesenchymal transition is not required for lung metastasis but contributes to chemoresistance. *Nature* **527**, 472-476 (2015).
 91. Pastushenko, I. *et al.* Identification of the tumour transition states occurring during EMT. *Nature* **556**, 463-468 (2018).
 92. Beerling, E. *et al.* Plasticity between Epithelial and Mesenchymal States Unlinks EMT from Metastasis-Enhancing Stem Cell Capacity. *Cell Rep* **14**, 2281-2288 (2016).
 93. Harper, K. L. *et al.* Mechanism of early dissemination and metastasis in Her2(+) mammary cancer. *Nature* **540**, 588-592 (2016).
 94. Biehs, B. *et al.* A cell identity switch allows residual BCC to survive Hedgehog pathway inhibition. *Nature* **562**, 429-433 (2018).
 95. van de Wetering, M. *et al.* Prospective derivation of a living organoid biobank of colorectal cancer patients. *Cell* **161**, 933-945 (2015).
 96. Fujii, M. *et al.* A Colorectal Tumor Organoid Library Demonstrates Progressive Loss of Niche Factor

- Requirements during Tumorigenesis. *Cell Stem Cell* **18**, 827-838 (2016).
97. Seino, T. *et al.* Human Pancreatic Tumor Organoids Reveal Loss of Stem Cell Niche Factor Dependence during Disease Progression. *Cell Stem Cell* **22**, 454-467 e456 (2018).
 98. Drost, J. *et al.* Sequential cancer mutations in cultured human intestinal stem cells. *Nature* **521**, 43-47 (2015).
 99. Bolhaqueiro, A. C. F. *et al.* Live imaging of cell division in 3D stem-cell organoid cultures. *Methods Cell Biol* **145**, 91-106 (2018).
 100. Verissimo, C. S. *et al.* Targeting mutant RAS in patient-derived colorectal cancer organoids by combinatorial drug screening. *Elife* **5** (2016).
 101. Rios, A. C. & Clevers, H. Imaging organoids: a bright future ahead. *Nat Methods* **15**, 24-26 (2018).
 102. Fumagalli, A. *et al.* Genetic dissection of colorectal cancer progression by orthotopic transplantation of engineered cancer organoids. *Proc Natl Acad Sci U S A* **114**, E2357-E2364 (2017).
 103. Ootani, A. *et al.* Sustained in vitro intestinal epithelial culture within a Wnt-dependent stem cell niche. *Nat Med* **15**, 701-706 (2009).
 104. Spence, J. R. *et al.* Directed differentiation of human pluripotent stem cells into intestinal tissue in vitro. *Nature* **470**, 105-109 (2011).
 105. McCracken, K. W. *et al.* Modelling human development and disease in pluripotent stem-cell-derived gastric organoids. *Nature* **516**, 400-404 (2014).
 106. Munera, J. O. *et al.* Differentiation of Human Pluripotent Stem Cells into Colonic Organoids via Transient Activation of BMP Signaling. *Cell Stem Cell* **21**, 51-64 e56 (2017).
 107. Dijkstra, K. K. *et al.* Generation of Tumor-Reactive T Cells by Co-culture of Peripheral Blood Lymphocytes and Tumor Organoids. *Cell* **174**, 1586-1598 e1512 (2018).
 108. Neal, J. T. *et al.* Organoid Modeling of the Tumor Immune Microenvironment. *Cell* **175**, 1972-1988 e1916 (2018).
 109. Sugimoto, S. *et al.* Reconstruction of the Human Colon Epithelium In Vivo. *Cell Stem Cell* **22**, 171-176 e175 (2018).



Chapter 2

Cellular Dynamics that Minimize the Accumulation of Mutations in the Intestinal Epithelium

Bruens L and van Rheenen J

Adapted from Swiss Medical Weekly 147: w14539. (2017)

ABSTRACT

The epithelial lining of the intestine is constantly exposed to a hostile environment containing a mixture of gastric acids, consumed harmful substances, and microbes. It is widely accepted that the dynamic nature of the intestinal epithelium protects against tissue damage. Here, we review three mechanisms that protect intestinal tissue against accumulation of somatic mutations: the conveyor belt-like structure, stem cell competition and crypt fusion. We highlight the events that can perturb these mechanisms, and their impact on accumulation of oncogenic mutations. Lastly, we review the potential of *in vitro* and intravital microscopy techniques to study the dynamics of these protection processes. These studies may identify new targets that can be used to manipulate the dynamics of the intestinal epithelium in such a way that accumulation of new mutations can be reduced. Importantly, reducing mutation accumulation has the potential to delay aging, and the initiation and progression of diseases such as colorectal cancer.

INTRODUCTION

The lumen of the intestine is a hostile environment and the intestinal epithelium is constantly challenged by intrinsic and extrinsic factors, such as gastric acids, consumed harmful substances, and pathogenic microbes. These challenges can result in damage, such as disruption of the epithelial lining and loss of stem cells. Under homeostatic conditions the intestine has an impressive capacity to protect itself against tissue damage. The very dynamic nature of the intestinal epithelium enables a fast regenerative response that can maintain epithelial integrity. Here we review how this dynamic nature of the intestinal epithelium also minimizes the accumulation of new mutations in the intestine, thereby protecting against aging and development of colorectal cancer. In addition, we focus on challenges that can perturb this protection against mutation accumulation.

CONVEYER BELT-LIKE ORGANIZATION

The vast majority of intestinal epithelial cells are short-lived

One way the intestine is protected against the accumulation of mutations is by imposing a short lifetime on the vast majority of intestinal cells. This is a result of the morphology of the intestinal epithelium, which is a repetitive sheet of crypt-villus units (**Figure 1**)¹. Intestinal stem cells that reside at the bottom of so-called crypts of Lieberkühn - little invaginations into the intestinal epithelium - fuel the fast turnover of the intestinal epithelium¹. These stem cells give rise to progenitor cells in the transit amplifying (TA) compartment, located a bit higher up the crypt-villus-axis, that subsequently differentiate into all specialized lineages while traveling upwards along the villus in a conveyer belt-like fashion (**Figure 1**)¹. The differentiated cells in the villus fulfill the physiological functions of the intestine, including nutrient uptake by enterocytes, hormone production by enteroendocrine cells and mucus production for protection and lubrication by goblet cells. Upon arrival at the tip of the villus, ~5 days after birth of the cells, differentiated cells are shed into the lumen¹. Only these short-lived differentiated villus cells are exposed to the hazardous environment of the intestinal lumen². Since they get shed into the lumen within a week, any genomic damage that occurs in these cells cannot manifest or be propagated. Of note, the colonic epithelium does not contain villi, but does function as a conveyer belt as differentiated cells are shed at the surface of the colonic epithelium.

Long-lived intestinal stem cells can accumulate new mutations

The small pool of long-lived stem cells that maintain the epithelium are positioned in the intestinal crypts, away from the lumen, which minimizes possible harm to these cells (**Figure 1**)². The fact that these multipotent stem cells can accommodate the fast turnover of the intestinal epithelium has been known for decades³. However, their exact identity remained uncertain for a long time. Already in the early 70s, Cheng and Leblond identified the proliferative crypt base columnar (CBC) cells residing at the bottom of the crypt interspersed between Paneth cells⁴. However, their functional role as stem cells was only confirmed relatively recently after leucine-rich repeat-containing G protein-coupled receptor 5 (Lgr5) was found to mark these CBC stem cells⁵. Lineage tracing experiments in which these cells are labeled with markers that are inherited by daughter cells showed that Lgr5+ CBC cells give rise to all differentiated cell types present in the intestine and that they can do so over prolonged periods of time⁵. Moreover, when single Lgr5+ cells are isolated and placed in defined culture conditions, they can form

mini-guts (i.e. organoids) that contain crypt-villus units and harbor all intestinal cell types⁶. Together, these findings show that Lgr5+ CBC cells are multipotent and have the capacity to self-renew, indicating that these cells are bona fide stem cells in the intestine.

Since the Lgr5+ stem cells are long-lived, while the differentiated cells in the intestine only have a short lifetime, the Lgr5+ stem cells are vulnerable for accumulation of mutations in, for example, cancer driver genes. In 2009, Barker *et al.* showed that Lgr5+ stem cells can indeed function as cells-of-origin for intestinal adenoma^{7,8}. Mice only developed intestinal adenomas when an *Apc* mutation was introduced in the long-lived Lgr5+ stem cells but not when the same mutation was introduced in the short-lived differentiated cells. Thus, the fast turnover of the intestine and its conveyor belt-like structure can protect against the accumulation of mutations in the vast majority of intestinal epithelial cells that are exposed to the hazardous environment of the lumen. Only a small pool of long-lived stem cells located at the bottom of shielded crypts can accumulate damage and mutations, and therefore have the potential to act as cells-of-origin for intestinal cancer.

The stem cell pool can be replenished upon tissue damage

Under homeostatic conditions, the chance to accumulate mutations depends on the lifetime of a cell, and this therefore happens, as discussed above, predominately in Lgr5+ stem cells. However, a large body of work suggests the existence of a pool of “reserve” stem cells that are in a relative quiescent state and characterized by DNA label-retention⁹ and the expression of Lrig1, Bmi1, mTert, Hopx, and Mex3a¹⁰⁻¹⁵. Since many of these proposed markers are enriched at the border of the stem cell niche, 4 cell diameters from the crypt bottom (+4 position), these cells are often referred to as +4 cells (**Figure 1**). However, the identity and even the very existence of quiescent “reserve” stem cells have been controversial and heavily debated¹⁶. It has been suggested that instead of being dedicated reserve stem cells, +4 cells are progenitors that can repopulate the Lgr5+ stem cell pool through dedifferentiation (for an review see¹⁷). This notion is supported by lineage tracing experiments that show that damage can induce the reversion of committed progenitors to Lgr5+ stem cells, including secretory progenitors^{18,19}, enterocyte precursors²⁰, Paneth cells²¹, and a population of goblet cells^{22,23}. This dedifferentiation is, at least in part, mediated by chromatin remodeling, which can make genomic regions important for stemness more accessible²³. The thought that there is no dedicated “reserve” stem cell pool is further strengthened by two independent studies that show that a key marker of the reserve stem cell pool (Bmi1) actually marks mature enteroendocrine cells and that these cells can be recalled into the stem cell compartment upon damage^{22,23}. Other studies show that the +4 markers do not mark a specific population of cells, but are expressed in cells throughout the crypt, including in Lgr5+ stem cells^{11,13,16,24,25}. This data indicates that, similar to mammary tissue²⁶, the identity, behavior, and fate of cells cannot always be linked to a single molecular profile or specific marker. Since cells are highly plastic and can gain or lose stem cell traits, it may be better to define a stem cell by its function than through markers.

Tissue damage drives progenitor dedifferentiation and affects accumulation of mutations

Regardless of the identity or state of stem cells, the current literature agrees on the existence of a pool of cells that has the potential to replenish Lgr5+ stem cells upon tissue damage. Consequently, mutations that are acquired in cells just above the stem cell zone can persist when these cells revert back to a stem cell state, which prevents cells from being transported to and lost at the tip of the

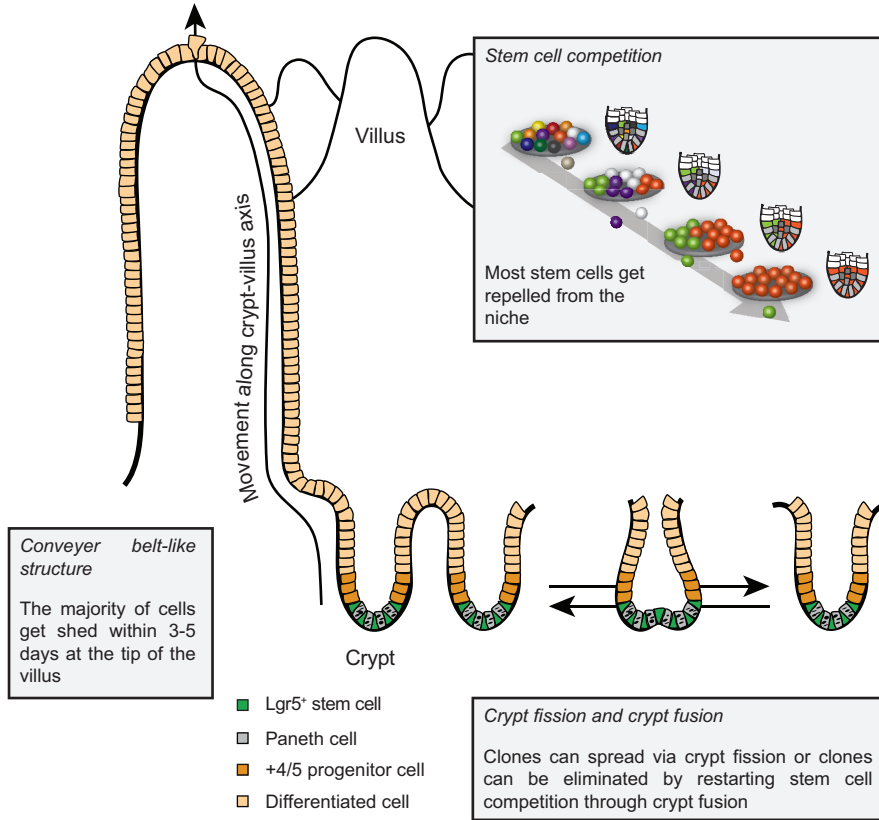


Figure 1. Cell and crypt dynamics that minimize the accumulation of mutations. Cartoon of the crypt-villus units of the small intestine. Shown are the three dynamic processes that minimize the retention of mutated cells: the conveyer belt-like structure, stem cell competition and crypt fusion.

villus. The activation of NFκB signaling seems to be required for this dedifferentiation^{27,28}. An activating mutation in the proto-oncogene *β-Catenin* in non-stem cells only leads to adenoma formation when NFκB signaling is simultaneously enhanced²⁷. In addition, *Apc* mutations in Dclk1+ tuft cells do not induce tumorigenesis under homeostatic conditions²⁹. However, when NFκB signaling is enhanced by dextran sulphate sodium-induced colitis, APC loss in tuft cells does lead to intestinal tumors²⁸. Thus, enhanced NFκB signaling may result in dedifferentiation of committed progenitors, thereby unmasking oncogenic events that can potentially lead to tumor initiation.

The route of cancer initiation via NFκB-induced dedifferentiation of committed progenitors may not be surprising. In colorectal cancers, and also pancreatic and gastric carcinomas, this pathway is often activated by inflammation or through mutations. NFκB signaling can for instance be enhanced by activating mutations in *Kras*, which occur in ~40% of all human colorectal cancers³⁰. In mice, simultaneous induction of *β-catenin* and *Kras* mutations within differentiated villus cells induces the re-expression of stem cell markers, and leads to dedifferentiation and stem cell potential²⁷. Moreover, in

these mice lesions are often formed at these villus regions suggesting that WNT and KRAS-mediated dedifferentiation enables cells to function as cells-of-origin²⁷. This phenomenon may explain the so-called 'top-down' adenomas that are observed in the clinic, where adenomas on the surface of the colorectal lumen form on top of "normal"-looking crypts³¹. However, it should be noted that these studies are predominantly performed in mouse models, in which whole populations of cells are transformed by oncogenic mutations. Future studies are required to indicate whether the route of dedifferentiation also occurs in human colorectal cancers, where adenomas arise from an oncogenic event in a single cell.

Taken together, the short life-time of the vast majority of cells is a strong protection mechanism in intestinal tissue since it results in loss of most newly acquired mutations. Therefore, mutations can only manifest in long-lived stem cells or in more differentiated cells that dedifferentiate into cells with stem cell characteristics that live long enough to induce a tumor.

STEM CELL COMPETITION

Most stem cells are lost over time due to stem cell competition

Although the geometry of the crypt-villus unit protects long-lived stem cells better than short-lived differentiated cells against harmful substances present in the intestine², new mutations can get introduced in the stem cells upon proliferation. Fortunately, not all mutations that arise in stem cells are propagated due to a second protection mechanism present in the crypt: stem cell competition^{32,33}. The crypt contains ~14-16 Lgr5+ stem cells that are interspersed with Paneth cells, which together with the stroma, function as a niche for stem cell maintenance³⁴. On average, Lgr5+ stem cells proliferate symmetrically every 21.5 hours³⁵, and as soon as stem cells lose touch with a Paneth cell, they get primed for differentiation and move up along the crypt-villus axis (**Figure 1**). This process was illustrated by lineage-tracing experiments in Lgr5-multi-color 'confetti-mice'³². In these mice, injection of tamoxifen results in recombination of a confetti-construct, which stochastically induces expression of one of four confetti colors specifically in Lgr5+ stem cells, and this color is inherited by all daughter cells³². Despite induction of different confetti colors in different individual Lgr5+ stem cells within the same crypt, most crypts contain stem cells of a single confetti color after 1-6 months (**Figure 1**). This data led to the neutral drift stem cell competition model: upon each stem cell division, the number of stem cells exceeds the available positions within the niche, which is counterbalanced by loss of a stem cell from the niche. This constant stem cell division and stem cell loss leads to the expansion or extinction of stem cell clones and ultimately to clonality of all stem cells in the niche (**Figure 1**). By multi-day intravital microscopy, we directly visualized this process and showed that stem cells can be passively displaced from the stem cell niche after the division of proximate cells implying that stem cell fate can be uncoupled from division³⁶. Moreover, our experiments showed that all Lgr5+ stem cells (~14-16) are able to contribute to the stem cell competition. However, cells at the border are more susceptible to be passively displaced from the niche than those located at the center³⁶. Since cells constantly gain or lose favorable positions by changing position, they function as a single stem cell pool with a combined output equal to ~5-7 equipotent functional stem cells as was predicted by mathematical modeling^{32,36,37}. Importantly, similar data have been obtained in human intestinal tissue³⁸.

Stem cell competition can eradicate mutant cells

The model of stem cell competition predicts that a mutation can only remain in a crypt long-term

when it is present in the one stem cell that wins the competition; mutations in the other stem cells will get lost. To test this, two independent studies were done using sporadic induction of oncogenic mutations often found in colorectal cancer (*Apc*, *Kras* or *TP53*) in combination with lineage tracing and demonstrated that oncogenic clones can indeed get lost from the stem cell niche^{39,40}. However, the stem cell competition is not always completely neutral. For example, instead of having a 50% chance of displacing a neighboring stem cell in neutral competition, *Apc*^{het} and *Kras*^{G12D} mutations lead to a respectively 62% and 78% chance to outcompete a neighbor^{39,40}. Interestingly, a *TP53* mutation does not affect stem cell competition under homeostatic conditions, while it gives a competitive advantage (58%) when colitis is induced³⁹. Mutations can potentially also give a disadvantage in the competition. Using time-lapse microscopy of organoids, it has recently been shown that Ras^{V12}-transformed cells have an altered metabolism that promotes active extrusion of these cells from non-transformed epithelial tissues⁴¹. Obviously, if this also holds true for Ras^{V12}-transformed intestinal stem cells, this mechanism decreases the strength of these cells in stem cell competition and therefore the ability of the Ras^{V12} mutation to be maintained in intestinal epithelial tissues.

Even in a non-neutral competition, a stem cell that acquires a mutation is likely to be outcompeted by one of the ~15 wild-type stem cells, and as a consequence this mutant cell will be repelled from the niche and transported to and lost at the villus tip^{39,40}. Thus, acquisition of an oncogenic mutation may influence the fitness of a cell in the stem competition, but is not deterministic, and can be eradicated due to stem cell competition.

Perturbation of niche factors alters stem cell niche and stem cell competition

Stem cell competition can be quite accurately described by a relatively simple one-dimensional stochastic model based on only two parameters: the number of stem cells per crypt and the rate at which they are replaced by a neighbor and get lost^{32,33,37} (for more information see review¹⁷). The number of stem cells determines the chance of an individual stem cell to win the competition, while both parameters determine the speed of the competition. These parameters are tightly controlled by the stem cell niche. The niche provides cues to accurately balance stem cell proliferation and differentiation, controlling the number of stem cells and therefore also the protection potential of stem cell competition⁴². The niche factors that control stem cell numbers are produced by Paneth and mesenchymal cells and include WNT ligands (e.g. Wnt3a), Notch ligands (Dll1, Dll4), BMP antagonists (e.g. Noggin and Gremlin) and epidermal growth factor (EGF)^{34,43-48}. Importantly, the stem cell zone, and therefore stem cell competition, is altered when these signals are perturbed. For example, blocking Delta-Notch signaling between stem and Paneth cells results in quick differentiation of stem and progenitor cells into postmitotic Goblet cells^{44,49}. Moreover, inhibition of BMP signaling by Gremlin or Noggin leads to hyperproliferative crypts and the formation of ectopic crypts at the villus compartment^{50,51}. In addition, when WNT signaling is reduced by manipulating WNT proteins directly or by manipulating a regulator of WNT signaling R-spondin, the number of stem cells is decreased (described in Chapter 4)⁵². As predicted by the one-dimensional stochastic model for stem cell competition described above, lineage tracing experiments showed that reducing the number of Lgr5+ stem cells results in faster stem cell competition, observed as accelerated drift of stem cells toward monoclonality⁵². Together these studies shows that niche factors tightly control the number of stem cells and the composition of the crypt, thereby controlling stem cell competition and its ability to minimize the accumulation of new mutations.

CRYPT DYNAMICS

Crypt fission and fusion can influence stem cell dynamics

As a result of stem cell competition, stem cells within crypts become monoclonal over time. However, this is not a static situation: crypts can undergo fission and fusion events (**Figure 1**). During crypt fission one crypt divides into two crypts⁵³, and this process mostly takes place during postnatal intestinal elongation and during regenerative responses⁵⁴⁻⁵⁷. In adulthood, crypt fission remains present during homeostasis, although at lower levels⁵⁸⁻⁶⁰. Using intravital microscopy, we recently uncovered crypt fusion, which seems to be an almost exact reverse phenomenon of crypt fission where two crypts fuse into one daughter crypt⁶¹ (**Figure 1**). At homeostatic conditions, crypt fission and fusion occur at near similar frequencies and on average a crypt should at least undergo a fission or fusion event every 3 months^{58,61}.

Crypt fission has the potential to spread monoclonal mutant crypts over the epithelium, and has been shown to be a mechanism through which mutant cells can expand beyond crypt borders⁶². This spread creates fields of genetically altered crypts that can predispose a tissue for cancer development (field cancerization)^{63,64}. In the human intestine, fields of KRAS-mutated crypts have been observed surrounding colorectal cancers, indicating that this can be an initiating event in cancer development^{65,66}. In addition, fields of APC-deficient crypts have been found that may play an important role in adenoma formation and expansion⁶⁷⁻⁶⁹. Thus, crypt fission can induce the spread of mutated cells over the epithelium which may enhance tumor initiation.

In contrast to the spread of mutations via crypt fission, crypt fusion has the potential to eradicate mutations from the epithelium, since it enables stem cell competition to eradicate mutant cells even in the situation where all stem cells in a crypt contain a particular mutation. When a crypt containing mutant stem cells fuses with a wild-type crypt, the stem cell competition “restarts” and the mutant cells can be outcompeted by the wild-type cells (**Figure 1**). Therefore, crypt fusion may be a third mechanism that could protect against accumulation of mutations, and has the potential to counteract the spread of mutations by crypt fission. Since crypt fission and fusion significantly influence stem cell competition, it will be important to investigate the stem cell dynamics during crypt fission and fusion. Moreover, both processes should be incorporated into models describing stem cell competition in the intestine.

Tissue damage alters crypt dynamics

As mentioned before, crypt fission and fusion can influence stem cell competition. Because of its recent discovery, the molecular mechanisms underlying crypt fusion are yet unknown, while more is known about crypt fission. For example, it has been found that crypt fission occurs more frequently in response to damage, including intestinal resection, irradiation and chemotherapy treatment^{54,55,70,71}. This response may (partly) function through the TGF β signaling pathway, since loss of TGF β R2 significantly reduces crypt fission events⁷². Interestingly, increased crypt fission is also observed in diseased colonic epithelia from patients with Crohn's disease and ulcerative colitis⁷³, which both induce an inflammatory response and lead to an increased risk of colorectal cancer. Thus, damage and inflammation induce crypt fission, which may be linked to tumor initiation. In addition to damage and inflammation, crypt fission may also be induced by genetic mutations. For example, in the mouse small intestine, the number of crypts monoclonal for the KRAS^{G12D} mutation can expand by crypt fission with an increased rate compared to wild type crypts (>30-fold), and this creates fields of KRAS^{G12D} mutated crypts⁴⁰. As

mentioned before, activating KRAS mutations can enhance NFκB signaling, which is associated with inflammation, again suggesting a link between inflammation and colorectal tumor initiation.

FUTURE PERSPECTIVES

In this review we have given an overview of the current knowledge about how the dynamics of the intestinal epithelium minimize accumulation of new mutations, including the conveyor belt-like structure, stem cell competition and crypt fusion. Future research is required to reveal the exact dynamics of these processes and how each of them contributes to the protection against the accumulation of mutations. Interestingly, once we understand these processes in more detail, one could think about manipulating them to optimize their protective capacity. For example, inhibition of crypt fission may lead to decreased spread of new mutations over the epithelium. On the other hand, induction of crypt fusion may result in the depletion of mutant crypts and a reduced spread of oncogenic mutations. In addition, expanding the number of stem cells per crypt may increase the chance that a mutant stem cell will be repelled from the niche and be depleted from the tissue.

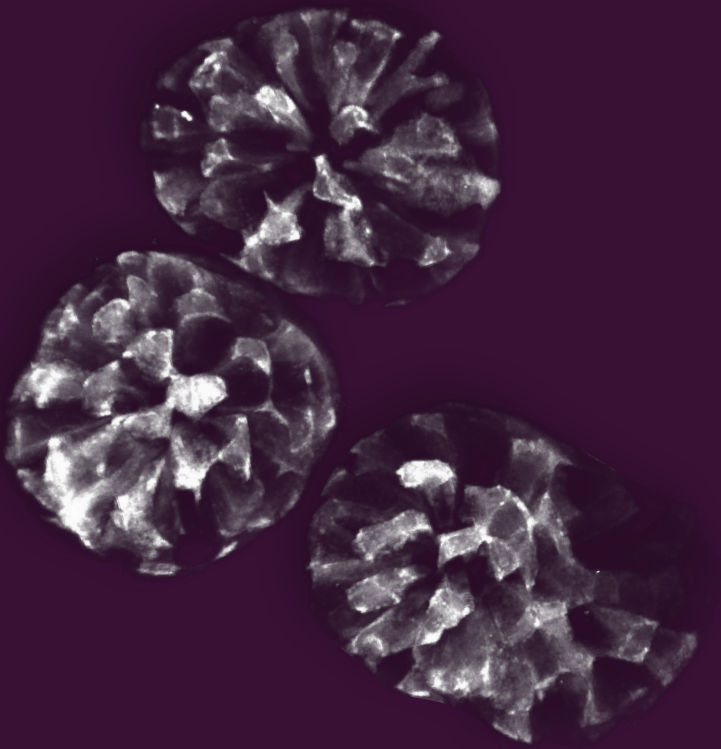
Live imaging of the intestinal epithelium, such as organoid imaging and intravital microscopy, will greatly help in understanding the cellular protection mechanisms and in finding ways to manipulate them. In contrast to techniques that draw a static picture of the dynamic nature of intestinal tissues, live microscopy can be used to visualize intestinal tissues, cells and processes over time. Organoid imaging will be instrumental in monitoring intestinal dynamics at subcellular resolution (e.g. ^{41,74,75}). However, it is important to realize that organoids - as any other 3D culture model - lack the *in vivo* microenvironment, such as the surrounding stroma and immune cells. Recent advantages in high resolution intravital microscopy, and the development of a variety of imaging windows⁷⁶, enable the visualization of the fate and behavior cells and lineages in living mice for several days⁷⁷⁻⁷⁹. We recently developed the abdominal imaging window^{80,81}, which was used to study intestinal tissue homeostasis^{36,61} and intestinal tumor progression⁸². In addition, it enabled us to uncover new aspects of epithelial dynamics, such as the identification of crypt fusion, which on static images cannot be discriminated from crypt fission⁶¹. In the future, live imaging technologies will be instrumental in understanding whether and how manipulating intestinal cell and crypt dynamics affects tissue homeostasis and how this affects the fate of cells that have acquired mutations in for example cancer driver genes. We believe that manipulation intestinal cell and crypt dynamics gives us the ability to reduce the accumulation of new mutations, which provides great potential to influence aging and the induction and progression of diseases such as cancer. With new microscopy techniques, we expect to make big steps in this direction in the near future.

REFERENCES

1. Clevers, H. The Intestinal Crypt, A Prototype Stem Cell Compartment. *Cell* **154**, 274–284 (2013).
2. Kaiko, G. E. *et al.* The Colonic Crypt Protects Stem Cells from Microbiota-Derived Metabolites The architecture of intestinal crypts protects the stem cells at their base from a growth-inhibiting metabolite derived from the gut microbiome. Might these findings suggest co-evolution of mammalian anatomy with commensal flora? The Colonic Crypt Protects Stem Cells from Microbiota-Derived Metabolites. *Cell* **165**, 1708–1720 (2016).
3. Wright, N. A. Epithelial stem cell repertoire in the gut: clues to the origin of cell lineages, proliferative units and cancer. *Int. J. Exp. Pathol.* **81**, 117–43 (2000).
4. Cheng, H. & Leblond, C. P. Origin, differentiation and renewal of the four main epithelial cell types in the mouse small intestine V. Unitarian theory of the origin of the four epithelial cell types. *Am. J. Anat.* **141**, 537–561 (1974).
5. Barker, N. *et al.* Identification of stem cells in small intestine and colon by marker gene Lgr5. *Nature* **449**, 1003–1007 (2007).
6. Sato, T. *et al.* Single Lgr5 stem cells build crypt–villus structures in vitro without a mesenchymal niche. *Nature* **459**, (2009).
7. Barker, N. *et al.* Crypt stem cells as the cells-of-origin of intestinal cancer. *Nature* **457**, 608–611 (2009).
8. Zhu, L. *et al.* Prominin 1 marks intestinal stem cells that are susceptible to neoplastic transformation. *Nature* **457**, 603–7 (2009).
9. Potten, C. S., Kovacs, L. & Hamilton, E. Continuous labelling studies on mouse skin and intestine. *Cell Tissue Kinet.* **7**, 271–83 (1974).
10. Breault, D. T. *et al.* Generation of mTert-GFP mice as a model to identify and study tissue progenitor cells. *Proc Natl Acad Sci* **105**, 10420-5 (2008).
11. Powell, A. E. *et al.* The Pan-ErbB Negative Regulator Lrig1 Is an Intestinal Stem Cell Marker that Functions as a Tumor Suppressor. *Cell* **149**, 146–158 (2012).
12. Sangiorgi, E. & Capecchi, M. R. Bmi1 is expressed in vivo in intestinal stem cells. *Nat. Genet.* **40**, 915–920 (2008).
13. Montgomery, R. K. *et al.* Mouse telomerase reverse transcriptase (mTert) expression marks slowly cycling intestinal stem cells. *Proc Natl Acad Sci* **108**: 179-84
14. Takeda, N. *et al.* Interconversion Between Intestinal Stem Cell Populations in Distinct Niches. *Science* **334**, 1420–1424 (2011).
15. Barriga, F. M. *et al.* Mex3a Marks a Slowly Dividing Subpopulation of Lgr5+ Intestinal Stem Cells. *Cell Stem Cell* **20**, 801–816.e7 (2017).
16. Muñoz, J. *et al.* The Lgr5 intestinal stem cell signature: robust expression of proposed quiescent ‘+4’ cell markers. *EMBO J.* **31**, 3079–3091 (2012).
17. Vermeulen, L. & Snippert, H. J. Stem cell dynamics in homeostasis and cancer of the intestine. *Nat. Rev. Cancer* **14**, 468–80 (2014).
18. van Es, J. H. *et al.* Dll1+ secretory progenitor cells revert to stem cells upon crypt damage. *Nat. Cell Biol.* **14**, 1099–1104 (2012).
19. Buczaccki, S. J. A. *et al.* Intestinal label-retaining cells are secretory precursors expressing Lgr5. *Nature* **495**, 65–9 (2013).
20. Tetteh, P. W. *et al.* Replacement of Lost Lgr5-Positive Stem Cells through Plasticity of Their Enterocyte-Lineage Daughters. *Cell Stem Cell* **18**, 203–13 (2016).
21. Roth, S. *et al.* Paneth Cells in Intestinal Homeostasis and Tissue Injury. *PLoS One* **7**, e38965 (2012).
22. Yan, K. S. *et al.* Intestinal Enteroendocrine Lineage Cells Possess Homeostatic and Injury-Inducible Stem Cell Activity. *Cell Stem Cell* **21**, 78–90.e6 (2017).
23. Jadhav, U. *et al.* Dynamic Reorganization of Chromatin Accessibility Signatures during Dedifferentiation of Secretory Precursors into Lgr5+ Intestinal Stem Cells. *Cell Stem Cell* **21**, 65–77.e5 (2017).
24. Li, N. *et al.* Single-Cell Analysis of Proxy Reporter Allele-Marked Epithelial Cells Establishes Intestinal Stem Cell Hierarchy. *Stem Cell Reports* **3**, 876–891 (2014).
25. Grün, D. *et al.* Single-cell messenger RNA sequencing reveals rare intestinal cell types. *Nature* **525**, 251-5 (2015)
26. Scheele, C. L. G. J. *et al.* Identity and dynamics of mammary stem cells during branching morphogenesis. *Nature* **542**, 313–317 (2017).
27. Schwitalla, S. *et al.* Intestinal tumorigenesis initiated by dedifferentiation and acquisition of stem-cell-like properties. *Cell* **152**, 25–38 (2013).
28. Westphalen, C. B. *et al.* Long-lived intestinal tuft cells serve as colon cancer-initiating cells. *J. Clin. Invest.* **124**, 1283–95 (2014).
29. Nakanishi, Y. *et al.* Dclk1 distinguishes between tumor and normal stem cells in the intestine. *Nat. Genet.* **45**, 98–103 (2013).

30. Cancer Genome Atlas Network, T. C. G. A. Comprehensive molecular characterization of human colon and rectal cancer. *Nature* **487**, 330–7 (2012).
31. Shih, I. M. *et al.* Top-down morphogenesis of colorectal tumors. *Proc. Natl. Acad. Sci. U. S. A.* **98**, 2640–5 (2001).
32. Snippert, H. J. *et al.* Intestinal crypt homeostasis results from neutral competition between symmetrically dividing Lgr5 stem cells. *Cell* **143**, 134–144 (2010).
33. Lopez-Garcia, C., Klein, A. M., Simons, B. D. & Winton, D. J. Intestinal stem cell replacement follows a pattern of neutral drift. *Science*. **330**, 822–825 (2010).
34. Sato, T. *et al.* Paneth cells constitute the niche for Lgr5 stem cells in intestinal crypts. *Nature* **469**, 415–418 (2011).
35. Schepers, A. G., Vries, R., van den Born, M., van de Wetering, M. & Clevers, H. Lgr5 intestinal stem cells have high telomerase activity and randomly segregate their chromosomes. *EMBO J.* **30**, 1104–9 (2011).
36. Ritsma, L. *et al.* Intestinal crypt homeostasis revealed at single-stem-cell level by in vivo live imaging. *Nature* **507**, (2014).
37. Kozar, S. *et al.* Continuous Clonal Labeling Reveals Small Numbers of Functional Stem Cells in Intestinal Crypts and Adenomas. *Cell Stem Cell* **13**, 626–633 (2013).
38. Baker, A. M. *et al.* Quantification of Crypt and Stem Cell Evolution in the Normal and Neoplastic Human Colon. *Cell Reports* **8**, 940-7 (2014)
39. Vermeulen, L. *et al.* Defining stem cell dynamics in models of intestinal tumor initiation. *Science* **342**, 995–8 (2013).
40. Snippert, H. J., Schepers, A. G., Van Es, J. H., Simons, B. D. & Clevers, H. Biased competition between Lgr5 intestinal stem cells driven by oncogenic mutation induces clonal expansion. *EMBO Rep.* **15**, 62–69 (2014).
41. Kon, S. *et al.* Cell competition with normal epithelial cells promotes apical extrusion of transformed cells through metabolic changes. *Nat. Cell Biol.* **19**, 530–541 (2017).
42. Simons, B. D. & Clevers, H. Leading Edge Review Strategies for Homeostatic Stem Cell Self-Renewal in Adult Tissues. *Cell* **145**, 851-62 (2011)
43. Pinto, D., Gregorieff, A., Begthel, H. & Clevers, H. Canonical Wnt signals are essential for homeostasis of the intestinal epithelium. *Genes Dev.* **17**, 1709–1713 (2003).
44. van Es, J. H. *et al.* Notch/γ-secretase inhibition turns proliferative cells in intestinal crypts and adenomas into goblet cells. *Nature* **435**, 959–963 (2005).
45. Hsu, D. R., Economides, A. N., Wang, X., Eimon, P. M. & Harland, R. M. The *Xenopus* dorsalizing factor Gremlin identifies a novel family of secreted proteins that antagonize BMP activities. *Mol. Cell* **1**, 673–83 (1998).
46. He, X. C. *et al.* BMP signaling inhibits intestinal stem cell self-renewal through suppression of Wnt-beta-catenin signaling. *Nat. Genet.* **36**, 1117–21 (2004).
47. Aoki, R. *et al.* Foxl1-expressing mesenchymal cells constitute the intestinal stem cell niche. *Cell. Mol. Gastroenterol. Hepatol.* **2**, 175–188 (2016).
48. Stzepourginski, I. *et al.* mesenchymal cells are a major component of the intestinal stem cells niche at homeostasis and after injury. *Proc Natl Acad Sci* **114**, E506-E513 (2017)
49. Fre, S. *et al.* Notch signals control the fate of immature progenitor cells in the intestine. *Nature* **435**, 964–968 (2005).
50. Haramis, A.-P. G. *et al.* De Novo Crypt Formation and Juvenile Polyposis on BMP Inhibition in Mouse Intestine. *Science* **303**, 1684-86 (2004)
51. Davis, H. *et al.* Aberrant epithelial GREM1 expression initiates colonic tumorigenesis from cells outside the stem cell niche. *Nat. Med.* **21**, 62–70 (2014).
52. Yan, K. S. *et al.* Non-equivalence of Wnt and R-spondin ligands during Lgr5+ intestinal stem-cell self-renewal. *Nature* **545**, 238–242 (2017).
53. Totafurno, J., Bjerknes, M. & Cheng, H. The crypt cycle. Crypt and villus production in the adult intestinal epithelium. *Biophys. J.* **52**, 279–294 (1987).
54. Cairnie, A. B. & Millen, B. H. Fission of crypts in the small intestine of the irradiated mouse. *Cell Prolif.* **8**, 189–196 (1975).
55. Cheng, H., McCulloch, C. & Bjerknes, M. Effects of 30% intestinal resection on whole population cell kinetics of mouse intestinal epithelium. *Anat. Rec.* **215**, 35–41 (1986).
56. Clarke, R. M. The effect of growth and of fasting on the number of villi and crypts in the small intestine of the albino rat. *J. Anat* **112**, 27–33 (1972).
57. Park, H. S., Goodlad, R. A. & Wright, N. A. Crypt fission in the small intestine and colon. A mechanism for the emergence of G6PD locus-mutated crypts after treatment with mutagens. *Am. J. Pathol.* **147**, 1416–27 (1995).
58. Bjerknes, M. A test of the stochastic theory of stem cell differentiation. *Biophys. J.* **49**, 1223–7 (1986).
59. Cheng, H. & Bjerknes, M. Whole population cell kinetics and postnatal development of the mouse intestinal epithelium. *Anat. Rec.* **211**, 420–426 (1985).

60. Langlands, A. J. *et al.* Paneth Cell-Rich Regions Separated by a Cluster of Lgr5+ Cells Initiate Crypt Fission in the Intestinal Stem Cell Niche. *PLoS Biol.* **14**, e1002491 (2016).
61. Bruens, L., Ellenbroek, S. I. J., van Rheenen, J. & Snippert, H. J. In vivo Imaging Reveals Existence of Crypt Fission and Fusion in Adult Mouse Intestine. *Gastroenterology* **153**, 674-677 (2017)
62. Greaves, L. C. *et al.* Mitochondrial DNA mutations are established in human colonic stem cells, and mutated clones expand by crypt fission. *Proc. Natl. Acad. Sci. U. S. A.* **103**, 714-719 (2006).
63. Garcia, S. B., Park, H. S., Novelli, M. & Wright, N. A. Field cancerization, clonality, and epithelial stem cells: the spread of mutated clones in epithelial sheets. *J. Pathol.* **187**, 61-81 (1999).
64. Slaughter, D. P., Southwick, H. W. & Smejkal, W. Field cancerization in oral stratified squamous epithelium; clinical implications of multicentric origin. *Cancer* **6**, 963-8 (1953).
65. Zhu, D. *et al.* K-ras gene mutations in normal colorectal tissues from K-ras mutation-positive colorectal cancer patients. *Cancer Res.* **57**, 2485-92 (1997).
66. Aivado, M. *et al.* "Field cancerization" additional phenomenon in development of colon tumors? K-ras codon 12 mutations in normal colonic mucosa of patients with colorectal neoplasms. *Chirurg.* **71**, 1230-4-5 (2000).
67. Preston, S. L. *et al.* Bottom-up histogenesis of colorectal adenomas: origin in the monocryptal adenoma and initial expansion by crypt fission. *Cancer Res.* **63**, 3819-25 (2003).
68. Fischer, J. M., Schepers, A. G., Clevers, H., Shibata, D. & Liskay, R. M. Occult progression by Apc-deficient intestinal crypts as a target for chemoprevention. *Carcinogenesis* **35**, 237-46 (2014).
69. Wasan, H. S. *et al.* APC in the regulation of intestinal crypt fission. *J. Pathol.* **185**, 246-255 (1998).
70. Dekaney, C. M. *et al.* Expansion of intestinal stem cells associated with long-term adaptation following ileocecal resection in mice. *AJP Gastrointest. Liver Physiol.* **293**, G1013-G1022 (2007).
71. Dekaney, C. M., Gulati, A. S., Garrison, A. P., Helmrath, M. A. & Henning, S. J. Regeneration of intestinal stem/progenitor cells following doxorubicin treatment of mice. *Am. J. Physiol. - Gastrointest. Liver Physiol.* **297**, (2009).
72. Fischer, J. M. *et al.* Single cell lineage tracing reveals a role for Tgf β 2 in intestinal stem cell dynamics and differentiation. *Proc. Natl. Acad. Sci.* **113**, 12192-12197 (2016).
73. Cheng, H., Bjercknes, M., Amar, J. & Gardiner, G. Crypt production in normal and diseased human colonic epithelium. *Anat. Rec.* **216**, 44-48 (1986).
74. Verissimo, C. S. *et al.* Targeting mutant RAS in patient-derived colorectal cancer organoids by combinatorial drug screening. *Elife* **5**, (2016).
75. Drost, J. *et al.* Sequential cancer mutations in cultured human intestinal stem cells. *Nature* **521**, 43-47 (2015).
76. Alieva, M., Ritsma, L., Giedt, R. J., Weissleder, R. & van Rheenen, J. Imaging windows for long-term intravital imaging: General overview and technical insights. *Intravital* **3**, e29917 (2014).
77. Ellenbroek, S. I. J. & van Rheenen, J. Imaging hallmarks of cancer in living mice. *Nat. Rev. Cancer* **14**, 406-418 (2014).
78. Scheele, C. L. G. J., Maynard, C. & van Rheenen, J. Intravital Insights into Heterogeneity, Metastasis, and Therapy Responses. *Trends in cancer* **2**, 205-216 (2016).
79. Suijkerbuijk, S. J. E. & van Rheenen, J. From good to bad: Intravital imaging of the hijack of physiological processes by cancer cells. *Dev. Biol.* **428**, 328-337 (2017).
80. Ritsma, L. *et al.* Intravital microscopy through an abdominal imaging window reveals a pre-micrometastasis stage during liver metastasis. *Sci. Transl. Med.* **4**, 158ra145 (2012).
81. Ritsma, L. *et al.* Surgical implantation of an abdominal imaging window for intravital microscopy. *Nat. Protoc.* **8**, (2013).
82. Fumagalli, A. *et al.* Genetic dissection of colorectal cancer progression by orthotopic transplantation of engineered cancer organoids. *Proc. Natl. Acad. Sci. U. S. A.* **114**, E2357-E2364 (2017).



Chapter 3

Retrograde Movement Determines the Number of Cells with Stem Cell Potential in Small and Large Intestinal Crypts

Bruens L, Ellenbroek SJ*, Corominas-Murtra B*, Lafirenze SJA, Simons BD, Snippert HJ, Hannezo E and van Rheenen J*

Manuscript under review

* Equal contribution

ABSTRACT

Homeostasis in the intestinal epithelium is the consequence of neutral competition of dividing stem cells at the base of each crypt. Although markers, such as Lgr5, have been identified that label cells with stem cell properties, these markers do not necessarily label all or exclusively cells with stem cell potential. Here, we used a combination of intravital microscopy and modeling to reveal what determines the ability of cells to function as a stem cell in the small and large intestine. Repetitive intravital microscopy showed that most cell movements go along the crypt-lumen axis, following a conveyor belt-like dynamics fueled by proliferation at the crypt bottom. In parallel to this upward advection, we observed random cell relocation resulting in retrograde movement towards the crypt base. Surprisingly, while we observed this retrograde cell movement in the small intestine, it was near absent in the large intestine. We found that the scale of retrograde movement determines the size of the stem cell compartment, as this enables cells to away from the bottom of the crypt to continuously reposition to the base region. From our study we concluded that stem cell behavior is not a cell-intrinsic property, but rather a potential that can be gained or lost, and that random relocations resulting in retrograde movement determines the number of cells that possess stem cell potential.

INTRODUCTION

The intestinal tract consists of multiple compartments with different functions, which together ensure digestion and uptake of nutrients, absorption of water and expelling remainders of food intake. The small intestinal (SI) region comprises villi and invaginations, called crypts. In the large intestine (LI, comprising cecum and colon) the surface is flat, but a similar architecture of mitotic stem cell compartments at the bottom of crypts and more differentiated epithelial towards the intestinal lumen is found in all regions of the intestinal tract. The entire intestinal tube is lined with a single layer of epithelial cells that get renewed every few days. This high turnover has been shown to be the consequence of dividing stem cells that compete neutrally for niche space at the base of each crypt^{1,2}. At each cell division, a cell gets displaced from the base moving up along the crypt-lumen axis to differentiate into specialized cells such as goblet cell and enterocytes. Markers, such as Lgr5, have been identified that label cells with the ability to generate all differentiated cells along the crypt-lumen axis³. However, such markers do not necessarily label all or exclusively cells that have the potential to function as a stem cell⁴⁻⁸. Here, we use a combination of intravital microscopy and modeling to compare the cellular dynamics at the base of small and large intestinal crypts and how these dynamics determine functional stemness. We reveal that different scales of retrograde movement result in different sizes of the stem cell pool in small and large intestinal crypts.

RESULTS

Distribution of proliferating Lgr5+ cells in crypts along the intestinal tract

Cells at the crypt base express Leucine-rich repeat-containing G-protein coupled receptor 5 (Lgr5) (**Figure 1a,b**)³. These cells have been shown to function as stem cells, since they can give rise to all differentiated cells along the crypt-lumen axis³. Moreover, the position of Lgr5+ cells within the base of the crypt is important for their ability to displace other Lgr5+ cells (i.e. competitive strength)⁹. Therefore, we first determined the total average number of Lgr5+ cells at the base of the crypts of the SI and LI of Lgr5eGFP-Ires-CreERT2 mice, dividing populations into two regions: the centre and border region (**Figure 1c,d**). In both regions, we observed comparable numbers of Lgr5-expressing cells, with a total of approximately 20 Lgr5+ cells per crypt (**Figure 1c,d**). In addition to the number and distribution of Lgr5+ cells, the proliferation rate and the position of proliferating cells are important contributors to the dynamics of stem cell competition, since together they determine the rate at which stem cells are replaced in the niche. We compared the presence of proliferating cells in the different intestinal compartments by quantifying the number of cells in S-phase (measured through short-term EdU incorporation) and the number of cells in mitosis (positive for phospho-histone H3), both showing similar results. Although comparable numbers of proliferating cells were found in the central crypt region in the SI and LI, our analyses revealed that more cells in the border of the SI crypt were proliferating compared to those in the LI (**Figure 1e-g**). Together, this resulted in a slightly higher fraction of proliferative cells in the SI. Of note, the transit-amplifying zone, the proliferative zone above the Lgr5+ zone, is significantly less pronounced in the colonic epithelium, compared to the SI, when looking at BrdU incorporation (**Supplementary Figure 1**). Together, these results show that the distribution of Lgr5+ cells within crypts was comparable between the different intestinal compartments, but in the LI crypts proliferation predominantly takes place in the centre, whilst in the SI crypts proliferation takes place both in the centre and border regions of the Lgr5+ zone.

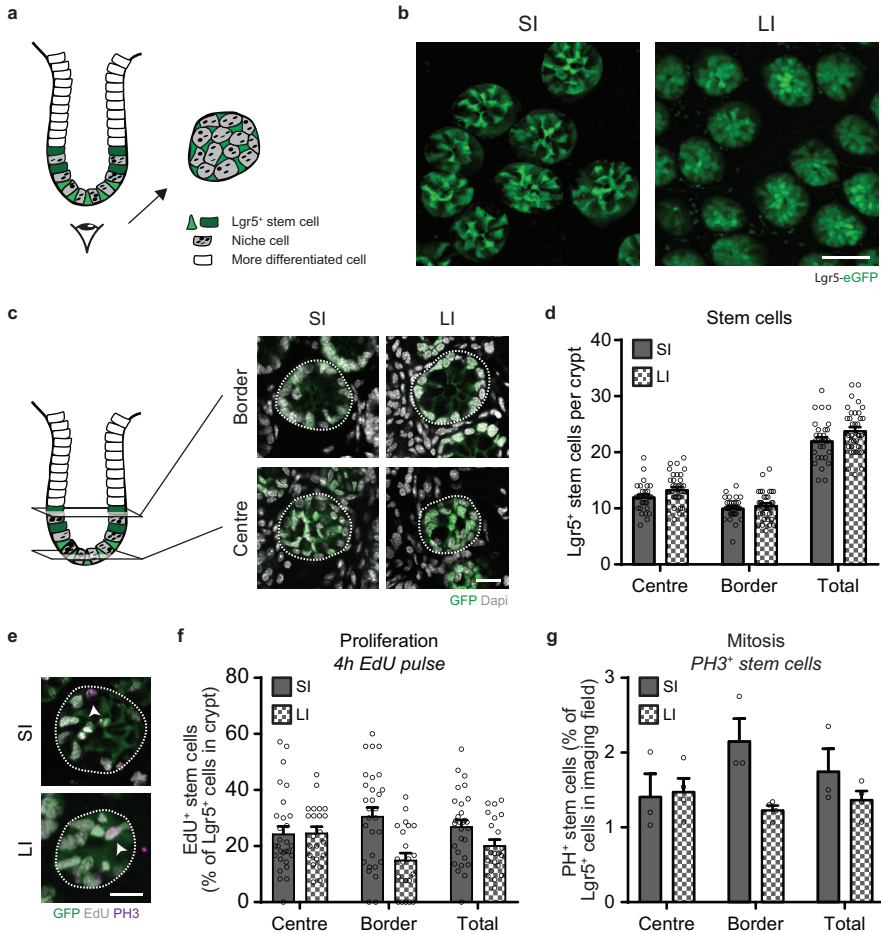
Not all Lgr5+ cells in LI function as stem cells

We have previously shown in the SI that the location within the crypt base determines the chance that Lgr5+ cells become displaced from the niche and lost⁹. Since we observed that proliferation in the LI crypts was predominantly localized in the centre, we hypothesized that the border cells of the LI crypts get displaced more often and potentially have lower competitive fitness than border cells in SI crypts. To test our hypothesis, we performed repetitive intravital imaging in lineage-traced Lgr5eGFP-Ires-CreERT2;R26R-Confetti/LSL-tdTomato mice (**Figure 2a**). We could retrace crypts in the SI and LI in large overview images by using vasculature and patchiness of Lgr5 expression as landmarks (**Figure 2b-d**). This allowed us to record the location of clones in the crypt base 48 hour after onset of tracing and trace their fate 8 weeks later. Quantification of clonal persistence (i.e. the percentage of clones that remained present in the Lgr5+ zone) showed that centre clones were more likely to persist than border clones, as expected based on previous research⁹. Strikingly, no border-derived clones in the LI remained in the stem cell niche 8 weeks after onset of tracing while ~15% of border-derived clones continued to persist in the SI (**Figure 2e**). Dissection of the different positions within the crypt base showed that the gradient of positional advantage (decreasing from centre to border) was remarkably stronger in the LI as compared to SI (**Figure 2e**). These results indicate that not all Lgr5+ cells in the LI function as stem cells, since the cells higher up on the crypt base do not participate in the stem cell competition because they are displaced and lost.

Modelling of stem cell dynamics: the stochastic conveyor belt

Given this striking difference between the positional retention advantage of Lgr5+ cells in crypts of the SI versus LI, we turned to a statistical modelling-based approach to address the mechanism underlying these differences. In contrast to previous studies that have sought to model the neutral drift dynamics of clones around the crypt circumference using a minimal one-dimensional scheme^{1,2,10}, we developed a model that took into account the two-dimensional organization and potential cellular rearrangements at the crypt base to capture the positional dependence of survival probability (see **Supplemental Theory**). In particular, we modeled the intestinal crypts as a regular two-dimensional cylindrical grid (denoting +0,+1,+2,+3,... as the cell position along the crypt axis). Through numerical analyses, we found that a more faithful geometry that captured the tapered organization of the stem cell compartment at the crypt base did not change significantly our findings. Our modeling strategy was then based on two core processes (sketched in **Figure 2f**): 1) the upward transfer of cells along the crypt axis arising from cell division at rate k_d (with random division orientation and leading to symmetric fate outcome), and 2) a process of random relocation of cells to adjacent rows at rate k_r leading to an exchange of cells either within or between adjacent rows. Notably, since the lateral dispersion of cells through division or exchange involves represents a neutral process, the relative survival advantage of cells along the crypt axis could be captured by considering the effective one-dimensional dynamics along the crypt axis, which we term the stochastic conveyor belt model. This dynamics is a particular case of an Ornstein-Uhlenbeck process with positive drift^{11,12}. Importantly, predictions of this model were found to be insensitive to details of how cell relocation was implemented.

Consistent with the results of the repetitive imaging, the model predicts a decrease in the probability that clones are retained over the long-term as a function of their position along the crypt axis at the time of induction. In particular, an analysis of the clone dynamics shows that this probability takes the form of a simple and Gaussian-like distribution (**Figure 2g**). In particular, the retention probability, and thus stem



cell potential, depends only on the dimensionless ratio between k_r (the rate of random relocation) and k_d (the rate of upward transfer due to cell proliferation). This single free parameter provides a measure of spatial competition, quantifying the relative strength of cell relocation within the niche over advection

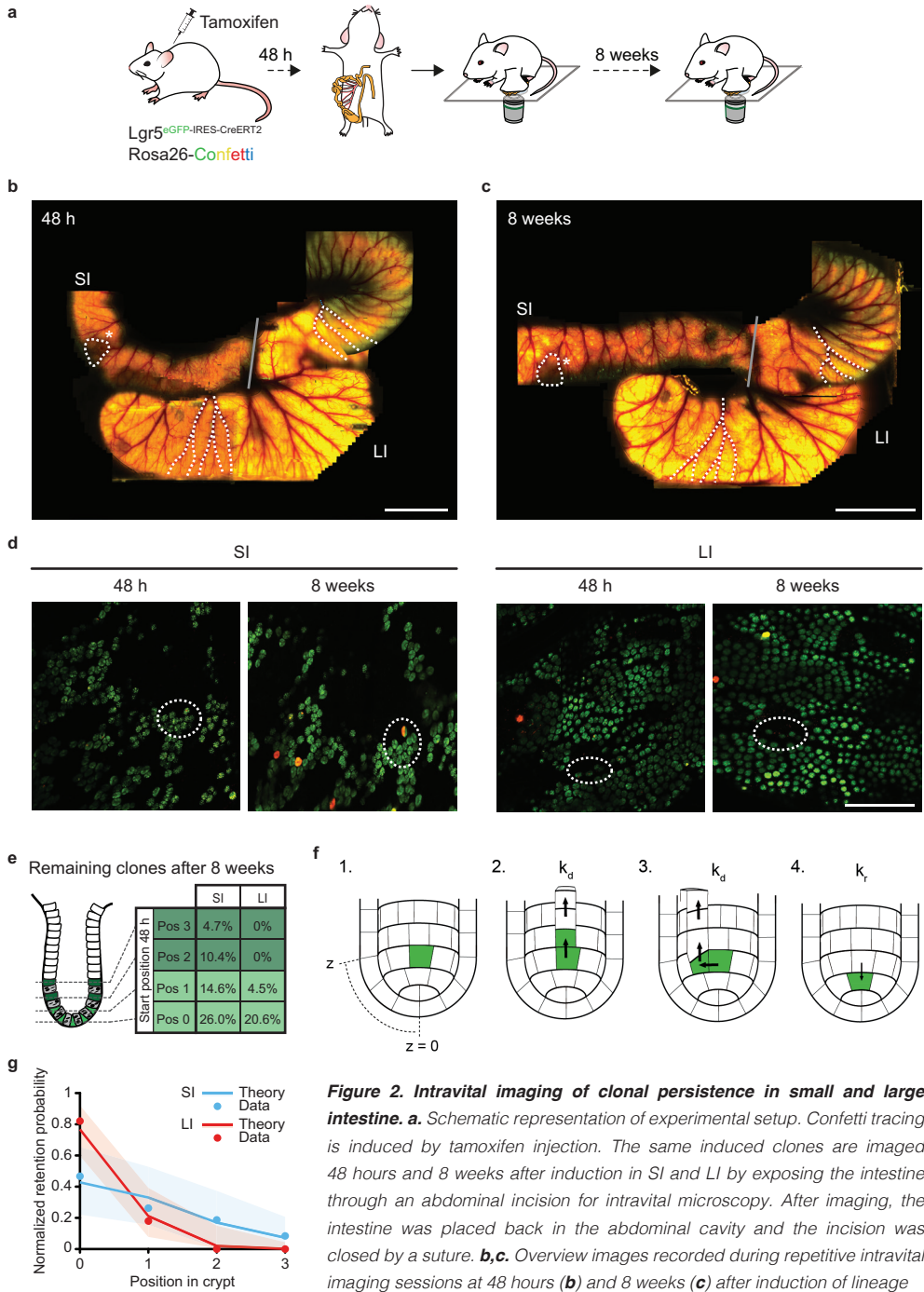


Figure 2. Intravital imaging of clonal persistence in small and large intestine. **a.** Schematic representation of experimental setup. Confetti tracing is induced by tamoxifen injection. The same induced clones are imaged 48 hours and 8 weeks after induction in SI and LI by exposing the intestine through an abdominal incision for intravital microscopy. After imaging, the intestine was placed back in the abdominal cavity and the incision was closed by a suture. **b,c.** Overview images recorded during repetitive intravital imaging sessions at 48 hours (**b**) and 8 weeks (**c**) after induction of lineage

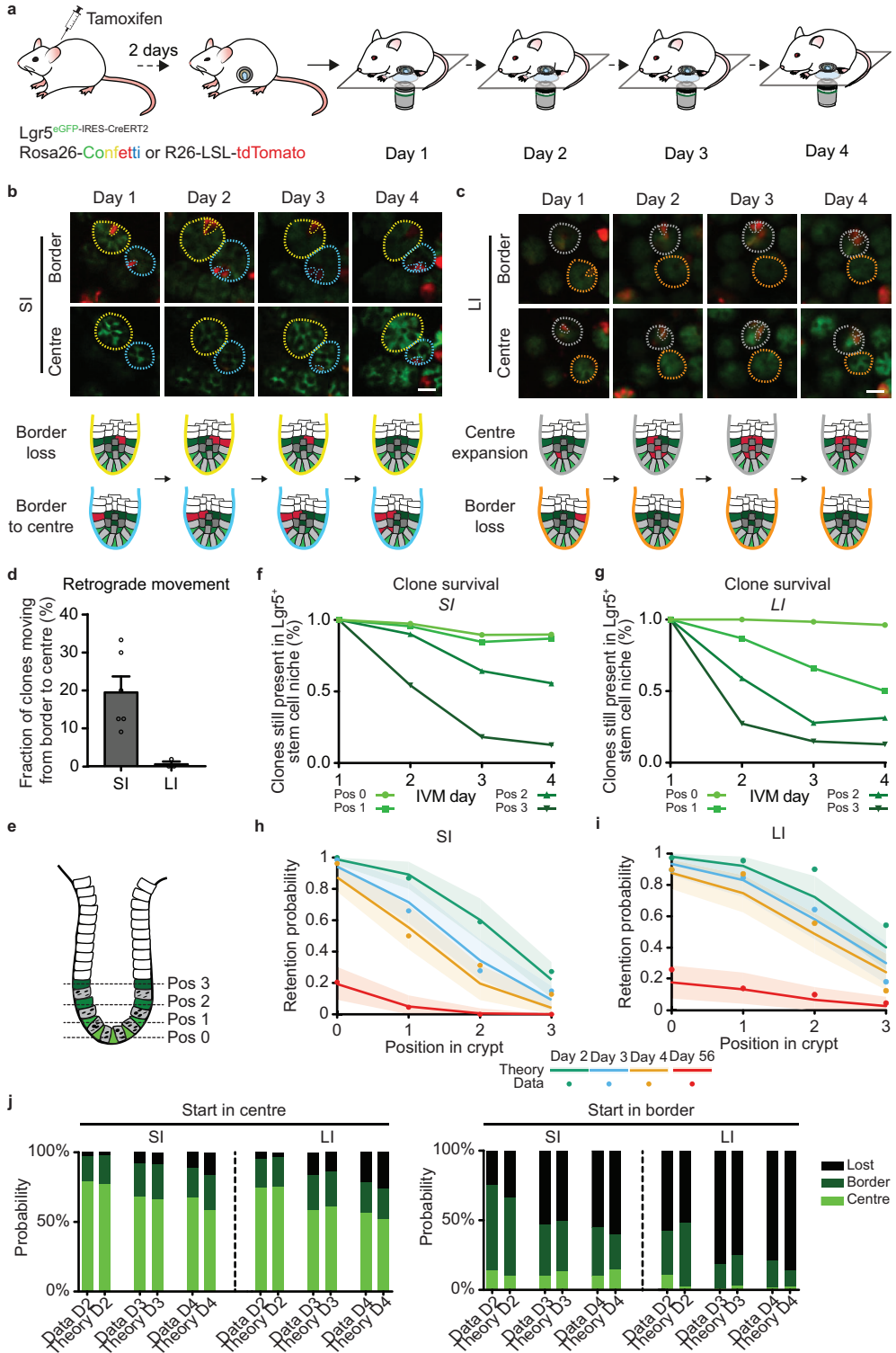
away from the niche centre. From a fit of the predicted Gaussian-like distribution of the clone persistence at the 8 week time point (**Figure 2g**), the ratio of k_r/k_d could be extracted in both the SI and LI ($k_r/k_d=0.3$ in LI and $k_r/k_d=2$ in SI). The higher value of k_r/k_d in the SI, combined with a near equal rate of cell division and therefore upward cell movement (k_d), implies that there is more random repositioning (k_r) in SI crypts than in LI crypts. Due to random repositioning, cells can move down in SI crypts, thereby (re-)gaining a more favorable position for survival in the niche, increasing the stem cell renewal potential. Thus, our modeling shows that the self-renewal potential of cells within the crypt is determined by the retrograde movement of cells (i.e. downward movement in the crypt), implying that stem cell potential is not a binary property, but varies continuously along the axis of the crypt.

Correctly predicted short-term behavior and fate of cells at various positions in the crypt

To test whether there is indeed more retrograde movement of cells in SI crypts than in LI crypts as predicted by our modeling, we performed short-term multi-day intravital microscopy to follow the movement of individual cells over time in living Lgr5GFP-Ires-CreERT2/R26R-Confetti or Lgr5GFP-Ires-CreERT2/R26-LSL-tdTomato mice (**Figure 3a**). Injection of a low-dose of tamoxifen resulted in Cre-mediated recombination and activation of one of the Confetti colours (CFP, YFP and RFP, respectively) or tdTomato, respectively, in individual Lgr5-expressing cells. Using intravital imaging on consecutive days, we monitored cell movement and clonal evolution of cells originally located at central or border locations over time in both the SI and LI (**Figure 3b,c**). The position and clone persistence were determined and quantified. As expected, many clones became lost from the Lgr5-zone over time (**Figure 3b,c**). Moreover, as predicted by our modeling, we observed retrograde movement of labelled cells in crypts of the SI, which was near absent in the crypts of the LI (**Figure 3d**). In line with the differences in retrograde

tracing of SI and LI. The vasculature was used as a landmarks to retrace previously recorded images. Dotted lines represent the same areas in SI and LI. Asterisk shows Peyers patch and grey line indicates boundary between SI and LI. Scale bar, 5 mm. d. Intravital images showing fields of individual Lgr5-expressing crypts. Patterning of Lgr5 expression was used to retrace the same clones 8 weeks (right panels) after the first imaging session (left panels) (retraced areas are indicated by dotted lines). Lgr5-expressing stem cells are marked with eGFP (green). Clones are randomly marked with YFP (yellow), RFP (red) or CFP (blue) driven from the R26R-Confetti locus. Scale bar, 500 μ m. e. Quantification of clone maintenance after 8 weeks of tracing starting from different positions within the stem cell niche in SI and LI. Note that clones starting from large intestinal border cells are lost at 8 weeks of tracing, whereas a fraction of border-started SI clones is still present. SI: n=267 clones in 6 mice; LI: n=294 clones in 6 mice. f. Schematic representation of the model parameters used to study the dynamics underlying clone behaviour in epithelial tissue. The geometry of the intestine crypt is abstracted as a cylinder coupled to a hemispheric region. Each cube represents a cell. 1. A cell is labelled for the study at $t=0$. Its position, $z=3$, in units of cell length, describes the distance to the bottom of the crypt along the coordinate through which advective force due to duplication is exerted. 2. This cell duplicates at rate k_d and its daughter cells can either occupy a position up in the organ and push up the column over the labelled cell or 3. its daughter cell moves to one side of the labelled cells at the same 'level' and it, in turn, pushes up the column of cells located above. 4. Finally, random relocations of cells are expected at rate k_r , and this may imply that, in spite the dominant advection dynamics due to duplication, retrograde movements are possible, thereby giving a non-zero probability for lineages belonging to cells located away from the bottom of the crypt to eventually colonize the entire crypt. g. Normalized retention probability over 8 weeks for cells at different starting position. Lines represent the Gaussian-predictions ($\sim \exp[-k_r/2k_d]$) of the model, shaded regions represent the 95% confidence interval, necessary due to the finite size of data, and dots represent data. Predictions have been obtained from numerical simulations using a grid with periodic boundary conditions. For the SI (blue), we estimate $k_r/k_d \sim 2$, whereas for the LI (red) $k_r/k_d \sim 0.3$.

Chapter 3



movement, we observed that clones were lost faster from border positions of the LI (cell positions +2 and +3) than from border positions of the SI (**Figure 3e-g**). Importantly, when comparing the dynamics to the predictions of our modelling scheme, with values of k_r/k_d determined from the previous fit to the long-term persistence probabilities, we observed a good quantitative agreement at all time points for both the SI and LI (**Figure 3h,i**). Note that the short-term dynamics depends both in the ratio k_r/k_d and on the absolute value of the cell division rate, which was slower than expected in SI with a symmetric division every 3 days. In addition, the model and data showed an excellent quantitative agreement when looking at the movement of clones between centre and border compartments, arguing that (differences in) both short and long-term dynamics in SI and LI can be captured by this simple model (**Figure 3j**). Thus, the analysis of the short-term dynamics corroborate the findings of long-term data and the values of k_r/k_d extracted above, again showing more cellular rearrangement and thus retrograde movement in the SI compared to LI.

The consequence of retrograde movement on monoclonal conversion

The more stem cells compete for space at the base of the crypt, the longer it takes for one clone to outcompete all other cells. Since we observed fewer cells that can function as a stem cell in the LI crypts compared to SI crypts due to less retrograde movement, we hypothesized that monoclonality is reached faster in the LI than in the SI. To test this, we used whole mount preparations of Lgr5eGFP-Ires-CreERT2/R26R-Confetti mice sacrificed at different time points after onset of lineage tracing (**Figure 4a,b**). As predicted from our modeling, we observed differences in clonal expansion over time within the Lgr5+ zone of SI and LI crypts, with faster evolution (growth) of LI clones than SI clones (**Figure 4c**). The observed growth patterns showed that monoclonality was reached faster in the LI than in the SI. Whereas only ~40% of SI crypts was monoclonal at 6 weeks after onset of tracing, the vast majority of large LI crypts were already monoclonal at that time. Importantly, this evolution was quantitatively predicted by the two-dimensional stochastic conveyor belt model (**Figure 4d**), with only the measured ratio k_r/k_d (i.e. stochastic rearrangement/division rate) differing between the regions (while the geometry and average division rate were assumed the same), arguing that the process of crypt monoclonal drift

Figure 3. Intravital imaging of short-term stem cell dynamics in small and large intestine. **a.** schematic representation of experimental setup. Tamoxifen injection induces tdTomato or Confetti labeling of individual Lgr5-expressing cells and their progeny. Implantation of an abdominal imaging window enables intravital monitoring of clonal evolution of labeled cells on multiple consecutive days. **b,c.** Intravital images of clonal evolution of Lgr5-expressing labeled cells (dotted line) starting from central and border positions in crypts of SI (**b**) and LI (**c**). Bottom panels show cells in central region, top panels show cells in border regions. Lgr5-expressing stem cells are marked with eGFP (green). Clones are pseudo-colored (red). Scale bar, 25 μ m. **d.** Quantification of retrograde movement from border to centre region in SI and LI. Mean \pm S.E.M. and dots represent individual mice. **e.** Representation of different cell positions within crypt base. Position 0 and 1 represent centre region, while position 2 and 3 represent the border region. **f,g.** Quantification of intravital imaging of clone survival within the stem cell niche of labelled Lgr5 cells starting from different positions in the niche in SI (**f**) and LI (**g**). SI: n=281 clones in 8 mice; LI: n=350 clones in 5 mice. **h,i.** Probability of a clone to retain in the Lgr5+ zone for the different starting positions (x-axis) over time (solid lines) in SI (**h**) and LI (**i**). Solid lines represent theoretic model predictions, shaded regions represent the 95% confidence interval and dots represent real data. **j.** Probability in percentage of a clone starting either in niche centre (pos. 0 and 1, left panel) or at the niche border (pos. 2 and 3, right panel) to be present in the niche centre, niche border or to be lost from the Lgr5+ zone over time. Data (left bar) and theory (right bar) are compared.

is faster in the LI due to reduced cellular rearrangements, and thus reduced retrograde movement, at the crypt base.

FINAL REMARKS

Stem cells are defined by their potential to self-renew and give rise to differentiated progenies. Traditionally, stem cell potential has been thought to be intrinsic property, characterized by signature expression of molecular markers. However, stem cell potential does not translate to stem cell function⁹. For example, whilst *Lgr5*+ cells in the intestinal crypt have the intrinsic capacity to give rise to all differentiated cell types, and to form *in vitro* organoid cultures, *Lgr5* expression does not necessarily

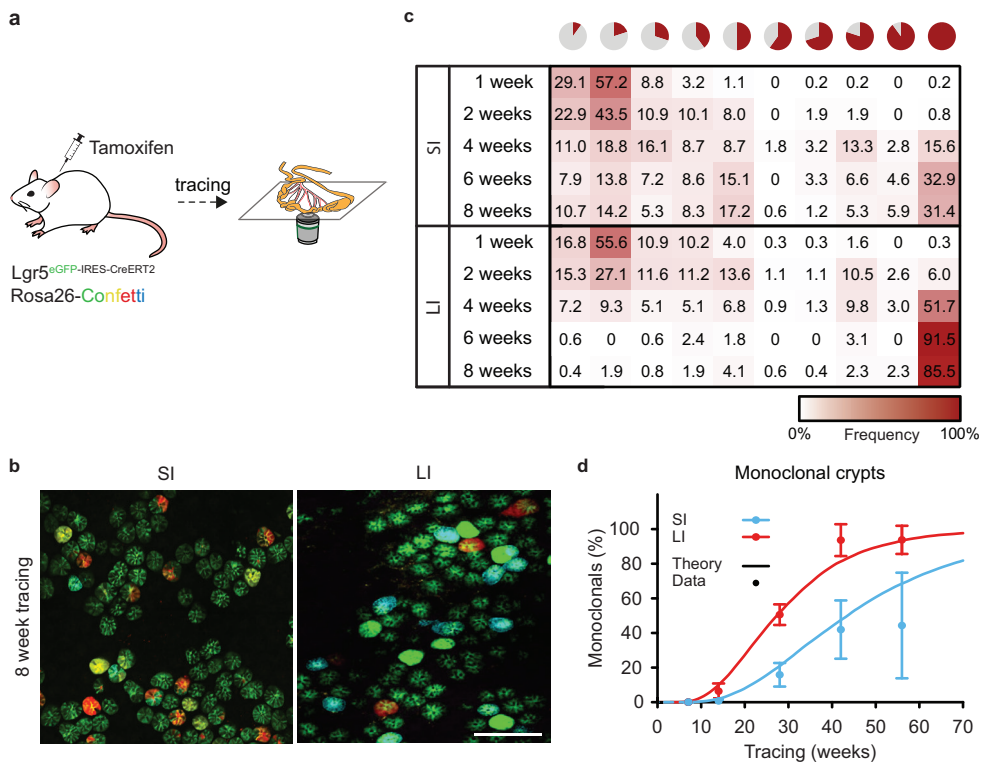


Figure 4. Comparing clonal evolution and fixation speed between small and large intestine. a. Schematic representation of experimental setup. Animals are sacrificed at different time points after induction of lineage tracing. Whole mounts of small and large intestines were imaged to determine clone sizes. **b.** Examples of maximum projections of confocal images of crypt bottoms at 8 weeks after induction of sporadic tracing in SI and LI (SI on the left and LI on the right). *Lgr5*-expressing stem cells are marked with eGFP (green). Clones are randomly marked with YFP (yellow), RFP (red) or CFP (blue) driven from the *R26R-Confetti* locus. Scale bar, 200 μ m. **c.** Heat map showing clonal expansion in stem cell zones of SI and LI over time. Data is presented as percentages of clones with clones sizes indicated above the heat map for each time point. **d.** Quantification of monoclonal crypts (100% labeled) in SI and LI at different time points after induction of labeling. Lines represent theoretic model predictions and dots represent real data. Mean \pm standard deviation and $n > 150$ clones in > 3 mice per time point.

overlap with the ensemble of cells showing functional stem cell activity⁴⁻⁸. Here we have shown that the balance between the rate of random cell repositioning (resulting in retrograde cell movement) and the rate of cell proliferation provides a determinant of the range of functional stem cell potential in the intestinal crypt. We find that, due to a lack of retrograde movement in the LI, Lgr5+ cells at the border of the crypt base (cell positions +2 and +3) are already destined to be displaced irreversibly from the Lgr5+ zone, thereby preventing their long-term self-renewal and production of differentiated progenies. This shows that, in the LI, Lgr5+ border cells do not function as long-term stem cells. By contrast, due to the presence of retrograde movement in the SI, cells at the border of the crypt base, including those outside of the Lgr5 zone, can relocate the crypt base, albeit with diminishing probability, self-renew and give rise to differentiated progenies. We therefore conclude that stem cell identity is not cell-intrinsic that is marked by molecular signatures, but rather a potential that can be gained or lost, and which is highly dependent on the retrograde movement of cells within the crypts.

Based on our experimental data and mathematical modeling, we observed the importance of random cell relocation resulting in retrograde movement for stem cell potential. In our study, we developed a mathematical framework that captures the two-dimensional organization of the crypt, mimicking the mechanism of a conveyor belt with stochastic rearrangements. Our model is based on only a single dimensionless parameter involving the ratio between random cell repositioning and the movement away from the crypt base due to cell division (k_r/k_d). We found that the differential rate of cell repositioning and retrograde movement was the sole factor explaining the differential dynamics underlying competition for niche space in the SI and LI. These differences in stem cell dynamics eventually lead to faster clonal evolution and shorter fixation times in LI compared to SI. In conclusion, despite similarities in crypt architecture, different parts of the intestinal tract not only serve different functions, but also display different stem cell dynamics regulating epithelial turnover as predicted by our modelling. Longitudinal movement of cells is a critical determinant for the acquisition of stem cell potential, allowing cells to gain positions favorable for long-term maintenance and self-renewal capacity. These differences may provide crucial clues to understand known differences in susceptibility to disease along the intestinal tract.

MATERIALS AND METHODS

Mice

All experiments were carried out in accordance with the guidelines of the animal welfare committee of the Netherlands Cancer Institute. For lineage tracing experiments *Lgr5^{eGFP-ires-CreERT2}/R26R-Confetti* and *Lgr5^{eGFP-ires-CreERT2}/LSL-tdTomato* mice were used. Random double heterozygous male and female mice mixed or B16 background were housed under standard laboratory conditions and received standard laboratory chow and water ad libitum. Male and female mice between 8 and 50 weeks of age were used for static lineage tracing and IVM experiments. For whole mount imaging and imaging of isolated crypts, intestines from 8–50 week-old male and female mice were used.

Surgery

All surgical procedures were performed under ~2% isoflurane (v/v) inhalation anesthesia. Before and 8-12 hours after surgery, the mice were treated with a dose of buprenorphine (subcutaneous, 100 µg/kg mouse, Temgesic; BD Pharmaceutical System). Rimadyl (64 µg/ml, Carprofen; Zoetis B.V.) was given in drinking water for 3 days after the surgery. For short-term intravital imaging an AIW was placed as described previously¹³. In short, the left lateral flank of the mouse was shaved and disinfected. An incision was made through the skin and peritoneum of the mouse and a purse string suture was placed along the edge of the wound. The ileum (SI) or cecum (LI) was exposed and a disinfected abdominal imaging window (AIW) (>1h in 70% (v/v) ethanol) was placed on top. In case of the ileum, the mesentery was fixed to the cover glass using Cyanoacrylate Glue (Pattex) and CyGel (BioStatus Limited) was added on top to prevent liquid accumulation. In case of the cecum, it was fixed to the titanium ring of the AIW using Cyanoacrylate Glue (Pattex). After these substances were dry, the intestine and AIW were placed back in the abdominal cavity and the skin and abdominal wall were placed into the groove of the AIW. Subsequently, the suture was tightened. After surgery, the mice were closely monitored daily for reactivity, behavior, appearance and defecation. For repetitive long-term imaging, parts of the intestine that were imaged were exteriorized through a midline abdominal incision. Tissue hydration was maintained by creating a wet chamber, covering the mice with parafilm and the exposed tissue with PBS drenched gauze. After the imaging session placed back in the abdomen and the abdomen was closed using vicryl absorbable sutures (GMED Healthcare BVBA).

Intravital imaging

For every imaging session, mice were sedated by using isoflurane inhalation anesthesia (~1.5% isoflurane/O₂ mixture), and placed in a custom-designed imaging box. For short-term imaging, mice were imaged once a day for a maximum of 3 h. For long-term imaging, mice were imaged 2-3 d after label-induction and 8 weeks thereafter. Z-stacks and overview images were recorded using the Navigator function from Leica. The patchy pattern of the *Lgr5* knock-in allele, in combination with specific landmarks such as blood vessels, allowed repeated identification of imaged areas over consecutive days. After imaging, the acquired images were analyzed using basic functions in ImageJ software.

Whole mount preparation

For whole mount imaging, intestines were harvested and the lumen was flushed with ice-cold PBSO. The tissues were opened longitudinally and for the ileum, villi were removed from the luminal

surface using a cover glass. The tissues were washed in ice-cold PBSO and fixed for 30 min in 4% formaldehyde solution (w/v) (Klinipath) or periodate-lysine-4% paraformaldehyde (PLP) overnight at 4°C¹⁴. For antibody labeling, the tissues were permeabilized in 3% BSA, and 0.8% Triton X-100 in PBS. Subsequently, stretches of ~2 cm of fixed tissue, were mounted between 2 coverslips and embedded in Vectashield HardSet Antifade Mounting Medium (Vector Laboratories). Crypts were imaged from the bottom using the same equipment and settings as for intravital microscopy described below. For storage, PLP fixed tissues were incubated in sucrose for >6 hours and frozen in OCT at -80°C.

Crypt isolation

For crypt isolation, intestines were harvested and lumen was flushed with ice-cold PBS. Tissue was opened longitudinally, villi were removed from the luminal surface of distal ileum. Parts of approximately 3 cm of ileum and intact but opened cecum were incubated with 30mM EDTA in HBSS at room temperature for 20 minutes. After vigorously shaking the release of the epithelium from the mesenchyme was checked using a microscope. Suspensions were filtered (100µm) before spinning down (5 minutes at 4°C, 88 rcf). Pellets containing isolated crypts were washed with cold PBS, fixed in 4% PFA (30 minutes at room temperature), permeabilized in 1% triton X-100 (45 minutes at room temperature), blocked in blocking buffer for 30 minutes at room temperature (1% BSA, 3% horse serum, 0.2% Triton X-100 in PBS) before antibody labeling.

Cell proliferation and antibody labeling

To label cells in S-phase, 1 mg of 5-ethynyl-2-deoxyuridine (EdU, 200 µl in PBS) or 2 mg bromodeoxyuridine (BrdU, 200 µl in PBS) was injected intraperitoneally 4 hours prior to sacrifice. Tissues were processed for whole mount analysis or crypt isolation as described above. Click-it staining reaction was performed according to the manufacturer's protocol (Click-it EdU, ThermoFisher/Invitrogen). For labeling of BrdU incorporation, crypts were incubated in 2N HCl at 37°C for 15 minutes to denature the DNA followed by 15 minutes in 0.1 M sodium borate for neutralization before incubation with BrdU antibody (Abcam, 3626) and GFP-antibody (Abcam, 6673) overnight. To label cells in mitosis phospho-Histone H3 antibody was used (Millipore, 06-570). Stainings were finalized by incubation with alexa secondary antibodies (Invitrogen) combined with DAPI followed by mounting in antifading mounting medium (Vectashield, Vector laboratories).

Microscopy equipment and settings

Tissues were imaged with an inverted Leica TCS SP8 confocal microscope. All images were collected in 12 bit with 25X water immersion objective (HC FLUOTAR L N.A. 0.95 W VISIR 0.17 FWD 2.4 mm).

AUTHOR CONTRIBUTIONS

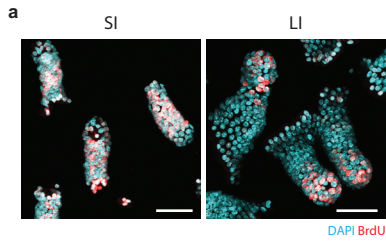
SIJE, LB, EH, HJS and JvR conceived the study. SIJE, LB and SJAL performed the experiments. BCM, BDS, and EH performed the mathematical modeling. All authors contributed to writing and have approved the manuscript.

ACKNOWLEDGMENTS

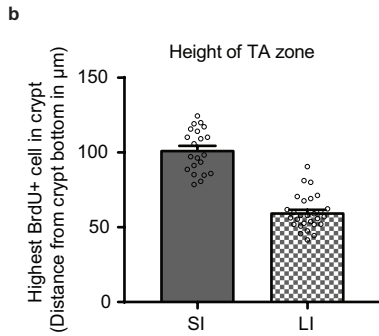
We thank members of the Van Rheezen laboratory for critically reading the manuscript. This work was financially supported by the Netherlands Organization of Scientific Research NWO (Veni grant 863.15.011 to SIJE), European Research Council Grant CANCER-RECURRENCE 648804 (to JvR), and the CancerGenomics.nl (Netherlands Organisation for Scientific Research) program (to JvR) the Doctor Josef Steiner Foundation (to JvR) and the European Union's Horizon 2020 research and innovation program under the Marie Skłodowska-Curie grant agreement No 642866 (both to JvR).

REFERENCES

1. Snippert, H. J. *et al.* Intestinal crypt homeostasis results from neutral competition between symmetrically dividing Lgr5 stem cells. *Cell* **143**, 134–144 (2010).
2. Lopez-Garcia, C., Klein, A. M., Simons, B. D. & Winton, D. J. Intestinal stem cell replacement follows a pattern of neutral drift. *Science* **330**, 822–825 (2010).
3. Barker, N. *et al.* Identification of stem cells in small intestine and colon by marker gene Lgr5. *Nature* **449**, 1003–1007 (2007).
4. Breault, D. T. *et al.* Generation of mTert-GFP mice as a model to identify and study tissue progenitor cells. *Proc Natl Acad Sci* **105**, 10420–5 (2008).
5. Powell, A. E. *et al.* The Pan-ErbB Negative Regulator Lrig1 Is an Intestinal Stem Cell Marker that Functions as a Tumor Suppressor. *Cell* **149**, 146–158 (2012).
6. Sangiorgi, E. & Capecchi, M. R. Bmi1 is expressed in vivo in intestinal stem cells. *Nat. Genet.* **40**, 915–920 (2008).
7. Takeda, N. *et al.* Interconversion Between Intestinal Stem Cell Populations in Distinct Niches. *Science* **334**, 1420–1424 (2011).
8. Barriga, F. M. *et al.* Mex3a Marks a Slowly Dividing Subpopulation of Lgr5+ Intestinal Stem Cells. *Cell Stem Cell* **20**, 801–816.e7 (2017).
9. Ritsma, L. *et al.* Intestinal crypt homeostasis revealed at single-stem-cell level by in vivo live imaging. *Nature* **507**, (2014).
10. Kozar, S. *et al.* Continuous Clonal Labeling Reveals Small Numbers of Functional Stem Cells in Intestinal Crypts and Adenomas. *Cell Stem Cell* **13**, 626–633 (2013).
11. Gardiner, C. W. *Handbook of Stochastic Methods.* (1983).
12. Kampen, N. G. Van. *Stochastic Processes in Physics and Chemistry.* (2007).
13. Ritsma, L. *et al.* Surgical implantation of an abdominal imaging window for intravital microscopy. *Nat. Protoc.* **8**, 583–94 (2013).
14. McLean, I. W. & Nakane, P. K. Periodate lysine paraformaldehyde fixative. A new fixative for immunoelectron microscopy. *J. Histochem. Cytochem.* **22**, 1077–1083 (1974).



Supplementary Figure 1. Visualizing the transit amplifying compartment in SI and LI. **a.** Confocal images of isolated crypts of SI (left), and LI (right) in which proliferating cells were identified by BrdU-incorporation (cells in S-phase, red). Nuclei were labeled using DAPI (blue). Scale bar, 50 μm . **b.** Quantification of the height of the proliferative zone. Dots represent individual crypts.



SUPPLEMENTAL THEORY

Basic dynamics

The simplest abstraction of our system is composed by a column of cells arranged in a finite segment $[0, N]$, in which the length unit is scaled to the average length of a cell. Each cell divides at constant rate k_d . We consider that the system can only grow towards the positive axis and that the density of cells remains constant. This division creates a positive push up force because newly born cells occupy upper adjacent positions in the array, pushing the cells that were there to higher positions. As long as a cell reaches the position N and is pushed, it disappears from the system. The coordinate x or z through which the dynamics take place will depict only the distance to the origin of the organ, without assumptions on the global movement of it: In the crypt that will represent the distance to the bottom. In addition, the position of the cells can fluctuate stochastically at rate k_r (either via local cell-cell rearrangements, or more global movements of cells relative to the niche, see sections below for more details). Importantly, the results that we derive, as described below, are highly generic to different types of assumptions on the microscopic dynamics, as long as the basis features of advection and rearrangements exist in a system.

Single cell dynamics

This process is a mixture of Brownian motion with a given amplitude k_r and a drift parameter that depends on the position. In the continuous limit, the position of the cell, x , can be described as a random variable satisfying the following stochastic equation:

$$dx = k_d x dt + \sqrt{k_r} dW \quad , \quad (1)$$

being dW the differential of the standard Wiener process with mean 0 and variance 1. In other words, we are describing a kind of *Ornstein-Uhlenbeck* process, with positive drift k_d ^{1,2}. The above described stochastic process has no stationary solutions, which is in agreement to the conveyor belt-like dynamics of the systems under study: all cells will sooner or later be pushed out from the system. One can still compute the time-dependent solutions, considering initial conditions $t_0 = 0$, $x_0 = \delta(x - k)$ and natural boundary conditions* as follows: First we observe that:

* A rigorous approach to this problem would require a reflecting boundary condition at $x = 0$. Imposing such boundary condition would make the whole problem much more difficult and, eventually intractable. The reason by which we adopted natural boundary conditions is due to the fact that the dynamics in this system is extremely imbalanced and runs essentially in only one direction. If one takes equation (5) at $x = 0$ we observe that the probability of being at $x = 0$ decays as $\sim e^{-\tau}$, for any starting point $k > 0$, as it is the case in our system. This tells us that the probability of visiting regions $x < 0$ is, to our purposes, negligible.

$$d(e^{-k_d t} X(t)) = dX(t)e^{-k_d t} - k_d e^{-k_d t} X(t) dt \quad .$$

Then, multiplying both sides of equation (1) by $e^{-k_d t}$, and after some algebra, one finds that:

$$d(e^{-k_d t} X(t)) = \sqrt{k_r} e^{-k_d t} dW \quad ,$$

leading to:

$$X(t) = x_0 e^{k_d t} + \int_0^t \sqrt{k_r} e^{k_d(t-s)} dW \quad . \quad (2)$$

The integral is a standard stochastic integral with respect to a *Wiener process*. According to *Ito's isometry*⁸ one has that the law governing the random variable described by the integral is a normal distribution $N(0, \sigma^2(t))$. In our case this reads:

$$\int_0^t e^{k_d(t-s)} \sqrt{k_r} dW \sim N\left(0, \int_0^t |\sqrt{k_r} e^{k_d(t-s)}|^2 ds\right) \quad ,$$

which means that the explicit form of $\sigma^2(t)$, is thus given by:

$$\sigma^2(t) = \int_0^t |\sqrt{k_r} e^{k_d(t-s)}|^2 ds = \frac{k_r}{2k_d} (e^{2k_d t} - 1) \quad . \quad (3)$$

Finally, from equation (2), we conclude that the time dependent mean, $\mu(t)$, is:

$$\mu(t, x_0) = x_0 e^{k_d t} \quad .$$

By setting

$$\tau \equiv k_d t \quad , \quad (4)$$

and $x_0 = k$ as the starting position, one gets the time evolution of the probability distribution of for the position of the random walker which started at k :

$$p_k(x, \tau) = \sqrt{\frac{k_d}{2\pi k_r (e^{2\tau} - 1)}} \exp\left\{-\frac{k_d}{2k_r} \frac{(x - ke^\tau)^2}{(e^{2\tau} - 1)}\right\} \quad . \quad (5)$$

In words, the solution is given by random variable following a normal distribution whose mean and variance run exponentially fast in time through the positive axis. In **Figure 1a** of this SI, we plotted some snapshots of this time dependent probability.

Lineage dynamics

The Fokker-Planck equation accounting for the probability that a given random walker starting at k will be at x at a given time τ —as defined in equation (4)—, for the stochastic process described by equation (1), $p_k(x, \tau)$, is given by:

$$\frac{\partial p_k}{\partial \tau} = -\frac{\partial}{\partial x}(x p_k) + \frac{k_r}{2k_d} \frac{\partial^2 p_k}{\partial x^2} \quad . \quad (6)$$

If we want to study the density of cells of the lineage started by cell k in a given position, $\rho_k(x, \tau)$, we have to take into account that, in a given time step, $\rho_k(x, \tau)$ new cells of the lineage will emerge in such a position. Therefore, to describe the whole process, we need a diffusive part, given by the differential operator $-\frac{\partial}{\partial x}x + \frac{k_r}{k_d}\frac{\partial^2}{\partial x^2}$ of equation (6) and a reactive part, given by $\rho_k(x, \tau)$. To derive the reactive part, we take into account the following reasoning: If the density of a given lineage at position x at time τ is $\rho_k(x, \tau)$, one expects that, in average, new $\rho_k(x, \tau)$ cells will emerge within this interval in a time unit –as it is standard in the exponential growth. So, one has that the equation accounting for the time evolution –in units of $\tau = k_d t$ – of such density is:

$$\frac{\partial \rho_k}{\partial \tau} = -\frac{\partial}{\partial x}(x\rho_k) + \frac{k_r}{k_d}\frac{\partial^2 \rho_k}{\partial x^2} + \rho_k \quad . \quad (7)$$

The above equation is a reaction diffusion equation whose diffusive part observes a Ornstein-Uhlenbeck processes with positive drift and whose reaction part is given by an standard exponential growth. Knowing that the solution of equation (6) is given by $p_k(x, \tau)$ as defined in equation (5), the solution of equation (7), with initial conditions $\rho_k(x, 0) = \delta(k - x)$, is given by:

$$\rho_k(x, \tau) = A \cdot e^\tau p_k(x, \tau) \quad . \quad (8)$$

We observe that, according to equation (8), the term $e^\tau p_k(x, \tau)$ can be safely approximated by

$$e^\tau p_k(x, \tau) \approx \sqrt{\frac{k_d}{2\pi k_r}} \exp\left\{-\frac{k_d}{2k_r}\left(\frac{x - ke^\tau}{e^\tau}\right)^2\right\} \quad . \quad (9)$$

Determination of the integration constant

We observe that, even though random fluctuations in cell positions are allowed, epithelial tissues remain confluent ⁴, and maintain a constant density at homeostasis. This imposes that, in the limit of a continuous array of cells and for $\tau \rightarrow \infty$, the overall density of cells of the site x must stabilize to 1, and must not depend on the position x . We will call that condition the *confluent tissue condition*. Consistent with the above reasoning, we observe that:

$$\int_0^N e^\tau p_x(x', \tau) dx \rightarrow c \in \mathbb{R}^+ \quad .$$

To determine the constant A of equation (8), we impose the *confluent tissue condition*. According to the above equation, this is satisfied by:

$$A \equiv \frac{1}{c} \quad .$$

Let us remark that we consider $x \in [0, N]$. Then, knowing that, in this case:

$$\lim_{\tau \rightarrow \infty} \int_0^N e^\tau p_x(x', \tau) dx = \int_0^N \lim_{\tau \rightarrow \infty} \{e^\tau p_x(x', \tau)\} dx \quad ,$$

we compute the limit, taking into account equation (9):

$$\lim_{\tau \rightarrow \infty} e^{\tau} p_x(x', \tau) = \sqrt{\frac{k_d}{2\pi k_r}} \exp\left\{-\frac{k_d}{2k_r} x'^2\right\} ,$$

which is a gaussian with zero mean and $\sigma^2 = k_r/k_d$. so that:

$$\begin{aligned} c &= \int_0^N \sqrt{\frac{k_d}{2\pi k_r}} \exp\left\{-\frac{k_d}{2k_r} x^2\right\} dx \\ &= \frac{1}{2} \operatorname{erf}\left(N \sqrt{\frac{k_d}{2k_r}}\right) \\ &\approx \frac{1}{2} , \end{aligned}$$

where $\operatorname{erf}(x)$ is the *error function*. The approximation $c \approx 1/2$ holds as soon as $N \gg 1$. Therefore, in that approximation, $A = 2$.

By setting the integration constant $A = 2$, the process fills up space in a correct manner that is: The density of cells is always conserved as 1 cell \times length unit, as expected for a confluent homeostatic tissue. The final expression for $\rho(k, \tau)$ will thus be:

$$\rho_k(x, \tau) \approx \sqrt{\frac{2k_d}{\pi k_r}} \exp\left\{-\frac{k_d}{2k_r} \left(\frac{x - ke^{\tau}}{e^{\tau}}\right)^2\right\} . \quad (10)$$

In **Figure 1b** of this SI we plotted some snapshots of this time dependent density.

Lineage survival probability

The first task is to demonstrate that the above dynamics leads, in the long term, to a system composed by descendants of the same cell, i.e. that only a single lineage is present in the system for $\tau \gg 1$. In the case of a 1D system defined over the interval $[0, N]$ with $k_r = 0$, this result is trivial, since the lineage of the cell located at the bottom of the system will occupy the whole system whenever it has divided enough times to cover all the positions from 0 to N . In the case $k_r > 0$, the strategy to see that it runs towards monoclonality is the following: Let Ω_N be all the potential configurations the system can have in terms of lineage configuration whenever the system has 2, 3, ..., N lineages alive. That is $\sigma \in \Omega_N$ will be a sequence of N numbers each labelling the lineage the cell in a given position belongs to:

$$\sigma = \sigma^1, \dots, \sigma^N ; \quad \sigma^k \in \{0, 1, \dots, N\} .$$

In units of τ and given a configuration σ of lineages, for $\Delta\tau > \frac{1}{k_d} \log_2 N$ all the cells will potentially have produced more than N new cells. Therefore, the probability that a lineage has been expelled by the system will be larger than zero. Let us call this probability $p(\downarrow, \Delta\tau)$. Let us define \tilde{p}_Ω as:

$$\tilde{p}_\Omega = \min_{\sigma \in \Omega} \{p(\downarrow, \Delta\tau)\} ,$$

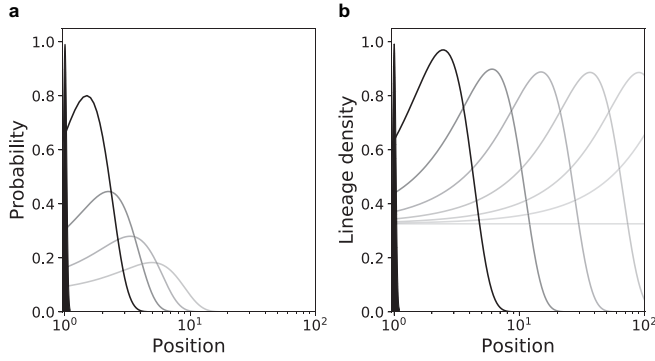


Figure 1 - Temporal evolution of the stochastic conveyor belt dynamics (black to grey indicates time). **a.** Evolution in time of the probability for cells starting at a given position to occupy the location x according to the theoretical prediction given by equation (5). Observe that the dynamics does not run to a stationary state, so all cells will eventually abandon the system with probability 1 as long as time grows. **b.** Evolution in time of the density of a lineage starting in the same position across all positions, according to the solution of the reaction diffusion equation (7) given in equation (10). Observe that the reaction diffusion dynamics displays a front that runs exponentially towards the outside of the system. However, we observe that the density reaches a non-zero stationary value, that is proportional to the probability of the lineage to remain and colonize the whole system. The initial black, elongated triangle at position 1 shows the initial conditions i.e., $k = 1$ and $k_r = 1$, $k_d = 1$. These values have been chosen only for the sake of clarity.

that is, the configuration for which the probability of losing a lineage after $\Delta\tau$ steps is minimum. By construction, we know that from whatever configuration containing more than a single lineage has a non-zero probability of losing at least one of them after $\Delta\tau$, so:

$$\tilde{p}_n > 0 \quad .$$

The probability of not losing any lineage whatever the configuration of the system after n steps of duration $\Delta\tau$, $p(=, n\Delta\tau)$ will be bounded as:

$$0 \leq p(=, n\Delta\tau) \leq (1 - \tilde{p}_n)^n \quad ,$$

and the probability of losing at least one lineage will be bounded as well as:

$$1 \geq p(\downarrow, \Delta\tau) \geq 1 - (1 - \tilde{p}_n)^n \quad .$$

In consequence,

$$\begin{aligned} p(=, n\Delta\tau) &\rightarrow 0 \\ p(\downarrow, \Delta\tau) &\rightarrow 1 \quad . \end{aligned}$$

Since the loss of a lineage is a completely irreversible process, the above equation tells us that it is expected that the system will lose lineages until only one survives. Note that for a 2D geometry but $k_r = 0$, the system reduces to the stochastic voter model along a 1D ring (the N_0 cells at position 0) which was proposed and tested experimentally in Ref. 5, and where the process of monoclonal conversion is diffusive, occurring on time scales of N_0^2/k_d .

Now that we know that the system will reach monoclonality, the next question is to ask which lineage will win the competition. In particular, we are interested in the probability that a given lineage colonizes the whole system as a function of the position of the cell that defined the lineage at $t = 0$. To that end, we first compute the asymptotic lineage density, $\rho_k(\infty)$, that reads:

$$\rho_k(\infty) \equiv \lim_{\tau \rightarrow \infty} \rho_k(x, \tau) = \sqrt{\frac{2k_d}{\pi k_r}} e^{-\frac{k_d}{2k_r} k^2} . \quad (11)$$

We observe that this density is independent of x –see **Figure 1b** of this SI. Now we make the following assumption: The competition between cells at different levels term is absorbed in a mean field approach by the drift push-up force. In this context, we conclude that the probability of lineage survival $p(c_k)$ –that is, the probability that the whole tissue from 0 to N will be occupied by cells of the lineage k – can be derived directly from the normalization of the asymptotic densities $\rho_k(\infty)$:

$$p(c_k) \propto \frac{\rho_k(\infty)}{\sum_j \rho_j(\infty)} ,$$

which leads to:

$$p(c_k) = \frac{1}{Z_N} \exp\left\{-\frac{k_d}{2k_r} k^2\right\} , \quad (12)$$

being Z_N the normalization constant, namely, $Z_N \equiv \sum_{j \leq N} \exp\left\{-\frac{k_d}{2k_r} j^2\right\}$.

Time dependent clone survival probability

We work under the assumption that the exclusion principle governing site positions and the correlations arising from the duplication dynamics vanish if we take an ensemble picture. In that frame, the strength of a given lineage is assumed to be proportional to the density. Therefore, the probability for a lineage k to survive after time τ , $p(c_k, \tau)$ will observe the following relation:

$$\frac{p(c_k, \tau)}{p(c_0, \tau)} = \int_0^L \rho_k(x, \tau) dx \left(\int_0^L \rho_0(x, \tau) dx \right)^{-1} . \quad (13)$$

Dynamics in more general geometries

In general we will assume that there is a coordinate z over which the displacement induced by the division takes place. All the dynamics will be, in consequence, studied from its projection over this coordinate –see **Figure 2** of this SI for the special cases of hemispheric and spheric geometries. In the case of a 1D-system, as the one described above, this coordinate is the length, x . In the case of a hemisphere, assuming that the push-up force is exerted from the bottom pole, this coordinate is the arc length defined from the position of the cell to the bottom pole itself –see **Figure 2a** of this SI. To gain intuition, consider the surface of the hemisphere with radius R : The cells at the bottom pole divide and push the ones on top of them up through the surface. The cell under consideration is located at whatever position defining an arc from the bottom pole equal to $z = R\varphi_k = z_k$, where φ_k is the polar angle, meaning that there is an arc of k cells from the given cell to the pole of the hemisphere –see **Figure 2a**

of this SI. The successive divisions of cells located at $z_i < z_k$ will result into a net displacement along the angular coordinate φ of the cell located initially at $z_k = R\varphi_k$, going from $z_k = R\varphi_k$ to $z_{k'} = R\varphi_{k'}$, with $\varphi_{k'} > \varphi_k$. The linear displacement along the surface will be $\Delta z = R(\varphi_{k'} - \varphi_k)$. Displacements along the other coordinate will have no effect in the push up force.

Drift term

The push-up force or drift term will be described by the function $h(z)$, and will be defined as:

$$h(z) = \frac{dz}{dt} \quad . \quad (14)$$

In the case of a 1D-system, as the one described by equation (7), one has that $h(z) = k_d z$. To properly study these dynamics over more general geometries, let us consider a Riemannian manifold equipped with a metric tensor g , with components g_{ij} ⁶. Crucial to our purposes is the property of *local flatness*^{6,7}. Roughly speaking, this implies that, for small enough regions of the manifold, the geometry has euclidean properties. Let us consider that the push up force due to duplications has an origin and is exerted along the direction of a single coordinate z as well. As we did above, the surface/volume units are given such that an average cell has a surface/volume of 1 in the corresponding units. Consider the starting position of our cell to be z_k along the coordinate z along which the displacement due to the push up force takes place. If the other coordinates are given by x_1, \dots, x_{n-1} , the surface/volume encapsulated below this position is given by:

$$S_k = \int \dots \int_0^{z_k} \sqrt{g} dx_1 \dots dz \quad ,$$

where g is the determiner of the metric tensor, i.e.:

$$g = \begin{vmatrix} g_{11} & g_{12} & \cdot & \cdot & \cdot \\ g_{21} & g_{22} & & & \\ \cdot & & \cdot & & \\ \cdot & & & \cdot & \\ \cdot & & & & \cdot \end{vmatrix}$$

Cells are assumed to divide at rate k_d . That implies that $k_d S_k$ new cells will be produced below the cell located at z_k . This will create an extra surface/volume of:

$$\frac{dS_k}{dt} = k_d S_k \quad ,$$

that will project into the coordinate z . Using that:

$$\frac{dS_k}{dt} = \frac{dS_k}{dz} \frac{dz}{dt} \quad ,$$

and, then, equation (14), one can find the general expression for this projection, which reads:

$$h(z) = k_d \left(\frac{dS_k}{dz} \right)^{-1} S_k \quad . \quad (15)$$

Projection of the fluctuations

We are only interested on the projection of the dynamics over the coordinate z along which the system grows, as in the other coordinates the competition is neutral and has no net effect in the lineage survival statistics. If the reported fluctuations are k_r , we will refer to the projection to the coordinate z as k_r^z . In general, k_r^z will be a function $k_r^z = f(k_r, z)$. According to the above results, we will have that the general equation for the evolution of cell lineage densities along the coordinate z will read:

$$\frac{\partial \rho_k}{\partial t} = -\frac{\partial}{\partial z}(h(z)\rho_k) + \frac{k_r^z}{2} \frac{\partial^2 \rho_k}{\partial z^2} + \rho_k \quad . \quad (16)$$

In the case $h(z)$ can be approached as a linear function, i.e., $h(z) \sim ak_d z$ and k_r^z as $k_r^z = bf(k_r)$, one can reproduce the reasoning provided to derive the lineage survival probability, equation (12), and obtain:

$$p(c_k) \propto \exp\left\{-\frac{a}{2b} \frac{k_d}{f(k_r)} k^2\right\} \quad .$$

To gain intuition, imagine that we report experimental fluctuations of amplitude k_r –see **Figure 3** of this SI. That is, in a time unit, the cells move randomly over the manifold k_r steps. We are in a 2D isotropic, locally flat surface with generic orthogonal coordinates y, z –for example, $R \times$ the azimuthal angle θ and $R \times$ the polar angle φ over a sphere surface. The amplitude of the fluctuations after time t is known to be $\sim \sqrt{k_r t}$, a distance defined over the surface. In the case we consider the projection over the coordinate z , thanks to the local flatness⁷, assuming that $\sqrt{k_r} \ll R$ and using only symmetry reasonings, one has that since the displacement is given by $(\Delta y, \Delta z) = (\sqrt{k_r^y}, \sqrt{k_r^z})$:

$$\sqrt{(\sqrt{k_r^y})^2 + (\sqrt{k_r^z})^2} = \sqrt{k_r} \quad ,$$

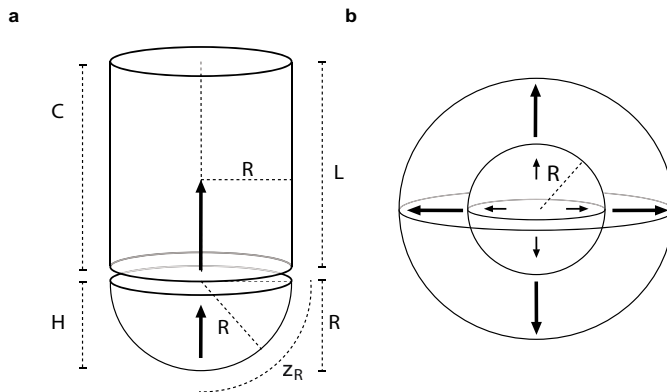


Figure 2 - Schematic representation of the crypt a. Schematic characterization of the structure of the crypt as a hemispherical region H coupled to a cylinder region of the same radius, R . **b.** The expansion of the tissue in a 3D abstract setting where there is radial symmetry. The growing of the inner cells creates a push up force. In addition, the stochastic fluctuations in the position determine the probability of lineage survival as a function of the starting point, as in the case of low dimensional approaches.

and the fluctuations are isotropic, then:

$$k_r^z = k_r^y \quad ,$$

and the only solution to the above problem is that:

$$k_r^z = \frac{k_r}{2} \quad . \quad (17)$$

In the case we are dealing with a spherical surface, we are projecting the fluctuations over the polar angle $z = R\varphi$ –see **Figure 3** of this SI. The stochastic differential equation that will describe the movement of a single cell in this manifold will be, for $z \leq \frac{\pi}{2}R$:

$$dz = h(z)dt + \sqrt{\frac{k_r}{2}} dW \quad ,$$

where dW is the differential of the standard Brownian motion with average 0 and variance 1 in one dimension.

Evolution of densities: Hemispherical approach

Let us now consider a detailed version of the geometry of the crypt. This consists in a half sphere, H , whose arc length from the bottom pole to the end is $z_R = \frac{\pi}{2}R$ coupled to a cylinder C of length L and radius R . The cells populate both the surface of the hemisphere and the cylinder. The push-up force is directed towards the top of the cylinder –see **Figure 2a** of this SI. In the arc that goes from the bottom pole to the end of the hemisphere there are z_R cells. Again, the units are given considering the average size of the cell as the length/surface/volume unit. Therefore, the cells will be labelled in terms of the geodesic distance over the hemisphere to the bottom pole. The density of the lineages will be given by:

$$(\rho_0, \rho_1, \rho_2, \dots, \rho_{z_R-1}, \rho_{z_R}) \quad .$$

Since the coordinate R is constant, the only dynamically relevant information will come from the angle φ . Each position k in the arc $(0, 1, 2, \dots, z_k, \dots, z_R - 1, z_R)$ describing the initial point of a cell lineage can be rewritten as:

$$z_k = R\varphi_k \quad , \quad \varphi_k \in \left(0, \frac{\pi}{2}\right) \quad .$$

i.e., $\varphi_k = \frac{z_k}{R}$. The metric tensor for this hemispheric surface is:

$$g = \begin{pmatrix} R^2 & 0 \\ 0 & R^2 \sin^2(\varphi) \end{pmatrix} \quad .$$

Computing the determiner of g , g :

$$g = \begin{vmatrix} R^2 & 0 \\ 0 & R^2 \sin^2(\varphi) \end{vmatrix} = R^4 \sin^2 \varphi \quad .$$

one can compute the surface element as ⁷:

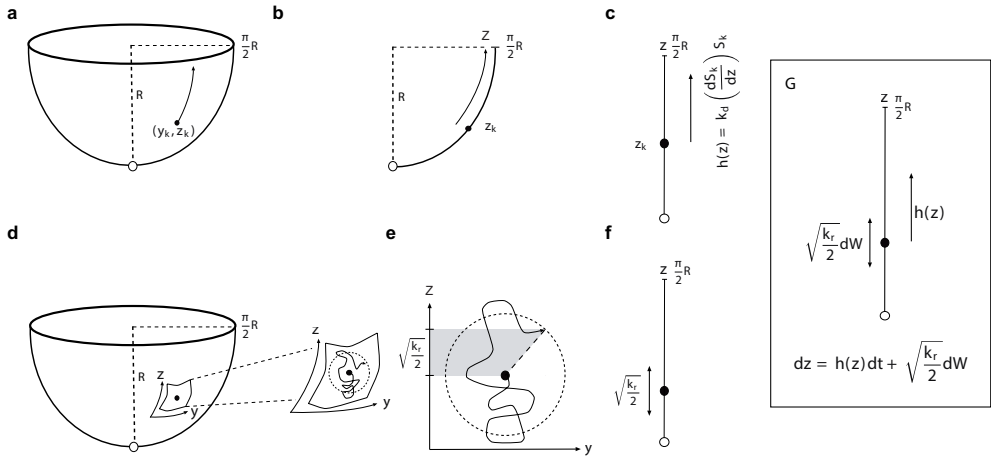


Figure 3 – Constructing the dynamical equation for a general kind of manifold and projecting it onto the 1D coordinate system along which the push-up force is exerted. a. A cell is located in a point in a manifold –in that case, a hemisphere–, described by two orthogonal coordinates y_k, z_k . In this case $y_k = R\theta_k$, where θ is the azimuthal angle, and $y_k = R\varphi_k$, where φ is the polar angle. **b.** the push up force due to duplication is only exerted along the z coordinate. **c.** $h(z)$ is the drift term that enters the equation, and refers to the amount of new surface that has been created below the point z_k in the z coordinate that results in pushing up the cells above. **d.** the same point y_k, z_k also observes fluctuations due to random noise. In particular, the rate of these fluctuations is externally reported as k_r . **e.** Thanks to the local flatness property, if $\sqrt{k_r} \ll R$, then the fluctuations take place locally in a flat space, and the average distance from the starting point, after a unit time interval, will be $\sqrt{k_r}$. Since the coordinate system y, z is orthogonal and locally flat, and the random fluctuations occur isotropically in space, the projection of the fluctuations over the coordinate y, k_r^y , will be the same than in the coordinate z, k_r^z . Since $\sqrt{k_r} = \sqrt{k_r^y + k_r^z}$, the only solution for this projection is that, $k_r^z = k_r/2$, as described in **(f)**. **g.** Combining **(c)** and **(f)** we have that the growing process can be described along the z coordinate as a Ornstein-Uhlenbeck process with push up force $h(z)$ and random fluctuations $\sqrt{\frac{k_r}{2}} dW$, where dW is the standard Brownian motion with mean 0 and variance 1.

$$dS = \sqrt{g} d\theta d\varphi \quad .$$

In consequence, the area under the position of the cell k in the in the hemisphere H , located at the arc position z_k , will be:

$$S_k^H = \int_0^{2\pi} \int_0^{\frac{z_k}{R}} \sqrt{g} d\theta d\varphi = 2\pi R^2 \left(1 - \cos\left(\frac{z_k}{R}\right) \right) \quad .$$

By direct application of equation (15), we have that the push-up force inside the hemisphere H is given by:

$$h^H(z) = k_d R \left[\frac{1 - \cos\left(\frac{z}{R}\right)}{\sin\left(\frac{z}{R}\right)} \right] \quad . \quad (18)$$

Finally, from equation (17) we know that –see also **Figure 3** of this SI:

$$k_z^2 = \frac{k_r}{2} ,$$

leading, according to equation (16) to the general dynamical equation for $0 \leq z \leq \frac{\pi}{2}R$ in a hemispherical surface to be:

$$\frac{\partial \rho_k}{\partial t} = -k_d R \frac{\partial}{\partial z} \left(\frac{1 - \cos\left(\frac{z_k}{R}\right)}{\sin\left(\frac{z_k}{R}\right)} \rho_k \right) + \frac{k_r}{4} \frac{\partial^2 \rho_k}{\partial z^2} + \rho_k . \quad (19)$$

The above equation is difficult to deal with. However, we observe that in the region of interest, $z \in \left[0, \frac{\pi}{2}R\right]$, equation (18) can be approximated as:

$$\tilde{h}(z) \sim \frac{2k_d}{\pi} z , \quad (20)$$

leading to an error bounded as:

$$\max_{z \in \left[0, \frac{\pi}{2}R\right]} \left| \left| h(z) - \frac{2k_d}{\pi} z \right| \right| < 0.09 k_d R ,$$

according to numerical tests. With this approximation, we have that equation (19) can be rewritten approximately as:

$$\frac{\partial \rho_k}{\partial t} \approx -\frac{2k_d}{\pi} \frac{\partial}{\partial z} (z \rho_k) + \frac{k_r}{4} \frac{\partial^2 \rho_k}{\partial z^2} + \rho_k , \quad (21)$$

which is the general kind of Ornstein-Uhlenbeck equations we have been working so far.

Coupling to a cylinder

In the case the cell is at the position k in the cylindrical region \mathcal{C} , the area under it will be given by $S_{\frac{\pi}{2}R}^H$, the area of the whole hemisphere, and the remaining surface due to the cell is the cylinder. Knowing that for the cylindrical coordinates $\sqrt{g} = R$, then:

$$S_k^{\mathcal{C}} = S_{\frac{\pi}{2}R}^H + \int_0^{2\pi} d\theta \int_{\frac{\pi}{2}R}^{z_k} \sqrt{g} dz = S_{\frac{\pi}{2}R}^H + 2\pi R \left(z_k - \frac{\pi}{2}R \right) .$$

Completing the picture, the push force felt by a cell in the cylindrical region \mathcal{C} is given by:

$$h^{\mathcal{C}}(z) = k_d \left(z_k + \left(1 - \frac{\pi}{2}\right) R \right) . \quad (22)$$

It is easy to check that:

$$\begin{aligned} \lim_{z \rightarrow \frac{\pi}{2}R^+} h^H(z) &= \lim_{z \rightarrow \frac{\pi}{2}R^-} h^{\mathcal{C}}(z) \\ \lim_{z \rightarrow \frac{\pi}{2}R^+} \frac{d}{dz} h^H(z) &= \lim_{z \rightarrow \frac{\pi}{2}R^-} \frac{d}{dz} h^{\mathcal{C}}(z) . \end{aligned}$$

Therefore, one can define a function, $h(z)$ as:

$$h^{H,C}(z) = \begin{cases} h^H(z) & \text{if } z \leq \frac{\pi}{2}R \\ h^C(z) & \text{if } z > \frac{\pi}{2}R \end{cases} , \quad (23)$$

which is always well defined. In addition, the projection of the fluctuations will be the same in both regions, since the only relevant property is the local dimension, which in both cases is 2, leading to a $k_r^z = k_r/2$. Consequently, equation (16) can be rewritten consistently for all the hemisphere/cylinder system as:

$$\frac{\partial \rho_k}{\partial t} = -\frac{\partial}{\partial z}(h^{H,C}(z)\rho_k) + \frac{k_r}{4} \frac{\partial^2 \rho_k}{\partial z^2} + \rho_k \quad . \quad (24)$$

Lineage survival: Detailed geometry approach

To guess the probability of lineage survival, we restrict ourselves to the hemispheric region H of the crypt. As discussed in section 'Dynamics in more general geometries' of this SI, the existence of linear functions approximating the drift and fluctuation parameters of the general reaction-diffusion equation (16) leads to gaussian-like lineage survival probabilities. According to the approximations leading to equation (21), we have that, considering the hemispheric region of the crypt:

$$p(c_k) \propto \exp\left\{-\frac{2k_d}{\pi k_r}k^2\right\} \quad . \quad (25)$$

Coupling to a cluster with different k_d

In this section we deal with the case where the duplication rate is not constant throughout the organ. Specifically, we consider the case where the cells located at $(0, \ell)$ duplicate at rate k_d and the cells located at positions $(\ell + 1, L)$ duplicate at rate k_d' . We consider that $k_d' < k_d$. The push-up force sensed by these cells corresponds to the division of the first cluster, resulting into ℓk_d and the push up force caused by the cells belonging to the second cluster yet under the cell under study, namely $(z - \ell)k_d'$, with $z > \ell$. In this region, the stochastic dynamics will be governed by the following Langevin-like equation:

$$\frac{dZ}{dt} = \ell k_d + (Z - \ell)k_d' + \sqrt{k_r} \frac{dW}{dt} \quad . \quad (26)$$

To solve this equation, we perform the following coordinate change:

$$Z \rightarrow U = \ell \left(\frac{k_d}{k_d'} - 1 \right) + Z \quad ,$$

one observes that:

$$\frac{dU}{dt} = \frac{dZ}{dt} \quad ,$$

since the term $\ell \left(\frac{k_d}{k_d'} - 1 \right)$ is constant. Therefore, one can rewrite equation (26) as:

$$\frac{dU}{dt} = k_d' U + \sqrt{k_r} \frac{dW}{dt} .$$

In this context, the reaction-diffusion equation accounting for the lineage density at the region $z > \ell$, implying $u > \ell \left(\frac{k_d}{k_d'} \right)$, reads:

$$\frac{\partial \rho_k}{\partial t} = -k_d' \frac{\partial \rho_k}{\partial u} (u \rho_k) + \frac{k_r}{2} \frac{\partial^2 \rho_k}{\partial u^2} + k_d' \rho_k . \quad (27)$$

We need to also rescale the starting position k into the new coordinate system. In this new frame:

$$k \rightarrow k_u = k + \ell \left(\frac{k_d}{k_d'} - 1 \right) .$$

Then, the solutions of equation (27) are of the form:

$$\rho_k(u, t) \propto e^{k_d' t} \sqrt{\frac{k_d'}{2\pi k_r (e^{2k_d' t} - 1)}} \exp \left\{ -\frac{k_d'}{2k_r} \frac{(u - k_u e^{k_d' t})^2}{e^{2k_d' t} - 1} \right\}$$

Notice that the above equation is defined in the space defined by the coordinate $u = z + \ell \left(\frac{k_d}{k_d'} - 1 \right)$.

The coupling to a non-dividing cluster

A case of particular interest is corresponding to the $k_d' \rightarrow 0$, which would describe a non-dividing cluster. In this frame, the dynamics would correspond to a Brownian motion with drift parameter $k_d \ell$. Indeed, let us use the following approach for small x :

$$e^x = 1 + x + \dots ,$$

and the following identity, derived from the coordinate change:

$$\begin{aligned} u - k_u(1 + k_d' t) &= \ell \left(\frac{k_d}{k_d'} - 1 \right) + z - \ell \left(\frac{k_d}{k_d'} - 1 \right) - \\ &\quad - k - k_d \ell t + (z - \ell) k_d' t \\ &= z - k - k_d \ell t + (z - \ell) k_d' t , \end{aligned}$$

which leads to:

$$\lim_{k_d' \rightarrow 0} (u - k_u(1 + k_d' t)) = z - k - k_d \ell t . \quad (28)$$

With the above result one is led, after some algebra, to:

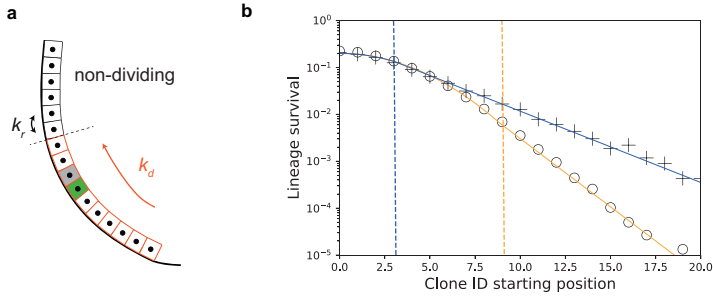


Figure 4 – a. Schematic of the model of stochastic conveyor belt with two regions: a dividing region (red) with rate k_r and a non-dividing region (black). Both regions experience random intercalation at the same rate k_r , assumed constant. **b.** Numerical simulations of the steady state survival probability of a lineage as a function of its starting position, for the non-dividing starting either at position $n^* = 3$ (crosses and blue dashed lines), or at position $n^* = 9$ (dots and orange dashed lines). Full lines display the fit of the model (Gaussian distribution in the dividing region and exponential distribution in the non-dividing region), showing excellent agreement.

$$\lim_{k_d \ell \rightarrow 0} \rho_k(u, t) = \sqrt{\frac{1}{4\pi k_r t}} \exp\left\{-\frac{1}{4k_r t} (z - k - k_d \ell t)^2\right\} ,$$

The above equation corresponds, as expected, to a Brownian motion with drift parameter $k_d \ell$. In particular:

$$\frac{p(c_k, \infty)}{p(c_\ell, \infty)} = \exp\left\{-\frac{k_d}{2k_r} (k - \ell)\ell\right\} . \quad (29)$$

Under the assumption of continuity, one has that, if the dynamics runs until position ℓ with the k_d :

$$\frac{p(c_\ell, \infty)}{p(c_0, \infty)} = \exp\left\{-\frac{k_d}{2k_r} \ell^2\right\} ,$$

leading to a prediction for the survival of the lineages from the non-dividing cluster –i.e., $k > \ell$ – of:

$$\frac{p(c_k, \infty)}{p(c_0, \infty)} = \exp\left\{-\frac{k_d}{2k_r} k\ell\right\} . \quad (30)$$

In **Figure 4** of this SI we confront the above result with numerical simulations, obtaining an excellent fit.

Noise in the stochastic conveyor-belt from “tectonic” epithelial movements

In this section, we explore an alternative source for noise in determining the number of functional stem cells, i.e. the possibility of global rearrangements of the epithelium relative to the optimal position (bottom of the crypt/edge of the tip –see **Figure 5a** of this SI for a sketch. This is motivated by observations in experiments in intestinal morphogenesis.

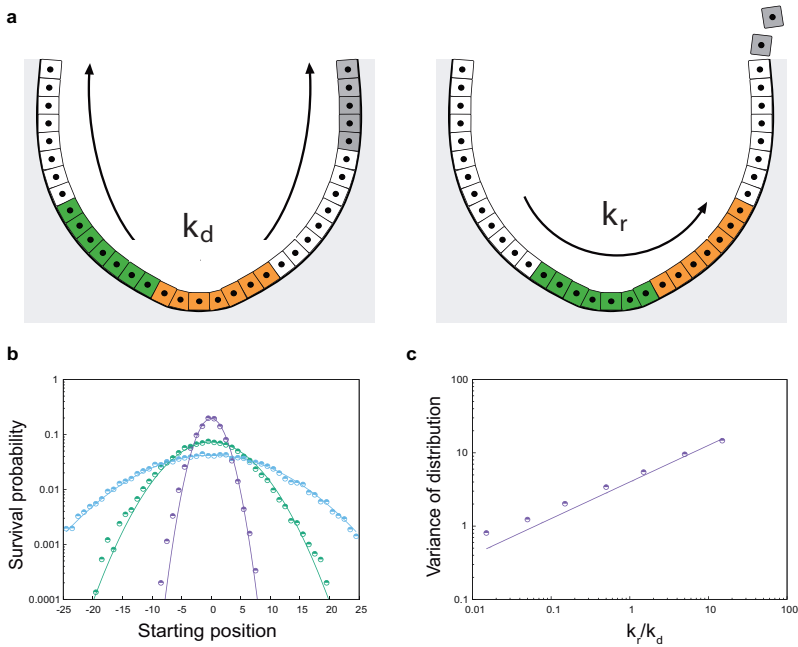


Figure 5 – a. Schematic of the model of stochastic conveyor belt with tectonic movements: cell division can occur for every cell, which pushes all cells above, but repositioning relative to the bottom of the crypt/tip can only occur via global movements of the layer, at rate k_r , (two clones shown competing before and after a movement). **b.** Computational predictions of the 1D stochastic conveyor belt dynamics in the presence of tectonic movements, with increasing rates k_r (purple to blue), in terms of survival probability as a function of starting position of the clone. All curves are very well fitted by normal distributions, as expected by our model. **c.** Variance of survival probability as a function of starting position (i.e. functional stem cell number) as a function of the tectonic movements rates normalized by division rate k_r/k_d (dots), and theoretical prediction ($\sqrt{k_r/k_d}$, continuous line) from the stochastic conveyor belt model, showing that the system undergoes the same dynamics as for random stochastic intercalations.

Importantly, performing full stochastic simulations of this process in one-dimensions revealed a strikingly similar paradigm compared to the version of the model with higher dimensions, with survival probabilities decaying as normal distributions away from the central, optimal position for survival –see **Figure 5b** of this SI. Moreover, the variance of these probabilities, which define the number of functional stem cells, also scale as k_r/k_d as expected in the model –see **Figure 5c** of this SI.

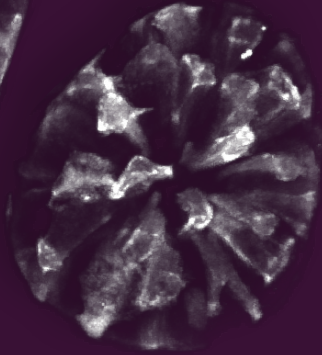
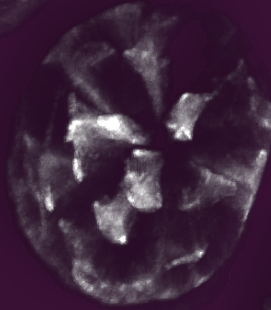
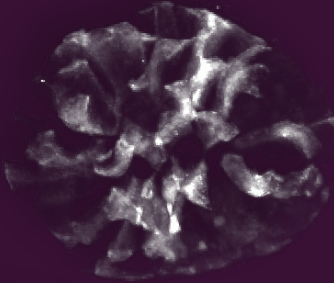
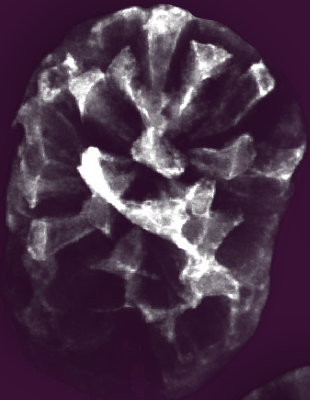
This confirms that such tectonic movements can also be described in our coarse-grained model, simply renormalizing in long-term dynamics the intensity of the noise term k_r in the system (although one would expect tectonic movements to significantly change the short-term dynamics). Interestingly, this allows for the system to be “noisy”, i.e. many functional stem cells to contribute to the long-term dynamics, without any clonal dispersion, showing that one must be careful in equating the two directly. This would in particular be relevant for the dynamics of intestinal crypts, where cells away from starting position 0 have been shown experimentally to still contribute long-term, but where little clonal

Chapter 3

fragmentation was observed (raising the possibility that such tectonic collective movements could occur to reposition cells towards/away from the best location).

References

1. C. W. Gardiner: Handbook of Stochastic Methods for Physics, Chemistry and the Natural Sciences Springer-Verlag:Berlin. (1983)
2. N. G. Van Kampen. Stochastic Processes in Physics and Chemistry third edition, North Holland. (2007)
3. I. Karatzas, and S. E. Shreve. Brownian Motion and Stochastic Calculus Springer-Verlag:Berlin. (1988)
4. C. Guillot, and T. Lecuit. Mechanics of epithelial tissue homeostasis and morphogenesis Science 340, 1185–1189 (2013)
5. C. López-García *et al.* Intestinal stem cell replacement follows a pattern of neutral drift. Science 330:822–825 (2010)
6. W. Klingenberg. A course on differential geometry Translated by D. Hoffman. Springer-Verlag:Berlin. (1978)
7. W. Kühnel. Differential Geometry: Curves–Surfaces–Manifolds 2nd Edition. (Student Mathematical Library series, 77) American Mathematical Society:New york. (2006)



Chapter 4

Wnt Ligands Influence Tumour Initiation by Controlling the Number of Intestinal Stem Cells

Huels DJ, Bruens L, Hodder MC, Cammareri P, Campbell AD, Ridgway RA, Gay DM, Solar-Abboud M, Faller WJ, Nixon C, Zeiger LB, McLaughlin ME, Morrissey E, Winton DJ, Snippert HJ, van Rheenen J and Sansom OJ

Adapted from Nature Communications 9(1):1132 (2018)

ABSTRACT

Many epithelial stem cell populations follow a pattern of stochastic stem cell divisions called 'neutral drift'. It is hypothesised that neutral competition between stem cells protects against the acquisition of deleterious mutations. Here we use a Porcupine inhibitor to reduce Wnt secretion at a dose where intestinal homeostasis is maintained despite a reduction of Lgr5+ stem cells. Functionally, there is a marked acceleration in monoclonal conversion, so that crypts become rapidly derived from a single stem cell. Stem cells located further from the base are lost and the pool of competing stem cells is reduced. We tested whether this loss of stem cell competition would modify tumorigenesis. Reduction of Wnt ligand secretion accelerates fixation of Apc-deficient cells within the crypt leading to accelerated tumorigenesis. Therefore, ligand-based Wnt signalling influences the number of stem cells, fixation speed of Apc mutations and the speed and likelihood of adenoma formation.

INTRODUCTION

The intestinal epithelium is constantly renewing and new epithelial cells are continuously produced by a small number of intestinal stem cells (ISCs) located at the base of the crypt^{1,2}. These crypt columnar stem cells exhibit the highest levels of Wnt signalling demonstrated by nuclear β -catenin staining and high expression of a number of Wnt target genes including *Lgr5*. The expression of *Lgr5* within these cells amplifies Wnt ligand signalling as R-spondin binds to the LGR5 receptor to agonise Wnt signalling³. Wnt ligands are produced by the epithelium (Wnt3 from the Paneth cells) and the mesenchyme⁴, which also produces R-spondin. Although excellent evidence exists showing that *Lgr5*+ cells can act as functional stem cells in the adult intestinal epithelium, these cells are dispensable for homeostasis (over the measured time period of 10 days), though they are required for regeneration post irradiation^{5,6}. Over recent years it has been accepted that these *Lgr5*+ ISCs are not long lived but rather replace each other in a stochastic fashion termed 'neutral drift'. Functionally, the progeny of one stem cell displaces all other stem cells from the niche and becomes fixed in the crypt^{7,8}. This stochastic replacement also explains stem cell dynamics in other proliferating tissues like skin or during spermatogenesis⁹. Through this process it is hypothesised that cells that have acquired deleterious mutations would be likely displaced by their neighbouring wild-type ISCs. *In vivo* imaging studies have monitored this competition in real time. These studies have shown that stem cells at border regions (higher up from the base of the crypt) can be pushed into the transit amplifying zone of the crypt, while stem cells at the centre/base of the crypt are more likely to be retained. Importantly border stem cells can also return to the centre position and regain functional stem cell properties¹. The Wnt signalling pathway has been shown to be required for intestinal homeostasis. Genetic loss of the Wnt transcription factor *Tcf4*/ β -catenin or suppression of Wnt ligand-based signaling via *Dkk* overexpression led to rapid loss of small intestinal crypts¹⁰⁻¹². Additionally, R-spondins are essential for ISCs and crypt maintenance, since complete inhibition by blocking their *Lgr5* and *Znrf3/Rnf43* binding domains results in crypt death. However, inhibition of only one of the binding domains results in a reduced number of *Lgr5*+ cells but otherwise normal crypt homeostasis. This reduction in *Lgr5*+ cells resulted in a rapid fixation of the remaining ISCs in the crypt¹³. This model where stem cells compete with each other has also been applied to examine oncogenic events that might confer advantages to ISCs carrying that mutation. Common mutations in CRC (*Kras*G12D mutation and *Apc* deletion) have been targeted to ISCs in the mouse and have been shown to influence the neutral drift. In both cases there was a greater chance for these mutated stem cells to replace other wild-type cells in the crypt^{14,15}. One technical caveat to these studies is the methodology used to mark crypts in the mouse and determine ISC dynamics. The studies comparing the advantages of a specific mutation relied on cre-mediated expression of *KRAS*G12D mutation or *Apc* gene deletion within ISCs. Tracking of mutant clones were all performed using a reporter gene from the *Rosa26* promoter (e.g. *Rosa26*-Lox-Stop-Lox-tdTomato) allele rather than assaying recombination at the *Kras* or *Apc* locus itself. Importantly previous studies have suggested there may be discordance between reporter alleles¹⁶; therefore, there is a possibility that the precise rates of advantages of these alleles may be different if there are clones that fail to recombine the gene of interest and only the reporter gene (and vice versa). Moreover, it is important to realise that even if mutations are non-neutral, these mutations are not deterministic: mutated stem cells are still surrounded by nonmutated stem cells and therefore have a high chance to be replaced by wild-type cells. Instead of complete inhibition, reduction of Wnt signalling by Wnt ligand inhibitors in adult mice and humans has shown that these inhibitors can

be well tolerated, though do result in dramatically fewer stem cells¹⁷. Here we have used a Porcupine inhibitor to reduce Wnt secretion and test the consequences of lowering the number of functional stem cells per crypt and its effect on stem cell competition. We find that crypts are rapidly derived from a single stem cell and using *in vivo* imaging we show the reason for this is that stem cells at border regions are rapidly lost. To test the functional relevance of this reduction of stem cell competition for tumorigenesis, we examined whether this would accelerate the fixation of *Apc*-deficient cells in the intestine. Importantly, we discovered that the widely used R26tdTomato reporter poorly reports efficient recombination of the two *Apc* alleles *in vivo*. Using RNA in situ and immunohistochemistry to report loss of *Apc* we show that reduction of Wnt ligands results in more efficient tumorigenesis due to the rapid fixation of *Apc*-deficient crypts. Together our data suggest neutral drift and stem cell competition require an optimal level of ligand driven Wnt signaling that has evolved to allow the rapid loss of deleterious mutation but also to protect against the acquisition of advantageous tumour-promoting mutations.

RESULTS

Wnt inhibition only has minor effects on homeostasis

We assessed intestinal homeostasis after treatment with a Porcupine inhibitor LGK974, otherwise known as WNT97417. Consistent with previous studies targeting Porcupine and other strategies to dampen Wnt ligand-based signalling¹⁸, reduction of Wnt ligand secretion did not change rates of crypt proliferation (**Figure 1a,b**). Although the total number of proliferating cells per crypt did not change, there was a small yet significant alteration in the distribution of the proliferative cells. Following porcupine treatment all the proliferative cells are found lower in the crypt compared to the vehicle/untreated mice (**Supplementary Figure 1**). The most striking impact of Wnt inhibition was the marked downregulation of several ISC genes, e.g. *Lgr5*, *Olfm4* and *Lrig1* (**Figure 1a,c**). Interestingly, there was no change in *Bmi1* expression (**Figure 1c**). We performed RNA sequencing from whole intestine to analyse the effect of reduced Wnt signalling on global gene expression (**Supplementary Figure 2a**), which revealed only a small number of significantly deregulated genes (22 upregulated, 44 downregulated). Among the downregulated genes was the canonical Wnt target gene *Axin2*, and the ISC genes *Olfm4* and *CD133*. We observed a reduced number of Paneth cells only after long-term treatment (~30 days), which indicates the requirement of Wnt ligands for the generation of new Paneth cells (**Supplementary Figure 2b**).

Given this relatively mild effect on homeostasis we wanted to test if intestinal regeneration following irradiation was affected as this is a Wnt regulated process and requires *Lgr5*⁺ cells^{11,19}. We observed an inhibition of intestinal regeneration after irradiation (**Supplementary Figure 2c**) consistent with previous studies¹⁸. We also investigated whether Porcupine inhibition could suppress hyperproliferation and increase crypt number induced by oncogenic mutations (either *Braf*^{V600E/+} or *Braf*^{V600E/+} *Pten*^{fl/fl}) and again saw a marked impact on these phenotypes (**Supplementary Figure 3**). Finally given the previous genetic studies showing that complete Wnt ligand inhibition caused the loss of crypts¹², we examined if Porcupine inhibition in combination with reduced β -catenin levels might disrupt tissue homeostasis. The Porcupine inhibitor at the used dosage is well tolerated and mice can be treated for several weeks. Mice with reduced expression of β -catenin are viable and display no phenotype throughout their life. However, a reduction of β -catenin expression by 50% renders these mice sensitive to the Porcupine inhibitor and resulted in rapid crypt loss within 8–12 days (**Figure 1d,e**). Together these data highlight

that the intestinal epithelium can tolerate a reduction in Wnt ligand signalling but further reduction of β -catenin causes a complete loss of crypts. This is consistent with previous work using higher doses of Porcupine inhibitors^{17,18}.

Reduced Wnt ligand secretion decreases crypt fixation time

Given the very selective effect of Wnt ligand reduction via Porcupine inhibition upon *Lgr5* and other ISC genes, we wanted to assess the impact this had upon ISC dynamics. To do this we used well-established techniques examining the ability of single stem cells (labelled by tomato) to repopulate entire crypts.

This was achieved using the *Lgr5-EGFP-CreER* (*Lgr5CreER*) mouse crossed to the *R26R-LoxStopLox-tdTomato* (*tdTom^{fl}*) mouse. Induction with a previously established low tamoxifen concentration resulted in recombination of very few *Lgr5*+ cells per crypt which are then permanently labelled by expression of the tdTom reporter. The fate of these stem cells can be monitored to see if they are lost or take over the full crypt. *Lgr5CreER tdTom^{fl}* mice were induced and treated from 24 h post induction with either LGK974 or vehicle. After treatment with LGK974 we observed a reduction in the *Lgr5*-GFP signal consistent with our previous qRT-PCR and ISH data (**Figure 2a**). Importantly, we saw a dramatic increase in the average clone size after administration of the Porcupine inhibitor. This was observable 4 days post induction and further increased during the time course (**Figure 2b,c**). This resulted in a striking increase in the number of fully fixed clones (**Figure 2d**), with more than 80% of crypts fully fixed after 3 weeks (<20% in the vehicle control), a process which usually takes about 2–4 months^{7,8}. The competition between labelled and unlabelled cells within a crypt resulted in many crypts losing the tdTom label, in accordance with neutral drift. The vehicle treatment resulted in a progressive decline in the number of tdTom+ crypts, whereas treatment with LGK974 accelerated this process and the final number of tdTom+ crypts was reached after 10 days (**Figure 2e**). This analysis also confirmed that an equal number of crypts were recombined before the start of the treatment (**Figure 2e**, day 4). To investigate clonal dynamics using a system that is not limited to recombination in only *Lgr5*-positive stem cells, we repeated this experiment using another inducible cre (*AhCre^{ER}*, not driven by *Lgr5*), which has previously been used for stem cell dynamic studies¹⁴. Using an established low dose induction of *AhCre^{ER}* mice, crossed to the *Rosa26 tdTom^{fl}* mice, we observed a similar increase in the average clone size after LGK974 treatment compared to vehicle treatment 10 days after induction (**Supplementary Figure 4a**).

Border stem cells are lost after reduction of Wnt ligand secretion

The dramatic increase in clone size at early time points following Porcupine inhibitor treatment gave us an excellent opportunity to image the *Lgr5Cre^{ER} tdTom^{fl}* mice *in vivo* to elucidate why the stem cell dynamics were altered. The *in situ* hybridisation analysis for *Lgr5* and *Olfm4* showed that there is a reduction in the expression of these ISC markers. These data imply that either ISCs reduce expression of these genes, while still participating in the competition, or that there is a decrease in the number of functional stem cells per crypt.

To investigate this, we tracked the fate of single *Lgr5*+ cells via multiphoton intravital microscopy through an abdominal imaging window¹. The *Lgr5Cre^{ER} tdTom^{fl}* mice were induced with a low dose of tamoxifen and tdTom+ clones were followed over a period of 4 days (**Figure 3a**). On average, an increase of clonal progeny (tdTom+) derived from the *Lgr5*+ cells was observed in both treatment groups with similar kinetics (**Figure 3b**). It has been previously established that the fate of individual

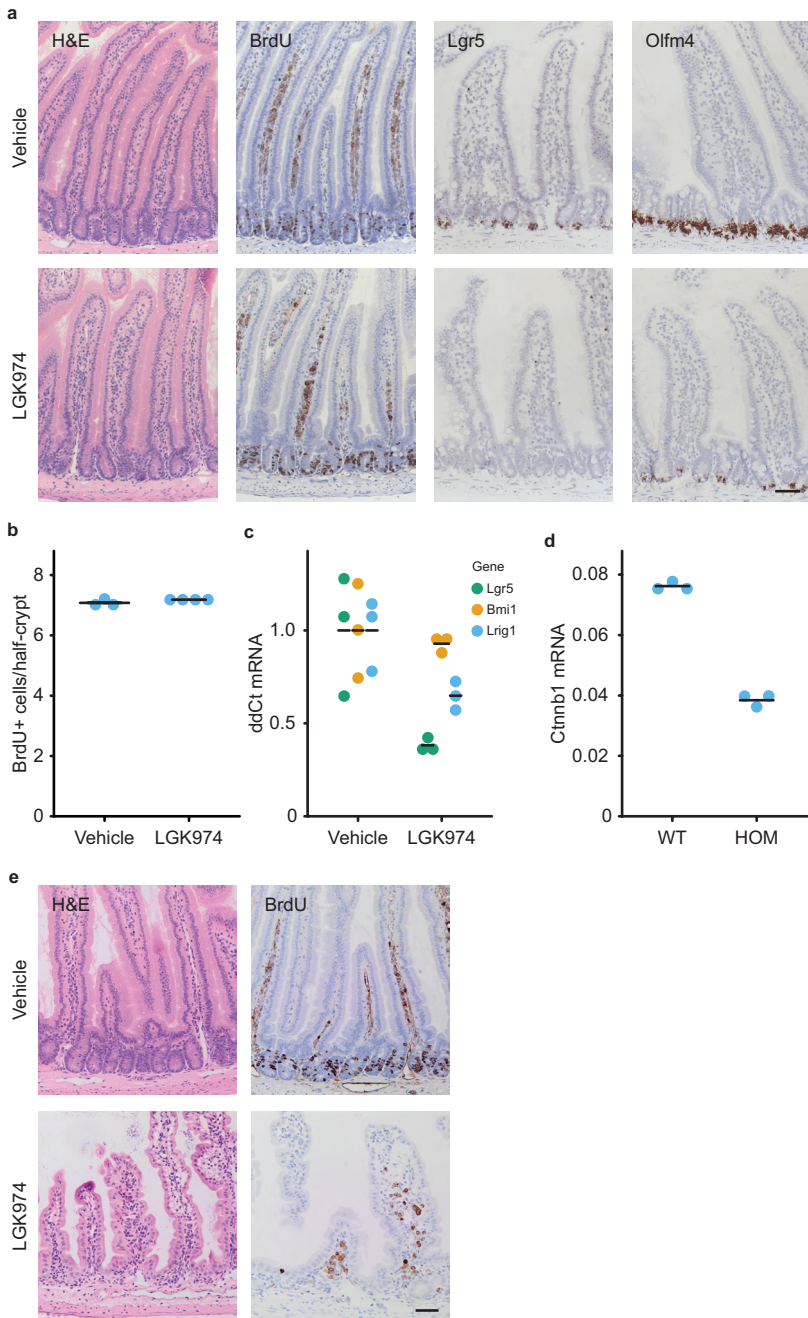


Figure 1. Homeostasis is unperturbed after LGK974 treatment. **a.** C57BL/6 mice were treated with LGK974 for 4.5 days. The small intestine showed no toxicity and no difference in proliferation (BrdU). Treatment of LGK974 leads to downregulation of the intestinal stem cell genes Lgr5 and Olfm4 as confirmed by RNA in situ hybridisation. Note only a few cells at the bottom of the crypt still express Olfm4 after LGK974 treatment (N = 3 for both groups). **b.** Quantification

stem cells is determined by its position in the crypt. Depending on the position, Lgr5+ cells can be grouped as 'border stem cells' at the upper part of the stem cell niche and 'centre stem cells' positioned at the bottom of the crypt¹. Despite loss of Lgr5-GFP expression after LGK974 treatment, originally labelled centre stem cells persisted at the centre and proliferated similar to the control cells (**Figure 3c,d**). In contrast, following the fate of labelled clones at the border of the stem cell niche, we observed a reduction in the number of tdTom+ clones that remained after treatment with LGK974 (**Figure 3e,f**). This suggests that reduction of Wnt ligand secretion leads to specific loss of stem cell activity at the upper part of the stem cell niche. The cells at the bottom of the crypt show no difference in clonal growth, despite downregulation of the ISC gene *Lgr5*. Thus, Wnt ligand inhibition is reducing the number of stem cells in the niche. Due to the resulting decreased competition, cells at the centre have a higher chance of repopulating the crypt quickly when compared with vehicle or untreated mice.

Reduced stem cell pool facilitates adenoma formation

The neutral drift of the ISCs is defined by two parameters, the number of stem cells and the stem cell replacement rate¹⁴. We observed that reduction of Wnt ligand secretion led to a reduction in the number of stem cells, namely the border stem cells, but otherwise normal kinetics of the centre stem cells. This is accompanied by an acceleration of single clones to become fixed. We next examined if these changes have consequences for tumour initiation.

Colorectal cancer is characterised by loss of the tumour suppressor gene APC and our previous studies have shown that this is sufficient to result in Wnt deregulation and adenoma initiation *in vivo*²⁰. Importantly, organoid cultures from *Apc*-deficient cells grow as spheres and do not require R-Spondin, suggesting they are independent of Wnt ligand²¹. We tested if *Apc*-deficient cells are truly independent of secreted Wnt ligands *in vivo*. *VillinCre^{ER} APC^{fl/fl}* mice were induced and treated with either vehicle or LGK974. As expected, we saw no impact of the crypt progenitor phenotype after LGK974 treatment, with marked hyperproliferation in both vehicle and LGK974-treated mice (**Figure 4a, Supplementary Figure 4b**).

It has been reported that certain mutations (e.g. *Kras^{G12D/+}* or *Apc^{-/+}*) impart an advantage on ISCs when compared with their neighbouring wild-type stem cells. This advantage is reflected in an increased probability for a mutant stem cell to replace its neighbour and ultimately become fixed so that all cells in the crypt derive from the same mutant clone^{14,15}. Our data suggest that a reduction of the stem cell pool also led to a dramatic acceleration in the time it takes for crypts to become monoclonal. This leads to the prediction that LGK974 might accelerate the rate of adenoma initiation through altering stem cell dynamics, despite not having an impact on *Apc*-deficient cells.

Previous studies have assumed an equivalent level of recombination between the *R26R-LSL-tdTomato* and the gene of interest. However in our experience we only obtain a robust tumorigenic

*of BrdU+ cells/half-crypt (at least 30 crypts per mouse were analysed). Each dot represents the average per mouse, red bar = mean per group. Vehicle (VEH) N = 3, LGK974 (LGK) N = 4. c. qRT-PCR confirms downregulation of several stem cell genes, whereas expression of Bmi1 is unchanged. Each dot represents single mouse sample, black bar indicates mean per group, N = 3 per group. d. Uninduced *Catnb^{lox(ex3)/lox(ex3)}* are hypomorphs with about 50% reduced expression of β -catenin (*Ctnnb1*), as confirmed by qRT-PCR (N = 3). e. Reduced expression of β -catenin results in hyper-sensitivity to LGK974 and loss of the (small) intestinal crypts within 10 days (mean survival), N = 8. Scale bar = 50 μ m*

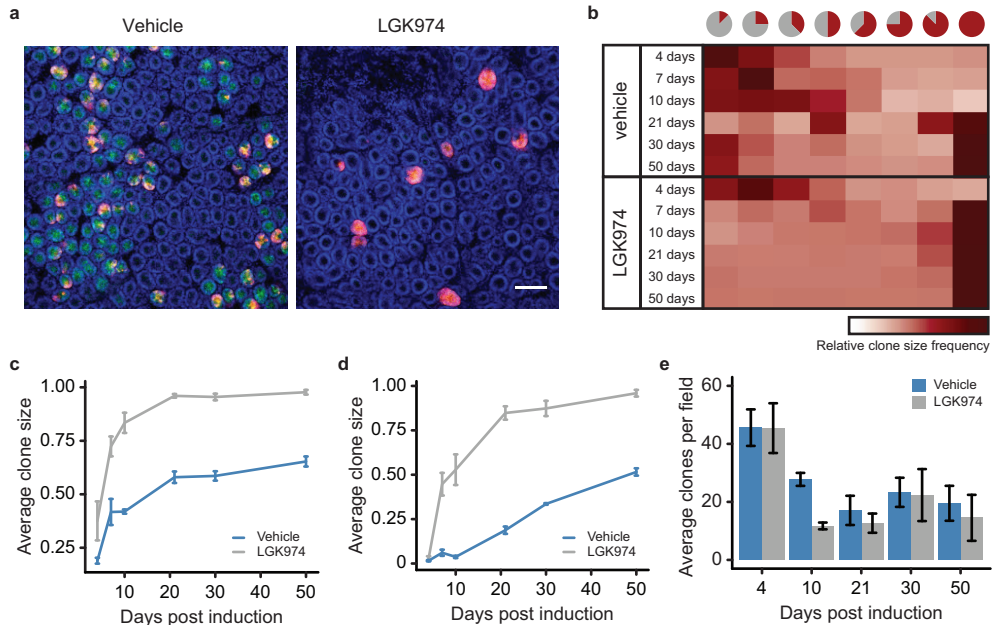


Figure 2. Stem cell replacement rate is accelerated after LGK974 treatment. Mice were induced with 0.15 mg tamoxifen to induce *tdTom^{fl}* recombination in few *Lgr5-CreER-EGFP+* cells. **a.** Mosaic expression of the *Lgr5-eGFP* (green) and the recombined *tdTom+* cells (red). Nuclei were stained with DAPI (blue). Representative pictures at day 10, note the loss of GFP expression and clones are fully labelled by *tdTom+* cells in Porcupine inhibitor-treated mice (LGK974). Scale bar = 100 μ m. **b.** Clone size was counted in 'eighths', at time indicated after induction. At least 200 clones per mouse were counted, vehicle (VEH) N = 3, 3, 4, 4, 3, 3 and LGK974 (LGK) N = 2, 4, 3, 5, 3, 3 for each timepoint, respectively. Heatmap shows all counted clones per timepoint/group. Note that LGK974 has an increased clone size at day 4 and the mean clone size from day 7 is almost at its maximum. Graph shows the mean clone size (**c**) or the number of fully fixed crypts (**d**) at different time points as shown in **b**. Error bars, s.e.m. **e.** Number of *tdTom+* clones per field. The number of crypts with at least one *tdTom+* cell were counted per field, ≥ 19 images per mouse, error bars = s.e.m. Note the similar number of clones at day 4 but the greater reduction in clones after LGK974 treatment at day 10. Vehicle (VEH) N = 3, 3, 4, 4, 3, 3 and LGK974 (LGK) N = 2, 4, 3, 5, 3, 3 for each timepoint respectively.

phenotype in *Lgr5Cre^{ER} Apc^{fl/fl}* mice with a single injection of high concentration tamoxifen22 (≥ 2 mg tamoxifen, **Supplementary Figure 4c**). We therefore first decided to test whether LGK974 could lead to tumour formation following low-level deletion (0.15 mg) in *Lgr5Cre^{ER} Apc^{fl/fl}*. Mice were induced with the low-level tamoxifen and treated 24 h after induction, which assures recombination of the same number of cells before treatment. We observed that LGK974 treatment resulted in a number of macroscopic adenomas, whereas none of the vehicle or untreated mice had any visible adenomas (**Figure 4b**). We then examined if microscopically there were more lesions on the intestines dissected from these mice. These can be visualised by immunohistochemistry for β -catenin (as *Apc* is deleted). Histological analysis of an intestinal 'swiss roll' showed that the majority of vehicle and untreated mice had no lesions (3/5 and 4/7, respectively) with the other mice containing only a single microadenoma. In contrast, almost all the LGK974-treated mice had several adenomas per section (6/7 mice, **Figure 4c**). These data suggest that Porcupine inhibition does affect tumorigenesis in this murine model of colorectal cancer.

However, the low number of histological lesions in the control mice did not match the high number of recombined tdTom+ crypts, we would expect based on our clonal analysis with the same low tamoxifen induction (**Figure 2e**). We thought of two possibilities that could explain this discrepancy: 1. both copies of *Apc* are deleted in a large number of crypts, but only few of them accumulate β -catenin and progress to adenoma formation; 2. That loss of *Apc* was occurring at a much lower frequency than the tdTom reporter would suggest.

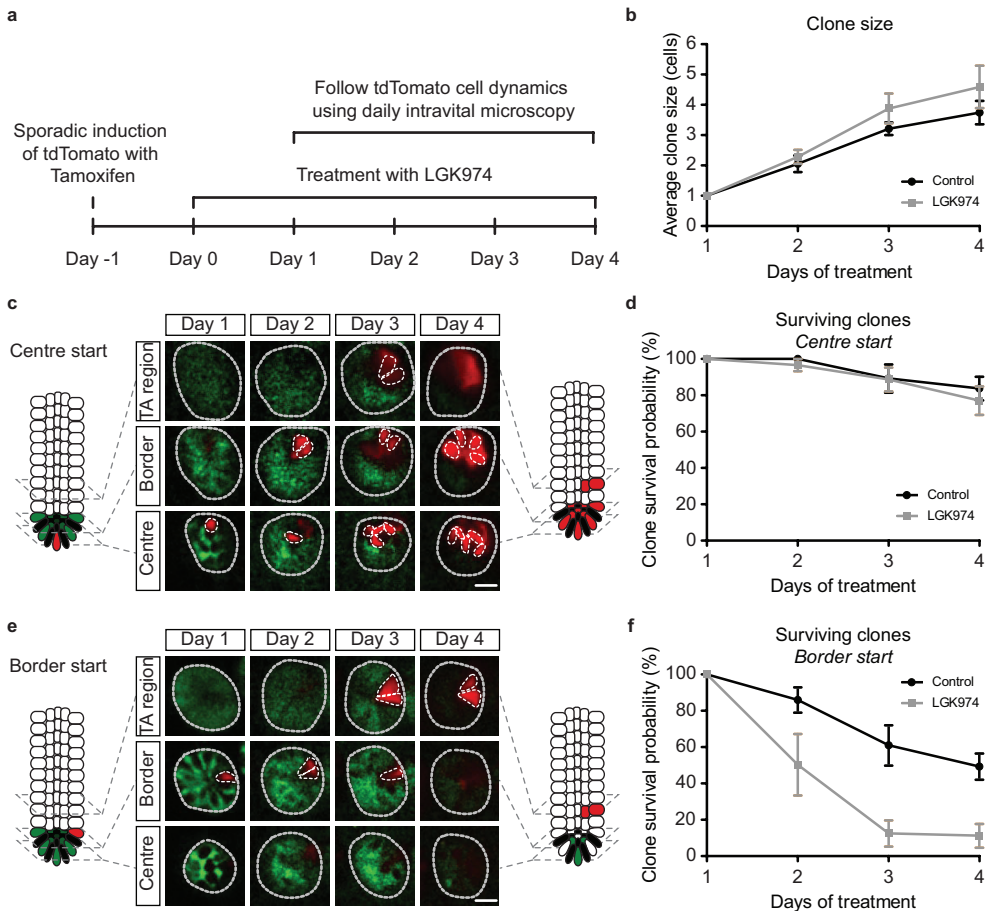


Figure 3. In vivo live imaging shows specific loss of border stem cells after LGK974 treatment. **a.** Graphical representation of the experimental setup. One day before LGK974 treatment, *Lgr5Cre^{ERT2}tdTom^{fl}* mice were injected with 0.05 mg tamoxifen IP to induce recombination in single cells. Mice (N = 4) were treated with LGK974 and daily intravital imaging was performed starting 1 day after first LGK974 treatment and compared to control mice (N = 5). **b.** Graph shows mean clone size (43 crypts, control; 56 crypts, LGK974 on day 1) of surviving clones (clones with at least one cell in centre or border) over time within the centre and border. Note that cells in the transit amplifying (TA) cell region are not counted. **c,e** Intravital images of the same crypt on days 1–4 following a clone starting in the centre (**c**) and a clone starting in the border (**e**). **d,f** Graphs show the percentage of clones that still have at least one cell in the centre or border starting from centre cell (17 crypts, control; 36 crypts, LGK974) (**d**) or from border cell (26 crypts, control; 20 crypts, LGK974) (**f**). Error bars = s.e.m. Scale bar, 20 μ m.

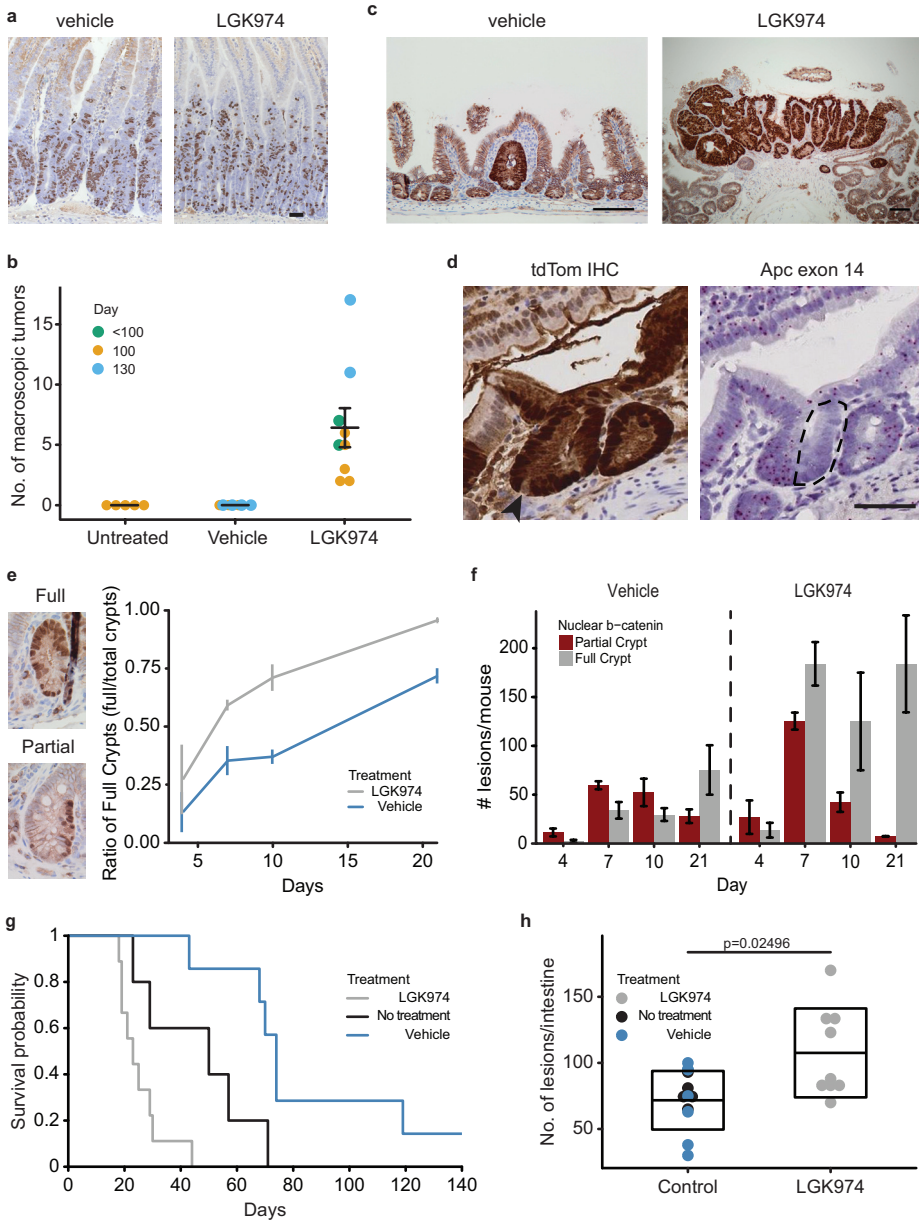


Figure 4. Reduced Wnt ligand secretion does not affect Apc-deficient cell growth but accelerates tumorigenesis. **a.** $VilCre^{ER}Apc^{fl/fl}$ mice were induced and treated with LGK974 starting the following day. Mice were sampled at day 4 post induction, and proliferation assessed by BrdU staining. Scale bar = 50 μ m. **b.** $Lgr5Cre^{ER}Apc^{fl/fl}$ mice induced with 0.15mg tamoxifen and treated with LGK974/vehicle 1 day p.i. The number of macroscopic adenomas was scored when mice showed signs of intestinal adenomas or at 100/130 day timepoint. Each dot represents one mouse, untreated N=5, vehicle N=7 and LGK974 N=9, black dot = mean, error bars = s.e.m., Mann-Whitney U test: untreated vs. LGK974 $p=0.002639$, vehicle vs. LGK974 $p=0.0006014$. **c.** Immunohistochemistry for β -catenin showed only small microadenomas in the vehicle group, in contrast to adenomas found after LGK974

To test the latter possibility, we utilised the latest in situ hybridisation technology 'Basescope'. This technology allows accurate detection of RNA transcripts by use of short RNA detection probes. We designed probes that enabled the detection of exon 14 (117 bp) of *Apc*, which is deleted following recombination. We confirmed the specificity of the RNA in situ probes on established adenomas from *Lgr5Cre^{ER} Apc^{fl/fl}* mice, both for the unrecombined and the recombined *Apc* allele (**Supplementary Figure 5a,b**). Using these probes, we examined the level of *Apc* deletion after a single injection of high concentration tamoxifen (3 mg *Lgr5Cre^{ER} Apc^{fl/fl}*). Surprisingly we found very few crypts that had recombined *Apc*, despite being positive for the tdTom reporter (**Supplementary Figure 5c**). This is not due to leakiness of the reporter since we observed crypts which had partially recombined for *Apc*, whereas almost the entire crypt is positive for tdTom apart from the Paneth cells which have a longer turnover time (**Figure 4d**).

The asynchronous expression of the tdTom reporter and loss of *Apc* also holds true with a lower induction of 0.15 mg tamoxifen in *Lgr5Cre^{ER} Apc^{fl/fl}* and with a similar low-level induction in *AhCre^{ER} Apc^{fl/fl}* mice (**Supplementary Figure 5d**). Furthermore, serial sections revealed that if the *Apc* gene is lost, this coincides with accumulation of nuclear β -catenin in the *Apc*-deficient cells (**Supplementary Figure 5e**).

To analyse the stem cell dynamics of *Apc*-deficient cells without use of the tdTom reporter, we analysed *Lgr5Cre^{ER} Apc^{fl/fl}* mice using a higher concentration of tamoxifen induction (3 mg) by immunohistochemistry for β -catenin. We could differentiate between partially recombined crypts and fully recombined crypts (**Figure 4e**), thus allowing us to perform a similar analysis on stem cell dynamics using nuclear β -catenin as a surrogate.

The first detection of nuclear β -catenin+ cell clones was between 4 and 7 days. We observed a shift towards fully recombined crypts from day 4 to day 21 in vehicle-treated mice, suggesting that the β -catenin+ clones replace the WT stem cells and become fixed in the crypt. This shift is accelerated after LGK974 treatment, where at day 7 most of the crypts are fully populated by β -catenin+ clones (**Figure 4e,f**). This confirms our observation in wild-type mice that treatment with the Porcupine inhibitor accelerates the stem cell dynamics. The reduction in partially populated crypts could either result in a fully populated crypt or the removal of these clones from the crypt. Interestingly, when treated with the Porcupine inhibitor, crypts appeared to be fully clonal by day 7 - resulting in loss of partial crypts while the number of full crypts remained comparable from day 7 through day 21 (**Figure 4f**). The accelerated fixation time of *Apc*-deficient crypts was confirmed when we aged *Lgr5Cre^{ER} Apc^{fl/fl}* mice induced with 3

treatment. Scale bar = 100 μ m. **d.** Example image of *Lgr5Cre^{ER}Apc^{fl/fl}tdTom^{fl/+}* mouse 10 days post induction (3mg, LGK974 treatment). Immunohistochemistry for tdTomato (RFP) shows fully labelled crypt. Arrow marks unlabelled cell (probably Paneth cell), suggesting a newly labelled crypt. RNA in situ for *Apc* exon 14 shows that only half of the crypt has recombined (dashed area). Scale bar = 50 μ m. **e.** *Lgr5Cre^{ER} Apc^{fl/fl}* mice were induced with 3mg tamoxifen and treated with LGK974/vehicle starting at day 1 p.i. Crypts were scored based on immunohistochemistry for β -catenin and categorised into partial and full crypts. The ratio of full crypts is in relation to the sum of full and partial crypts. **f.** Scoring of partial and full crypts at different timepoints in absolute numbers. N = 3 mice for each timepoint and each group, error bars = s.e.m. **g.** *Lgr5Cre^{ER} Apc^{fl/fl}* mice induced with 3mg tamoxifen were treated with LGK974 or vehicle starting at day 1 p.i. Mice were sampled when signs of intestinal tumour burden were apparent. Untreated N = 5, vehicle (VEH) N = 7, LGK974 N = 9 mice, log-rank test: vehicle vs. LGK974 $p = 0.00019$, untreated vs. LGK974 $p = 0.0222$. **h.** Number of adenomas scored on histological sections. Untreated N = 5, vehicle (VEH) N = 6, LGK974 N = 9 mice. Each dot represents number of lesions per mouse; box indicates mean \pm standard deviation. Mann-Whitney U test for LGK974 vs. control mice (untreated and vehicle) $p = 0.02496$.

mg of tamoxifen and treated with Porcupine inhibitor. Here, we observed a dramatic decrease in the time to intestinal tumorigenesis (**Figure 4g**). Histological analysis revealed that these mice had numerous intestinal adenomas (**Figure 4h**). Interestingly, we observed many lesions in the proximal small intestine, whereas the majority of lesions in control mice were confined to the distal part of the small intestine (**Supplementary Figure 6a**). This tumour distribution is also reflected in the ratio of *Apc* deletion. Whereas the tdTom reporter would suggest a higher number of recombined crypts in the proximal compared with the distal small intestine (**Supplementary Figure 6b**), we observed the opposite in terms of *Apc* deletion. Analysis of several mice revealed that about 70% of the tdTom+ crypts still expressed *Apc* based on the RNA in situ probe signal in the proximal small intestine (duodenum). Only a small fraction of crypts (<5%) were positive for the tdTom reporter and had lost *Apc* exon 14 expression in the majority of cells. In the distal part (ileum) we observed a higher fraction of tdTom+ cells that had also lost *Apc* (>20%) (**Supplementary Figure 6c**). This correlates with the high number of adenomas in the distal small intestine compared to the proximal part.

To show that our finding is not simply a reflection of the *Lgr5Cre^{ER}*-mediated deletion we treated *VilCre Apc^{fl/+}* mice with the Porcupine inhibitor, similarly induced with a low concentration of tamoxifen. Again, we observed a decreased survival of treated mice, whereas control mice showed no signs of intestinal adenoma burden within 100 days p.i (**Supplementary Figure 7a**). We saw a high frequency of adenomas within the proximal small intestine, whereas no macroscopic adenomas were found in control mice (**Supplementary Figure 7b**). Microscopic analysis revealed that control mice only had few small lesions, compared to numerous adenomas in mice after treatment with LGK974 (**Supplementary Figure 7c**).

DISCUSSION

In summary, we show that the number of ISCs is regulated by secreted Wnt ligands. Reduction of Wnt ligand secretion reduced the stem cell pool and led to a faster fixation of a single ISC clone, probably due to reduced competition for the stem cell niche (Supplementary Figure 8). Despite downregulation of several stem cell genes (e.g. *Lgr5*), the cells at the centre of the crypt are functional stem cells and maintain intestinal homeostasis.

Reducing Wnt ligand secretion led to a reduced number of ISCs. If the ISCs carry a mutation in *Apc*, this decreased cell competition results in faster population of the crypt by the *Apc*-deficient cells and hence accelerated tumorigenesis. Importantly we see this across multiple different models of *Apc* loss (*Lgr5* mediated deletion of both copies of *Apc*, and in *VilCre^{ER} Apc^{fl/+}* followed by loss of heterozygosity of the remaining wild-type allele).

Our work raises an important technical consideration for previous work looking at selective advantages/disadvantages of particular alleles using the tdTom reporter. It may be that the problem of overestimating the recombination efficiency is unique to the *Apc^{580S}* allele in combination with the *R26-LSL-tdTom* allele. In this case, a total of three alleles need to be recombined to turn on the reporter and achieve homozygous deletion of *Apc*. However previous studies have shown discordant recombination even if two reporter alleles are at the R26 locus¹⁶.

It should be noted that, as the *Apc^{580S}* mouse is a hypomorph, any changes in previously published work might be down to the reduced expression of *Apc* compared to wild-type mice. Moreover, it raises important questions on work suggesting that *Apc* loss does not lead to Wnt signalling activation and

there may be existence of occult *Apc*-deficient crypts. Using the RNA in situ probes, we do not observe deleted *Apc* crypts that have not accumulated nuclear β -catenin and the associated phenotypes.

The low efficiency of *Apc* loss in 3mg tamoxifen-treated mice is also reflected in the distribution of adenomas in these models. However, we believe the most likely way to explain this phenotype is via differences in the Wnt gradient along the small intestine and maybe partly due to different recombination efficiencies. Previous studies have suggested that the mouse proximal small intestine may have a higher levels of basal Wnt signalling, making it suboptimal for tumorigenesis with certain *Apc* mutations, e.g. *Apc*^{Min/+}²³. Here by using a Wnt inhibitor we make the proximal intestine more permissive for tumorigenesis following *Apc* loss, again reinforcing the 'just right' hypothesis of Wnt signalling.

A recent study found a similar role in limiting the number of ISCs by blocking the R-spondin ligands. Inhibition of R-spondins also led to disappearance of Lgr5+ ISCs, despite normal homeostasis. Similarly the authors observed a shorter time to monoclonality, suggesting that reduction of Wnt ligands or R-spondin can lead to the observed stem cell dynamic changes¹³.

One question that arises from our study is why we observed only a minor impact in homeostasis in long-term porcupine inhibitor-treated intestines. Our current hypothesis is that even reduced Wnt signalling at the base of the crypt is sufficient to maintain epithelial homeostasis, despite a reduction in the number of ISCs. A recent study in intestinal organoids may also support this paradigm. Here, Wnt3 did not freely diffuse but is bound to the membrane and spreads passively due to cell division²⁴. In this case, we could imagine that a reduction of the Wnt ligands bound to the membrane are sufficient for the ISCs in the centre of the niche, but since proliferation is not changed the cells further away receive less Wnt ligands and are therefore lost from the ISC pool. Therefore, further reduction of Wnt signalling with higher doses of Porcupine inhibitor or lowering β -catenin expression can then affect the stem cells in the centre as well, leading to their differentiation and loss of the intestinal crypts.

Our work has also shown that the increase in the number of crypts per circumference after MAPK pathway activation is Wnt ligand dependent. Here, we were able to stop the additional crypt fission by treatment with the Porcupine inhibitor (**Supplementary Figure 3**). Therefore, Wnt inhibition may prevent tumours developing from more serrated routes, which are often associated with a lack of *APC* mutation and carry *BRAF* or *KRAS* mutations.

MATERIALS AND METHODS

Mice and treatment

All experiments were performed following the UK Home Office guidelines. All mice were maintained under non-barrier conditions and given a standard diet and water ad libitum. The following mouse strains were used: *VilCre^{ER}* (ref. 25), *Lgr5Cre^{ER}* (ref. 26), *AhCre^{ER}* (ref. 27), *R26R LSL-tdTomato (tdTom^{fl})* (ref. 28), *Apc^{fl}* (ref. 29), *Catnb^{lox(ex3)}* (ref. 30), *Bra^{fl600E}* (ref. 31), *PTEN^{fl}* (ref. 32). The *Lgr5Cre^{ER} Apc^{fl/fl}* and *VilCre^{ER} Apc^{fl/+}* mice were on a C57/B6 background (backcrossed ≥ 10 generations). The Porcupine inhibitor LGK974 (also referred to as WNT974) was administered in a concentration of 5 mg/kg BID (oral) in a vehicle of 0.5% Tween-80/0.5% methylcellulose. *AhCre^{ER}* mice were induced with 1 mg β -naphthoflavone (Sigma) and 0.15 mg tamoxifen (Sigma) IP. *VilCre^{ER}* and *Lgr5Cre^{ER}* mice were induced with tamoxifen (Sigma) IP at the concentrations indicated throughout the manuscript.

Immunohistochemistry/RNA in situ hybridisation

Standard immunohistochemistry techniques were used throughout this study. The following primary antibodies were used: BrdU (1/200, #347580, BD Biosciences), β -catenin (1/50 #610154, BD Biosciences), lysozyme (1/200, DAKO #A0099), RFP (1/200, Rockland #600-401-379). RNA in situ hybridisation (RNAscope) was performed according to the manufacturer's protocol (ACD RNAscope 2.0 High Definition–Brown) for *Lgr5* and *Olfm4*. BaseScope (also ACD) *Apc* EX14 #701641 (detects wild-type APC exon 14) and *Apc* E14E16 #703011 (detects floxed APC) were used according to the manufacturer's instructions. Staining for nuclear β -catenin and RNA in situ hybridisation was performed on tissue samples fixed at 4 °C for less than 24 h in 10% formalin prior to processing. RNAseq. Whole tissue from the small intestine was used for RNA purification. The RNA Integrity was analysed with a NanoChip (Agilent RNA 6000 Nanokit #5067- 1511). A total of 2 μ g of RNA per sample was purified via Poly-A selection. The count matrix returned from the SAM tools was analysed with the R-package DESeq³³ which returned differentially expressed genes with threshold of the adjusted p-value (padj) of < 0.1 . A heatmap of the significantly deregulated genes was created based on the shape of gene expression by Pearson correlation.

In vivo imaging

The *in vivo* imaging was performed as previously described¹. *Lgr5Cre^{ER} R26R-LSL-tdTomato* mice (*tdTom^{fl}*) were induced with 0.05 mg tamoxifen. After placing the abdominal imaging window (AIW), mice were kept under anaesthesia and were imaged once a day. After the imaging sessions the mice were allowed to wake up to maintain their body temperature. After imaging, acquired z-stacks were corrected for z and xy shifts using a customdesigned VisualBasic software program and further processed and analysed using basic functions in ImageJ software (linear contrasting, blurring, median filtering).

Clonal counting

Lgr5Cre^{ER} tdTom^{fl} mice were induced with 0.15 mg tamoxifen (IP) as previously described¹⁴. *AhCre^{ER} tdTom^{fl}* mice were induced with 1 mg β -naphthoflavone and 0.15 mg tamoxifen (IP). The small intestines of mice were sampled at different time points and fixed with 4% paraformaldehyde for 3 h at room temperature. The small intestinal tissue was then incubated with DAPI (10 μ g/ml) in 0.1% PBS-Tween20 (PBS-T) overnight. Whole mount sections were then imaged using a Zeiss 710 confocal microscope.

Regeneration

C57/B6 mice were irradiated with 10 Gy and treated with LGK974/ WNT974 (Porcupine inhibitor) or vehicle 6 h after irradiation. The mice were sampled 72 h after irradiation. The number of regenerating crypts per circumference (10 per mouse) of the small intestine was scored and the average of regenerating crypts per mouse represented in the graph.

Statistics

All data were analysed with R³⁴ and the use of the ggplot2 package³⁵ and the survival package³⁶.

Data availability

Microarray data that support the findings of this study have been deposited in the ArrayExpress database (www.ebi.ac.uk/arrayexpress) under accession number E-MTAB-4178.

ACKNOWLEDGEMENTS

The research was supported by Cancer Research UK core grant C596/A17196 and grant to OS A12481, and DJH was funded by the European Union Seventh Framework Programme FP7/2007-2013 under grant agreement number 278568. OJS is funded by an ERC Starting grant COLONCAN under agreement number 311301. This work was financially supported by European Research Council Grant CANCERRECURRENCE 648804 (to JvR), by the CancerGenomics.nl (Netherlands Organisation for Scientific Research) program (to JvR), by the Doctor Josef Steiner Foundation (to JvR) and by the European Union's Horizon 2020 research and innovation program under Marie Skłodowska-Curie grant agreement no. 642866 (to JvR).

AUTHOR CONTRIBUTIONS:

DJH and OJS contributed to study design; DJH, LB, MCH, PC, ADC, DMG, MSA, CN, LBZ and R.A.R. to acquisition of data; DJH, MCH, DJW, EM, LB, MEM, WJF, JvR, HJS and OJS to analysis and interpretation of the data; and DJH, MCH and OJS to drafting the manuscript.

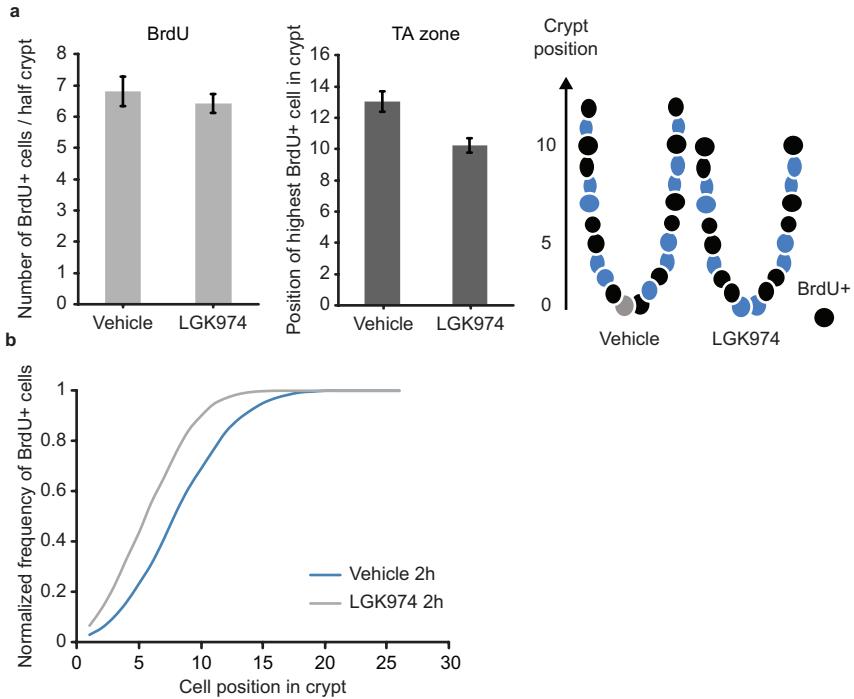
Supplementary Data 1 can be found at <https://www.nature.com/articles/s41467-018-03426-2>

Raw reads of the significantly deregulated genes between vehicle and Porcupine inhibitor treated mice.

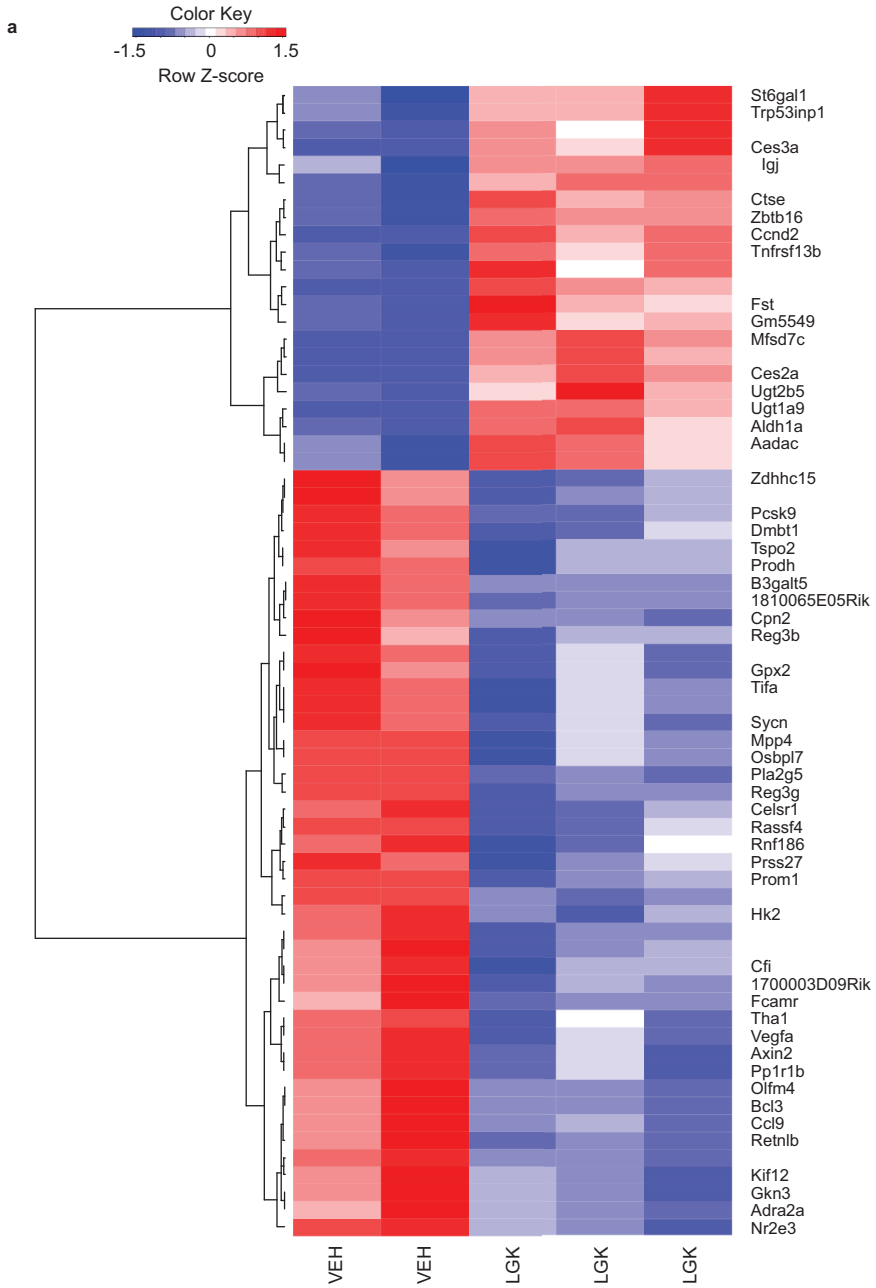
REFERENCES

1. Ritsma, L. et al. Intestinal crypt homeostasis revealed at single-stem-cell level by in vivo live imaging. *Nature* **507**, 362–365 (2014).
2. Kozar, S. et al. Continuous clonal labeling reveals small numbers of functional stem cells in intestinal crypts and adenomas. *Cell Stem Cell* **13**, 626–633 (2013).
3. de Lau, W. et al. Lgr5 homologues associate with Wnt receptors and mediate R-spondin signalling. *Nature* **476**, 293–297 (2011).
4. Farin, H. F., Van Es, J. H. & Clevers, H. Redundant sources of Wnt regulate intestinal stem cells and promote formation of Paneth cells. *Gastroenterology* **143**, 1518–1529 (2012).
5. Tian, H. et al. A reserve stem cell population in small intestine renders Lgr5- positive cells dispensable. *Nature* **478**, 255–259 (2011).
6. Metcalfe, C., Klijavin, N. M., Ybarra, R. & de Sauvage, F. J. Lgr5+ stem cells are indispensable for radiation-induced intestinal regeneration. *Cell Stem Cell* **14**, 149–159 (2014).
7. Snippert, H. J. et al. Intestinal crypt homeostasis results from neutral competition between symmetrically dividing Lgr5 stem cells. *Cell* **143**, 134–144 (2010).
8. Lopez-Garcia, C., Klein, A. M., Simons, B. D. & Winton, D. J. Intestinal stem cell replacement follows a pattern of neutral drift. *Science* **330**, 822–825 (2010).
9. Klein, A. M. & Simons, B. D. Universal patterns of stem cell fate in cycling adult tissues. *Development* **138**, 3103–3111 (2011).
10. Korinek, V. et al. Depletion of epithelial stem-cell compartments in the small intestine of mice lacking Tcf-4. *Nat. Genet.* **19**, 379–383 (1998).
11. Ireland, H. et al. Inducible Cre-mediated control of gene expression in the murine gastrointestinal tract: effect of loss of beta-catenin. *Gastroenterology* **126**, 1236–1246 (2004).
12. Pinto, D., Gregorieff, A., Begthel, H. & Clevers, H. Canonical Wnt signals are essential for homeostasis of the intestinal epithelium. *Genes Dev.* **17**, 1709–1713 (2003).
13. Yan, K. S. et al. Non-equivalence of Wnt and R-spondin ligands during Lgr5+ intestinal stem-cell self-renewal. *Nature* **545**, 238–242 (2017).
14. Vermeulen, L. et al. Defining stem cell dynamics in models of intestinal tumor initiation. *Science* **342**, 995–998 (2013).
15. Snippert, H. J., Schepers, A. G., Van Es, J. H., Simons, B. D. & Clevers, H. Biased competition between Lgr5 intestinal stem cells driven by oncogenic mutation induces clonal expansion. *EMBO Rep.* **15**, 62–69 (2014).
16. McCutcheon, S. C. et al. Characterization of a heat resistant β -glucosidase as a new reporter in cells and mice. *BMC Biol.* **8**, 89 (2010).
17. Liu, J. et al. Targeting Wnt-driven cancer through the inhibition of Porcupine by LGK974. *Proc. Natl. Acad. Sci. USA* **110**, 20224–20229 (2013).
18. Kabiri, Z. et al. Stroma provides an intestinal stem cell niche in the absence of epithelial Wnts. *Development* **141**, 2206–2215 (2014).
19. Muncan, V. et al. Rapid loss of intestinal crypts upon conditional deletion of the Wnt/Tcf-4 target gene c-Myc. *Mol. Cell. Biol.* **26**, 8418–8426 (2006).
20. Sansom, O. J. et al. Loss of Apc in vivo immediately perturbs Wnt signaling, differentiation, and migration. *Genes Dev.* **18**, 1385–1390 (2004).
21. Sato, T. et al. Paneth cells constitute the niche for Lgr5 stem cells in intestinal crypts. *Nature* **469**, 415–418 (2011).
22. Barker, N. et al. Crypt stem cells as the cells-of-origin of intestinal cancer. *Nature* **457**, 608–611 (2009).
23. Leedham, S. J. et al. A basal gradient of Wnt and stem-cell number influences regional tumour distribution in human and mouse intestinal tracts. *Gut* **62**, 83–93 (2012).
24. Farin, H. F. et al. Visualization of a short-range Wnt gradient in the intestinal stem-cell niche. *Nature* **530**, 340–343 (2016).
25. El Marjou, F. et al. Tissue-specific and inducible Cre-mediated recombination in the gut epithelium. *Genesis* **39**, 186–193 (2004).
26. Barker, N. et al. Identification of stem cells in small intestine and colon by marker gene Lgr5. *Nature* **449**, 1003–1007 (2007).
27. Kemp, R. et al. Elimination of background recombination: somatic induction of Cre by combined transcriptional regulation and hormone binding affinity. *Nucleic Acids Res.* **32**, e92 (2004).

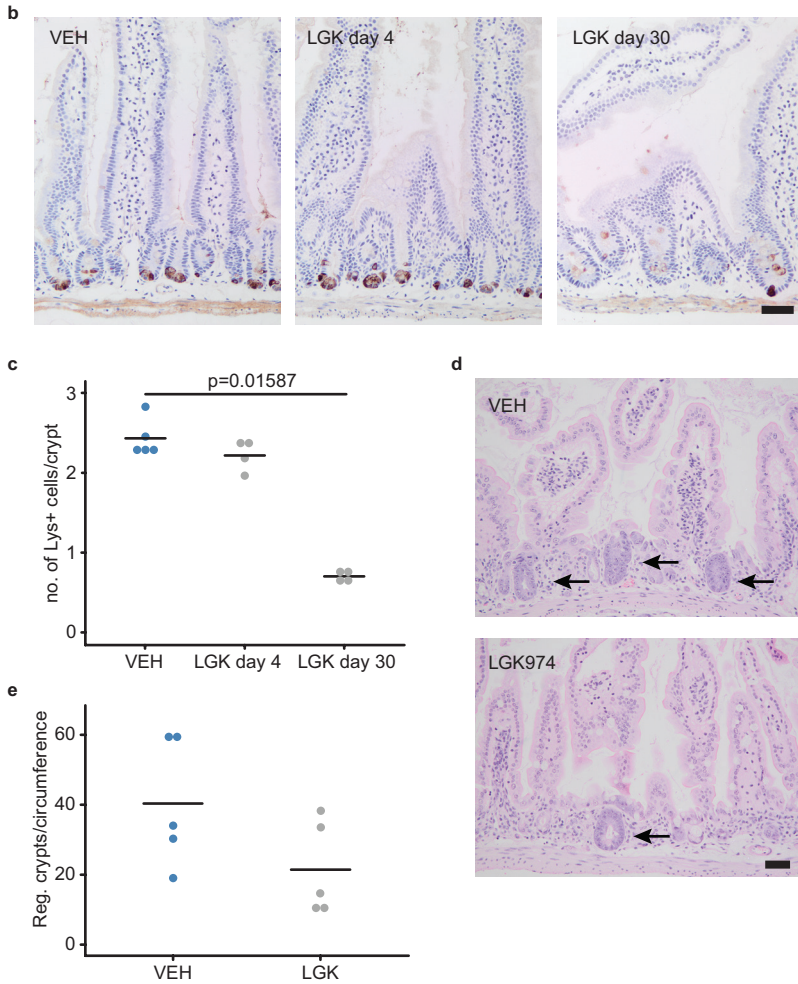
28. Madisen, L. et al. A robust and high-throughput Cre reporting and characterization system for the whole mouse brain. *Nat. Neurosci.* **13**, 133–140 (2010).
29. Shibata, H. et al. Rapid colorectal adenoma formation initiated by conditional targeting of the Apc gene. *Science* **278**, 120–123 (1997).
30. Harada, N. et al Intestinal polyposis in mice with a dominant stable mutation of the β -catenin gene. *EMBO J.* **18**, 5931–5942 (1999).
31. Mercer, K. et al. Expression of endogenous oncogenic V600E-*raf* induces proliferation and developmental defects in mice and transformation of primary fibroblasts. *Cancer Res.* **65**, 11493–11500 (2005).
32. Suzuki, A. et al. T cell-specific loss of Pten leads to defects in central and peripheral tolerance. *Immunity* **14**, 523–534 (2001).
33. Anders, S. & Huber, W. Differential expression analysis for sequence count data. **11**, R106 (2010).
34. R Development Core Team. R: A Language and Environment for Statistical Computing (R Foundation for Statistical Computing, Vienna, Austria, 2013) <http://www.R-project.org>.
35. Wickham, H. ggplot2 Elegant Graphics for Data Analysis. Media.doi: [https:// doi.org/10.1007/978-0-387-98141-3](https://doi.org/10.1007/978-0-387-98141-3) (2009).
36. Therneau, T. M. A Package for Survival Analysis in S. <https://cran.r-project.org/package=survival> (2015).



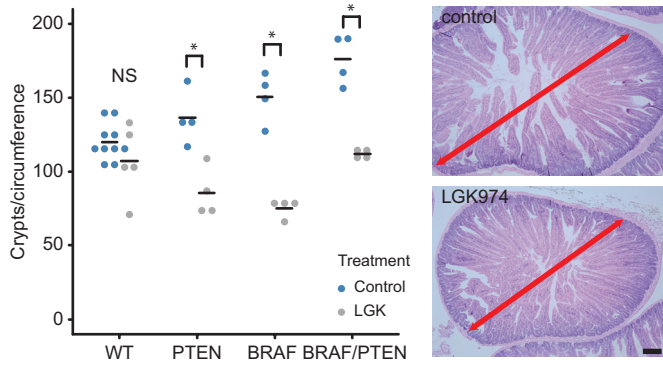
Supplementary Figure 1. Porcupine Inhibition changes size of proliferative zone. a. Although the number of BrdU+ cells per crypt did not change, there is a reduction in the height of the proliferative zone (TA zone). The last BrdU+ cell in vehicle treated mice is about +13, whereas after LGK974 treatment the last positive BrdU+ cell is at position +10 (N=3 mice per group). **b.** Scoring of BrdU+ cells per position reveals the distribution of the proliferative cells along the crypt-villus axis. For example, whereas 50% of all proliferative cells in the vehicle mice are found until position +8, 50% of all the proliferative cells are found until position +5 (N=3 mice, at least 30 crypts per mouse analysed).



Continued on next page

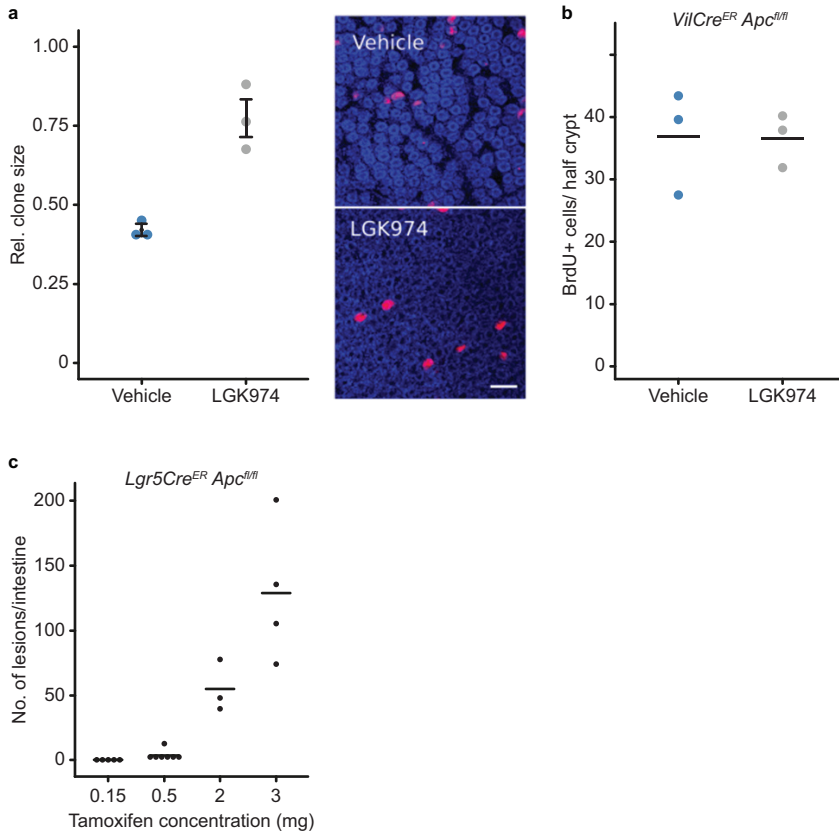


Supplementary Figure 2. Changes of Porcupine treatment on homeostasis and regeneration. **a.** Heatmap of Pearson correlation of significantly de-regulated genes after LGK974 treatment. Whole small intestinal tissue (proximal small intestine) was analysed. There were 22 genes upregulated (red), and 44 genes downregulated (blue), N=2 vehicle, N=3 LGK974 (see also Supplementary Table 1) **b,c.** The number of Paneth cells were scored by lysozyme IHC. Graph depicts mean per mouse of lysozyme+ cells per crypt (100 crypts per mouse scored, N=5 vehicle (treated for 4 days), N=4 LGK974 (treated for 4 and 30 days), statistics: Mann-Whitney U. Scale bar = 50 μ m. **d,e.** Whole body irradiation (10Gy) was performed and treatment with LGK974 started after 6 hrs, mice were sampled 72h post irradiation. Regenerating crypts (arrow) per small intestinal circumference were scored, at least 10 circumferences per mouse were analysed. Each dot represents the mean per mouse; the red line indicates the mean per group. N=5 mice per group, Scale bar = 50 μ m.



Supplementary Figure 3. Increased crypt number in BRAF and BRAF PTEN mice is dependent on Wnt ligands.

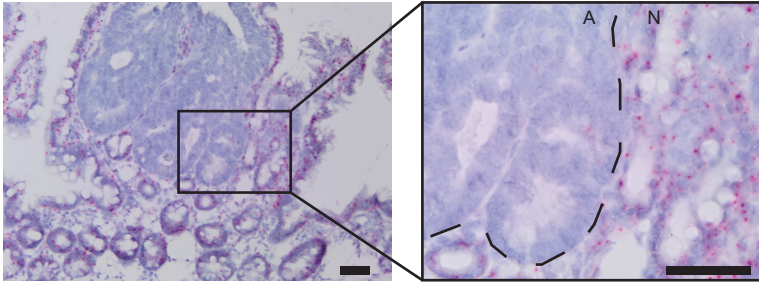
The number of crypts per circumference in the small intestine was quantified. At least 10 circumferences per mouse were scored; each dot represents mean per mouse. Wildtype (WT), ViiCre^{ER} Braf^{V600E/+} (BRAF), ViiCreER Pten^{fl/fl} (PTEN) and ViiCre^{ER} Braf^{V600E/+} Pten^{fl/fl} (BRAF PTEN) were sampled 30 days after induction. The H&E show the circumference of a BRAF PTEN mouse untreated (control) or treated with LGK974 (starting 1 day after induction). The red arrow indicates difference in crypt diameter. Scale bar = 100 μ m. Statistics: Mann-Whitney U test between CNTRL and LGK treatment, WT (CNTRL: N=10, LGK: N=5): $p=0.371$, PTEN, BRAF and BRAF PTEN (N=4 in each group): $p=0.02857$ (*).



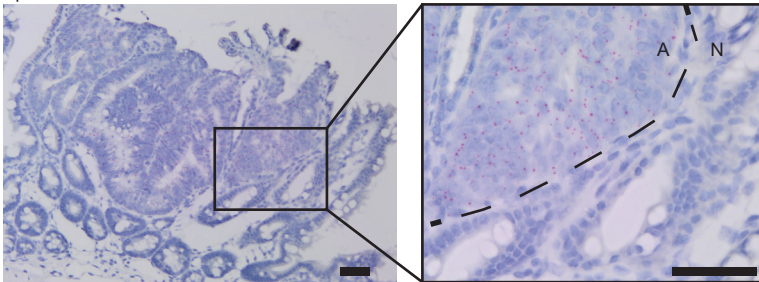
Supplementary Figure 4. Effect of Porcupine treatment on stem cells and proliferation. **a.** AhCre^{ER} tdTom^{fl/+} Apc^{fl/+} mice were induced with 1mg β -Naphthoflavone and 0.15 mg tamoxifen and treated with Vehicle/LGK974 24hrs after induction until sampling. The base of the crypt was analysed 10 days after induction. For each mouse, ≥ 60 clones from the proximal small intestine were scored for the average clone size. Each red dot represents the mean for each mouse (N=3); the crossbar is mean per group \pm s.e.m. Representative images, tdTom (red), DAPI (blue), scale bar = 100 μ m. **b.** The number of BrdU+ cells per half-crypt (at least 30 crypts per mouse) was scored. Each dot represents the mean of one mouse, red bar indicates mean per group. N=3 for each group. Mann-Whitney U test, $p=1$. **c.** Lgr5Cre^{ER} Apc^{fl/fl} (untreated) were induced with different concentrations of tamoxifen (IP) and sampled at 100 days p.i. or when signs of intestinal adenomas were apparent. Data show the number of lesions on a single H&E section of the full length of the small intestine. Each dot represents a single mouse, the box is constructed by the mean \pm standard deviation.

Supplementary Figure 5. RNA in situ probe to detect recombined Apc allele. **a.** RNA in situ probe for the wildtype Apc exon 14 allele (red dots) and **b.** RNA in situ probe (red dots) for the recombined allele ($\Delta 14$) in an established adenoma of a Lgr5Cre^{ER} Apc^{fl/fl} (3mg tamoxifen). Inserts show specificity of probes between adenoma (A) and normal tissue (N). **c.** Immunohistochemistry for tdTom (RFP) staining and RNA in situ for the deletion of Apc on serial sections from Lgr5Cre^{ER} Apc^{fl/fl} mice induced with 3mg tamoxifen, day 10 p.i. **d.** Low-level induction in AhCre^{ER} Apc^{fl/fl} tdTom^{fl/fl} mice with 0.15mg tamoxifen and 1mg β -naphthoflavone at day 21. Scale bars = 50 μ m. **e.** Loss of Apc exon 14 coincides with accumulation of nuclear β -catenin (arrow - Lgr5Cre^{ER} Apc^{fl/fl} day 10 p.i, 3mg tamoxifen).

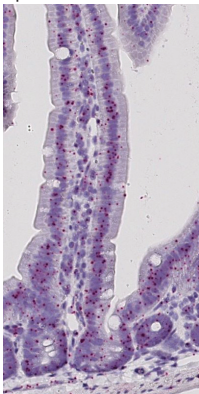
a Apc exon 14



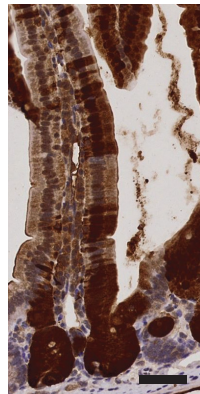
b Apc Δ 14



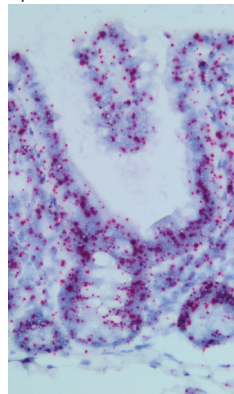
c Apc exon 14



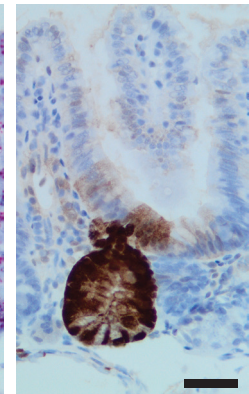
tdTomato



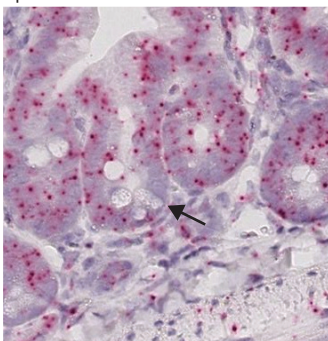
d Apc exon 14



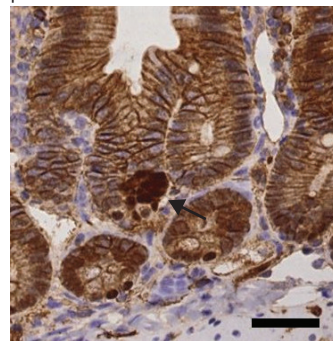
tdTomato

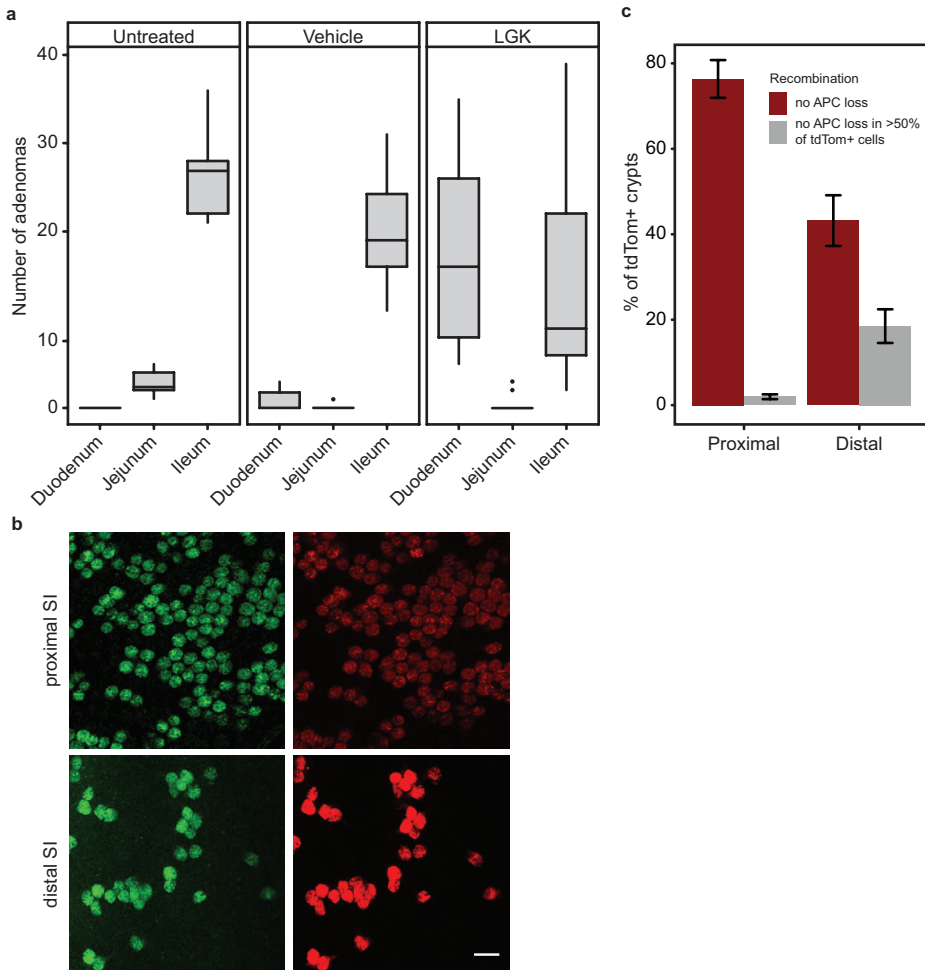


e Apc exon 14

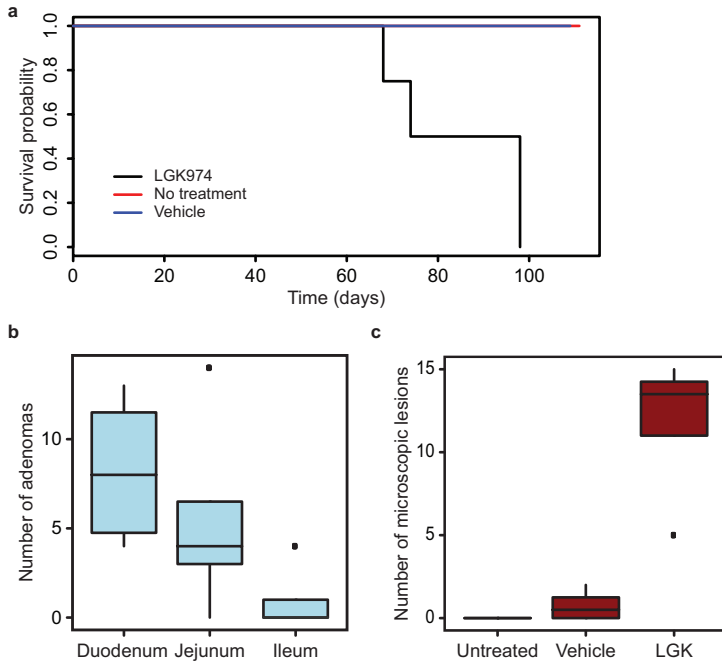


β -catenin

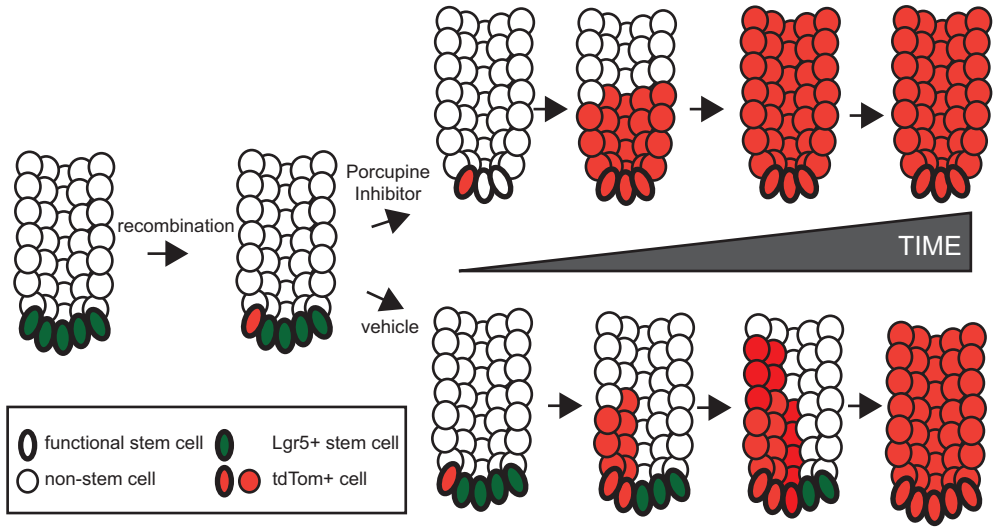




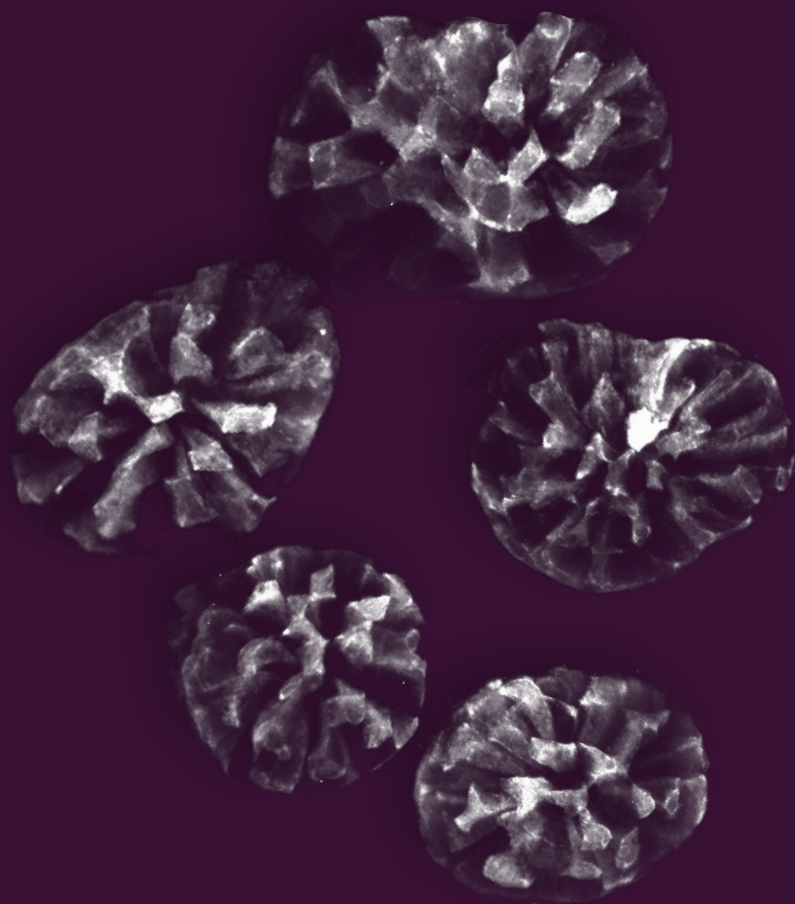
Supplementary Figure 6. Effect of Porcupine treatment on adenoma distribution and discrepancy between *tdTom* reporter and *Apc* recombination. **a.** *Lgr5Cre^{ER} Apc^{fl/fl}* mice were induced (3mg tamoxifen) and sampled when signs of intestinal adenoma burden were apparent. The small intestine was equally divided into 3 sections, from proximal to distal (duodenum, jejunum and ileum) and the number of adenomas per section was quantified microscopically. Note the increased number of adenomas specifically in the duodenum after LGK974 treatment. **b.** *Lgr5CreER tdTom^{fl}* mice induced with 3mg tamoxifen (IP) were analysed at day 3 p.i. All *Lgr5*-GFP positive crypts were fully labelled by *tdTom*. Scale bar = 100 μ m. **c.** *Lgr5Cre^{ER} Apc^{fl/fl}* mice, induced with 3mg tamoxifen and sampled day 10 p.i. Serial sections were stained for *tdTom* (RFP) and RNA in situ for *Apc* loss show that the majority of *tdTom*+ crypts still express *Apc*. Note, the increased efficiency of *Apc* deletion in the distal SI (Ileum). N=3 mice with ≥ 100 crypts scored per region per mouse, error bars = s.e.m.



Supplementary Figure 7. Increased tumorigenesis in *VilCre^{ER} Apc^{fl/+}* mice after Porcupine treatment. *VilCre^{ER} Apc^{fl/+}* mice were induced with 0.15mg tamoxifen (IP) and treated with LGK974 or vehicle from day 1 p.i. continuously. **a.** Mice were sampled when signs of intestinal adenoma burden were apparent. All remaining mice were finally sampled at day 100-105 p.i. **b.** The small intestine was arbitrarily divided in 3 equal parts and the number of macroscopically visible adenomas per mouse was counted. Only LGK974 treated mice had visible adenomas. **c.** Microscopic analysis showed only very few small adenomas in vehicle treated mice, whereas LGK974 had several adenomas per section. *N*=5 for untreated and vehicle treated mice, *N*=4 for LGK974 treated mice. The boxplots show the median (black line) and the first and third quartiles (box).



Supplementary Figure 8. Overview of changed stem cell dynamics after Porcupine inhibition. After recombination in a limited number of intestinal stem cells, treatment with Porcupine inhibitor LGK974 reduced the number of functional stem cells in the crypt. The labelled intestinal stem cell competes with the reduced number of intestinal stem cells, which have lost *Lgr5* expression, resulting in a quicker fixation of the *tdTom*⁺ clone. The same principle applies to loss of *Apc* in few intestinal stem cells instead of *tdTom* labelling.



Chapter 5

Calorie Restriction Decreases Retention of
Intestinal Mutations by Increasing the Number of
Wild-type Stem Cell Competitors

Bruens L, Ellenbroek SJ, Suikerbuik SJE, Hale AJ, Toonen P, Snippert HJ and van Rheenen J

Manuscript in revision

ABSTRACT

Calorie restriction (CR) is known to extend lifespan by several mechanisms including increased DNA repair leading to less DNA mutations that cause age-related pathologies such as cancer. Here, by intravital microscopy of intestinal stem cells, we identify an additional mode of action of CR that affects DNA mutation retention in intestinal tissues. We visualized in real time how dividing Lgr5+ stem cells at the base of crypts compete for niche space, and showed that mutations can only retain long-term in intestinal tissues if the mutated stem cell outcompetes all wild-type stem cells. We observed that CR leads to enlarged crypts and increased number of stem cells. Consequently a mutant cell competes with more wild-type cells resulting in slower competition and higher chance to be replaced. Thus, in addition to lowering the acquisition of DNA mutations, our study shows that CR lowers the retention of mutations that have been acquired, as CR enhances the number of wild-type competitors that can outcompete mutant stem cells.

INTRODUCTION

Aging, and age-related pathologies such as cancer, are the consequence of deleterious changes in cells and tissues over time, including the progressive accumulation of DNA mutations¹. Calorie restriction (CR) can prevent many of these age-related changes resulting in extended lifespan and reduced age-related pathologies through a reduction of dietary calories while maintaining adequate nutrition²⁻⁴. Several mechanisms through which calorie restriction can reduce the accumulation of mutations have been identified, including attenuating oxidative stress and enhancing DNA repair⁵. However, additional mechanisms may be at play, especially in tissues exposed to hostile environments which potentiates mutation incidence, such as intestinal tissues.

The intestinal epithelium is curved into a single-cell layered sheet of crypt-villus units where proliferative cells are located at the bottom of the crypt, giving rise to more differentiated cells that travel upwards in a conveyor belt-like fashion⁶. As a protective barrier against the external environment, this epithelial sheet is constantly exposed to potentially DNA-damaging substances. However, most mutated cells are eliminated due to the highly dynamic self-renewing nature of the epithelium. This imposes a short life time on the majority of the cells as they are shed at the tip of villi within a few days, preventing manifestation or propagation of genomic damage⁷. Lgr5+ stem cells at the bottom of the crypt are long-lived and can thus accumulate mutations⁸. However, these Lgr5+ stem cells compete for niche space resulting in loss of most stem cells⁸⁻¹⁰. As a result, the progeny of one stem cell will ultimately replace all other stem cells meaning that mutations will only be retained if they occur the stem cell winning the stem cell competition⁷. Even in the case of non-neutral mutations, a mutant stem cell is outnumbered by wild-type cells and is likely outcompeted and expelled from the niche to be transported and lost at the villus tip^{11,12}.

We and others have recently shown that the chance that a mutated cell wins the stem cell competition can be manipulated by decreasing the number of stem cells through pharmacologically inhibiting Wnt gradients^{13,14}. We showed that with fewer wild-type competitors, Apc-deficient cells can take over crypts more rapidly, leading to faster tumorigenesis¹³. Thus, mutated stem cells can more rapidly spread in the crypt when there are fewer competing stem cells. Interestingly, calorie restriction (CR) has been shown to increase the number of stem cells. Whether the reverse, increasing the strength of SC competition by increasing stem cell numbers, leads to slower competition and reduce spread of mutations, is unknown. Therefore, in this study, we use CR to enlarge the stem cell pool and investigate whether this results in slower, but stronger stem cell competition.

RESULTS AND DISCUSSION

To study the effect of CR on stem cell competition in the intestinal epithelium, we set up a CR protocol resulting in 40% reduced calorie intake while maintaining adequate nutrition¹⁵. After 8 weeks on CR, animals showed a 25.1±/7.4% reduced bodyweight compared to animals on control food, while intestine width and length were unaltered (**Figure 1a-c**). In line with previous reports^{16,17}, we found that this CR protocol resulted in increased numbers of Lgr5+ stem cells and their niche cells (i.e. Lysozyme+ Paneth cells), resulting in larger crypt diameters (**Figure 1d-g**). Interestingly, this phenotype was fully reversible when diets were reverted (**Figure 1h**).

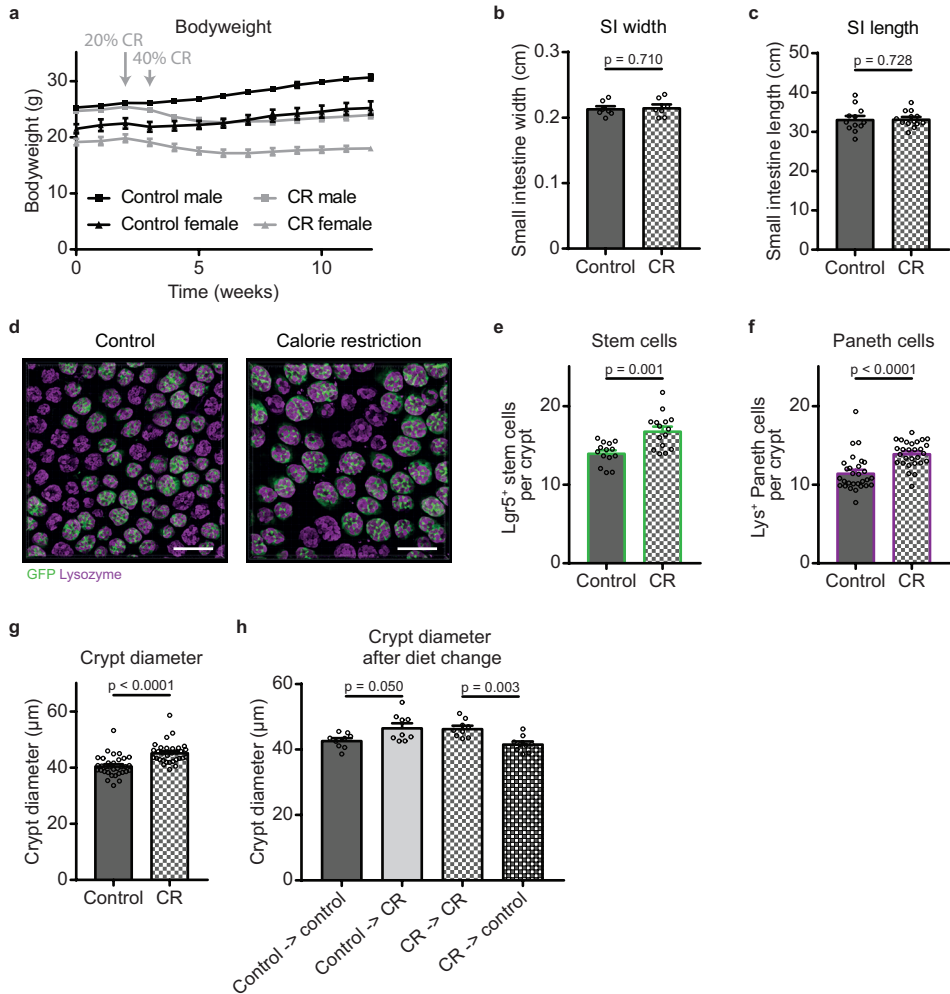


Figure 1. Calorie restriction reversibly alters crypt morphology. Upon CR, (a) bodyweight is reduced compared to control fed mice ($n > 15$ mice per group), while (b) small intestinal width ($n=7$ mice) and (c) length are unaltered ($n > 12$ mice per group). (d) Staining for Lgr5⁺ stem cells and Lysozyme⁺ Paneth cells (scale bar = 100μm) shows that (e,f) both cell populations are bigger under CR (e, $n > 14$ mice per group) (f, $n=28$ mice), which (g) results in a larger crypt diameter ($n > 31$ per group). (h) After change of the diets (8-16 weeks on first diet, 8 weeks on second diet), crypt diameter ($n > 9$ mice per group) is reversed. Mean \pm s.e.m. Dots represent individual mice.

We previously demonstrated the existence of crypt fusion during which two separate crypts can fuse into one, counterbalancing crypt fission¹⁸. Therefore, the expansion of the number of stem cells per crypt can be the result of an increased number of stem cells in each crypt, but also the results of a redistribution of the same number of stem cells over a lower number of crypts by altering the balance of crypt fission and fusion. To distinguish between these two possibilities, we performed repetitive intravital microscopy (IVM) experiments in which we imaged the same crypts before and after diet change *in vivo* (Figure 2a). We used landmarks such as vessels, confetti-colored crypts and patchy pattern of Lgr5-

GFP expression to validate successful retracing of the imaging areas (**Supplementary Figure 1**). After the first imaging session, the diet was reversed in half of the mice resulting in 4 experimental groups: control to control diet, control to CR diet, CR to CR diet and CR to control diet. Eight weeks after the first imaging session, we did not observe a significant number of crypts that were gained or lost (**Figure 2b,c**), confirmed by the finding that the same number of crypts feed into one villus (**Supplementary Figure 2**). However, we did observe the expected increase in crypt diameter when diet was changed from control to CR, and decrease in crypt diameter with the reverse dietary change (from CR to control diet) (**Figure 2d**). Together, these data indicates that the number of crypts is not altered upon CR, but that the number of stem cells is increased in each crypt rather than that the same number of stem cells are redistributed over a smaller number of crypts.

Previously, we have shown that decreasing the number of Lgr5+ stem cells concomitantly lowers the chance of mutant stem cells to be outcompeted by wild-type cells¹³. To investigate whether the reverse

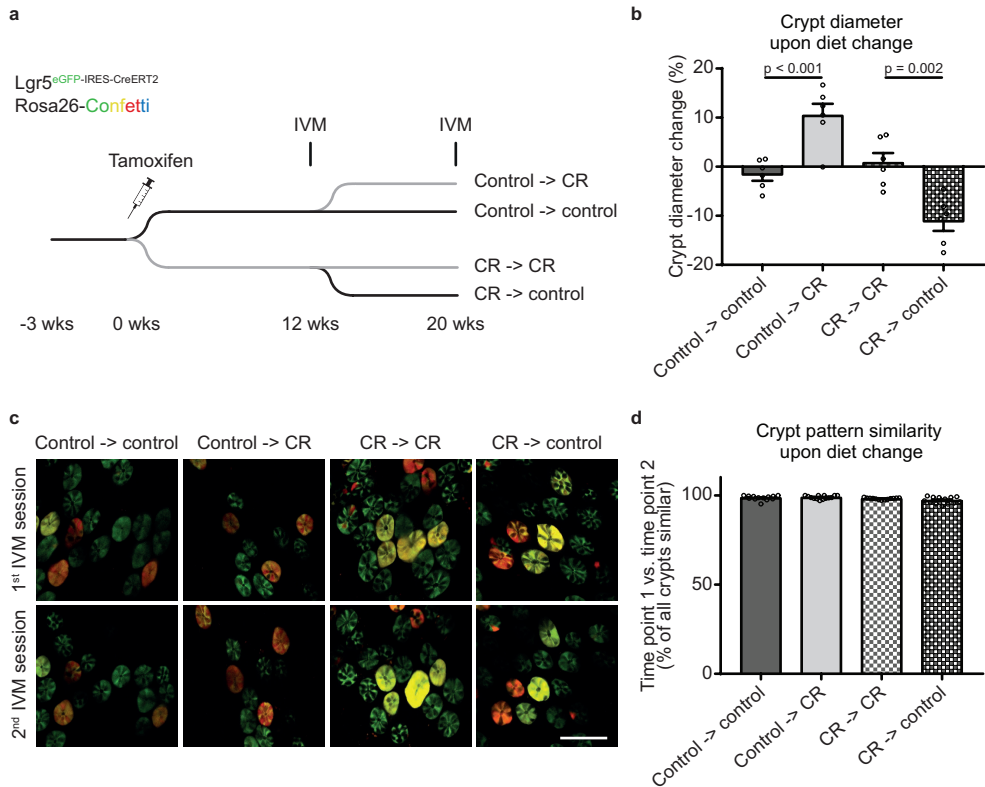
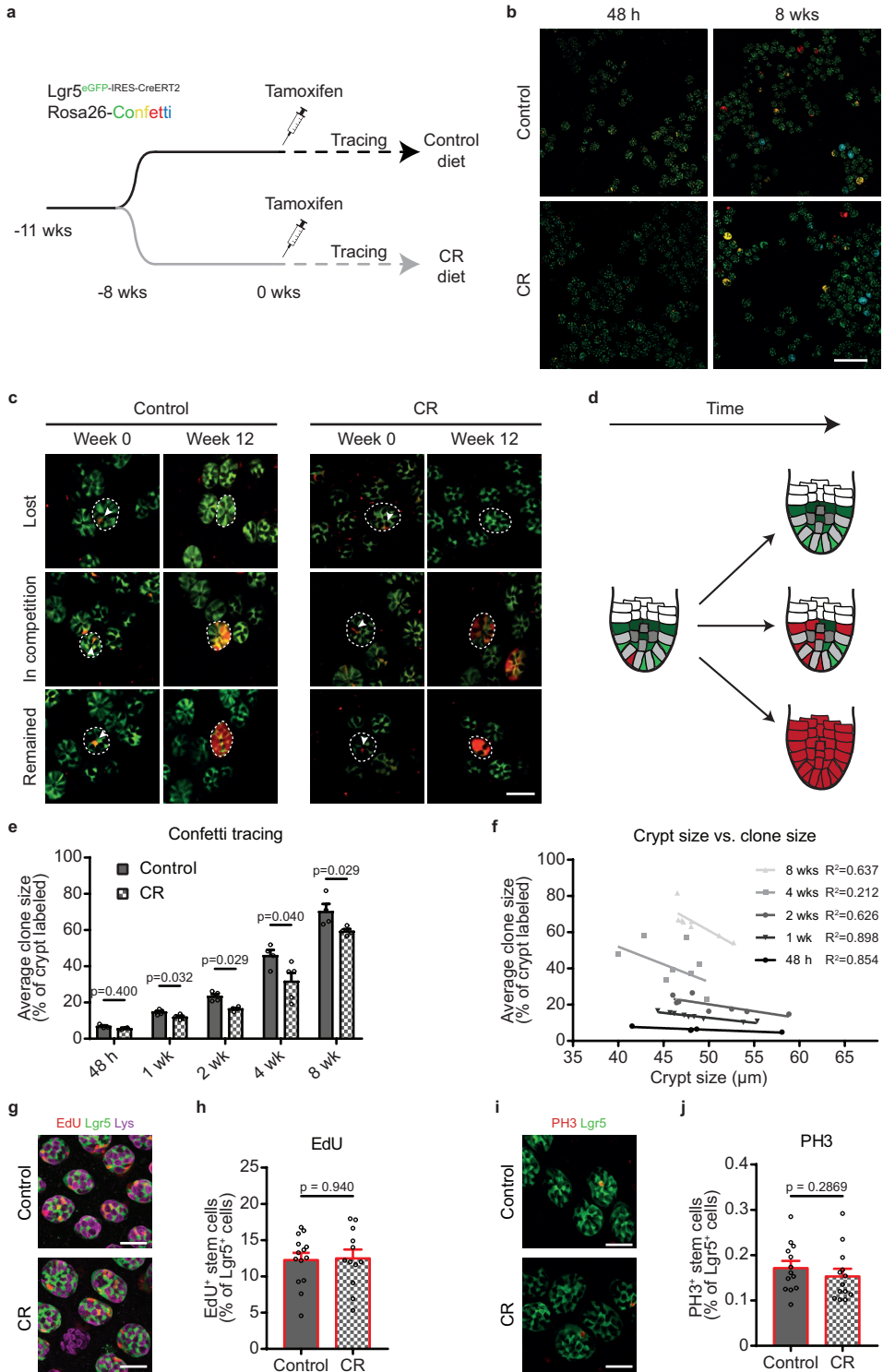


Figure 2. Calorie restriction does not affect crypt numbers. Repetitive intravital microscopy experiment (schematic representation in **a**) was performed to see whether crypt density is changed upon CR. A high dose of tamoxifen was injected to create a recognizable crypt pattern. After 12 weeks, the crypt pattern was imaged after which the diet was reversed for half the mice. 8 weeks later the same pattern was imaged. (**b,c**) No significant change was found in crypt pattern showing that crypt density is unaltered upon CR ($n > 13$ positions in 6 mice per group, based on >3000 crypts per group) (scale bar = $100\mu\text{m}$). (**d**) Diet reversal did result in reversal of the crypt diameter phenotype ($n > 6$ mice per group). Mean \pm s.e.m. Dots represent individual mice, except in **d** each dot represents single imaging field.



holds true when increasing the number of Lgr5+ stem cells upon CR, we performed lineage tracing experiments in Lgr5^{eGFP-ires-CreERT2};confetti mice (**Figure 3a,b**). In either control or CR mice, we injected a low dose of tamoxifen to activate Cre in one stem cell every ~10 crypts. The DNA recombination activity of Cre induces a defined mutation in the confetti locus leading to expression of one of four confetti colors. Each of the four DNA mutations (i.e. confetti color) is inherited by all progeny resulting in clonal tracing. By visualizing the confetti-labelled stem cells over time, we could observe mutant stem cells that were outcompeted by wild-type cells (i.e. clones that were lost), mutant stem cells that were still in competition with wild-type cells (crypts in which a part of the stem cells were confetti labelled), and mutant stem cells that outcompeted all wild-type cells (crypts in which all stem cells were confetti labelled) (**Figure 3c,d**). When we analyzed the stem cell clones that were still in competition, as expected for neutral competition, we observed a drop in the number of confetti clones over time (**Figure 3c**). Consequently, the remaining clones became larger (**Figure 3e**). Strikingly, the average size of confetti mutant clones was smaller in CR animals than in control animals, which illustrated that it takes longer to outcompete the wild-type stem cells (**Figure 3e**). This slower stem cell competition in CR mice was significantly correlated with a larger crypt size (**Figure 3f**). Slower stem cell competition can be both caused by higher number of stem cells that compete, or by slower proliferation rate of the competing stem cells. Importantly we found that proliferation was not altered upon CR, as EdU incorporation to mark S-phase and the number of Phospho-Histone H3 positive cells (marking mitosis) was not different for the crypts in the CR and control animals (**Figure 3g,h**). Taken together, this shows that the reduced speed of monoclonal conversion is the consequence of an increased number of competitors in enlarged crypts.

To investigate the consequence of increased number of stem cell competitors and stronger competition, we again made use of the power of our repetitive intravital imaging to follow the fate of mutated stem cells in control and CR crypts. We induced confetti mutations by Cre activation and imaged the same mutated clones 48 hours and 8 weeks after induction using our repetitive imaging approach described above (**Figure 4a-c**). This enabled us to determine how many mutations remained in the epithelium after 8 weeks. While in control crypts 15.21% of all mutations (96 out of 631 clones) were still present, only 11.82% of all mutations were present after 8 weeks in CR crypts (**Figure 3d**). This shows that mutations in crypts of CR mice have 22.29% less chance to remain in the epithelium than mutations in control mice. Taken together, we show that CR leads to enlarged crypts with more stem cells that compete for niche space. This results in slower but stronger competition and a higher chance for a mutation to be outcompeted by wild-type stem cells.

Figure 3. Lineage tracing shows slower and stronger stem cell competition under calorie restriction. Lineage tracing was performed as schematically depicted in **(a)**. Mice were put on diet for 8 weeks to let the phenotype manifest before starting lineage tracing by tamoxifen injection. Mice were clonally induced (max. 1 cell per crypt). **(b)** Representative images of 48 hours and 8 weeks of tracing (scale bar = 200µm). **(c,d)** When looking at the same clones 48 hours and 12 weeks after induction using intravital imaging, clones can be found that are lost (top panel), still in competition (middle panel), or clones that have taken over the whole crypt, which is schematically represented in **d**. **(e)** When looking at the average clone size of clones still present in the crypt (% of crypt labeled with confetti color) at different time points after tracing, it could be observed that SC competition was more slowly resolved under CR ($n > 3$ mice per time point). **(f)** Clone size correlates with crypt diameter. **(g,h)** Slower SC competition is not explained by altered proliferation upon CR as shown by a 4 hour EdU pulse to measure S-phase or PH3 staining labeling mitosis. Representative image in left panel (scale bar = 40µm) and quantification in right panel ($n > 12$ mice per group). Mean \pm s.e.m. Dots represent individual mice.

CR has been shown to reduce the formation of DNA mutations that cause ageing, and age-related pathologies such as cancer. For example, CR reduces tumor initiation and progression in many tumor models, including intestinal polyp formation in APC^{min} mice¹⁹. While mechanisms such as reduced DNA damage and improved DNA repair may reduce the acquisition of mutations under CR, CR may also have other modes of action. Indeed, here we showed that when a mutation occurs, the chance that this mutation retains in intestinal tissues is smaller upon CR, since mutant stem cells have a higher chance to be outcompeted by the higher number of wild-type stem cells. This newly identified mode of action of CR may explain previous reported observations. A prior study reported that mutation frequencies in the *LacZ* gene in CR mice demonstrated reduced accumulation of mutations in the stem cells of small intestinal epithelium, but not in organs (i.e. liver and spleen) where stem cell competition does not take place²⁰. This further illustrates the importance of the here identified mode of action of CR to eliminate DNA mutations by altering stem cell competition.

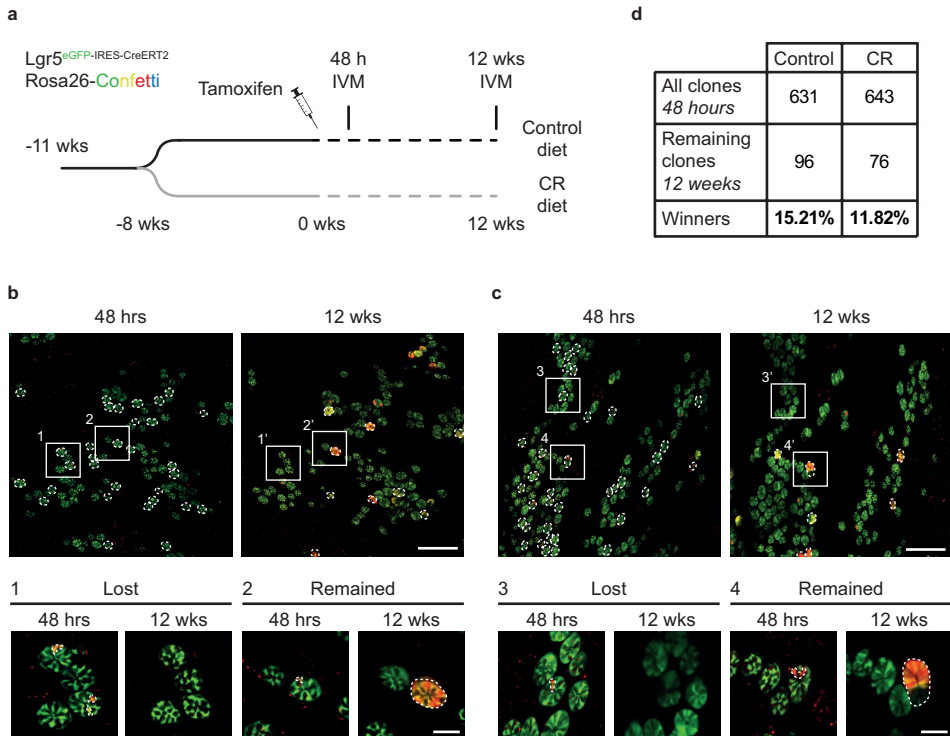


Figure 4. Repetitive intravital imaging reveals that less mutations are remained in CR crypts than in control crypts. Clonal persistence was measured using repetitive intravital imaging as schematically depicted in (a). After 8 weeks on control or CR diet, clones were induced by tamoxifen injection and imaged 48h after induction. The same clones were imaged 12 weeks later (b,c), and the number of clones that got lost and clones that remained were determined (c) ($n > 7$ mice per group).

MATERIALS AND METHODS

Mice

All experiments were carried out in accordance with the guidelines of the animal welfare committee of the Netherlands Cancer Institute. *Lgr5*^{EGFP-ires-CreERT2} and *Lgr5*^{EGFP-ires-CreERT2::R26-confetti} (double) heterozygous male and female mice (Bl6 background) were housed under standard laboratory conditions and received standard laboratory chow and water ad libitum prior to start of the experiment. Mice entered the experiment between 8-12 weeks of age.

Diet

Calorie restriction in mice was performed according to established protocols¹⁵. All mice were fed a AIN-93M control diet (Plexx B.V.; F05312) ad libitum for 2 weeks to get used to the food. The third week, mice were housed individually and food intake was measured three times. The fourth week, mice were randomly divided into two groups: CR mice received 80% of their ad libitum food intake using AIN-93M 20% CR diet (Plexx B.V.; F06298), while control mice received 90% of their ad libitum food intake using the AIN-93M control diet. After one week, CR mice were switched to AIN-93M 40% CR diet (Plexx B.V.; F05314) and fed 60% of their ad libitum food intake, while control mice received 90% of their ad libitum food intake using the control diet. For diet switching experiments, diets were switched from control to CR and from CR to control after 8-16 weeks with a transition period of 1 week for both groups on 80% of ad libitum food intake of AIN-93M 20% CR diet. The mice were then on the diet for 8 weeks.

Lineage tracing

For lineage tracing experiments, mice received an intraperitoneal injection with 1 mg / 30 g bodyweight tamoxifen (Sigma, T5648) dissolved in oil resulting in maximally 1 labeled cell per crypt. For crypt pattern experiments, mice received 5 mg / 30 g bodyweight tamoxifen. Mice were sacrificed at specified time points.

Repetitive in vivo imaging

Before and 8-12 hour after surgery mice received buprenorphine (subcutaneous, 100 µg/kg mouse, Temgesic; BD Pharmaceutical System). In addition, mice received Rimadyl (64 µg/ml, Carprofen; Zoetis B.V.) in the drinking water from 1 day prior to surgery till 3 days post-surgery. For surgery, mice were anesthetized through inhalation of 2% isoflurane (v/v). The abdomen was shaved and sterilized using povidone-iodine solution (Betadine). A midline abdominal incision was made and the small intestine was exposed and placed on sterile, PBS drenched gauze. The animal was placed in a custom made imaging box and tissue hydration was maintained by creating a wet chamber, covering the mice with parafilm and the exposed tissue with PBS drenched gauze. During imaging, anesthesia was maintained with 1.5% isoflurane (v/v). The mice were imaged 12 weeks after clone induction for crypt density experiment to create a recognizable pattern and 48 h after clone induction for persistence experiment. The second imaging session was 8-12 weeks after the first session. Images were recorded using an inverted Leica TCS SP8 multiphoton microscope. All images were collected in 12 bit with 25X water immersion objective (HC FLUOTAR L N.A. 0.95 W VISIR 0.17 FWD 2.4 mm). Overview images were recorded using a color camera and the Navigator function in the Leica LasX software. After imaging, the intestine was placed back and the abdomen was closed using resorbable sutures (GMED Healthcare BVBA). For diet

Chapter 5

switching experiments, the day after the first imaging session the diets were switched for half the mice in the control and CR groups.

Whole mount preparation

To prepare intestinal whole mounts, the distal small intestine was harvested and directly put on ice. After flushing three times with ice cold PBSO and it was cut open along its length. Using a cover glass, the villi were scraped off and the tissue was washed in ice cold PBSO. After fixing the tissue for 30 min in 4% formaldehyde solution (w/v) (Klinipath), the tissue was washed and either directly mounted between two coverslips using Vectashield HardSet Antifade Mounting Medium (Vector Laboratories) or further processed for immunofluorescence (see below). For long-term storage while maintaining endogenous fluorescence, tissues were fixed in periodate-lysine-4% paraformaldehyde (PLP) buffer²¹ overnight at 4°C, incubated in 30% sucrose >6h at 4°C and embedded in Tissue Freezing medium (Leica Biosystems).

Immunofluorescence

Stainings were performed on either 4% formaldehyde (w/v) (Klinipath) fixed or PLP fixed whole mounts. Tissues were blocked and permeabilized using a 3% bovine serum albumin (w/v) (BSA) and 0.8% Triton X-100 in PBS. The stainings were performed with the following primary antibodies: anti-GFP (Abcam, cat. no. ab6673), anti-RFP (Rockland, cat. no. 600-401-379), anti-lysozyme (DAKO, A0099) and anti-Phospho-Histone H3 (Ser10) (Millipore, 06-570). Secondary antibodies were combined with DAPI and/or phalloidin (Life Technologies, A-22287) and the tissue was mounted using Vectashield HardSet Antifade Mounting Medium (Vector Laboratories). To visualize the whole crypt-villus axis, tissues were cleared using FUnGI as described in Rios et al. 2019²². Whole mounts were imaged with TCS SP8 confocal and multiphoton microscopes (Mannheim, Germany). All images were collected with 20X dry (HCX IRAPO N.A. 0.70 WD 0.5 mm) or 25X water immersion (HC FLUOTAR L N.A. 0.95 W VISIR 0.17 FWD 2.4 mm) objectives in 12 bit. Images were only if necessary, corrected for bleed through, cropped, smoothed, rotated and contrasted linearly in Fiji. Quantification was performed in Fiji.

Cell proliferation

To label cells in S-phase, 1 mg of 5-ethynyl-2-deoxyuridine (EdU, 200 ul in PBS) was injected intraperitoneally. After 4 hours, the intestine was isolated and whole mounts were prepared as described above. Click-it staining reaction was performed according to the manufacturers protocol (Click-it EdU, cat. no. C10340; ThermoFisher). The tissues were incubated with a GFP (Abcam, cat. no. ab6673) and lysozyme (DAKO; cat. no. A0099) primary antibody. DAPI was combined with the secondary antibodies after which the tissues were mounted using Vectashield HardSet Antifade Mounting Medium (Vector Laboratories).

Quantification and statistical analysis

A Mann-Whitney test was performed using GraphPad Prism (GraphPad Software, LA Jolla, CA) to determine statistical significant differences between two means. Differences were considered statistical significant when $p < 0.05$. R^2 was determined using linear regression in GraphPad Prism (GraphPad Software, LA Jolla, CA).

ACKNOWLEDGMENTS

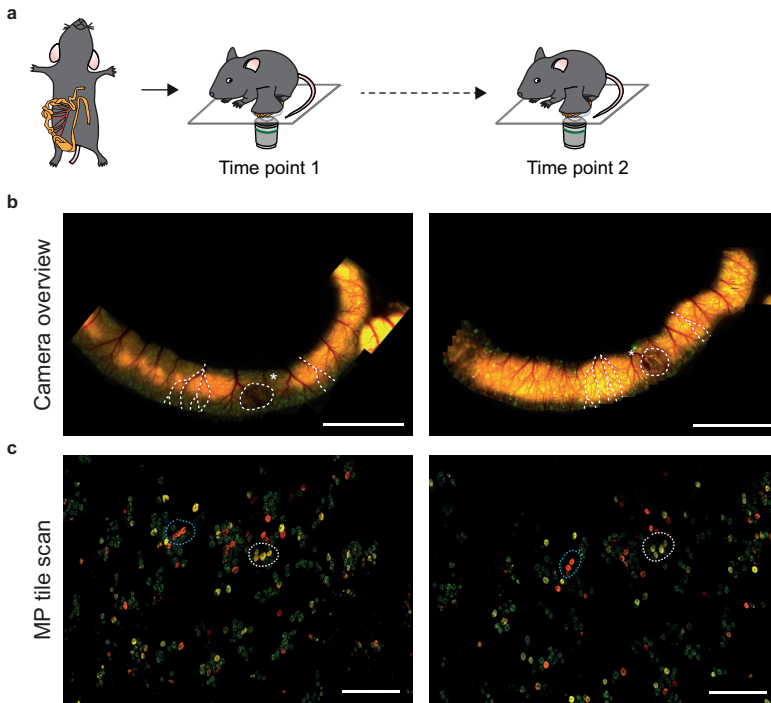
The authors would like to thank the staff at The Hubrecht Institute animal facility and The Netherlands Cancer Institute (NKI) animal facility and bioimaging facility for technical support and input, and members of the van Rheenen laboratory for discussions. This work was supported by the Netherlands Organization of Scientific Research NWO (Veni grant 863.15.011 to SIJE, Cancer Genomics Netherlands to JvR), the European Research Council (consolidator grant 648804 to JvR), the Worldwide Cancer Research (grant 13-0297 to JvR), the Dutch Cancer Society KWF (2013-6070 to HJS), and the Doctor Josef Steiner Foundation (to JvR).

AUTHOR CONTRIBUTIONS

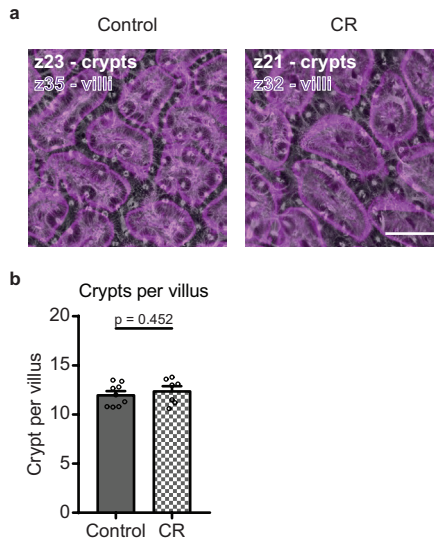
LB, HJS and JvR perceived the conceptual ideas, designed the experiments, and LS, SIJE, HJS and JvR wrote the manuscript. LB, SIJE, SJES, AJH, and PT performed experiments.

REFERENCES

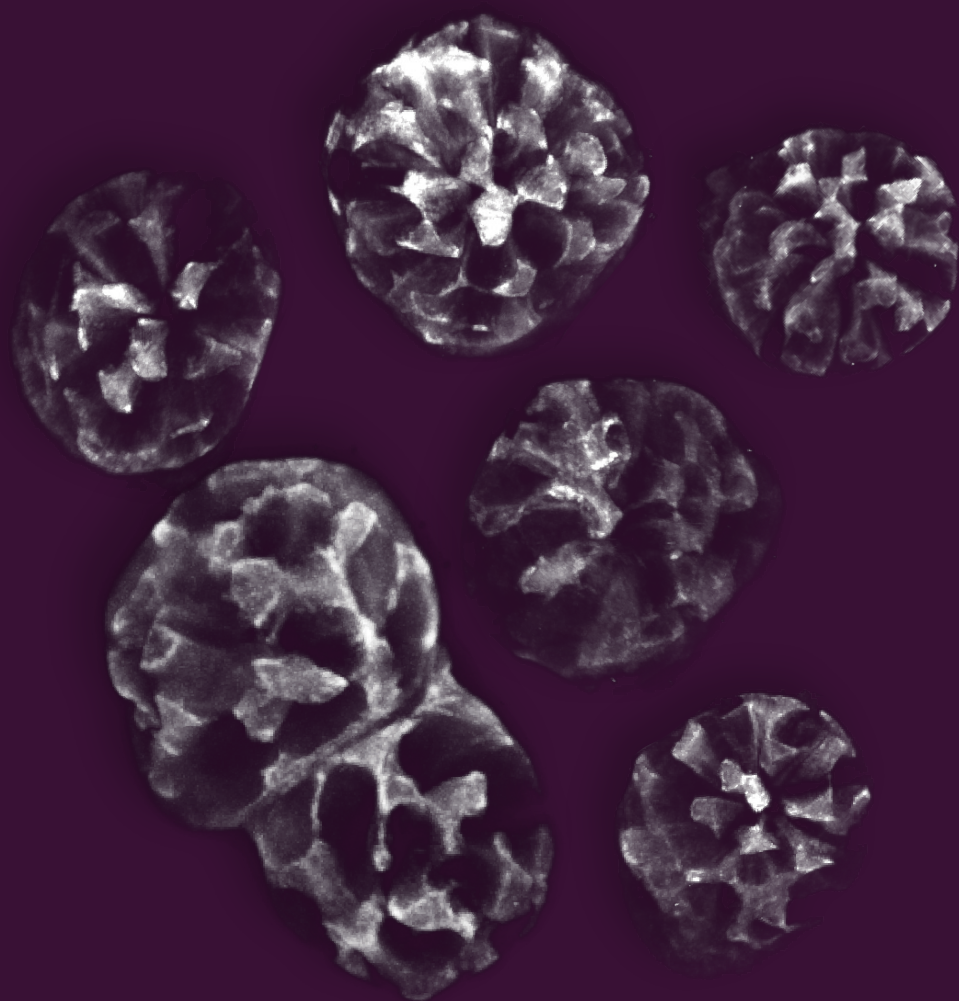
1. López-Otín, C., Blasco, M. A., Partridge, L., Serrano, M. & Kroemer, G. The hallmarks of aging. *Cell* **153** 1194 (2013).
2. Sohal, R. S. & Weindruch, R. Oxidative stress, caloric restriction, and aging. *Science* **273**, 59–63 (1996).
3. Bartke, A. *et al.* Extending the lifespan of long-lived mice. *Nature* **414**, 412 (2001).
4. Colman, R. J. *et al.* Caloric restriction delays disease onset and mortality in rhesus monkeys. *Science* **325**, 201–204 (2009).
5. Heydari, A. R., Unnikrishnan, A., Lucente, L. V. & Richardson, A. Caloric restriction and genomic stability. *Nucleic Acids Res.* **35**, 7485–7496 (2007).
6. Clevers, H. The Intestinal Crypt, A Prototype Stem Cell Compartment. *Cell* **154**, 274–284 (2013).
7. Rheeinen, J. van & Bruens, L. Cellular protection mechanisms that minimise accumulation of mutations in intestinal tissue. *Swiss Med. Wkly.* **147**, (2017).
8. Barker, N. *et al.* Identification of stem cells in small intestine and colon by marker gene Lgr5. *Nature* **449**, 1003–1007 (2007).
9. Snippert, H. J. *et al.* Intestinal crypt homeostasis results from neutral competition between symmetrically dividing Lgr5 stem cells. *Cell* **143**, 134–144 (2010).
10. Ritsma, L. *et al.* Intestinal crypt homeostasis revealed at single-stem-cell level by in vivo live imaging. *Nature* **507**, (2014).
11. Snippert, H. J., Schepers, A. G., Van Es, J. H., Simons, B. D. & Clevers, H. Biased competition between Lgr5 intestinal stem cells driven by oncogenic mutation induces clonal expansion. *EMBO Rep.* **15**, 62–69 (2014).
12. Vermeulen, L. *et al.* Defining stem cell dynamics in models of intestinal tumor initiation. *Science* **342**, 995–8 (2013).
13. Huels, D. J. *et al.* Wnt ligands influence tumour initiation by controlling the number of intestinal stem cells. *Nat. Commun.* **9**, 1132 (2018).
14. Yan, K. S. *et al.* Non-equivalence of Wnt and R-spondin ligands during Lgr5+ intestinal stem-cell self-renewal. *Nature* **545**, 238–242 (2017).
15. Pugh, T. D., Klopp, R. G. & Weindruch, R. Controlling caloric consumption: protocols for rodents and rhesus monkeys. *Neurobiol. Aging* **20**, 157–65 (1999).
16. Beyaz, S. *et al.* High-fat diet enhances stemness and tumorigenicity of intestinal progenitors. *Nature* **531**, 53–58 (2016).
17. Igarashi, M. & Guarente, L. mTORC1 and SIRT1 Cooperate to Foster Expansion of Gut Adult Stem Cells during Calorie Restriction. *Cell* **166**, 436–450 (2016).
18. Bruens, L., Ellenbroek, S. I. J., van Rheeinen, J. & Snippert, H. J. In vivo Imaging Reveals Existence of Crypt Fission and Fusion in Adult Mouse Intestine. *Gastroenterology* **163**: 674-677 (2017)
19. Mai, V. *et al.* Calorie restriction and diet composition modulate spontaneous intestinal tumorigenesis in Apc(Min) mice through different mechanisms. *Cancer Res.* **63**, 1752–5 (2003).
20. He, D. *et al.* Effects of calorie restriction on the age-dependent accumulation of mutations in the small intestine of lacZ-transgenic mice. *Mech. Ageing Dev.* **132**, 117–122 (2011).
21. McLean, I. W. & Nakane, P. K. Periodate lysine paraformaldehyde fixative. A new fixative for immunoelectron microscopy. *J. Histochem. Cytochem.* **22**, 1077–1083 (1974).
22. Rios, A. C. *et al.* Intracлонаl Plasticity in Mammary Tumors Revealed through Large-Scale Single-Cell Resolution 3D Imaging. *Cancer Cell* **35**, 618–632.e6 (2019).



Supplementary Figure 1. Repetitive intravital microscopy to find back the same crypt region. (a) Schematic overview of repetitive intravital microscopy experiment, where the same crypts are imaged with an 8/12 week interval. The same regions are found back using (b) the vessel structure imaged with a color camera overview in the Leica Navigator software (scale bar = 5mm) and (c) the patchy pattern of *Lgr5*-eGFP expression recorded using the multiphoton (MP) laser (scale bar = 500 μ m).



Supplementary Figure 2. 3D imaging of crypt-villus axis shows same number of crypts per villus in CR compared to control (a) Representative image of an overlay of crypts (grey) feeding into a villus (magenta) from a cleared whole mount sample (scale bar = 100 μ m). **(b)** the number of crypts feeding into a villus is unaltered by CR ($n > 7$ mice per group).



Chapter 6

In Vivo Imaging Reveals Existence of Crypt Fission and Fusion in Adult Mouse Intestine

Bruens L, Ellenbroek SJ, van Rheenen J, Snippert, H

Adapted from Gastroenterology 153: 674-677 (2017)

ABSTRACT

The intestinal epithelium is a repetitive sheet of crypt and villus units with stem cells at the bottom of the crypts. During postnatal development, crypts multiply via fission, generating two daughter crypts from one parental crypt. In the adult intestine, crypt fission is observed at a low frequency. Using intravital microscopy in *Lgr5EGFP-Ires-CreERT2* mice, we monitored individual crypt dynamics over multiple days with single-cell resolution. We discovered the existence of crypt fusion, an almost exact reverse phenomenon of crypt fission, in which two crypts fuse into one daughter crypt. Examining 819 crypts in 4 mice, we found that 3.5%–0.6% of all crypts were in the process of fission, whereas 4.1–0.9% of all crypts were undergoing crypt fusion. As counteracting processes, crypt fission and fusion could regulate crypt numbers during the lifetime of a mouse. Identifying the mechanisms that regulate rates of crypt fission and fusion could provide insights into intestinal adaptation to altered environmental conditions and disease pathogenesis.

MAIN TEXT

Crypts of Lieberkühn are central elements of the self-renewing nature of the intestine because they harbor active cycling stem cells at their base and progenitor cells along the flanks. During postnatal development, crypts are dynamic structures that undergo multiple rounds of replication via a process called crypt fission to accommodate the elongation of the intestinal tract¹. In general, this process occurs through bifurcation of individual crypts where branching starts at the base and elongates toward the villus in a zipper-like fashion. This bifurcation is thought to be completed within 1 week². In addition to elongation of the intestinal tract, this process has been shown to play an essential role in the regenerative response after irradiation and tissue resection^{3,4}.

Interestingly, generation of new crypts does not completely disappear in adulthood, where fission remains continuously present^{2,5}. Intriguingly however, the relative high number of crypt fission events^{2,5} seems to be at odds with the observation that small intestinal length only slightly increases during aging, while both small intestinal width and crypt density remain constant (**Supplementary Figure 1**). In addition, analyses of crypt ancestry by Cre-induced lineage tracing⁶ or mutation-induced marker systems⁷ also indicate that fewer crypt fission events have occurred than the frequency of crypt branching events suggest. Previously, the concept of the crypt cycle has been proposed to describe the continuous growth and bifurcation of crypts analogous to the cell cycle⁸. Mechanisms that counterbalance the continuous production of new crypts have been postulated, including crypt death, but direct evidence has never been reported.

Recently, we developed intravital microscopy (IVM) techniques that enable us to monitor intestinal stem cells, crypt size, composition, and dynamics over multiple days with single-cell resolution⁹. To identify mechanisms that have the ability to counterbalance the continuous production of new crypts, the small intestine of mice was positioned behind an abdominal imaging window and imaged over multiple consecutive days. Using Lgr5EGFP-Ires CreERT2 knock-in mice (See Materials and Methods), we took advantage of the fluorescent marking of intestinal stem cells at the crypt bottom, ie, Lgr5+ crypt base columnar cells. Following crypt morphology over time using IVM, we indeed observed crypts undergoing fission in line with previous observations^{5,10}.

Surprisingly, in addition to previously described crypt fission, we observed crypt fusion events where two independent crypts merge together to form one daughter crypt with one central lumen (**Figure 1a**). Intriguingly, based on the evolving crypt morphology during the process, a fusion event seems to be an almost exact reversal phenomenon of a crypt fission process (**Figure 1b,c**). As such, crypt fusion has the potential to act as a counterbalancing mechanism for the continuous birth of crypts via crypt fission.

To confirm that crypt fusion involves two autonomous and independent crypts rather than being a reversal of incomplete crypt fission, we crossed Lgr5EGFP-ires-CreERT2 mice with the Cre-reporter mouse strain LSL-tdTomato. In this mouse model, the LSL-tdTomato allele recombines at very low background levels (0.86% ± 0.31% of all Lgr5+ crypts, 4 mice; **Supplementary Figure 2a**), thereby occasionally giving rise to individual, fully tdTomato-labeled crypts as a result of neutral drift^{11,12}. As expected, we found tdTomato-labeled crypts with an 8-shaped crypt circumference that is representative of the intermediate state of either crypt fission or fusion (**Figure 2a**). The distribution pattern of tdTomato-labelled cells within 8-shaped crypts allowed us to discriminate between these two processes (**Supplementary Figure 2b**). Crypt fission events were scored when 8-shaped crypts were fully labeled because the chance of independent labeling events in two neighboring crypts before

fusion could be neglected because of the low labeling frequency. In contrast, 8-shaped crypts in which labeling was restricted to one half were scored as crypt fusion events because fissions of non-clonal crypts were not observed (for further explanation see **Supplementary Figure 2b**). After examining 819 fully labeled crypts (4 mice), we found that $3.5\% \pm 0.6\%$ of all labeled crypts were in the process of crypt fission, while $4.1\% \pm 0.9\%$ of all labeled crypts were in the process of crypt fusion (**Figure 2a,b; Supplementary Figure 2c**).

Next, using IVM we monitored a substantial amount of sporadically tdTomato-marked crypts and identified a fusion event between two independent *Lgr5*^{EGFP+} crypts (**Figure 2a**). Interestingly, 24 hours after central lumen formation, tdTomato+ cells started to intermingle with non-marked cells, indicating that both stem cell pools are now united and participate within the same neutral drift toward clonality^{11,12}.

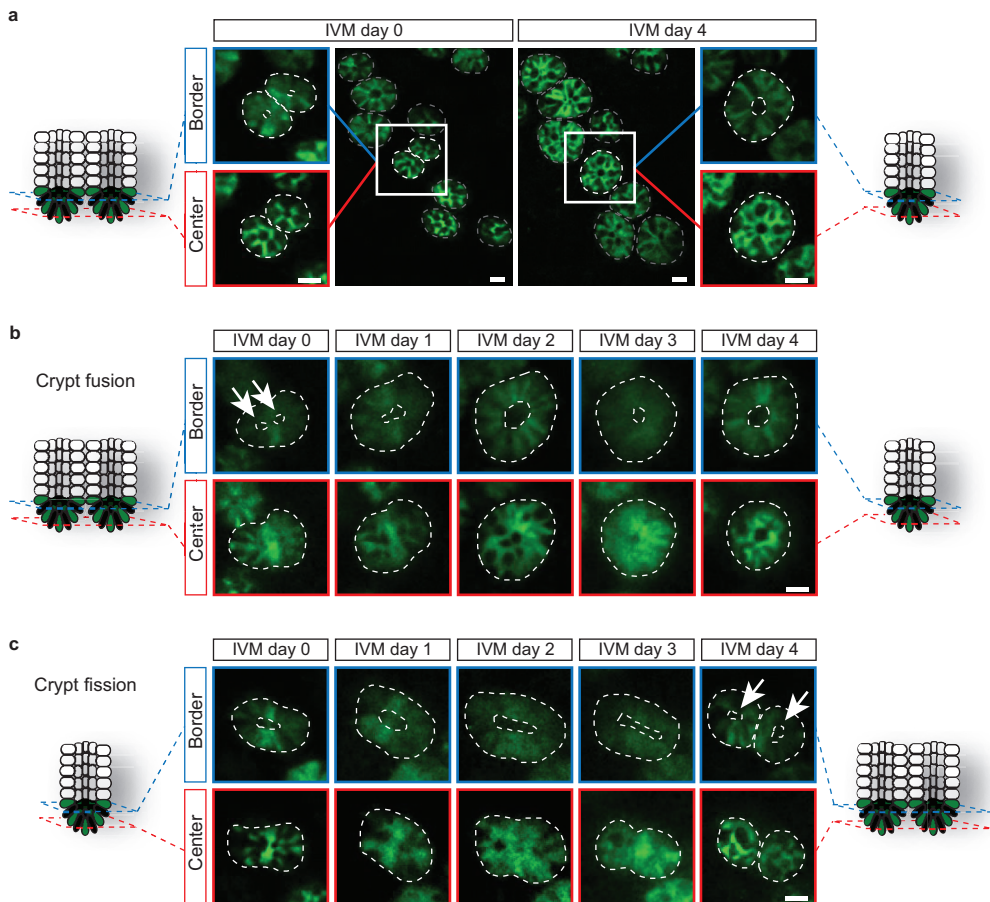


Figure 1. Crypt dynamics includes both crypt fission and crypt fusion. a. Crypt fusion event where 2 separate crypts (day 0) merged into 1 crypt (day 4). Overview panels (middle) show crypt pattern to confirm crypt identity. Outer panels show enlargement of imaging planes at center and border of stem cell zone. **b.** Representative examples of crypt fusion and **(c)** fission where a single event is followed over 5 consecutive days by IVM. Arrows point at separate lumen. Dotted lines indicate outlines of *Lgr5*^{EGFP+} (green) crypts and lumen. Cartoons illustrate process at beginning (left) and end (right). Scale bars: 20 μ m.

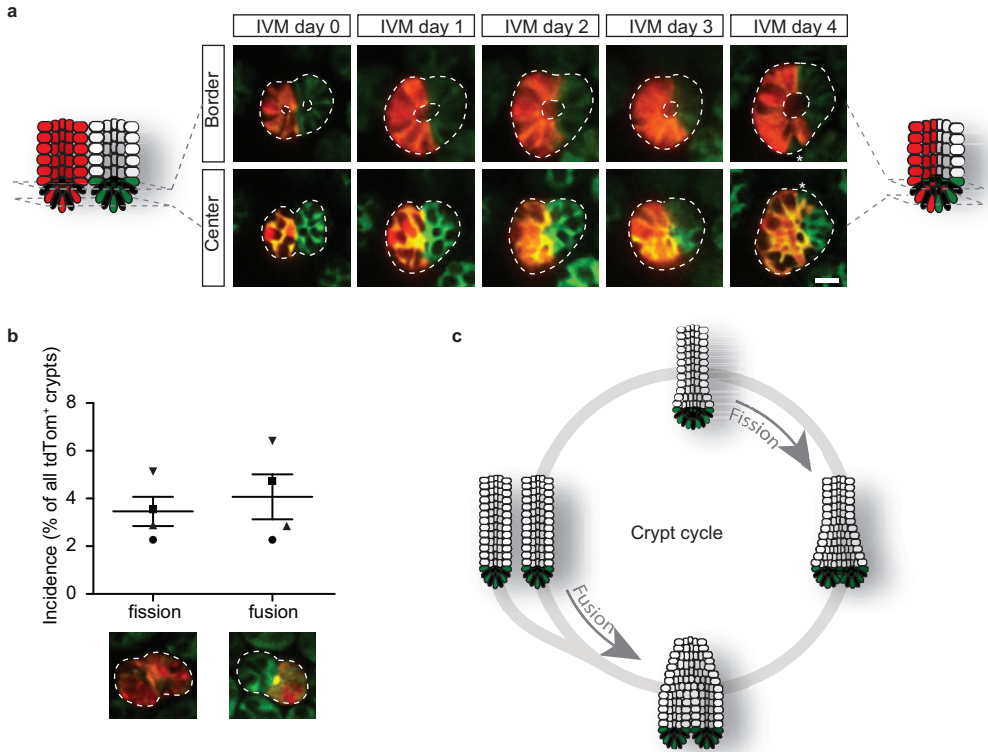


Figure 2. Fusion events of 2 independent crypts. **a.** IVM images of 5 consecutive days reveals crypt fusion between *tdTomato+* (red) and non-labelled crypt. Cartoons illustrate process at beginning (left) and end (right). Dotted lines indicate outlines of *Lgr5^{EGFP+}* (green) crypts and lumen. Asterisks indicate competing cells within neutral drift. Scale bar: 20 μ m. **b.** Quantification of fission and fusion events in fixed whole mount samples of proximal and distal intestine (819 *tdTomato+* crypts, 4 mice). Symbols indicate individual mice. Representative examples of crypt fission (left) and fusion (right) are depicted below. **c.** Schematic representation of crypt cycle that includes crypt fission and fusion.

Our ability to monitor evolving crypt morphology over time provided the opportunity to identify the existence of crypt fusion during homeostatic conditions in adulthood. Because crypt fission and fusion occur at approximately similar frequency, it can be speculated that, as counteracting mechanisms, they are involved in regulating crypt numbers. However, many variables concerning fission and fusion are poorly understood, underscoring why both frequencies are not exactly in line with the slight increase of intestinal length during aging. For instance, minor deviations in duration of both processes or differences in frequencies per region along the gastrointestinal tract or during aging might explain the discrepancy. Moreover, other non-discovered counterbalancing mechanisms cannot be excluded.

Although opposite processes, crypt fission and fusion are morphologically nearly identical, explaining why crypt fusion has not been identified with conventional analyses of fixed tissue. Identification of immunohistochemistry markers to discriminate between fission and fusion would facilitate studies on human samples. One way to identify such markers would be by combining laser capture microdissection with genomic approaches. Indeed, laser capture microdissection on bifurcating human crypts has

Chapter 6

already been performed to study methylation patterns^{13,14}. Intriguingly, adjacent crypts in human colon, and even 2 arms of a bifurcating crypt, can be as dissimilar to one another as two unrelated distantly located crypts^{14,15}. The presence of crypt fusions could very well explain these counterintuitive observations.

Crypt fusion exists in adulthood during homeostasis and is a counterbalancing process for the continuous birth of new crypts (**Figure 2c**). It is well known that crypt fission underlies the regenerative response of the intestinal epithelium. Identifying the mechanisms that modulate the rates of crypt fission and fusion is of high interest to understand intestinal adaptation to altered environmental conditions in health and disease.

MATERIALS AND METHODS

Mice

Lgr5^{EGFP-ires-CreERT2} and Lgr5^{EGFP-ires-CreERT2}:LSL-tdTomato male and female mice (mixed background between C57BL/6 and 129/Ola) were housed under standard laboratory conditions and received standard laboratory chow and water ad libitum. Random (double) heterozygous mice were used for the experiments. Male and female mice between 12–14 weeks old were used for IVM. For whole mount imaging intestines from 8–79-week-old male and female mice were used. Background recombination frequency was determined in 4 mice. Quantification of crypt fission and crypt fusion in whole mount samples was based on 819 fully labeled crypts in 4 mice. All experiments were carried out in accordance with the guidelines of the Animal Welfare Committee of the Royal Netherlands Academy of Arts and Sciences.

Whole mount preparation

To prepare whole mounts, the small intestine was harvested and directly put on ice. It was flushed 3 times with ice-cold PBSO and cut open along its length. The villi were removed using a cover glass and the tissue was washed in ice-cold PBSO. After fixing the tissue for 30 min in 4% formaldehyde solution (w/v) (Klinipath), it was mounted between 2 coverslips using Vectashield HardSet Antifade Mounting Medium (Vector Laboratories). Crypts were imaged from the bottom using the same equipment and settings as for intravital microscopy described below.

Abdominal imaging window surgery

The abdominal imaging window (AIW) surgery was performed as previously described.⁹ In short, before surgery buprenorphine (100 µg/kg mouse; Temgesic, BD Pharmaceutical Systems) was administered via a subcutaneous injection. All surgical procedures were performed under anesthesia via 2% isoflurane (v/v) inhalation. At the start of the surgery, the skin of the mouse was shaved and disinfected with 70% (v/v) ethanol and a left lateral flank incision was made through skin and peritoneum of the mouse. Next, a purse string suture was placed along the wound edge. The ileum was taken out of the abdominal cavity and placed on top of a disinfected AIW (>1 h in 70% [v/v] ethanol) that was positioned glass-side down. The mesenterium was fixed to the cover glass using Cyanoacrylate Glue (Pattex) and CyGel (BioStatus Limited) was added on top of the ileum to reduce peristaltic movement. After allowing the Ultra Gel and CyGel to dry for 1 min, the AIW, together with the ileum, was inverted and placed into the mouse, ensuring that the skin and abdominal wall were placed into the groove of the AIW. Next, the suture was tightened to secure the AIW into the mouse. After surgery, the mice were closely monitored daily for reactivity, behavior, appearance, and defecation. The mice were provided with food and water ad libitum.

Equipment and settings

Intravital microscopy was performed as previously described⁹. An inverted Leica TCS SP5 AOBS 2-photon microscope was used with a chameleon Ti:Sapphire pumped optical parametric oscillator (Coherent) equipped with 4 non-descanned detectors (NDDs) and a ×25 (HCX IRAPO NA0.95 WD 2.5mm) water objective. The NDDs collect the wavelengths: NDD1 (HyD1): 555–680 nm, NDD2 (HyD2): 505–550 nm, NDD3 (PMT1): 455–505 nm, NDD4 (PMT2): <455 nm. Scanning was performed

Chapter 6

at 940nm wavelength. Re-identification of the same crypts over multiple days was accomplished by storing *xy* coordinates of different positions using the 'multiple position' function in the LAS-AF software and using the vasculature and the typical patchy Lgr5⁺ crypt pattern as visual landmarks.

Multi-day crypt imaging

Following the AIW surgery, mice were kept under anesthesia with isoflurane (1% [v/v]) for imaging and placed in a custom-designed imaging box as previously described⁹. After each imaging session mice were allowed to recover before being placed back in their cage. The following 3–4 days, mice were imaged daily for a maximum of 4 h. The climate chamber around the microscope was kept at 36°C and body temperature of the animals was monitored using a rectal probe. The patchy pattern of the Lgr5 knock-in allele, in combination with specific landmarks such as blood vessels, enabled us to discriminate individual crypts that could be repeatedly identified over consecutive days. After imaging, the acquired z-stacks were further processed and analyzed using basic functions in ImageJ software.

AUTHOR CONTRIBUTIONS

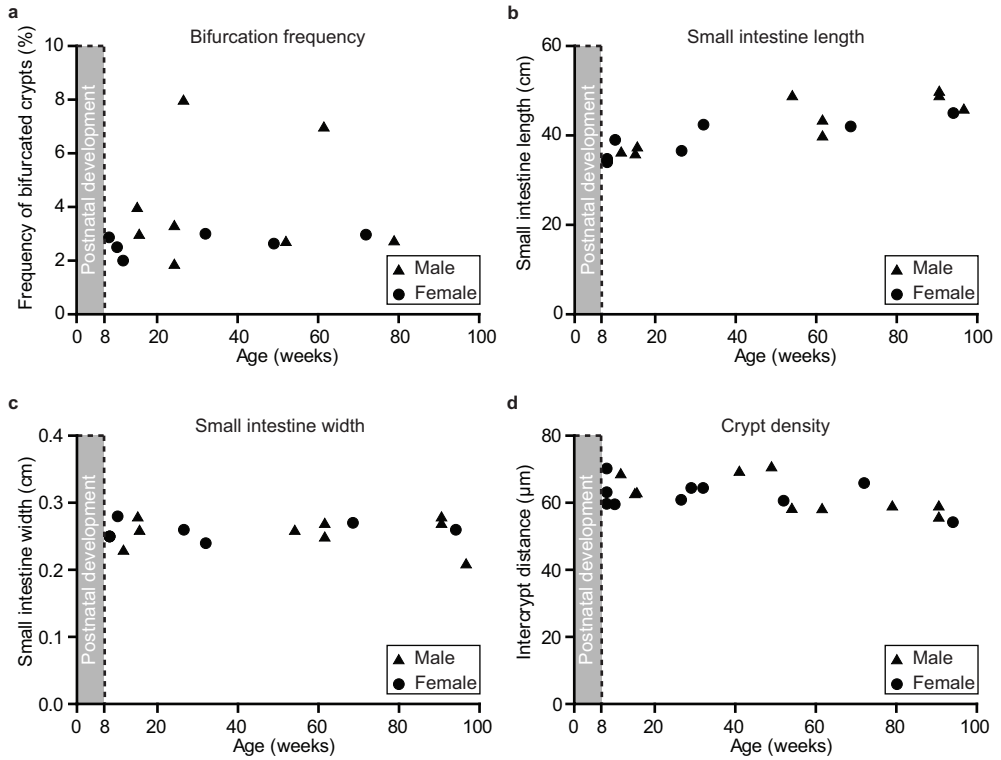
JvR and HJS conceived the study and designed the experiments. LB and SIJE performed experiments and analyses. All authors contributed to the writing and have approved the final manuscript. JvR and HJS contributed equally to this work.

ACKNOWLEDGMENTS

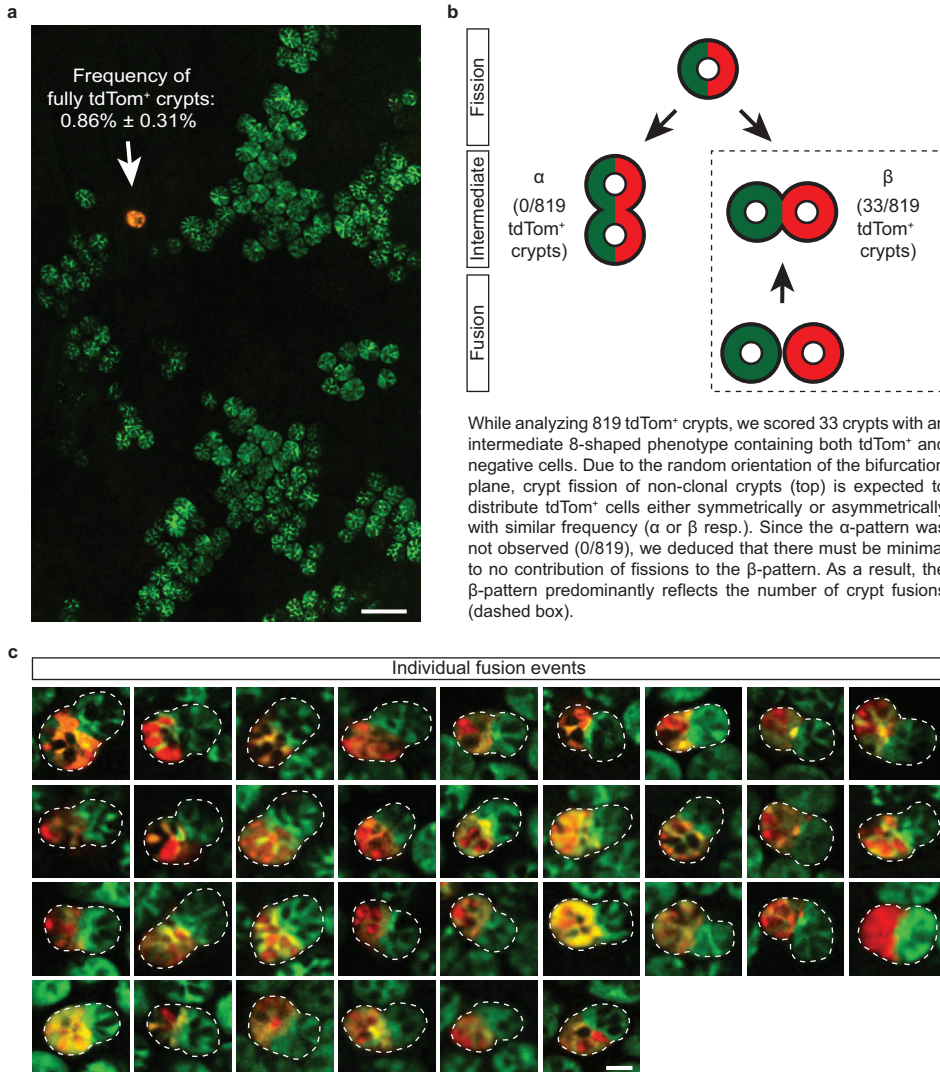
This work was supported by the Netherlands Organization of Scientific Research NWO (Veni grant 863.15.011 to SIJE), the European Research Council (consolidator grant 648804 to JvR), the Worldwide Cancer Research (grant 13-0297 to JvR), and the Dutch Cancer Society KWF (2013-6070 to HJS)

REFERENCES:

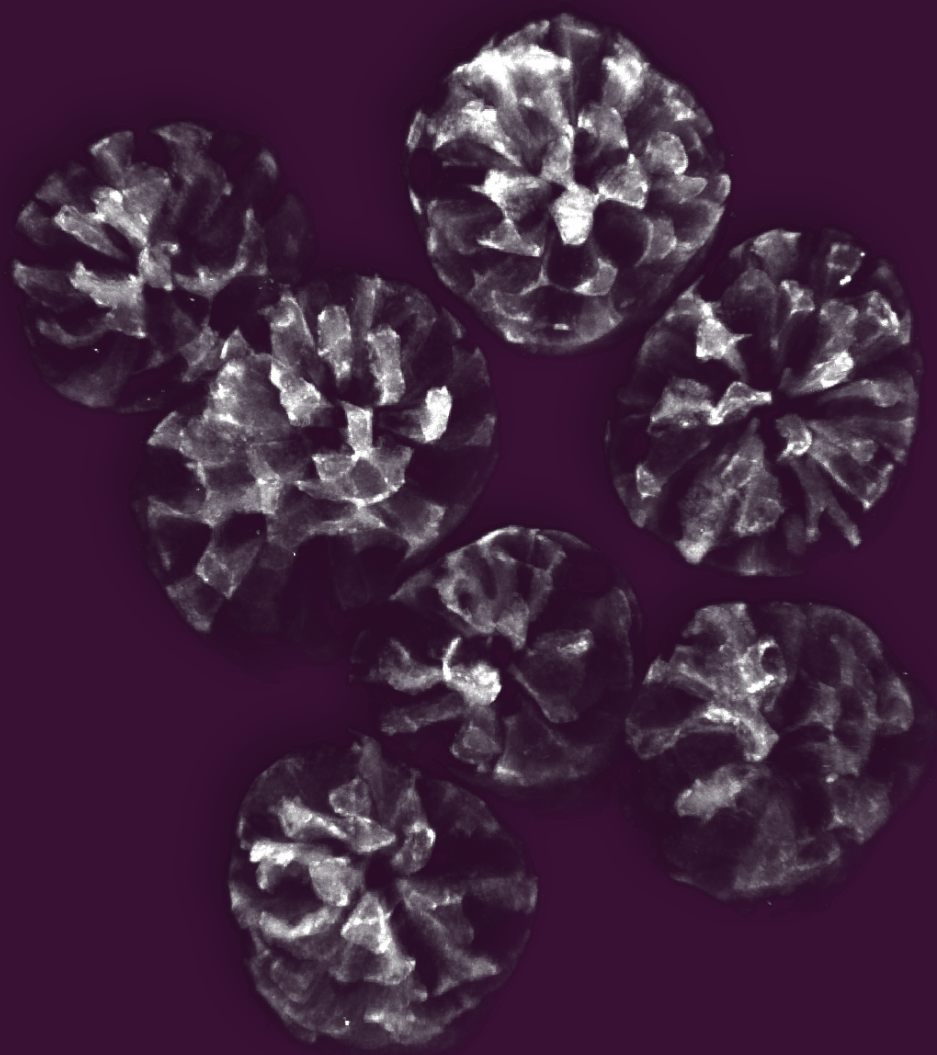
1. Clarke, R. M. The effect of growth and of fasting on the number of villi and crypts in the small intestine of the albino rat. *J. Anat* **112**, 27–33 (1972).
2. Bjerknes, M. A test of the stochastic theory of stem cell differentiation. *Biophys. J.* **49**, 1223–1227 (1986).
3. Cheng, H., McCulloch, C. & Bjerknes, M. Effects of 30% intestinal resection on whole population cell kinetics of mouse intestinal epithelium. *Anat. Rec.* **215**, 35–41 (1986).
4. Cairnie, A. B. & Millen, B. H. Fission of crypts in the small intestine of the irradiated mouse. *Cell Prolif.* **8**, 189–196 (1975).
5. Cheng, H. & Bjerknes, M. Whole population cell kinetics and postnatal development of the mouse intestinal epithelium. *Anat. Rec.* **211**, 420–426 (1985).
6. Snippert, H. J., Schepers, A. G., Van Es, J. H., Simons, B. D. & Clevers, H. Biased competition between Lgr5 intestinal stem cells driven by oncogenic mutation induces clonal expansion. *EMBO Rep.* **15**, 62–69 (2014).
7. Li, Y. Q., Roberts, S. a, Paulus, U., Loeffler, M. & Potten, C. S. The crypt cycle in mouse small intestinal epithelium. *J. Cell Sci.* **107** (Pt 1, 3271–3279 (1994).
8. Totafurno, J., Bjerknes, M. & Cheng, H. The crypt cycle. Crypt and villus production in the adult intestinal epithelium. *Biophys. J.* **52**, 279–294 (1987).
9. Ritsma, L. *et al.* Intestinal crypt homeostasis revealed at single-stem-cell level by in vivo live imaging. *Nature* **507**, 362–5 (2014).
10. Langlands, A. J. *et al.* Paneth Cell-Rich Regions Separated by a Cluster of Lgr5+ Cells Initiate Crypt Fission in the Intestinal Stem Cell Niche. *PLoS Biol.* **14**, e1002491 (2016).
11. Greaves, L. C. *et al.* Mitochondrial DNA mutations are established in human colonic stem cells, and mutated clones expand by crypt fission. *Proc. Natl. Acad. Sci. U. S. A.* **103**, 714–719 (2006).
12. Graham, T. A. *et al.* Use of methylation patterns to determine expansion of stem cell clones in human colon tissue. *Gastroenterology* **140**, 1241–1250 (2011).
13. Kim, K.-M. & Shibata, D. Tracing ancestry with methylation patterns: most crypts appear distantly related in normal adult human colon. *BMC Gastroenterol.* **4**, 8 (2004).



Supplementary Figure 1. Dimensions of small intestine during aging. **a.** Frequency of all crypts with a bifurcation phenotype in mice of different ages, counted in whole mounts of distal intestine. **b,c.** Length (**b**) and (**c**) width of small intestine from mice of different ages. **d.** Crypt density, measured as average distance between centers of neighboring crypts, in mice of different ages.



Supplementary Figure 2. Discrimination between crypt fission and fusion. **a.** Representative image of whole mount sample of a field of *Lgr5^{EGFP+}* crypts (green) and a single *tdTomato⁺* crypt (red). Scale bar: 100 μ m. **b.** Schematic diagram illustrating the possible processes (fission and fusion) that can yield the 2 distribution patterns of *tdTomato⁺* cells over 2 branches of an 'intermediate' 8-shaped crypt. Number of observations of α and β pattern are indicated. Crypt fission contributes equally to both labeling patterns. Because a pattern is not observed, we deduced that crypt fusion is responsible for the 33 scored events of the β pattern. **c.** Images of all 33 observed fusion events. Scale bar: 20 μ m.



Chapter 7

Summarizing discussion

In this thesis, we investigated the role of stem cell competition in the elimination of mutations that arise in long-lived intestinal stem cells. In contrast to for instance stem cells in the hematopoietic system, intestinal stem cells are highly proliferative. This characteristic is inherent to the dual function of the intestine: taking up metabolites while functioning as a protective barrier against environmental insults. These tasks are carried out by a single-cell layer of postmitotic cells lining the villi that protrude into the intestinal lumen, thereby enlarging the absorptive area, but also exposing the epithelium to a hazardous environment. To minimize exposure to this harsh environment, the whole epithelial lining is replaced every 3-5 days, imposing a very short lifetime on the majority of epithelial cells¹. To achieve this, stem and progenitor cells at the bottom of the crypts proliferate approximately once a day pushing postmitotic cells upwards².

Crypts form invaginations in the intestinal wall where they are well protected from the hazardous environment. A narrow opening of ~6 μm between the crypt and the lumen limits diffusion, preventing direct contact of stem cells with the digestive process. In addition, stem cells secrete fluids to flush the crypt lumen, and Paneth cells produce antimicrobial products that, together with the mucus produced by Goblet cells, form a barrier to the intestinal lumen that ensures mucosal immunity^{3,4}. This architecture ensures the protection of stem cells from the harmful environment in the intestinal lumen.

Even though stem cells are well protected within their niche, mutations can still arise, for instance due to spontaneous processes^{5,6}. Somatic mutations can result in senescence or cell death and thereby contribute to ageing⁷. Alternatively, Fearon and Vogelstein described that accumulation of subsequent mutations can result in the initiation and progression of colorectal cancer⁸. However, the morphology of the intestinal epithelium is designed to minimize the retention and spread of mutations in the epithelium after they appear. For instance, compartmentalization of stem cells in crypts results in physical hindrance limiting the spread of mutated cells throughout the epithelium⁹. In addition, limited niche space at the bottom of these compartments and the proliferative capacity of stem cells result in stem cell competition leading to the loss of most mutated stem cells^{10,11}. In this thesis, we use intravital imaging to investigate intestinal stem cell and crypt dynamics and explore how this may affect the accumulation of mutations in the epithelium. We reviewed how live cell and intravital microscopy over the recent years have contributed to the understanding of stem cell dynamics and plasticity (**Chapter 1**) and we gave our perspective on how the dynamic nature of the intestinal epithelium results in expulsion of many mutated cells (**Chapter 2**). In addition, we explored the dynamics that underlie stem cell competition at the bottom of crypts in different parts along the intestinal tract (**Chapter 3**) and show that niche size affects this competition (**Chapter 4 & 5**). We also described the discovery of the phenomenon of crypt fusion that influences stem cell and crypt dynamics (**Chapter 6**). In this last chapter, I will summarize our findings and discuss them in the light of current literature.

Modeling the dynamics of stem cell competition

In **Chapter 3**, we described the stem cell dynamics that underlie stem cell competition in the distal small intestine (SI) and large intestine (LI). During stem cell competition, stem cells compete for niche space: upon each stem cell division, the number of stem cells exceeds the available positions within the niche, which is counter-balanced by loss of a stem cell from this niche. This constant stem cell division and stem cell loss leads to the expansion or extinction of stem cell clones and ultimately to clonality of all stem cells in the niche^{12,13} (**Chapter 2**, Figure 1). Many labs, including ours, have studied the dynamics of this process in the SI. Multi-day intravital microscopy has shown that all Lgr5⁺ stem cells

can contribute to the competition (¹⁴ and **Chapter 3**). However, cells at the border of the niche are more susceptible to displacement into the transit amplifying compartment than those located at the center. Since cells constantly gain or lose favorable positions by changing position, they function as a single stem cell pool with a combined output equal to 6 equipotent functional stem cells as was predicted by mathematical modeling^{14,15}. In the SI, all Lgr5⁺ cells participate in the stem cell competition. However, there is a gradient going from the bottom to the border of the stem cell zone with decreasing likelihood that a stem cell replaces all other stem cells in the niche. Already in 1995, it was shown that the process of stem cell competition is faster in the colon than in the SI, meaning that crypts reach a monoclonal state quicker¹⁶. In this study, a primitive form of lineage tracing was performed; the mutagen ethyl nitrosourea (ENU) was used to induce mutations in the enzyme glucose-6-phosphate dehydrogenase (G6PD) that could phenotypically be scored after histochemistry. While in the SI monoclonality was reached after ~12 weeks, it was reached between 4.6 and 7 weeks in the colon. Park *et al.* explain their observations by differences in the frequency of crypt fission¹⁶. They studied monoclonal conversion in mice at 6 weeks of age, when fission occurs frequently to accommodate the elongation of the intestine during postnatal development (more about crypt fission below). They found that the higher crypt fission frequency in the colon correlates with the faster drift towards monoclonality. Based on this, they propose that crypt fission speeds up the competition by segregating mutated and non-mutated cells into separate daughter crypts. However, we observe similar differences in fixation speed between small intestine and colon of adult mice in which fission rates are very low (see below: *What is the role of crypt fission and fusion?*). In collaboration with Ben Simons and Edouard Hannezo, we found that these low levels of crypt fission and fusion do not significantly affect stem cell competition during homeostasis (data not shown in this thesis). Therefore, we investigated alternative mechanisms to explain the differences in stem cell competition between small and large intestine.

Using our state-of-the-art intravital imaging techniques allowed direct and real-time visualization of the stem cell dynamics at the various sites of the intestinal tract. We found that in addition to cell movement along the crypt-lumen axis, there is also retrograde movement resulting in positional rearrangement of border and center cells within the niche. We found that this retrograde movement plays a pivotal role in the process of monoclonal conversion and that this is a crucial determinant of fixation speed (**Chapter 3**). Since there is a relative large amount of retrograde movement in the distal SI, both border and center stem cells can participate in the competition for niche space resulting in relatively slow drift. In the large intestine however, we observed an extremely low degree of retrograde movement suggesting only active participation of the stem cells at the bottom of the niche. Using repetitive intravital imaging we confirmed that large intestinal Lgr5⁺ cells at the border of the niche formed long-term clones with a very low frequency (undetectable in our experiments), uncoupling Lgr5 expression and stemness in this part of the intestine. Our results show that stemness is not a cell-intrinsic fate, but rather a potential that can be gained or lost, and that the retrograde movement determines the number of cells with such stem cell potential. In summary, due to low rates of retrograde movement in crypts of the large intestine, less cells have the potential to participate in stem cell competition for niche space. Ultimately this results in faster drift to clonality, compared to the SI where a higher rate of cellular mixing results in more competitors and therefore slower drift.

Interestingly, our findings seem in contrast with results obtained by the Winton group. Using a continuous clonal labeling approach, in combination with a simple mathematical model, they concluded that in the distal SI, the stem cell pool functions as 6 stem cells with equal stem cell potential, while in

Chapter 7

the colon the stem cell pool functions as 7 equal stem cells¹⁵. The rate that a stem cell is replaced per day was calculated to be 0.2 in the SI and 0.3 in the large intestine, meaning once every 5 days versus once every 3.3 days. Thus, they concluded that more stem cells replace each other at a faster rate in the colon and less stem cells replace each other at a slower rate in the SI. However, from Ritsma *et al.* and **Chapter 3**, we know that stem cells at the bottom of the crypt do not have equal stem cell potential; location within the niche determines the chance that a cell can function as a stem cell¹⁷. In the SI, border cells have for instance 3 times less chance to function as a stem cell than center cells. Therefore, a one dimensional model assuming equal stemness of all cells may not capture the full complexity of stem cell dynamics at the bottom of the crypt. In collaboration with the labs of Ben Simons and Edouard Hannezo, we are currently attempting to reconcile the findings by the Winton group and our own findings described in **Chapter 3**.

The effect of the number of stem cells

Our data in **Chapter 3** showed that the number of cells with stem cell potential is different for the small and large intestine. This difference affected the dynamics of stem cell competition in the crypt which could potentially affect the accumulation of mutations in these tissues. When investigating this effect, multiple factors should be considered, including the number of cells with stem cell potential that can participate in the competition. The neutral drift model of stem cell competition predicts that a mutation can only remain in a crypt long-term when it is present in the one stem cell that wins the competition; mutations in the other stem cells will get lost. This has indeed been shown for mutations in the oncogenes APC and KRAS¹⁸. Therefore, participation of more competitors in a larger stem cell zone increases the chance that a mutation is lost from the crypt, thus favoring a larger number of stem cells over a smaller number of stem cells to ensure protection against mutation accumulation. In addition, a mutation can fix more rapidly when a smaller number of stem cells compete, potentially speeding up tumor initiation (as shown in **Chapter 4**), while it takes more time in a larger stem cell zone (as shown in **Chapter 5**).

While a bigger stem cell pool may be protective against mutation accumulation, it also comes at a cost. For instance, bigger crypts harboring more stem cells can maintain a larger part of the epithelium. Therefore, when a mutation takes over a large crypt, it can take over a larger fraction of the epithelium creating a larger field of mutated cells. In addition, a larger stem cell zone can exert more selective pressure¹⁹. Since competition is slower in a larger stem cell zone, differences in stem cell fitness (e.g. effects on proliferation) have more time to manifest themselves. Mutations that result in increased fitness may therefore have a higher chance to take over the crypt. Interestingly however, it has been shown that the majority of mutations is neutral or reduces stem cell fitness²⁰. These mutations include many oncogenic mutations as these cause may delays in chromosomal segregation and therefore slow down proliferation. Both neutral mutations and mutations resulting in reduced fitness therefore have a higher chance to be outcompeted by wild-type neighbors in a larger stem cell zone. Thus, to minimize the accumulation and spread of mutations in the epithelium, an optimal stem cell number may balance the speed of competition and the chance to accumulate mutations (for which more stem cells are more beneficial), and the size of the clone once a mutation is fixed in a crypt (for which less stem cells are more beneficial). Of course, this is a simplistic view and other factors may play a role. For instance, the total number of stem cells and the mutation rate will impact the number of mutations that accumulate in the intestinal epithelium (discussed below).

Interestingly, in **Chapter 4** we found a correlation between the number of cells with stem cell potential and tumor initiation. In this chapter, we reduced the number functional of stem cells by inhibiting WNT with a porcupine inhibitor. Using intravital microscopy, we showed that in this scenario there is no retrograde movement of border cells and that only stem cells at the very bottom of small intestinal crypts can win the stem cell competition. Thus, porcupine inhibitor treatment resulted in less cells with stem cell potential, thereby speeding up stem cell competition. The total number of clones was not altered by porcupine inhibitor treatment, since the loss of clones originating in the crypt border, is balanced by the higher chance of clones in the crypt center to win the stem cell competition. When we introduced an APC mutation in Lgr5+ cells one day before porcupine treatment, we also saw that cells harboring this mutation take over crypts more rapidly. Interestingly, we found more APC-mutant clones in mice treated with the porcupine inhibitor than in untreated mice, which resulted in more adenomas (**Chapter 4**, figure 4f-h). This means that on top of speeding up the stem cell competition and mutant clone formation, porcupine inhibitor treatment results in a more permissive environment for adenoma formation. Remarkably, upon porcupine inhibitor treatment, adenomas started to form in the proximal SI (duodenum), while under control or vehicle conditions adenomas mainly form in the distal SI (ileum). This may be explained by differences in the WNT gradient along the SI. Previous studies have suggested that higher basal levels of WNT signaling in the proximal SI are suboptimal for certain APC mutations to initiate tumorigenesis²¹. By reducing WNT signaling, we may make the proximal intestine more permissive for tumorigenesis following APC loss. Thus, more factors than stem cell competition alone may be at play to enhance tumor initiation upon WNT inhibition.

Calorie restriction (CR) has been shown to reduce adenoma formation in APC^{min} mice²². These mice harbor a germline mutation in one APC allele and upon aging lose the second copy due to loss of heterozygosity resulting in adenoma growth. Although the decreased adenoma formation upon CR can in part be due to reduced mutation accumulation as a result of various types of DNA protection and repair systems²³, it could also be the result of enhanced expulsion of APC deficient cells through stronger stem cell competition. Remarkably, CR has been shown to increase the number of stem cells and reduce mutation accumulation in the SI, but not in the liver or in the spleen, organs without stem cell competition²⁴. Therefore, in **Chapter 5**, we used a CR diet to increase the number of cells with stem cell potential (opposed to decreasing the number of stem cells as in **Chapter 4**) and investigated the effect on stem cell competition. As expected, we found that a larger stem cell pool upon CR slows down stem cell competition (**Chapter 5**, Figure 3e). In addition, we showed that clones have a lower chance to remain in the crypt, and that less clones persist as a consequence of more competitors (**Chapter 5**, Figure 4d). This means that under CR there is a lower chance of clones to remain in the crypt. Thus, while reduced stem cell numbers speed up the stem cell competition potentially promoting mutation accumulation (**Chapter 4**), increased stem cell numbers slow down stem cell competition and may protect against mutation accumulation (**Chapter 5**).

While stem cell numbers per crypt affect the strength of stem cell competition and therefore the chance that a mutation can take over a crypt, the size of the total stem cell pool along the whole intestine should also be considered when looking at mutation accumulation. The total number of stem cells in the organ determines the number of cells that could potentially acquire a mutation. If a certain number of stem cells is distributed over a fewer but larger crypts, the number of cells that can acquire a mutation stays the same but the chance that a mutated cell will win the stem cell competition and remain in the crypt is reduced. Alternatively, when the number of crypts is unaltered but crypts become larger, the

resulting increase in the number of cells that can acquire a mutation is balanced by the lower chance that this mutation can remain in the crypt. Therefore, in **Chapter 5**, it was important to see whether an increased number of stem cells per crypt under CR led to a larger overall stem cell pool or whether stem cells were redistributed over less but larger crypts. When investigating this, we initially observed a lower crypt density in whole mount samples of CR mice compared to control mice (data not shown). However, repetitive intravital microscopy showed that crypt numbers did not change upon CR meaning that the observed changes in crypt density must have been an effect of sample preparation (**Chapter 5**, Figure 2b,c). Thus, CR increased the number of stem cells per crypt, but this was not accompanied by rearrangement of crypts. Therefore, under CR there are more stem cells that can acquire a mutation, but this is balanced by a lower chance that a mutated cell can persist in the crypt. Yet, as described above, when a mutation arises in the crypt, it has a lower chance to remain a larger crypt.

In addition to CR, several other diets have been shown to affect crypt size. For instance, high-fat diets or other diets increasing cellular cholesterol increase intestinal stem cell numbers and proliferation, while decreasing Paneth cell numbers^{25,26}. A ketogenic diet rich in proteins and fat increases the number of stem cells per crypt, while a diet supplemented with glucose decreases stem cell numbers²⁷. In addition, diets low in vitamin D compromise the function of Lgr5⁺ stem cells²⁸. Since dietary intake is linked to overall health, it is interesting to investigate in future studies whether these altered stem cell zones affect mutation accumulation and how dietary changes affect stemness in tumors, and hence tumor growth.

One important side note should be placed about dietary studies. Selecting the right control diet is crucial for correct interpretation of the results. Many studies use normal rodent chow as a control diet, while the composition of this diet is highly variable and thus non-controllable.

(Non-)stem cells as cells-of-origin

As mentioned before, already in 1990 Fearon and Vogelstein postulated that colorectal cancer is caused by the accumulation of subsequent mutations that result in tumor initiation and progression⁸. In this thesis, we focused on the long-lived stem cells of the intestine, as they are the cells that can accumulate mutations. But does this mean that these cells are the only cells that can act as cells-of-origin of colorectal cancer? It has indeed been shown that in the SI of mice, loss of APC in Lgr5⁺ stem cells results in the formation of large adenomas (also shown in **Chapter 4**), while the same mutation in short-lived more differentiated cells does not²⁹. Interestingly, APC loss in transit amplifying cells just above the stem cell zone results in a number of small lesions that rarely progress towards an adenoma.

Other processes may allow oncogenic cells arising outside the stem cell zone to remain in the epithelium, for instance by creating an ectopic stem cell niche. In mice, it has been shown that simultaneous induction of *Kras* and *β-catenin* mutations within differentiated villus cells induces the re-expression of a stem cell signature which leads to dedifferentiation. As a result, differentiated cells regain stemness, resulting in the emergence of lesions in the villus, suggesting that KRAS and WNT-mediated dedifferentiation enables cells in the villus to function as cells-of-origin³⁰. Similar observations have been done in mice overexpressing the mesenchymal bone morphogenetic protein antagonist, Grem1³¹. Also this overexpression results in ectopic crypt formation in which somatic mutations can accumulate that can initiate intestinal neoplasia. Together, these observation may explain the clinical phenomenon of so-called “top-down” adenomas, where adenomas form on top of “normal” looking crypts on the surface of the colorectal lumen³². However, it has to be noted that in most studies, whole

populations of cells were transformed. Whether or not transformed single cells can overcome getting shed from the villus will have to be shown.

In addition to the creation of an ectopic stem cell niche, mutated differentiated cells can also re-enter the stem cell niche at the bottom of the crypt through dedifferentiation. It has been shown that upon damage, cells just outside the stem cell zone can fall back and dedifferentiate^{17,33}. For instance, loss of APC in differentiated Tuft cells can induce tumorigenesis when damage is induced through colitis³⁴. Thus, oncogenic mutations outside the Lgr5⁺ zone may be maintained in the epithelium and ultimately lead to tumor initiation if they are able to reposition to the bottom of the crypt. However, plasticity resulting in stemness has mostly been studied in the SI. As described in **Chapter 3**, we observed no movement of cells from the border of the Lgr5⁺ zone back to the center in the large intestine. It is therefore of importance to investigate potential plasticity in the large intestinal stem cell zone. The number of cells that display long-term persistence (i.e. stemness) during homeostasis, and also upon damage and inflammation, may affect the incidence of tumor initiation.

What is the role of crypt fission and fusion in homeostasis, regeneration and tumor initiation?

The intestinal epithelium is a dynamic tissue, both at the level of individual cells within crypts and at the level of individual crypts. Under homeostatic conditions, crypts can be found with bifurcating morphology. For a long time, it was thought that these crypts were all undergoing crypt fission, a process during which two daughter crypts arise from one parental crypt. This process is the main mechanism through which the intestine elongates during postnatal development³⁵. In **Chapter 6** however, we described an exact reverse phenomenon that we named “crypt fusion”. During this process, two crypts fuse together in a zipper-like fashion starting at the top of the crypts ultimately resulting in one crypt. We quantified the prevalence of fission and fusion events using background recombination of the LSL-tdTomato reporter allele (**Chapter 6**, Figure 2b) and found that at any moment, 3-4% of all crypts are undergoing crypt fission, which is balanced by the same amount of crypts is undergoing crypt fusion. Based on our multi-day intravital imaging data we estimated that both processes take approximately one week. This is in concordance with the observation made by Bjerknes in 1986³⁶, who performed repetitive intravital imaging using transillumination with an almost closed condenser to provide the necessary contrast. He observed crypt fission in ~6% of all crypts one week after the first imaging session and in ~9% of all crypts two weeks later, also concluding that a fission event takes on average one week. Together, these results suggest that on average a crypt undergoes a fission or fusion event every 3-4 months. Based on this we can conclude that crypts in the intestinal epithelium are highly dynamic.

In **Chapter 5** we described experiments that altered our view on the prevalence of crypt fission and fusion. We performed repetitive intravital imaging similar to Bjerknes³⁶, but with multiphoton microscopy instead of transillumination allowing for more precise quantification. In an 8-week timeframe we only observed ~1% fission and ~0.5% fusion of all crypts in control mice, of which most events were not full events starting or ending in a bifurcating shape (based on **Chapter 5**, Figure 2b,c; data not shown in this thesis). In addition, we observed static events where crypts showed a bifurcating morphology at both time points (~0.5% of all crypt). Based on these data, we concluded that during homeostasis fission and fusion are rare events and that the processes take longer than the previously anticipated period of 1 week. This notion is supported by a recent paper by Baker *et al.* investigating fission and fusion in the human intestine³⁷. They found that a human crypt undergoes a fission or fusion event every ~45 years and that the average length of an event is ~9 weeks. Thus, during homeostasis fission and fusion are

slow and rare events in both mice and man.

The observation of more bifurcating crypts reported in **Chapter 6** than in the repetitive intravital microscopy experiment described in **Chapter 5** could be caused by different housing situations of the mice, as the first experiments were performed at the relatively dirty (i.e. low barrier level) mouse facility of the Hubrecht Institute (experiments in **Chapter 6**), while the later experiments were performed at the cleaner facility at the Netherlands Cancer Institute (i.e. high barrier level) (part of experiments in **Chapter 5**). This could be of influence on crypt fission and fusion since higher pathogen levels may lead to more inflammation and regeneration, which affects these processes. In addition, the surgery performed by Bjerknes in 1986 may have been suboptimal, leading to a regenerative response and thereby resulting in high fission rates.

While fission is a rare process during homeostasis, it is one of the main drivers of regeneration when the intestinal epithelium is damaged. For instance, when 30% of the SI of a mouse is resected, the epithelial surface area is restored via crypt fission resulting in more crypts feeding into one villus, increasing villus height and area³⁸. In addition, after X-ray irradiation which reduces crypt numbers by 77%, crypt fission restores the epithelium within 21 days³⁹. Miyoshi *et al.* describe the response of crypts to mucosal damage caused by a punch wound in great detail⁴⁰. Within 4 days after wounding, non-proliferative cells coming from adjacent intact crypts move into the wound bed to close it off from further harm. Subsequently, healthy crypts form wound channels into the damaged areas from which new crypts arise. Interestingly, to accommodate regeneration, the tissue transiently goes through a primitive state with fetal-like properties⁴¹. While performing the repetitive intravital microscopy experiments presented in **Chapter 3** and **Chapter 5**, we also laser-ablated patches of crypts (4-10 crypts) to investigate the recovery of the epithelium. Eight weeks later, the wound bed was closed but crypts were still undergoing fission (**Figure 1**). Thus, although the wound is closed within 4 days, restoration of normal homeostasis takes more than 8 weeks.

Inflammation, which is tightly linked to regeneration, also increases crypt fission rates. In situations of chronic inflammation, such as ulcerative colitis and Crohn's disease, up to as many as 35% of all crypts show a bifurcating morphology⁴². This high fission rate may contribute to the predisposition of these tissues to tumor initiation, since mutations can spread through fission resulting in field cancerization⁴³. For instance, patches of P53-negative crypts have been found in ulcerative colitis^{44,45}. Also, in patients with Familial Adenomatous Polyposis (FAP) - patients that lack one APC allele - higher levels of crypt fission have been observed contributing to tumor initiation and adenoma growth^{42,46-48}. Similar observations have been done in a mouse model for FAP, the APC^{min} mouse, that carries one wild type and one truncated copy of APC. In this model, crypt fission rates were increased by 61% in the SI and 75% in the colon. However, since there is approximately a 10-fold increase in tumor number in the SI versus colon additional factors must be influencing tumor initiation⁴⁶.

Oncogenic mutations in genes other than APC can also induce crypt fission. For instance, in a KRAS^{G12D}-inducible mouse model, KRAS-mutated crypts form large patches indicative of crypt fission, while wild type patches remain small¹⁰. In addition, in Supplementary Figure 3 of **Chapter 4**, we showed that a BRAF mutation, especially in combination with a PTEN mutation, resulted in more crypts per circumference of the intestine, indicating an induction of crypt fission. Interestingly, WNT inhibition through administration of a porcupine inhibitor reverted this phenotype. Since both KRAS and BRAF mutations resulted in increased proliferation^{49,50}, fission may be induced by an enlarged crypt size. By blocking WNT, crypt size is reduced thereby possibly reducing the need for crypt fission. However,

whether crypt fission is induced in an enlarged crypt to balance cell numbers still needs to be shown. We did not observe a change in crypt fission and fusion in the enlarged crypts upon CR (**Chapter 5**, Figure 2b)

Taken together, although crypt fission and fusion are rare events during homeostasis, crypt fission plays a big role during development and regeneration and can be activated by oncogenes. Future research is required to evaluate the role of crypt fusion in these processes. One can imagine that crypt regeneration is a tight balance between fission and fusion to prevent overshooting of crypt production. In addition, when oncogenic crypts spread over the epithelium, they may create space by taking over neighboring wild type crypts using crypt fusion. Contrarily, mutated clones may be eliminated from the epithelium by restarted stem cell competition upon crypt fusion.

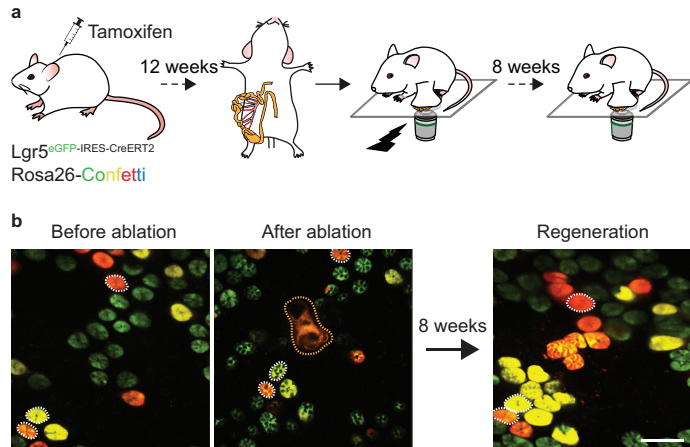


Figure 1. Crypt regeneration after laser ablation. **a.** A schematic overview of crypt ablation during intravital imaging. 12 weeks before the first imaging session, tamoxifen is injected into *Lgr5-eGFP-IRES-CreERT2;Rosa26-Confetti* mice to create a recognizable pattern of monoclonal crypts after 12 weeks. During the first intravital imaging session a patch of ~5 crypts is ablated after which the intestine is placed back and the mouse is allowed to wake up. 8 weeks later, the same crypts are imaged and crypt regeneration can be observed. **b.** Representative images of fields of crypts before ablation, immediately after ablation and 8 weeks after ablation. Green represents *Lgr5*⁺ cells, while red and yellow randomly label crypts. The ablation area is outlined by a dotted line. Scale bar = 100 μ m.

Translation from mouse to man

In this thesis, we used the mouse as a model system for the human situation. The human small intestinal epithelium is, like its murine counterpart, compartmentalized in crypt-villus units. The morphology of these crypts is also alike as Paneth cells are intermingled by small cells expressing *Lgr5*. In 2014, Baker *et al.* used somatic mtDNA mutations visualized by histochemistry to trace clonal lineages in human colonic crypts⁵¹. Based on the “wiggles” of a clone along the crypt-villus axis caused by expansion and regression of clones in the crypt, they concluded that 5 or 6 functional stem cells at the bottom of the human colonic crypt conform to neutral drift dynamics⁵¹. These results verify the murine crypt as a suitable model system to study intestinal dynamics.

Recently, however, human intestinal stem cell dynamics were further characterized. Nicholson *et al.* used two separate clonal markers to deduce functional stem cell numbers and replacement rate in human colonic crypts. They found that 7 functional stem cells rarely replace each other at the crypt base (0.65-2.7 stem cell replacements/crypt/year) resulting in very slow stem cell competition where monoclonal conversion takes many years (13 years for 90% conversion, median 6.3 years)⁵². This was in

Chapter 7

concordance with earlier studies that reported times to monoclonality in the order of years⁵³⁻⁵⁶. Reasons for this slow drift may include a larger crypt base (~23 cells per crypt circumference in mice vs. 41 cells in human⁵⁷), slower proliferation (~24 hours in mice vs ~140 hours in human⁵⁸) or predominantly asymmetric divisions at the human crypt base⁵⁹. Together, these studies show that stem cell competition in humans may be much slower than what we observe in mice. Consequently, it may take much longer for mutant cells to be outcompeted by wild-type competitors or to outcompete their wild-type competitors. Indeed, the development of colorectal adenomas and carcinomas can take >10 years in humans⁶⁰ whilst it takes weeks to months in mice⁶¹. Future studies are required to further determine the relevance of stem cell competition for human disease.

Concluding remarks

From this thesis, it became apparent that the intestinal epithelium is even more dynamic than it was previously thought to be. We added a layer of complexity to stem cell dynamics by defining that the degree of stem cell mixing determines stemness at the bottom of small and large intestinal crypts (**Chapter 3**). In addition, we showed that altering stem cell numbers affects stem cell competition (**Chapter 4 and 5**) and that crypt fusion can balance the production of crypts by crypt fission (**Chapter 6**). All these findings showed the power of intravital imaging, as static observations could not have revealed these dynamic processes. Therefore, I believe that intravital imaging holds great promise to the future and that it is even required for unraveling dynamic processes during homeostasis, tissue regeneration and cancer. The challenge will be translating these findings to the human situation. Therefore, future research and the development of new techniques should aim to study dynamic processes in human tissue.

REFERENCES:

1. Clevers, H. The Intestinal Crypt, A Prototype Stem Cell Compartment. *Cell* **154**, 274–284 (2013).
2. Schepers, A. G., Vries, R., van den Born, M., van de Wetering, M. & Clevers, H. Lgr5 intestinal stem cells have high telomerase activity and randomly segregate their chromosomes. *EMBO J.* **30**, 1104–1109 (2011).
3. Kaiko, G. E. *et al.* The Colonic Crypt Protects Stem Cells from Microbiota-Derived Metabolites The architecture of intestinal crypts protects the stem cells at their base from a growth-inhibiting metabolite derived from the gut microbiome. Might these findings suggest co-evolution of mammalian anatomy with commensal flora? The Colonic Crypt Protects Stem Cells from Microbiota-Derived Metabolites. *Cell* **165**, 1708–1720 (2016).
4. Allaire, J. M. *et al.* The Intestinal Epithelium: Central Coordinator of Mucosal Immunity. *Trends in Immunology* **39**, 677–696 (2018).
5. Blokzijl, F. *et al.* Tissue-specific mutation accumulation in human adult stem cells during life. *Nature* **538**, 260–264 (2016).
6. Lee-Six, H. *et al.* The landscape of somatic mutation in normal colorectal epithelial cells. *Nature* **574**, 532–537 (2019).
7. López-Otín, C., Blasco, M. A., Partridge, L., Serrano, M. & Kroemer, G. The hallmarks of aging. *Cell* **153**, 1194 (2013).
8. Fearon, E. R. & Vogelstein, B. A genetic model for colorectal tumorigenesis. *Cell* **61**, 759–767 (1990).
9. Cairns, J. Mutation selection and the natural history of cancer. *Nature* **255**, 197–200 (1975).
10. Snippert, H. J., Schepers, A. G., Van Es, J. H., Simons, B. D. & Clevers, H. Biased competition between Lgr5 intestinal stem cells driven by oncogenic mutation induces clonal expansion. *EMBO Rep.* **15**, 62–69 (2014).
11. Vermeulen, L. *et al.* Defining stem cell dynamics in models of intestinal tumor initiation. *Science* **342**, 995–8 (2013).
12. Lopez-Garcia, C., Klein, A. M., Simons, B. D. & Winton, D. J. Intestinal stem cell replacement follows a pattern of neutral drift. *Science*. **330**, 822–825 (2010).
13. Snippert, H. J. *et al.* Intestinal crypt homeostasis results from neutral competition between symmetrically dividing Lgr5 stem cells. *Cell* **143**, 134–144 (2010).
14. Ritsma, L. *et al.* Intestinal crypt homeostasis revealed at single-stem-cell level by in vivo live imaging. *Nature* **507**, 362–5 (2014).
15. Kozar, S. *et al.* Continuous Clonal Labeling Reveals Small Numbers of Functional Stem Cells in Intestinal Crypts and Adenomas. *Cell Stem Cell* **13**, 626–633 (2013).
16. Park, H. S., Goodlad, R. A. & Wright, N. A. Crypt fission in the small intestine and colon. A mechanism for the emergence of G6PD locus-mutated crypts after treatment with mutagens. *Am. J. Pathol.* **147**, 1416–27 (1995).
17. Ritsma, L. *et al.* Intestinal crypt homeostasis revealed at single-stem-cell level by in vivo live imaging. *Nature* **507**, (2014).
18. Vermeulen, L. & Snippert, H. J. Stem cell dynamics in homeostasis and cancer of the intestine. *Nat. Rev. Cancer* **14**, 468–80 (2014).
19. Cannataro, V. L., McKinley, S. A. & St Mary, C. M. The Evolutionary Trade-off between Stem Cell Niche Size, Aging, and Tumorigenesis. *Evol. Appl.* **10**, 590–602 (2016).
20. Eyre-Walker, A. & Keightley, P. D. The distribution of fitness effects of new mutations. *Nature Reviews Genetics* **8**, 610–618 (2007).
21. Leedham, S. J. *et al.* A basal gradient of Wnt and stem-cell number influences regional tumour distribution in human and mouse intestinal tracts. *Gut* **62**, 83–93 (2013).
22. Mai, V. *et al.* Calorie restriction and diet composition modulate spontaneous intestinal tumorigenesis in Apc(Min) mice through different mechanisms. *Cancer Res.* **63**, 1752–5 (2003).
23. Heydari, A. R., Unnikrishnan, A., Lucente, L. V. & Richardson, A. Caloric restriction and genomic stability. *Nucleic Acids Res.* **35**, 7485–7496 (2007).
24. He, D. *et al.* Effects of calorie restriction on the age-dependent accumulation of mutations in the small intestine of lacZ-transgenic mice. *Mech. Ageing Dev.* **132**, 117–22 (2011).
25. Beyaz, S. *et al.* High-fat diet enhances stemness and tumorigenicity of intestinal progenitors. *Nature* **531**, 53–58 (2016).
26. Wang, B. *et al.* Phospholipid Remodeling and Cholesterol Availability Regulate Intestinal Stemness and Tumorigenesis. *Cell Stem Cell* **22**, 206–220.e4 (2018).
27. Cheng, C. W. *et al.* Ketone Body Signaling Mediates Intestinal Stem Cell Homeostasis and Adaptation to Diet. *Cell* **178**, 1115–1131.e15 (2019).
28. Peregrina, K. *et al.* Vitamin D is a determinant of mouse intestinal Lgr5 stem cell functions. *Carcinogenesis* **36**, 25–31 (2015).
29. Barker, N. *et al.* Crypt stem cells as the cells-of-origin of intestinal cancer. *Nature* **457**, 608–611 (2009).
30. Schwitalla, S. *et al.* Intestinal Tumorigenesis Initiated by Dedifferentiation and Acquisition of Stem-Cell-like Properties. *Cell* **152**, 25–38 (2013).

31. Davis, H. *et al.* Aberrant epithelial GREM1 expression initiates colonic tumorigenesis from cells outside the stem cell niche. *Nat. Med.* **21**, 62–70 (2014).
32. Shih, I. M. *et al.* Top-down morphogenesis of colorectal tumors. *Proc. Natl. Acad. Sci. U. S. A.* **98**, 2640–5 (2001).
33. Tian, H. *et al.* A reserve stem cell population in small intestine renders Lgr5-positive cells dispensable. *Nature* **478**, 255–9 (2011).
34. Westphalen, C. B. *et al.* Long-lived intestinal tuft cells serve as colon cancer-initiating cells. *J. Clin. Invest.* **124**, 1283–95 (2014).
35. Clarke, R. M. The effect of growth and of fasting on the number of villi and crypts in the small intestine of the albino rat. *J. Anat.* **112**, 27–33 (1972).
36. Bjerknes, M. A test of the stochastic theory of stem cell differentiation. *Biophys. J.* **49**, 1223–1227 (1986).
37. Baker, A.-M. *et al.* Crypt fusion as a homeostatic mechanism in the human colon. *Gut* **68**, 1986–1993 (1986).
38. Cheng, H., McCulloch, C. & Bjerknes, M. Effects of 30% intestinal resection on whole population cell kinetics of mouse intestinal epithelium. *Anat. Rec.* **215**, 35–41 (1986).
39. Cairnie, A. B. & Millen, B. H. Fission of crypts in the small intestine of the irradiated mouse. *Cell Tissue Kinet.* **8**, 189–96 (1975).
40. Miyoshi, H., Ajima, R., Luo, C. T., Yamaguchi, T. P. & Stappenbeck, T. S. Wnt5a potentiates TGF- β signaling to promote colonic crypt regeneration after tissue injury. *Science (80-)*. **338**, 108–113 (2012).
41. Yui, S. *et al.* YAP/TAZ-Dependent Reprogramming of Colonic Epithelium Links ECM Remodeling to Tissue Regeneration. *Cell Stem Cell* **22**, 35–49.e7 (2018).
42. Cheng, H., Bjerknes, M., Amar, J. & Gardiner, G. Crypt production in normal and diseased human colonic epithelium. *Anat. Rec.* **216**, 44–48 (1986).
43. Galandiuk, S. *et al.* Field cancerization in the intestinal epithelium of patients with Crohn's ileocolitis. *Gastroenterology* **142**, (2012).
44. Chen, R. *et al.* The initiation of colon cancer in a chronic inflammatory setting. *Carcinogenesis* **26**, 1513–1519 (2005).
45. Leedham, S. J. *et al.* Clonality, Founder Mutations, and Field Cancerization in Human Ulcerative Colitis-Associated Neoplasia. *Gastroenterology* **136**, (2009).
46. Wasan, H. S. *et al.* APC in the regulation of intestinal crypt fission. *J. Pathol.* **185**, 246–255 (1998).
47. Wong, W.-M. *et al.* Histogenesis of human colorectal adenomas and hyperplastic polyps: the role of cell proliferation and crypt fission. *Gut* **50**, 212–7 (2002).
48. Preston, S. L. *et al.* Bottom-up histogenesis of colorectal adenomas: origin in the monocryptal adenoma and initial expansion by crypt fission. *Cancer Res.* **63**, 3819–25 (2003).
49. Feng, Y. *et al.* Mutant Kras Promotes Hyperplasia and Alters Differentiation in the Colon Epithelium but Does Not Expand the Presumptive Stem Cell Pool. *Gastroenterology* **141**, 1003–1013.e10 (2011).
50. Rad, R. *et al.* A Genetic Progression Model of BrafV600E-Induced Intestinal Tumorigenesis Reveals Targets for Therapeutic Intervention. *Cancer Cell* **24**, 15–29 (2013).
51. Baker, A. M. *et al.* Quantification of Crypt and Stem Cell Evolution in the Normal and Neoplastic Human Colon. *Cell Reports* **8**, 940–7 (2014).
52. Nicholson, A. M. *et al.* Fixation and Spread of Somatic Mutations in Adult Human Colonic Epithelium. *Cell Stem Cell* **22**, 909–918.e8 (2018).
53. Campbell, F. *et al.* Post-irradiation somatic mutation and clonal stabilisation time in the human colon. *Gut* **39**, 569–573 (1996).
54. Yatabe, Y., Tavaré, S. & Shibata, D. Investigating stem cells in human colon by using methylation patterns. *Proc. Natl. Acad. Sci. U. S. A.* **98**, 10839–10844 (2001).
55. Kim, K.-M. & Shibata, D. Methylation reveals a niche: stem cell succession in human colon crypts. *Oncogene* **21**, 5441–9 (2002).
56. Nicolas, P., Kim, K.-M., Shibata, D. & Tavaré, S. The Stem Cell Population of the Human Colon Crypt: Analysis via Methylation Patterns. *PLoS Comput. Biol.* **3**, e28 (2007).
57. Potten, C. S., Kellett, M., Roberts, S. A., Rew, D. A. & Wilson, G. D. Measurement of in vivo proliferation in human colorectal mucosa using bromodeoxyuridine. *Gut* **33**, 71–78 (1992).
58. Potten, C. S., Booth, C. & Hargreaves, D. The small intestine as a model for evaluating adult tissue stem cell drug targets1. *Cell Prolif.* **36**, 115–129 (2003).
59. Stamp, C. *et al.* Predominant Asymmetrical Stem Cell Fate Outcome Limits the Rate of Niche Succession in Human Colonic Crypts. *EBioMedicine* **31**, 166–173 (2018).
60. Beerenwinkel, N. *et al.* Genetic Progression and the Waiting Time to Cancer. *PLoS Comput. Biol.* **3**, e225 (2007).
61. Moser, A. R., Pitot, H. C. & Dove, W. F. A dominant mutation that predisposes to multiple intestinal neoplasia in the mouse. *Science* **247**, 322–324 (1990).

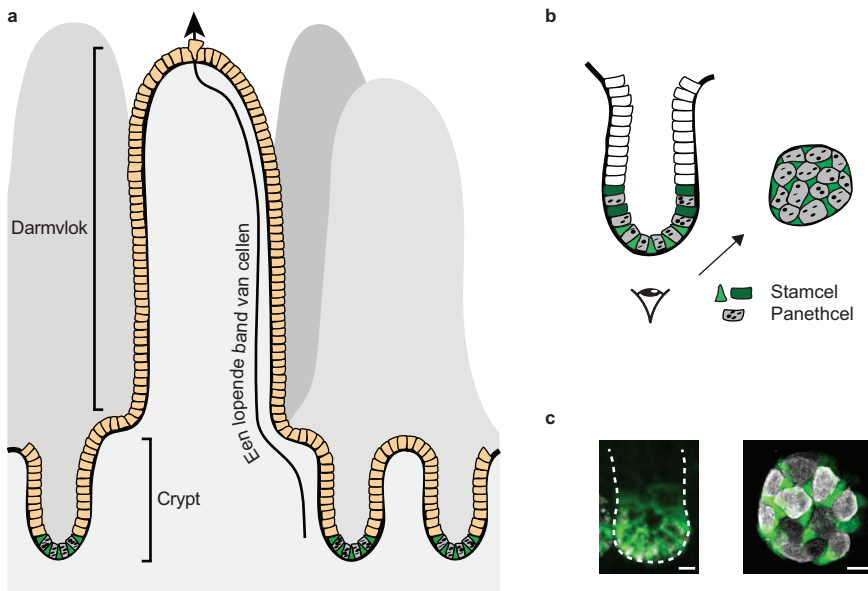


Addendum

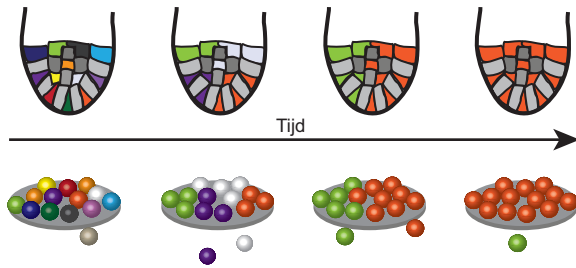
NEDERLANDSE SAMENVATTING

De binnenkant van onze dunne darm is bekleed met een laag cellen die het darmepitheel wordt genoemd. Dit darmepitheel is maar één cellaag dik en wordt constant blootgesteld aan alles wat door onze darm heen gaat, zoals de zure sappen uit de maag, maar ook bijvoorbeeld alle slechte dingen die wij eten en drinken. Om hier tegen te kunnen, wordt het hele epitheel elke 3-5 dagen vervangen. Daartoe heeft het darmepitheel een speciale vorm; het bestaat uit crypt-darmvlokeenheden (**Figuur 1a**). De darmvlokken steken uit naar de binnenkant van de darm waar ze de voedingsstoffen uit ons eten kunnen halen, terwijl de crypten beschermd weggestopt zitten dieper in de darmwand. In de crypten vinden de celdelingen plaats die ervoor zorgen dat het darmepitheel vernieuwd wordt. Doordat de cellen onderin de crypt ongeveer één keer per dag delen, worden alle cellen erboven richting het puntje van de darmvlok geduwd, als een lopende band (**Figuur 1a**). Wanneer een cel bovenin is aangekomen wordt hij uit het epitheel geduwd en opgenomen in de darm. Door dit mechanisme leven de meeste cellen in het darmepitheel maar heel kort en krijgen kapotte cellen niet de kans om schade aan te richten in de darm.

In tegenstelling tot het grootste deel van de epitheelcellen, leven de delende cellen onderin de crypt wel lang. Dit zijn de stamcellen van het darmepitheel. Deze zitten in een speciale niche, een plek waar ze de juiste signalen krijgen om stamcel te zijn (**Figuur 1b,c**). De niche wordt onder andere gevormd door de Panethcel. Zolang een cel naast een Panethcel zit is het een stamcel, maar zodra het contact verloren gaat zal de cel richting de darmvlok verdwijnen. Er is dus een beperkt aantal plekken in de darm waar een cel een stamcel is, namelijk de ongeveer 20 plekken naast de Panethcellen. Dit betekent dat als een stamcel deelt, er een stamcel uit de niche moet verdwijnen. Welke cel dit is, is vrij willekeurig, maar vaak is dit een stamcel net op het randje van de niche, aangezien deze het makkelijkst het



Figuur 1 - Morfologie van de darm. a. De darm bestaat uit crypt-darmvlokeenheden. **b,c.** Onderin de crypt bevinden zich stamcellen en Panethcellen, weergegeven als cartoon (**b**) en hoe ze eruit zien onder een microscoop (**c**).



Figuur 2 - Stamcelcompetitie in de crypt. In de crypt is er slechts plaats voor een beperkt aantal stamcellen, de stamcelzone. Dit kan worden weergegeven als knikers (stamcellen) op een schaalpje (stamcelzone). Doordat het aantal plaatsen beperkt is, moet een stamcel de zone verlaten op het moment dat er een andere stamcel bijkomt door celdeling. Door constante celdeling duwen stamcellen elkaar dus uit de stamcelzone. Als je dit proces lang genoeg volgt zie je dat uiteindelijk de nakomelingen van 1 stamcel alle andere stamcellen hebben verdrongen.

contact met de Panethcel verliest. Doordat de stamcellen delen duwen ze elkaar dus uit de niche en dit wordt stamcelcompetitie genoemd (**Figuur 2**). Als je dit proces maar lang genoeg volgt, dan zul je zien dat uiteindelijk de nakomelingen van één moederstamcel de niche overnemen. Deze hebben dan alle andere stamcellen uit de crypte geduwd. Eén op de ongeveer 20 stamcellen wint dus de stamcelcompetitie.

De stamcelcompetitie is van belang als je nadenkt over het verwerven van mutaties. Dit zijn veranderingen in het DNA die tot schade kunnen leiden en bij kunnen dragen aan veroudering of

het ontstaan van kanker. Op het moment dat er een mutatie optreedt in een cel in het darmepitheel, zal deze mutatie zeer waarschijnlijk verloren gaan. De gewone cellen in het epitheel leven immers maar kort en van de 20 stamcellen verliezen er 19 uiteindelijk de stamcelcompetitie. Een mutatie kan dus alleen in het darmepitheel blijven als deze optreedt in de stamcel die uiteindelijk de stamcelcompetitie wint.

In dit proefschrift bestudeer ik de stamcelcompetitie onder normale omstandigheden, homeostase genoemd, en in situaties waarin een verstoring plaatsvindt. Omdat stamcelcompetitie een erg dynamisch proces is, is het vrijwel onmogelijk dit te bestuderen aan de hand van enkel statische plaatjes. Daarom gebruik ik intravitale microscopie, ofwel het filmen in een levend organisme. Om dit mogelijk te maken heeft het lab een raampje ontwikkeld dat op de darm geplaatst kan worden en dat zo visuele toegang geeft tot de crypten (**Hoofdstuk 1**, Figuur 1c). Hierdoor kunnen we dezelfde crypt gedurende een aantal dagen volgen en zien hoe de stamcelcompetitie verloopt. In **Hoofdstuk 1** vat ik samen hoe intravitale microscopie over de afgelopen jaren bijgedragen heeft aan ons begrip van stamceldynamiek tijdens de ontwikkeling, homeostase, herstel na schade en het ontstaan van tumoren. In **Hoofdstuk 2** geef ik mijn perspectief op hoe de darmstamcel- en cryptodynamiek ervoor zorgt dat de meeste gemuteerde cellen verloren gaan en zo mutaties in het darmepitheel worden geminimaliseerd.

Onze huidige kennis van stamcelcompetitie is voornamelijk gebaseerd op bevindingen in de dunne darm. In **Hoofdstuk 3** beschrijven we hoe we intravitale microscopie hebben toegepast om de stamcellen in zowel de dunne als de dikke darm te filmen en deze te kunnen vergelijken. Ook al verschillen de functies van de dunne en dikke darm erg – in de dunne darm worden voornamelijk voedingsstoffen opgenomen terwijl in de dikke darm vooral water wordt onttrokken – zien de crypten er vergelijkbaar uit. Ze hebben een ongeveer gelijk aantal stamcellen, namelijk vier rijen van ~5 stamcellen, en deze cellen delen ook bijna even vaak. Toch vinden we grote verschillen wanneer we naar de dynamiek van deze stamcellen kijken. Terwijl in de dunne darm alle 20 stamcellen de stamcelcompetitie kunnen winnen zien we dat in de dikke darm alleen de onderste 10 stamcellen dit kunnen (**Hoofdstuk 3**, Figuur 2). De cellen daarboven gaan steevast verloren. Om te kunnen begrijpen waar dit verschil vandaan komt hebben we de hulp ingeroepen van biofysici die op basis van onze resultaten een model

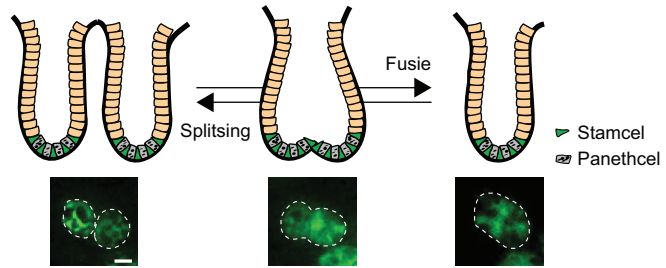
hebben ontwikkeld dat de bewegingen van stamcellen in de crypt beschrijft. Met behulp van dit model werd voorspeld dat in de dunne darm stamcellen aan de rand van de niche – die op het punt staan eruit geduwd te worden – naar beneden kunnen bewegen om zo een veiligere positie in te nemen beneden in de niche. In de dikke darm zou deze beweging omlaag volgens het model afwezig zijn, waardoor alleen de stamcellen onderin de crypt de stamcelcompetitie kunnen winnen. Deze voorspellingen hebben we vervolgens getoetst door met behulp van intravitale microscopie de cellen aan het randje van de niche te volgen en te kijken of deze cellen inderdaad omlaag konden bewegen richting het centrum van de niche. Zoals door het model voorspeld, zagen we alleen stamcellen in de dunne darm naar beneden bewegen terwijl stamcellen in de dikke darm alleen omhoog bewogen en verloren gingen (**Hoofdstuk 3**, Figuur 3). We kunnen dus concluderen dat er in de dunne darm meer verschillende stamcellen zijn die de stamcelcompetitie kunnen winnen dan in de dikke darm, doordat in de dunne darm stamcellen die verder verwijderd zijn van het centrum van de niche omlaag kunnen bewegen om zo toch weer een goede positie in de niche te kunnen bemachtigen. De consequentie hiervan is dat de hele competitie sneller gaat in de dikke darm dan in de dunne darm, omdat een stamcel hier maar ~9 andere stamcellen uit de niche hoeft te duwen terwijl dit er in de dunne darm ~19 zijn.

In **Hoofdstuk 4** gaan we verder in op de stamcelcompetitie. We beschrijven hoe we het aantal stamcellen in de dunne darm verminderen door een eiwit te blokkeren dat erg belangrijk is voor stamcellen, het Wnt-eiwit. We zien dat in deze situatie de hele stamcelcompetitie sneller gaat, en dat de dunne darm door Wnt-inhibitie op de dikke darm gaat lijken wat betreft de stamceldynamiek; de stamcellen verder weg van het centrum van de niche kunnen niet meer omlaag bewegen waardoor er minder stamcellen zijn die de stamcelcompetitie kunnen winnen. Vervolgens kijken we naar het effect van deze veranderingen op tumorinitiatie. We induceren in een aantal stamcellen in de darm een kankerverwekkende mutatie in het *Apc*-gen en zien dat na Wnt-inhibitie deze gemuteerde stamcellen sneller de competitie winnen dan in de normale dunne darm. Dit leidt vervolgens sneller tot tumoren. We kunnen dus concluderen dat Wnt-eiwitten tumorinitiatie beïnvloeden door het aantal stamcellen te reguleren en dat Wnt-inhibitie leidt tot meer tumorinitiatie.

In **Hoofdstuk 5** beschrijven we dat we het aantal stamcellen verhogen door een dieet met een beperkt aantal calorieën te geven, namelijk 40% minder dan normaal, een effect dat al eerder in de literatuur beschreven is. We zien dat onder deze omstandigheden de stamcelcompetitie langzamer wordt doordat er meer concurrerende stamcellen zijn, wat in overeenstemming is met de resultaten in **Hoofdstuk 4** waar we snellere competitie zagen bij een verminderd aantal stamcellen. We veronderstellen dat in dit scenario het moeilijker is voor een gemuteerde stamcel om de stamcelcompetitie te winnen aangezien er meer rivalen zijn. Om dit te testen hebben we met behulp van intravitale microscopie individuele mutaties gevolgd. Dit was mogelijk doordat de door ons geïntroduceerde mutaties zorgen voor de aanmaak van een gekleurd eiwit. Zo kunnen we op dag 1 kijken welke cellen mutaties hebben en kunnen we 8 weken later zien of de cellen met mutaties nog aanwezig zijn of niet (**Hoofdstuk 5**, Figuur 4). Zoals gedacht zien we dat onder caloriebeperking er minder gemuteerde cellen de stamcelcompetitie winnen en dat er dus minder mutaties aanwezig blijven in vergelijking met de situatie bij een normaal dieet. We kunnen dus concluderen dat caloriebeperking het behoud van mutaties in de darm vermindert door het aantal concurrerende stamcellen te vergroten.

In **Hoofdstuk 6** kijken we niet naar de dynamiek van de stamcellen in de crypt, maar naar de dynamiek van de crypten zelf. Het is al lang bekend dat crypten zich in tweeën kunnen splitsen om zich zo te vermenigvuldigen. Dit proces vindt voornamelijk plaats tijdens de ontwikkeling van de darm om de

lengte te laten toenemen, en op het moment dat er schade is en een beschadigde plek moet worden vervangen. Een splitsende crypt heeft een speciale vorm; als je vanaf de buitenkant van de darm naar de bodem van deze crypt zou kijken dan heeft hij de vorm van een achtje (Figuur 3). Tot nog toe is de algemene opvatting onder wetenschappers dat zo'n achtje een zich splitsende crypt is. In **Hoofdstuk 6**



Figuur 3 - Schematische weergave van cryptsplitsing en cryptfusie.

Tijdens cryptsplitsing worden er twee crypten gevormd uit een, terwijl er tijdens cryptfusie twee crypten samenkomen tot een crypt. Deze processen zijn spiegelbeelden van elkaar en verlopen via een tussenfase die wij een "achtje" noemen. Dit kan je zien als je vanaf de buitenkant van de darm naar de bodem van deze crypt kijkt (middelste panel onder de cartoon).

hebben wij het aantal achtjes geteld en we zagen dat dit aantal veel te groot was om ervanuit te kunnen gaan dat al deze achtjes splitsende crypten waren. Dan zou de muizendarm namelijk twee meter lang worden, terwijl deze in werkelijkheid ongeveer 30 centimeter lang is. Er moest dus een mechanisme zijn dat crypten weghaalt. Om dit mechanisme te vinden hebben we met behulp van intravitale microscopie door een raampje individuele crypten gevolgd gedurende 4-5 dagen. Tot onze verrassing zagen wij dat niet alle achtjes aan het splitsen waren, maar dat ongeveer de helft juist aan het fuseren was: twee crypten kwamen samen om te fuseren tot één crypt. We vonden dus een fenomeen dat de cryptvermeerdering door splitsing in balans bracht door crypten te laten fuseren. We zagen dat op het moment dat twee crypten fuseren, de stamcellen van beide crypten de competitie aangaan, die uiteindelijk door een stamcel wordt gewonnen. Dit kan ervoor zorgen dat óf de gemuteerde cellen in een crypt verloren gaan op het moment dat die crypt fuseert met een gezonde crypt en de competitie verliest, óf dat een gemuteerde crypt de plek van een gezonde crypt inneemt op het moment dat hij de competitie wint. In **Hoofdstuk 6** beschrijven we dus het nieuwe fenomeen cryptfusie dat een effect kan hebben op de verspreiding van mutaties binnen de darm.

Al met al beschrijf ik in dit proefschrift dat het darmepitheel nog dynamischer is dan eerder werd gedacht. De samenvatting en discussie zijn te vinden in **Hoofdstuk 7**. Mijn waarnemingen en conclusies hebben een laag van complexiteit toegevoegd aan het begrip stamceldynamiek door te definiëren dat stamcelbewegingen richting de bodem van de crypt bepalend zijn voor het aantal stamcellen in dunne- en dikkedarmcrypten dat de stamcelcompetitie kan winnen (**Hoofdstuk 3**). Bovendien heb ik aangetoond dat het veranderen van het aantal stamcellen per crypt de concurrentie tussen stamcellen beïnvloedt (**Hoofdstuk 4 en 5**) en dat cryptfusie de productie van crypten door cryptsplitsing kan compenseren (**Hoofdstuk 6**). Al deze bevindingen tonen de kracht van intravitale microscopie, want statische waarnemingen hadden deze dynamische processen niet kunnen onthullen. Daarom geloof ik dat intravitale microscopie uitermate veelbelovend is voor toekomstig onderzoek en dat deze methode nodig is voor het ontrafelen van dynamische processen tijdens homeostase, regeneratie en kanker. De uitdaging zal zijn om de bevindingen in muizen te vertalen naar de situatie in de mens. Daarom zal toekomstig onderzoek en de ontwikkeling van nieuwe technieken er ook op gericht moeten zijn om dynamische processen in menselijk weefsel te kunnen bestuderen.

CURRICULUM VITAE

Lotte Bruens werd op 11 januari 1990 in Neuss (D) geboren. In 2008 behaalde zij haar diploma aan het gymnasium van de Trevianum Scholengroep te Sittard met het profiel Natuur en Gezondheid. In september van hetzelfde jaar begon zij met de opleiding Biologie van de Universiteit Utrecht. Na afronding van deze bachelor begon zij in 2011 aan de master Cancer Genomics and Developmental Biology bij de Graduate School of Life Sciences van dezelfde universiteit. In het kader van deze master heeft Lotte een onderzoeksstage van twaalf maanden gedaan in het Hubrecht Instituut te Utrecht in de groep van Prof. dr. Niels Geijsen. Onder begeleiding van Maaïke Welling bestudeerde zij hoe embryonale stamcellen in een meer naïeve staat kunnen worden gebracht. Vervolgens is zij voor een tweede onderzoeksstage voor acht maanden naar de Verenigde Staten gegaan waar zij in het Harvard Stem Cell Institute in Cambridge, MA, werkte in de groep van prof. dr. Amy Wagers. Onder begeleiding van dr. Young Jang bestudeerde zij het effect van calorierestrictie op spierstamceltransplantaties. Na terugkomst heeft zij een extra-curriculaire minor gedaan binnen het masterprogramma Science and Business Management, genaamd Fundamentals of Business and Economics. Na het afronden van de Master is Lotte in augustus 2014 begonnen als gedeelde PhD student bij zowel de afdeling Molecular Cancer Research, UMC Utrecht, in het laboratorium van dr. Hugo Snippert als bij het Hubrecht Instituut in Utrecht in het laboratorium van prof. dr. Jacco van Rheenen. In november 2018 is zij met de groep van prof. dr. Jacco van Rheenen verhuisd naar het Nederlands Kanker Instituut in Amsterdam. De resultaten verkregen tijdens dit promotietraject staat beschreven in dit proefschrift.

LIST OF PUBLICATIONS

Published articles:

Fumagalli A*, Oost KC*, Kester L, Morgner J, Bornes L, **Bruens L**, Spaargaren L, Azkanaz M, Schelfhorst T, Beerling E, Heinz MC, Postrach D, Seinstra D, Sieuwerts AM, Martens JWM, van der Elst S, van Baalen M, Bhowmick D, Vrisekoop N, Ellenbroek SIJ, Suijkerbuijk SJE, Snippert HJ & van Rheeenen J. Lgr5-negative Cancer Cells Seed Metastases in Colorectal Cancer. *Cell Stem Cell*. (2020) In press

Fumagalli A*, **Bruens L***, Scheele CLGJ & van Rheeenen J. Capturing Stem Cell Behavior Using Intravital and Live Cell Microscopy. *Cold Spring Harb. Perspect. Biol.* a035949 (2019)

Huels DJ, **Bruens L**, Hodder MC, Cammareri P, Campbell AD, Ridgway RA, Gay DM, Solar-Abboud M, Faller WJ, Nixon C, Zeiger LB, McLaughlin ME, Morrissey E, Winton DJ, Snippert HJ, van Rheeenen J & Sansom OJ. Wnt Ligands Influence Tumour Initiation by Controlling the Number of Intestinal Stem Cells. *Nat. Commun.* 9, 1132 (2018).

Bruens L & Rheeenen J. Cellular Protection Mechanisms that Minimise Accumulation of Mutations in Intestinal Tissue. *Swiss Med. Wkly.* 147 (2017).

Bruens L & Snippert HJG. Expanding the Tissue Toolbox: Deriving Colon Tissue from Human Pluripotent Stem Cells. *Cell Stem Cell*. 21: 3–5 (2017). (Preview)

Bruens L, Ellenbroek SIJ, van Rheeenen J & Snippert HJ. In vivo Imaging Reveals Existence of Crypt Fission and Fusion in Adult Mouse Intestine. *Gastroenterology*. 153(3):674-677 (2017)

Manuscripts under review:

Bruens L*, Ellenbroek SIJ*, Corominas-Murtra B*, Lafirenze SJA, Simons BD, Snippert HJ, Hannezo E and van Rheeenen J. Retrograde Movements Determine Effective Stem Cell Numbers Intestinal Crypts.

Bruens L, Ellenbroek SIJ, Suijkerbuijk SJE, Hale AJ, Toonen P, Snippert HJ and van Rheeenen J. Calorie Restriction Decreases Retention of Mutations in the Intestine by Increasing the Number of Competing Stem Cells.

* Equal contribution

DANKWOORD

Wauw, het is af. Wat een reis is dit geweest. Pieken, dalen, hobbels, ik ben het (zoals het hoort) allemaal tegengekomen. In mijn eentje had ik het niet gekund, maar door alle lieve mensen om mij heen is het een fantastisch avontuur geweest. Daarom wil ik iedereen (voor zover dat kan) graag enorm bedanken. Daar gaan we...

Jacco en **Hugo**, mijn promotor en copromotor, wat ben ik blij dat ik zo'n enthousiast team begeleiders heb gehad. **Jacco**, ik weet een van onze gesprekken tijdens mijn sollicitatie nog goed te herinneren: jij leunde achterover met je benen op tafel en stelde me gerust dat werken op twee plekken aan twee totaal verschillende projecten helemaal goed zou komen. Je had helemaal gelijk. Ook tijdens de afgelopen jaren heb je me steeds weer weten te enthousiasmeren en motiveren op de momenten dat het even tegen zat. Dat waardeer ik enorm! Ik heb ontzettend veel van je geleerd. Ik ken weinig mensen die op een betere manier een verhaal kunnen opschrijven of kunnen presenteren. Door onze koppigheid hebben we ook wel eens wat onenigheid gehad, maar ik ben ervan overtuigd dat de projecten, presentaties en manuscripten hier alleen maar beter door zijn geworden. Bedankt voor vertrouwen in mij en in dit promotietraject. **Hugo**, ook mijn sollicitatiegesprek met jou weet ik nog goed. We hebben het over minstens tien projecten gehad en je was over het ene project nog enthousiaster dan over het andere. Je had het over Champions League spelen en over het mee te willen doen met de groten. Hier kon ik mij helemaal in vinden. Jammer genoeg heb ik dat maar een jaartje in jouw lab kunnen doen, maar ook daarna heb ik me altijd nog deel van het lab gevoeld. Onze koffiedates heb ik ook altijd enorm gewaardeerd. Je maakte tijd voor me vrij en we bespraken alles wat er speelde, zowel wetenschappelijk als daarbuiten. Ik heb altijd het gevoel dat je mij als een gelijke zag, niet als supervisor en student, en daar ben ik je erg dankbaar voor. **Jacco** en **Hugo**, bedankt voor alles!

Dearest members of the Van Rheenen lab. **Evelyne, Saskia (S), Jessica, Hendrik, Claire, Miguel, Kerstin, Colinda, Laura, Andreia, Ana, Rebeca, Maria, Jeroen** and **Tim**, thanks for being such great colleagues! You are a very special group of people. The group is open, smart, critical, supportive and most of all a lot of fun. I am really thankful to have been part of such an amazing bunch of people. **Colinda** and **Laura**, I feel so lucky to have had you as PhD buddies. Thanks for taking me on coffee walks when I needed them and for feeding me when I worked late (which was of course still early for you...). I enjoyed our movie night on the Hubrecht couch and I think we should have at least yearly birthday reunions. We should consider getting another snowman suit. **Colinda**, you are an amazing scientist. I learned so much from the way you navigated through your PhD. Besides being super dedicated to your projects, you are a truly nice person who I felt really comfortable sharing things with. Leuven can consider itself very lucky to have you. I am so happy that we can celebrate our graduation day together! **Laura**, I completely agree with you that I should not say that we are colleagues but that we are friends. I really enjoyed being office buddies with you for most of my PhD, to make sense of data together and to puzzle with Excel. I loved our coffee dates, New Year's Eves, Sunday board game afternoons, randomly joining you for team events and much more. Thanks for always being there. **Evelyne**, thanks for being you! Wat was het fijn om jou in het kantoor te hebben. Je bent doortastend, een aanpakker en een echte steunpilaar. Door je warme persoonlijkheid ben je echt een verbindende factor binnen het lab. Het was heerlijk om met jou op maandag het afgelopen weekend door te nemen en aan jou nieuwe (online) aankopen te kunnen showen. Jouw enthousiasme over escape rooms werkt erg aanstekelijk en ik vind dat we met

ons zeer stoere escape-groepje nog vaak moeten gaan ontsnappen. **Saskia** (S), ik kon altijd naar jou toe en ik weet niet hoe vaak ik daar wel niet gebruik van heb gemaakt. Je bedrijft wetenschap op de manier waarop ik het ook graag zou willen doen: grondig, georganiseerd en met veel enthousiasme. Daar heb ik erg veel waardering voor! Daarnaast ben je een ontzettend fijn en lief persoon en ik wil je graag bedanken voor alle tijd die je voor mij hebt vrijgemaakt. Ik zal aan je denken wanneer ik de roasted cauliflower soup maak of iets anders lekkers van de Minimalist Baker. **Jessica**, I don't know many people as passionate about science as you. Your enthusiasm is contagious and I loved looking at beautiful images of Collagen, Lamin, Laminin A or Laminin β 1 with you. Also, a big thanks for hosting great lab evenings and for spreading your beer knowledge. **Hendrik**, I really enjoyed having you in my office. Your occasional grumpiness made me just want to hug you but I realized that those hugs may not be appreciated. Thank you for your true interest, also in my job search. I am looking forward to seeing what comes out of your super cool flashy project. **Claire**, you have so much knowledge! I should have made use of that much more than I did. The lab is very lucky to have you and I'm sure that you are going to be very successful in whatever you do. **Miguel**, 3D printing king. I really appreciate your inventiveness and drive. I'm sure you'll make your mouse model work and it's going to be so cool! **Kerstin**, you are the coolest pathologist I know. I love how you're getting out of your comfort zone to learn anything and everything, while also sticking to your roots and sharing your knowledge about pathology with everyone. I wish you joined the lab earlier! **Andy**, over the years you really grew into the brain expert of the lab. I admire your perseverance and you can be super proud of what you're achieving. **Rebeca**, my neighbor. Thanks for having a food drawer that has saved me on multiple occasions! I should restock it before I leave... I'm sure all your hours in the T-building are going to pay off. **Ana**, you're so energetic and bubbling! I love it. Team cell competition is lucky to have you. **Maria**, mijn opvolgster. Ik vertrouw jou met een gerust hart 'Team Intestine' toe. Je bent slim, werkt hard en bent nieuwsgierig, en dat zijn volgens mij de juiste ingrediënten om goed onderzoek te doen. Veel succes en zorg goed voor de darm! **Jeroen**, wat heb jij gebuffeld! Respect!. Nu ben je een perfecte aanvulling op Eve en Tim, maar zorg je er wel voor dat je gevoel voor humor niet te veel aangetast wordt? Ik heb genoten van je gezelligheid en de dagelijkse tien minuten naast het Nespresso apparaat na lunch. **Tim**, wauw, jouw grappen. Die mogen niet ongenoemd blijven. Soms heb ik met mijn ogen gerold terwijl ik van binnen erg hard moest lachen. Je bent een gangmaker in de groep en bent samen met Eve en Jeroen een super goede fundatie van het lab! Bedankt!

Of course, I also want to thank the previous members of the Van Rheenen lab. **Arianna**, thanks for being a very good friend! I remember that in the beginning I was very intimidated by you! You looked at how I did my first surgery and I could not stop shaking. But, you taught me well and I don't find you intimidating anymore ;-). We shared many great moments together, like the weekend in Milan with all the food and drinks, and our US trip with Cliff and his peppermill, the apartment in Williamsburg (still very confused about this), our visit to Rockefeller and the whole conference... I loved it! I hope we will drink many more coffees together and share our frustrations but definitely also our victories. You are an amazing scientist and I'm very curious where your career is going to bring you. **SasE**, intestine buddy! Wat was het fijn om jou te hebben als teamgenoot. Ik heb ontzettend veel geleerd van jouw systematische aanpak en ik kan nog lang niet tippen aan jouw perfecte administratie, maar ik doe mijn best ;-). Ik heb erg genoten van de afgelopen maanden toen we samen het stamcelverhaal hebben afgemaakt. Ik ben er super trots op en bedankt dat ik eraan mee mocht werken! Je bent een ontzettend krachtig persoon en ik ben trots op je

Addendum

hoe je nu op zoek gaat naar de volgende stap. Heel veel succes! **Sander**, we go way back. Nou ja, tot het begin van onze master toen we allebei onze stage liepen in het Geijsen lab. Volgens mij bleek toen al dat we het erg goed met elkaar konden vinden en ik vond het dus ook super dat we allebei in hetzelfde lab terecht kwamen voor onze PhD. Wat heb jij heerlijk droge humor en wat kan je goed schelden. Dat heb ik het afgelopen jaar gemist! **Daniëlle**, hatseflats. Je enthousiasme, lach en energie zijn aanstekelijk. Ik vind het mooi om te zien dat je je plekje nu hebt gevonden binnen de Pathologie. **Lennart**, wat ben ik blij dat je het van Rheenen lab bent komen versterken! Je hebt een ontzettend fijn persoon om mee samen te werken door je vriendelijkheid, kennis en geduld. Heel veel succes bij het PMC! **Daniel**, I really enjoyed having you in the office citing Science papers from 1996. I don't know where you store all that knowledge! Good luck in Heidelberg and keep in touch. **Carrie**, little crazy ball of energy. I loved being your neighbor and all the craziness that happened in and out of the office. I loved the rum on Friday afternoon, our sport sessions, dinners, coffees, gossip sessions, etc. It was really hard to see you leave and there was definitely a drop in energy in the lab. Though, I'm glad to see that you found a spot where you are happy. **Amalie**, it was great to have you in the lab. Thanks for your support and enjoy your time at the facility! **Frank**, jij bent een echte mentor. Van jou heb ik geleerd dat je ontzettend moet genieten van het doen van wetenschap en dat het geen zin heeft om te streng te zijn op je eigen resultaten. Wijze lessen! Bedankt! Spanish **Maria**, I admire your creativity. I think you can make great use of that at the PMC with all the fancy technologies there. **Anoek**, jij was een goed voorbeeld toen ik mijn PhD begon. Jij beheerst de kunst om veel balletjes tegelijk in de lucht te kunnen houden. Daar kan ik nog wat van leren. **Pim**, jouw enthousiasme werkt aanstekelijk. Wat was het fijn om jou als helpende hand te hebben bij het calorie restriction project. Ook van jou heb ik geleerd om niet te streng voor mezelf te zijn en om lol te maken. Bedankt! **AJ**, een van de gangmakers van het Hubrecht met je taak als beer commander. Wat een top mails stuurde jij op de vrijdagmiddag. Het was een feest om je even in ons lab te hebben. Een grote stap van de vis naar de muis, maar dat maakte helemaal niks uit. Bedankt voor je gezelligheid en je hulp! **Anko**, bedank voor al jouw microscopiehulp en je magische kracht om door er gewoon te zijn, alle technische problemen op te lossen.

En dan het tweede lab, de Snippet groep, oftewel de Snippies. Wat een luxe om deel uit te maken van twee ontzettend leuke labs en om deze labs soms te kunnen verbinden. **Koen, Jasmin, Bas, Ingrid, Sander, Maria H, Yannik, Nizar, Michiel, Suzanne, Petra, Joris en Julian**. Ook al heb ik maar een jaar echt dagelijks in dit lab rondgelopen, toch voelt ook dit als thuis. Bedankt dat ik bij veel dingen nog ben betrokken en dat ik mee mocht op retreat. **Koen** en **Jasmin**, een komisch duo. Wat fijn om mijn PhD met jullie te beginnen! Spetses was natuurlijk een enorm hoogtepunt met goede dance moves, veel ice coffees en Cancer. **Jasmin**, wat een goede roomie was jij. Bedankt voor je gezelligheid en je soms grappige onhandigheid. Toch mooi dat we nu dezelfde stap willen gaan maken. Ik ben benieuwd waar je terecht gaat komen! **Koen**, mooi om aan het einde weer even in hetzelfde lab te staan! Door je enthousiasme en drive is het erg leuk om samen met jou wetenschap te bedrijven. En natuurlijk om samen weer naar een conferentie te gaan. Sorry voor mijn keuze voor een interessant hotel ;-). **Bas**, mijn allereerste buurman. Wat heb ik veel van jou geleerd! Je hebt mij een ontzettend goede basis in het imagen en het kloneren bijgebracht, wat best handig was voor de rest van mijn PhD... Je stelde altijd kritische, maar zeer rechtvaardige vragen die mijn verhalen beter hebben gemaakt. Bedankt! **Ingrid**, de steunpilaar van het lab. Bedankt voor je bereidbaarheid om altijd te helpen en vooral voor al jouw hulp met organoids! **Sander**, wat een heerlijke wetenschapper ben jij. Je enthousiasme is aanstekelijk! Ik ben benieuwd hoeveel jij met Jacco hebt geroddeld ;-). **Nizar**, ook jij bent ontzettend enthousiast. Je hebt een

uitnodigende persoonlijkheid en mede hierdoor heb ik mij nog altijd onderdeel gevoeld van het Snippert lab. **Maria H** and **Yannik**, you both started when I only occasionally visited the Snippert lab but I'm still happy that I got to hang out with you on retreats and meetings. **Maria**, your eagerness makes you a great scientist. I know that your projects are not the easiest but I'm very sure you will end up with a beautiful story! **Yannik**, jouw creativiteit en doorzettingsvermogen gaan jou ver brengen! **Michiel**, **Suzanne** en **Petra**, jullie zijn alle drie bij het lab gekomen toen ik al met Jacco mee naar het NKI was verhuisd. Ik had jullie heel graag beter leren kennen, want ik heb erg genoten van alle gekkigheid afgelopen jaar op de retreat. Volgens mij zijn jullie een super aanwinst voor het Snippert lab! **Joris** en **Julian**, welkom bij het lab! Ik hoop dat jullie net zoveel lol zullen hebben in het Snippert lab als dat ik heb gehad.

Everyone from the 3rd floor of the Stratenum, **Burgering**, **Gloerich** en **De Rooij** labs, thanks for all the fun and interesting retreats and borrels. **Hans**, **Boudewijn**, **Holger** and **Fried** thank you for your input and critical notes during work discussions or department meetings. **Lukas** en **WJ**, bedankt voor jullie gezelligheid! **Marianne** en **Christina** bedankt voor al jullie hulp met formulieren, applicaties en veel meer.

I would of course also like to thank the department of Molecular Pathology, **C2**, at the NKI. When our lab arrived at this department at the end of 2017, we were all a bit sceptical and hesitant, because we had to leave a great place at the Hubrecht. But you were warm and welcoming and now looking back I feel thankful that we moved and that I got to meet so many new nice people. **Ellen** en **Suus**, bedankt voor het makkelijker maken van alle kleine (en grote) dingen! Fijn om altijd bij jullie naar binnen te kunnen lopen. **Koen**, **Catrin**, **Stefan**, **Anna**, **Millie**, **Dario** and **all the rest**, thanks for nice retreats, borrels and coffee chats!

Then there is the **Hubrecht**. Most of you will remember how shocked the lab responded to the news that we were moving to the NKI. I think that that says it all. The Hubrecht is a great, exciting and warm place to work, with very cool science, but also with a lot of fun. I truly enjoyed the late borrels, random evenings in the city, Ardennes weekends, BBQs in the park, Christmas dinners, etc. etc. **Sven**, **Sasja**, **Caro** en **Tim**, thanks for being an awesome PV! **Bas**, purple pants **Bas**, **Ator**, **Javi**, **Wim**, **Rob**, **Judith**, **Geert**, **Anna**, **Kim**, **Ajit**, **Euclides**, **Hester**, **Margit**, **Corina**, **Suzanne**, **Annabel**, **Wouter**, **Charlotte**, **Kay**, **Chloé**, **Maartje**, **PJ**, **the IT guys** and **all the rest**, thank you for all the fun!

And then my students, **Eva**, **Konrad** and **Simona**, thank you for your help! **Eva**, although you were only briefly in the lab, you set up the organoid stainings, thanks! I hope you found a place where you are very happy! **Konrad**, my most independent student. You did an amazing amount of work and it actually may in the end fit into the paper that will come from Chapter 3! **Simona**, thanks for the fun! It was great to share the excitement with you, to pioneer new windows and to create awesome data. You can be super proud of what you achieved! I am really sure that with your curious and positive attitude you will do great in the Kops lab!

Some very important people that I should not forget to acknowledge, the **animal caretakers** of both the Hubrecht and the NKI, **Marieke**, **Ben** and the **intervention unit**. Thank you for all your help, especially with the calorie restriction project. I know it was a lot of work, but it was definitely worth it! You can read the results in Chapter 5. Thank you!

Of course I also need to thank all the **mice**. I tried my best to treat you the best as I could, but I realize that you made a big sacrifice. Thanks for helping bringing science further.

Addendum

Also, a big thanks to members of the **Sansom group** in Glasgow. **Owen**, your input during my PhD was very valuable and I'm very thankful that you pointed out that the APC mouse was a hypomorph. That explained a lot! I enjoyed our scientific discussions and your openness in sharing data. **David**, I really enjoyed collaborating and talking science with you. I'm glad we kept running in to each other over the past years and especially in Frankfurt. Hihi, I had to laugh about your punctuality when it comes to ICEs. **Michael** and **Dusty**, thank you both for being so helpful! I really enjoyed collaborating with you.

Bernat, Edouard and **Ben**, thank you for the great collaboration. I enjoyed our physics versus biology discussions a lot and I think they resulted in a great manuscript. Let's keep our fingers crossed now!

Francis, mijn paranimf, wat ben ik blij dat ik jou heb leren kennen tijdens mijn eerste masterclass. Fijn dat we hebben kunnen bonden over onze hoofdpijn, en dat dat voor ons allebei nu een kleiner probleem lijkt te zijn. Ik weet dat ik altijd bij jou terecht kan en ik geniet ervan om bij jou op de bank te zitten en over alles te kletsen (zoals keukentegels) terwijl Doris zo af en toe om aandacht vraagt. Spannend om allebei een nieuw avontuur aan te gaan! Ik kijk ernaar uit om te zien waar dit ons gaat brengen.

Lieve JC Helder, H², **Mariëtte, Marieke, Marieke, Franske, Sanne** en **Noukje**. Wat is het fijn om jullie om me heen te hebben en om elke vrijdag met een wijntje het weekend te kunnen beginnen. Het heeft mij de afgelopen vijf en een half jaar enorm geholpen om los te koppelen van werk en om te blijven realiseren dat er belangrijkere dingen zijn dan mijn resultaten in het lab. Jullie hebben mij bijgestaan tijdens alle pieken en dalen, en ik weet dat ik altijd bij jullie terecht kan. Bedankt lieve JC, ik kijk ernaar uit om nog vele jaren op vrijdag samen wijntjes te drinken.

Lieve bio-vriendinnetjes, **Ellen** en **Annelies**, jullie zijn erbij geweest tijdens mijn hele biologieavontuur. **Ellen**, jij letterlijk vanaf het eerste uur toen jij besloot dat van alle mensen in groepje 3 ik de beste kandidaat was als vriendin. Daar had je helemaal gelijk in. Jij weet mij uit mijn comfort zone te halen en mij te laten zien dat je je hart moet volgen en niet zo maar moet doen wat er van je verwacht wordt. Dankjewel voor alle mooie avonturen die we samen hebben beleefd! Ik kijk ernaar uit om nog veel meer samen te gaan ondernemen. **Annelies**, jij bent er altijd als het even niet zo lekker gaat. Je bent begripvol en weet het juiste te zeggen op het juiste moment. Ik bewonder je kracht en de manier waarop jij dit in je werk gebruikt. Ik geniet van onze avondjes Concertgebouw, onze shopsessies in Haarlem en de eindeloze hoeveelheid thee die we samen drinken met vaak een goed stuk taart erbij. En ik ben je natuurlijk enorm dankbaar dat je me aan mijn mooie huisje hebt geholpen! Ik ben blij met zulke lieve vriendinnetjes!

Laurien, mijn lieve lieve huisgenoot van de Adelaarstraat. Wat hadden wij een heerlijk plekje samen! Na een lange dag kon ik altijd bij jou op de bank ploffen of kwam je even boven om te kijken hoe het met mij ging. New Girl, een grote kop thee en een lekker bord eten waren goede ingrediënten voor een relaxte avond. Super dat we binnenkort ook jouw promotie kunnen vieren!

Charlotte, wat ben ik blij dat we elkaar hebben gevonden in Boston. We hebben daar veel samen meegemaakt en daar is een bijzondere vriendschap uit ontstaan. Bedankt voor je luisterend oor en voor je goede adviezen. Ik vind het enorm knap hoe je je over de afgelopen jaren heb ontwikkeld en hoe je je door moeilijke tijden hebt geworsteld. Je bent ontzettend sterk en weet wat je wil. Hier heb ik ontzettend veel respect voor!

Joost, Jostie, varkensbuddy. Mijn uitstapje naar de wereld van business and economics bleek een heel

goede beslissing aangezien wij toen ons fantastische project in het pittoreske Heeze mochten doen. Het was een top tijd en ik ben blij dat onze vriendschap hieruit is ontstaan. Laten we samen nog vele biertjes gaan drinken!

Guido, jij was mijn support tijdens de eerste jaren van mijn PhD en daar wil ik je enorm voor bedanken. Je was altijd geïnteresseerd en je liet merken hoe trots je op me was. Bedankt voor al je steun.

Ex-Enny's – **Martje, Niels, Julia, Ilja** en nu ook **Jorine** – nu verlies ik toch de wedstrijd door als laatste te promoveren... Och ja. Bedankt voor jullie support en gezelligheid! Ik ben erg dankbaar dat ik tijdens het begin van mijn studie jullie dagelijks om mijn heen heb mogen hebben. Het was een perfecte balans tussen gezelligheid en gekkigheid aan de ene kant, en ambitie aan de andere kant. Laten we onze traditie van spelletjesmiddagen en weekenden zeker doorzetten!

Lieve **Mirjam, Astrid, Anneli** en **Manou**, we go waayyy back. Harry Potter, Harry Potter, Harry Potter... Hermione! Voldemort! We hebben goede avonden samen doorgebracht en wat vind ik het enorm bijzonder dat het nog steeds zo fijn is als we met z'n allen zijn. **Mirjam**, jou ken ik het langst van al mijn vrienden en we hebben ontzettend veel samen gedaan. Jij was altijd net een klein beetje beter in alles en dat daagde mij uit om net een stapje extra te zetten. Toch gek dat we allebei een PhD zijn gaan doen en allebei zijn gaan kijken naar de darm! Heel veel succes met de laatste loodjes! **Astrid**, wat een heerlijk persoon ben jij. We zijn ontzettend anders maar toch werkt dat. Ook jij heel veel succes met de laatste beetjes van je PhD. **Anneli**, mijn hockeyvriendinnetje. Ik weet de avond nog goed dat ik jou mocht opbellen om te vragen of jij met mij op hockey wou. Ik ben blij dat je ja zei! Ik waardeer je heerlijke nuchterheid en wat was het mooi dat we bij jou terecht konden voor mooie avonden. **Manou**, fijn mens. Van jou heb ik geleerd dat kleine dingen heel mooi kunnen zijn en dat je vooral moet genieten. Je hebt een goede kijk op het leven! Lieve vriendinnetjes, ook al zien we elkaar niet vaak, ik ben blij dat ik jullie heb.

Tony, the craziness that we have been through together. I still cannot get over the fact that our families celebrated Christmas together... How cool is that! I also find it very special that our worlds merged a little bit. Many of my friends got to meet you and you became good friends with Danika. You are a wonderful person to spend time with and your ambition is inspiring. Although you are far away, you are a very valuable friend.

Danika, my Boston buddy. We must have spent 80% of the time together when I was in Boston and I loved every minute of it. It was so easy to hang out with you, to nerd out over science, to cook on Sundays, to order Thai and eat it on my balcony and to spend great evenings also together with **Nicole**. I loved my time in Boston thanks to you!

Sean, we have to thank craigslist for bringing us together. I still cannot believe how lucky I got to have you as my housemate during my Boston time. The time I did not spend with Danika, I spent with you. We hosted great parties, watched speed skating together, ate bitterballen and just had really nice long talks. I am thankful to have you as my friend.

Mark and Jenny, my second set of parents. I was 16 when I spent half a year as a true daughter in your family. This time really shaped me and it taught me that getting out of your comfort zone brings many wonderful things. A valuable lesson! Thank you for being so loving and for welcoming me into your family. I look forward to the day that you visit the Netherlands ;-)

Addendum

Lieve gekke **Bruens familie**. Wat een heerlijk stelletje zijn we toch met elkaar. Ik geniet van de momenten dat we met z'n allen zijn en dat dit dan altijd heel georganiseerd en toch chaotisch verloopt. Ik waardeer de oplossingsgerichtheid, de can-do mentaliteit en de kritische instelling van onze familie. Dit zijn eigenschappen die goed van pas kwamen tijdens mijn onderzoek. Bedankt voor jullie oprechte interesse in mijn promotietraject en voor mijn onderzoek!

Lieve **Linde**, van jou heb ik geleerd om goed om me heen te kijken en om schoonheid te zien in kleine dingen, dit geeft geluk. Je staat erg in contact met de dingen om je heen en dat vind ik heel mooi om te zien. Bedankt voor je lieve steun en voor de fijne berichtjes die je stuurt!

Grootmoeder, bedankt voor je enorme interesse in mijn onderzoek! Tijdens de eerste maanden van mijn biologiecarrière heb ik in Wageningen mogen logeren en daar heb ik hele warme herinneringen aan. De wetenschappelijke bijlages van de krant die op mij lagen te wachten als ik naar Wageningen kwam hebben vast en zeker bijgedragen aan mijn enthousiasme voor de wetenschap. Ik vind het erg bijzonder dat we het einde van mijn promotietraject samen kunnen vieren! Ik ben trots dat jij mijn grootmoeder bent!

Lieve **Lijs, Cas** en **Bien**, bedankt voor al jullie steun! Wat een warm en fijn nest hebben wij toch met elkaar. Lijs en Cas, jullie hebben mij met veel vrijheid op laten opgroeien. Jullie hebben mijn nieuwsgierigheid gevoed en mij alle kansen geboden om mij te ontwikkelen. Daar ben ik enorm dankbaar voor en ik besef hoeveel geluk ik hiermee heb gehad. **Lijs**, mijn liefde voor de biologie komt niet van een vreemde. Beestjes moesten buitengezet worden en we hebben eindeloos insectjes of waterbeestjes gevangen om die in ons loepotje te bekijken. Toen ik met muizen ging werken was dit dus ook wel een kleine shock, en jij vroeg me dan ook wel om elke muis te bedanken. Dat heb ik altijd gedaan! **Cas**, van jou heb ik mijn exacte en analytische kant. Onze gesprekken over investeringen, wetenschappelijk onderzoek of maatschappelijke ontwikkelingen hebben mij geleerd kritisch na te denken en om een mening te vormen, kwaliteiten die erg waardevol zijn tijdens een promotietraject. Lieve Lijs en Cas, bedankt voor al jullie liefde en steun! Lieve **Bien**, dit heb ik al vaak gezegd, maar wat ben ik blij dat jij mijn zusje bent. Ik kan altijd bij je terecht en dan weet je precies wat je moet zeggen. Je bent een enorm sociaal, doortastend en krachtig persoon, een combinatie van eigenschappen waar ik erg veel bewondering voor heb. Ik vind het erg bijzonder dat je mijn paranmf bent en dat we die dag zo samen met elkaar kunnen vieren. Bedankt dat jij mijn zusje bent en ik kijk erg uit naar ons volgende avontuur!

Axel, liefie, I am thankful to have you by my side. You support me by just being there, by putting things into perspective and most of all by saying that you are proud of me. You bring out my inner nerd, which I like more than I should admit, and you cherish it. Thank you for your love. I am really looking forward to make a next step with you along my side.

It was a wild ride, but I am thankful for every minute of it.

